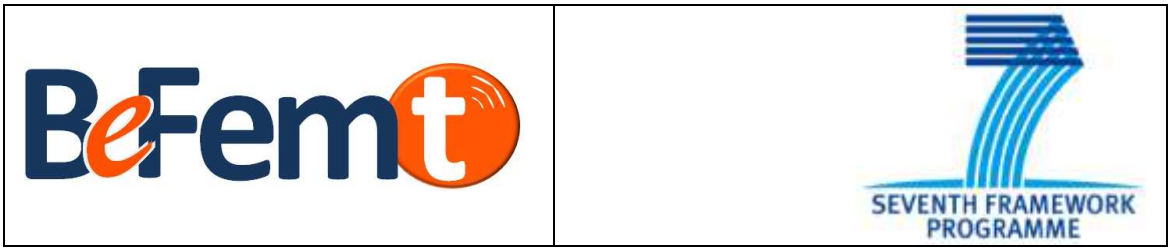

INFSO-ICT-248523 BeFEMTO

D4.3

Multi-cell RRM and self-optimisation for networked, fixed relay and mobile femtocells

Contractual Date of Delivery to the CEC:	**M24**
Actual Date of Delivery to the CEC:	**M24**
Author(s):	Antonio de Domenico, Emilio Calvanese Strinati, Sylvie Mayrargue, Lorenza Giupponi, Mischa Dohler, Stefan Brueck, Andrea Garavaglia, Mariano López, Carmen Palacios, Atta ul Quddus, Youngwook Ko, Ali Imran, Masood Maqbool, Massinissa Lalam, Mehdi Bennis, Francesco Pantisano, Simon Scott, Hirley Alves, Beatriz Solana, Serkan Uygungelen, Gunther Auer, Dimitry Marandin.
Participant(s):	*CEA, CTTC, mimoOn, QC, TTI, UNIS, SC, UOulu, TID, DOCOMO*
Workpackage:	WP4 (Self-Organizing Radio Access for Networked, Mobile and Fixed Relay Femtocells)
Estimated person months:	15 PM
Security:	**PU**
Nature:	**R**
Version:	Final
Total number of pages:	126

Abstract:

This deliverable provides a detailed analysis of multi-cell RRM and SON techniques for networked, fixed relay, and mobile femtocells. First, an overview of SON techniques and its architectural requirements is presented. An in-depth study of SON techniques for interference minimization, radio resource management, and energy efficiency are examined. Notably, it is shown that the BeFEMTO femtocell average spectral efficiency of 8bps/Hz is achieved in a MIMO macro-femtocell setting. SON-based radio resource management techniques are next dealt with through *docition*, femtocell- relay aided macrocell transmission and interference spatial coordination schemes. The issue of energy efficiency is examined within the context of SON where an admission control and resource allocation scheme is proposed, as well as a RF front-end functionality. Furthermore, the extension of SON techniques to the scenarios of fixed and moving femtocells relays is presented.

Keyword list:

SON, Q-learning, Game theory, Antenna Tilt, Power control, Frequency partitioning, Energy-aware, Interference management, Fixed and mobile femtocells

Executive Summary

Due to the expected high number and thus density of femtocells and their unplanned deployment, low cost deployment and management mandates the use of self-organization and self-optimization. Especially self-optimization of the radio access will allow reduction of interference, optimization of radio resource allocation and reduction of energy consumption while at the same time minimising the complexity of network management. This deliverable examines each one of these self-organization techniques, as well providing an extension to the mobile and fixed femtocell relay scenarios with preliminary results.

- **Section 2: Overview of SON Techniques.** An overview of the issue of self-organizing networking (SON) is provided with an in-depth taxonomy. State-of-the art literature on interference management in the context of SO, distributed machine learning and RF front-end functionalities is subsequently discussed. Major research projects and their contributions to standardization activities dedicated to SON activities are also discussed.

- **Section 3**: **Architectural requirements of SON 3GPP & BeFEMTO HeNB**: SON use case functionalities are discussed with a preliminary analysis of their relevance for the case of HeNB-HeNB as well as for the case of eNB-HeNB. In addition, a look into recent Release 10 additions to SON functions and the extension to interference management case is provided. Finally, an overview of ongoing work for Release 11, where a new Work Item on SON has been opened, and recent trends is included.

- **Section 4: SON for Interference Minimization**: The impacts of dominant interference conditions in the downlink when macro UEs are in close proximity of femtocells are assessed. Next, the performance of a macro/femto network equipped with MIMO spatial multiplexing mode is presented. By combining spatial multiplexing characterized by 4x4 antenna configuration and interference mitigation, the BeFEMTO average femtocell spectral efficiency target of 8bps/Hz is achieved. In addition, SON-enablers for interference minimization are examined as a means of minimizing the overall interference per resource block (RB) generated outside the femtocell coverage range while reducing the transmission power in each RB. Finally, spectral efficiency enhancement on the access link of outdoor fixed relay femtocells through SO of eNB antennas tilt is investigated.

- **Section 5: SON for Radio Resource Management: A** set of innovative SON-enablers for radio resource management are presented. First, the paradigm of docition is presented where a femto BS learns the interference control policy acquired by an already active neighboring femtocell, and thus saving significant energy during the startup and learning process. Second, femtocell-aided macrocell transmission is presented as a means of improving the performance of cell-edge macrocell users with a reward mechanisms using spectrum leasing for cooperative femtocells. Finally, interference coordination schemes in the spatial domain are analyzed and shown to improve the performance of UEs suffering from strong interference.

- **Section 6**: **SON for Energy Efficiency**: Focus is on energy efficiency within the context of SON where an admission control and resource allocation scheme are proposed, which aims at balancing the energy usage by femto cell users between the signalling and the data transmission. Finally, RF front-end functionalities for SON are presented including an implementation of power control for downlink that combines both open-loop and closed-loop.

- Finally**, Section 7** looks at the issue of fixed and mobile femtocell relays. Focus is first on the fixed femtocell relay where a femto BS is used as a relay in an indoor environment for coverage extension. Finally, moving relays are investigated with a main emphasis on in-band backhauling.

Authors

Partner	Name	Phone / Fax / e-mail
CEA		
	Antonio de Domenico	Phone: +33 4 38 78 18 17 e-mail: antonio.de-domenico@cea.fr
	Emilio Calvanese Strinati	Phone: +33 4 38 78 17 34 e-mail: emilio.calvanese-strinati@cea.fr
	Sylvie Mayrargue	Phone: +33 4 38 78 62 42 e-mail: sylvie.mayrargue@cea.fr
CTTC		
	Lorenza Giupponi	Phone: +34 93 645 29 22 e-mail: lorenza.giupponi@cttc.es
	Mischa Dohler	Phone: +34 679 094 *007* e-mail: mischa.dohler@cttc.es
DOCOMO		
	Serkan Uygungelen	Phone: +49 89 56824 226 e-mail: uygungelen@docomolab-euro.com
	Gunther Auer	Phone: +49 89 56824 219 e-mail: auer@docomolab-euro.com
mimoOn		
	Dimitry Marandin	Phone: +49 203 3064537 e-mail: dimitri.marandin@mimoOn.de
Sagemcom		
	Masood Maqbool	Phone: +33 1 57 61 13 63 e-mail: masood.maqbool@sagemcom.com
	Massinissa Lalam	Phone: +33 1 57 61 13 41 e-mail: massinissa.lalam@sagemcom.com
Qualcomm		
	Stefan Brueck	Phone: +49 911 54013-270 e-mail: sbrueck@qualcomm.com
	Andrea Garavaglia	Phone: +49 911 54013-530 e-mail: andreag@qualcomm.com
TTI		
	Carmen Palacios	Phone: +34 942291212 e-mail: mcpalacios@ttinorte.es
University of Surrey		
	Atta ul Quddus	Phone: +44 1483 683787 e-mail: a.quddus@surrey.ac.uk
	Youngwook Ko	Phone: +44 1483 683883 e-mail: y.ko@surrey.ac.uk
	Ali Imran	Phone : +44 1483 689330 e-mail: a.imran@surrey.ac.uk

UOulu		
	Mehdi Bennis	Phone: +358 40 8241 742 e-mail: bennis@ee.oulu.fi
	Francesco Pantisano	e-mail: fpantisa@ee.oulu.fi Phone: +358 46 6831 905
	Simon Scott	e-mail: simon.scott@ee.oulu.fi Phone: +358 40 8241 747
	Hirley Alves	e-mail : Hirley.Alves@oulu.fi Phone: +358 46 526 7197.

Table of Contents

List of Acronyms and Abbreviations

Acronym	Meaning
3G	3rd Generation
3GPP	3rd Generation Partnership Project
4G	4th Generation
AMMP	Active Macro Mobile Protection
ANR	Automatic Neighbour Relation
BLER	Block Error Rate
BOM	Bill of Material
BSCBS	Base Station Coordinated Beam Selection
BS	Base Station
BW	Bandwidth
CA	Carrier Aggregation
CDF	Cumulative Distribution Function
CLSM	Closed Loop Spectral Multiplexing
CQI	Channel Quality Indication
CRS	Cell-specific Reference Signal
CSG	Closed Subscriber Group
CSI	Channel State Information
CDMA	Code Division Multiple Access
CQI	Channel Quality Indicator
CoMP	Coordinated Multi-Point Transmission
DFP	Dynamic Frequency Planning
DL	Downlink
DSL	Digital Subscriber List
eICIC	enhanced Inter-Cell Interference Coordination
eNB	evolved Node B
E-UTRA	Evolved-Universal Terrestrial Radio Access
EVM	Error Vector Magnitude
FAP	Femto Access Point
FCC	Federal Communications Commission
FDD	Frequency Division Duplex
FFT	Fast Fourier Transform
FFR	Fractional Frequency Reuse
FUE	Femtocell User Equipment
GB-DFR	Graph Based Dynamic Frequency Reuse
GNSS	Global Navigation Satellite System
GPS	Global Positioning System
GT	Game Theory
GW	Gateway
HARQ	Hybrid Automatic Repeat Request
HBS	Home Base Station
HCS	Hierarchical Cell Structure
HeNB	Home evolved Node B
HetNet	Heterogeneous Network
HO	Handover
HSDPA	High-Speed Downlink Packet Access
ICI	Inter Carrier Interference
IoT	Interference over Thermal
ICIC	Inter-Cell Interference Coordination
ITU-R	International Telecommunication Union – Radio communication sector
KPI	Key Performance Indicator
LTE	Long-Term Evolution
LTE-A	Long-Term Evolution Advanced
MART	Mobile Assisted Range Tuning

MBSFN	Multicast Broadcast Single Frequency Network
MIC	Mean Instantaneous Capacity
MIMO	Multiple-Input Multiple-Output
MMSE	Minimum Mean Square Error
MRO	Mobility Robustness Optimization
MU-MIMO	Multi-User MIMO
MUE	Macrocell User Equipment
MS	Mobile Station
NL	Network Listen
NTP	Network Time Protocol
OFDM	Orthogonal Frequency Division Multiplexing
OFDMA	Orthogonal Frequency Division Multiple Access
OTA	Over The Air
PA	Power Amplifier
PHY	Physical Layer
PC	Power Control
PCI	Physical Cell Identity
PDF	Probability Distribution Function
PER	Packet Error Rate
PMI	Precoding Matrix Information
PTP	Precision Time Protocol
QoS	Quality of Service
PRB	Physical Resource Block
PRS	Positioning Reference Signals
RACH	Random Access Channel
RAN4	Radio Access Network (Working Group 4)
RBG	Resource Block Group
RF	Radio Frequency
RI	Rank Indicator
RIP	Received Interference Power
RL	Reinforcement Learning
RLF	Radio Link Failure
RPCD	Routing and Power Control Decomposition
RR	Restriction Request
RRC	Radio Resource Control
RRM	Radio Resource Management
RSS	Received Signal Strength
RSRQ	Reference Signal Received Quality
RSRP	Reference Signal Received Power
RSSI	Received Signal Strength Indicator
RSTD	Reference Signal Time Difference
SAS	Smart Antenna System
SFR	Soft Frequency Reuse
SINR	Signal to Interference plus Noise Ratio
SLS	System Level Simulator
SNR	Signal to Noise Ratio
SISO	Single Input Single Output
SO	Self-Organization
SoA	State-of-the-Art
SON	Self-Organizing Networks
SUI	Stanford University Interim channel models
SU-MIMO	Single User MIMO
TA	Timing Advance
TDOA	Time Difference of Arrival
TOA	Time of Arrival
TDD	Time Division Duplex
TNP	Thermal Noise Power

TTI	Transmission Time Interval
UAA	Uplink Adaptive Attenuation
UE	User Equipment
UL	Uplink
UMTS	Universal Mobile Telecommunication System
VGA	Variable Gain Amplifier
WCDMA	Wideband Code Division Multiple Access
WCS	Wireless Communication System
WiMAX	Worldwide interoperability for Microwave Access
WSN	Wireless Sensor Network

1. Introduction

The aim of this section is to introduce the vision and rationale of BeFEMTO WP4 activities.

1.1 BeFEMTO WP4 Vision & Goals

As outlined in the DoW [111], the BeFEMTO project aims at the investigation into development and optimisation of *indoor* and *outdoor* broadband femtocell technologies. The femtocell technologies designed have to be **autonomously self-managing** and provide **open and shared access**. As illustrated in Figure 1-1, BeFEMTO's WP4 vision comprises three major themes, indoor networked femtocells, outdoor fixed relay femtocell and outdoor mobile femtocell.

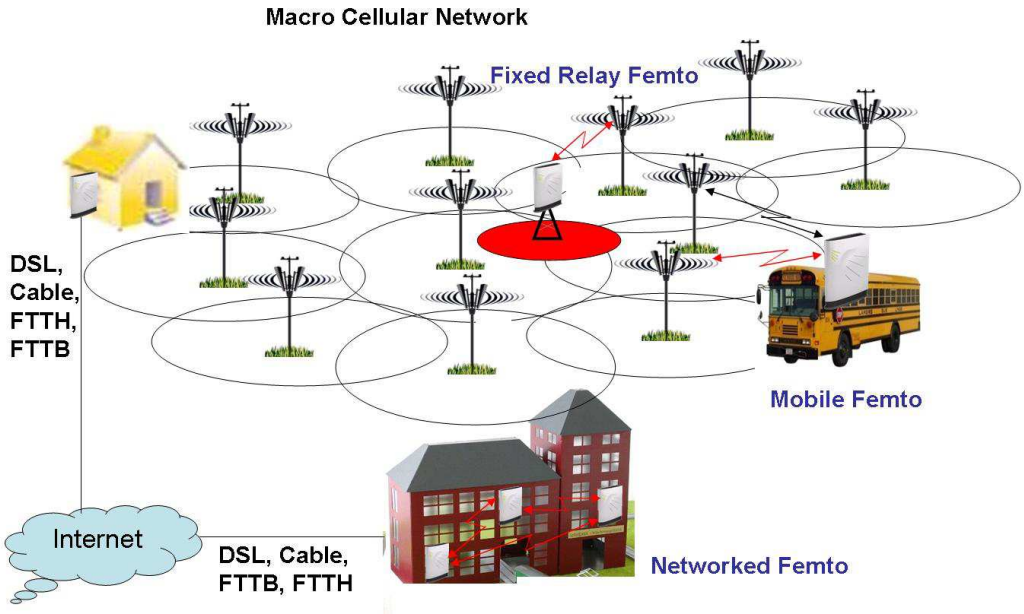

Figure 1-1: BeFEMTO WP4's vision of broadband evolved femtocells.

The theme of **indoor networked femtocells** is a long-term research theme that has only been slightly addressed in the research community, if ever. With networked femtocells, BeFEMTO will investigate on advanced cooperation between femtocells installed in buildings such as hospitals, offices or shopping malls. This approach goes far beyond any state-of-art femto technology and offers new service provisioning for home, office and enterprise environments, and, consequently, new market and business opportunities for service providers. From a technical perspective, networked femtocell requires novel concepts and algorithms with special focus on; resource and interference management, network synchronization, and architectural design facilitating a tight integration into macro and other infrastructure networks. The networks of femtocells could be formed by explicit wired connections or this networking could be wireless. The latter seems more plausible given the self-organising capabilities that BeFEMTO sees as an essential element of future femtocells.

Mobile & relay outdoor femtocells are also novel and they are to provide broadband communications to people outdoors walking or on the move using e.g. public transports. Consequently, we have to cope with a wireless backhaul link as opposed to the wireline link used for fixed or indoor stand-alone femto nodes. Moreover, moving and relay femtocells have to be tightly integrated into an overall heterogeneous network deployment without jeopardizing macro network capacity and quality. This again requires special attention for instance to radio resource management, interference management, group-handover and admission control techniques.

From a technical point of view, goal is to achieve a high **system spectral efficiency of at least 8bps/Hz/cell** (at a given outage level) and a **maximum mean transmit power of less than 10mW for indoors femtos**. Figure 1-2 illustrates these objectives in comparison to GSM and UMTS/LTE-based

cellular systems where spectral efficiency and base station output power values have been taken from [111].

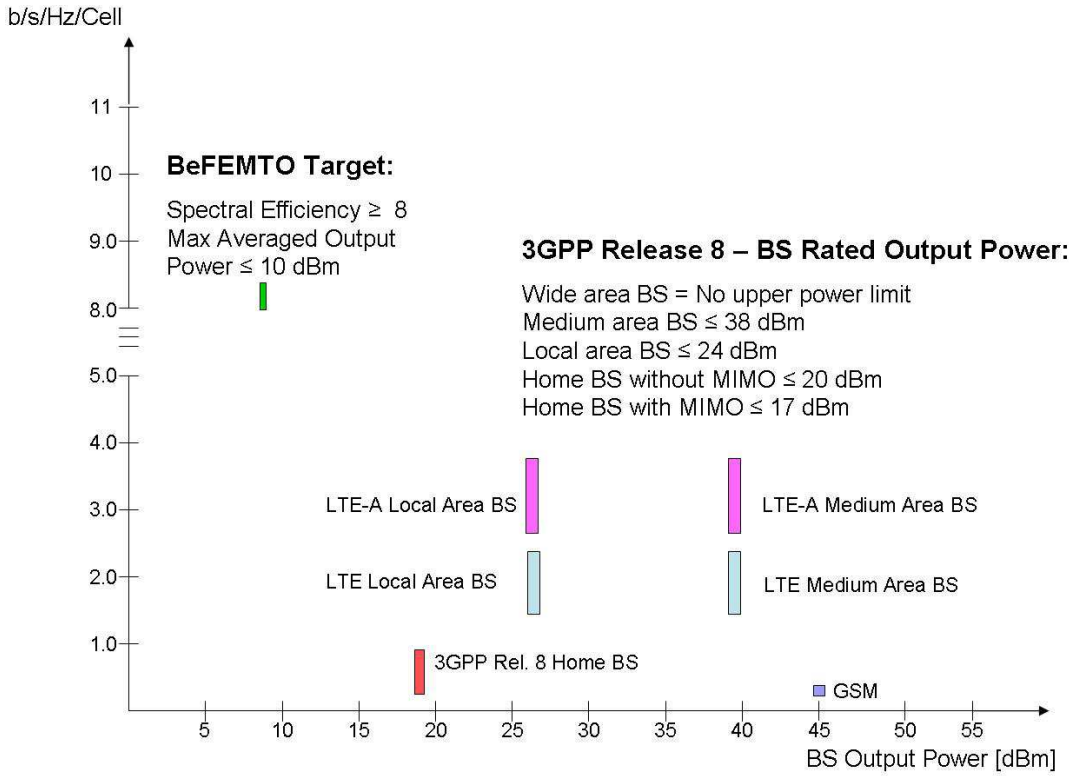

Figure 1-2: Illustration of BeFEMTO's targets in relation to 3GPP based cellular systems.

1.2 BeFEMTO WP4 Objectives & Challenges

To facilitate above vision and goals, WP4 aims at achieving the following objectives:

- **O4.1:** Development of new algorithms to allow accurate real-time geographic location of femtocells and autonomous coverage estimation for all the scenarios.
- **O4.2:** Development of radio context aware learning mechanisms, in centralized and decentralized fashion, and of network synchronization schemes, together with evaluation of implications on system stability and on the time-scales of different parameters involved in self-organisation.
- **O4.3:** Research on novel RRM solutions (interference management, resource allocation, scheduling, handover, admission control, flow control) tailored to the emerging paradigm of networked femtocells.
- **O4.4:** Enable integrated self-optimisation of radio access schemes and parameters taking into account the required signalling on the control plane as well as the associated energy requirements.
- **O4.5:** Adaptation and further improvement of above algorithms to the needs of fixed relay and mobile femtocells.

To meet these objectives, the following challenges were promised to be addressed:

- **Interference Management.** Assuming that femto nodes operate in the same frequency band as overlay networks such as macro or micro nodes, a strong challenge is to cope with the mutual interference caused. This is even a serious problem since femtocells are likely to be rollout unplanned, and, hence, without pre-determined network layout. In order to ensure a successful future deployment of femtocells, no matter which theme is considered, efficient interference management by coordination between femto and overlay systems with less control signalling overhead is of utmost importance. In this context, self-organizing and self-optimizing concepts play a significant role aiming for an easy and fast network deployment and operation.

BeFEMTO envisages indoor positioning schemes and femtocell coverage estimation techniques, as well as other related information, to be incorporated in self-optimisation algorithms to improve performance and, more importantly, stability of operation. By further including flexible transceiver technologies with interference cancellation properties and coordinated multi-point technologies into a cross-layer interference management, BeFEMTO envisages a high scalability and flexibility to handle wireless signals with very diverse QoS requirements efficiently to meet the high spectrum efficiency target of 8bps/Hz/cell (at a given outage level).

- **Link and Access Management.** Handover, admission control and, in general, resource management algorithms such as load balancing and flow control have to be designed to allow for a tight interworking of femto nodes with overlay systems. Especially the flat architecture of 3GPP LTE/LTE-A mandates the implementation of distributed management concepts, e.g. across femto and macro nodes, and it is a challenge to come up with optimal solutions requiring less control signalling effort whilst meeting power efficiency, high and diverse QoS constraints, as well as the different time-variant channel conditions.
- **Dynamic Bandwidth Allocation and Sharing.** Multi-operator band sharing for indoor standalone femtocells is a challenging task to be addressed as an approach to allow for efficient macro-femto coexistence and enhance capacity. For instance, a flexible allocation of a user being served by a femto node of which frequency bands are offered in a multi-operator shared fashion allows for assigning the user to the band that jeopardizes macro network transmissions at minimum. Furthermore, driven by the increasing diversity of QoS demands, it is required to fully exploit the OFDM air interface by allowing for flexible bandwidth allocation. This also includes handling backhaul (aggregated traffic) and user- specific signals simultaneously in case of fixed/mobile relay femto nodes and networked femtocells, but also takes into account the broader scope of jointly managing non-adjacent frequency bands allocated to mobile communication systems by regulatory bodies.

Taken from the DoW of BeFEMTO, the table below summarizes these challenges for WP4.

Table 1-1: WP4 challenges and innovations versus BeFEMTO themes.

Challenges / Innovations	Networked Femtocells	Fixed Relay Femtocells	Mobile Femtocells
Achieving 10 mW output power objective with same coverage & QoS	X		
Cooperative multipoint transmission	X	X	X
Integration between macro and relay femtocells		X	
Femto - macro co-existence: Interference characterisation, mitigation and coordination; centralized and de-centralized approaches	X	X	X
Capacity balancing between macro and femtocells	X		
Distributed resource management between macro and femtocells		X	X
Self-configuring & self-optimising femtocells		X	X
Scheduling for interference avoidance			
Interference mitigation through beamforming	X		
Decentralised resource allocation through game theoretic and learning approaches	X		
Range incorporated scheduling		X	X
Integrated femto hop selection and scheduling		X	X
Application of COMP technologies	X		
Resource-efficient and QoS-aware routing (including load balancing)	X		
Handover optimisations and efficient signalling			X
Handover in open access		X	X
Exchange of control information for radio resource management (may be a new X2 like interface)	X	X	
Cooperative positioning techniques	X		X
Automatic coverage estimation		X	X
Radio context aware learning mechanisms	X	X	X

Mobility management and context transfer	X		X
Centralised versus distributed learning mechanisms	X	X	X
Access control for local networks and services	X		
Dynamics and time scale for self- optimisation	X	X	X

1.3 Need for Self-Organization

Due to the **high number of femtocells** expected and their **unplanned deployment** in the above described scenarios, easy installation, low cost deployment and management makes the use of self-organization and self-optimization essential. Especially self-optimization of the radio access will allow reduction of interference, optimization of radio resource allocation and reduction of energy requirements, while at the same time minimising the complexity of network management. With the reduction of the deployment complexity CAPEX and OPEX can be reduced substantially paving the way for large-scale femtocell deployment. Therefore, to handle these challenges in a cost effective way **automatic, adaptive and autonomous self-organization techniques are needed**, which will reduce the cost of planning and deploying femtocells while achieving optimal capacity in a changing cellular environment.

The deployment of femtocells in an unplanned way will affect the performance of the overlaying macrocell network. The network capacity is expected to increase with the deployment of femtocells but the interference level for the macrocells will increase as well, thus affecting the capacity of the macrocells. This interference is called *cross-tier interference*. Moreover, neighbour femtocells may interfere with each other, which is called *co-tier interference*. The management of co-tier and cross-tier **interferences** in a self-organized manner is essential for the successful deployment of femtocells and needs to be investigated in detail. This will be analyzed by self-optimizing resource allocation and dynamic fractional frequency reuse schemes.

With interference at bay, an important issue is to determine when, how and whom to schedule resources to in the network of femtos. This is part of the **radio resource management** (RRM) functionalities which need to ensure that interference, coverage, capacity requirements and BeFEMTO's goals of 8bps/Hz/cell are met.

Due to the large number of femtocells the **energy requirements** of femtocells need to be taken into account in the self-organization of the femtocell networks in order to achieve the necessary trade-off between energy efficiency and performance. To this end, energy-aware resource allocation schemes are investigated. Additionally further energy savings due to power control, with respect to the RF transmitter, need to be evaluated.

In the open literature, as well as projects and standardisation activity, a number of specific functionalities have been identified which need application of self-organizing techniques. For example, SOCRATES project [77] presented an extensive list of 24 use cases most of which overlap with the use cases identified by 3GPP [79] and NGMN [78]. Most of these use cases can be summarised under following 9 specific categories:

1. coverage and capacity optimization;
2. energy savings;
3. interference reduction;
4. automated configuration of physical cell identity;
5. mobility robustness optimization;
6. mobility load balancing optimization;
7. random access channel (RACH) optimization;
8. automatic neighbour relation function; and
9. inter-cell interference coordination.

It must be noted that these use cases and the main objectives have strong coupling with each other making the overall optimization a difficult task. WP4 deals with the majority of these issues, as outlined subsequently.

1.4 Organization of D4.3

The remainder of the document is organized as follows.

In Section 2, an overview of the issue of self-organizing networking (SON) is provided with an in-depth taxonomy. State-of-the art literature on interference management in the context of SO, distributed

machine learning and RF front-end functionalities is subsequently discussed. Major research projects and their contributions to standardization activities dedicated to SON activities are also discussed.

In Section 3, SON use case functionalities are discussed with a preliminary analysis of their relevance for the case of HeNB-HeNB as well as for the case of eNB-HeNB (see Figure 3-1). In addition, a look into recent Rel. 10 additions to SON functions and the extension to interference management case is provided. Finally, an overview of ongoing work for Rel. 11, where a new Work Item on SON has been opened, and recent trends is included.

In Section 4,the impact of dominant interference conditions in the downlink when macro UEs are in close proximity of femtocells are assessed. Next, the performance of a macro/femto network equipped with MIMO spatial multiplexing mode is presented. By combining spatial multiplexing characterized by 4x4 antenna configuration and interference mitigation, a target of 8bps/Hz is attainable. The next contribution looks the enabling features for SON for interference minimization. First it is shown how to assign resources in unplanned wireless networks that are characterized by varying interference conditions. The proposed method takes the advantages of both central and autonomous resource assignment approaches. As the method relies on the measurements of UEs, it is able to dynamically adapt to the interference conditions faced in random deployments, thus balancing high spatial reuse of subbands with interference protection for cell-edge users. Furthermore, the method has less signaling overhead as existing LTE signaling procedures are used. The second SON-enabler for interference minimization is carried out by a novel resource management scheme that limits the overall interference per RB generated outside the coverage range of a femtocell while reducing the transmission power in each Resource Block (RB). The proposed approach shows coined “RRM ghost” significantly improves communication reliability for user equipment associated with both the macro base station and femtocells. Finally, the last contribution is focused on Spectral Efficiency (SE) enhancement on the access link of Outdoor Fixed Relay femtocells (OFR) through SO of eNB antennas tilt.

In Section 5, a set of innovative SON-enablers for interfrence management are presented. First, the novel paradigm of docition, where a femto BS can learn the interference control policy already acquired by a neighboring femtocell which has been active during a longer time, and thus saving significant energy during the startup and learning process. Second, femtocell-aided macrocell transmission is presented as a means of improving the performance of cell-edge macrocell users with a reward mechanisms using spectrum leasing for cooperative femtocells. Finally, interference coordination schemes in spatial domain (BSCBS) are analyzed and it has been shown that BSCBS allows improving the performance of UEs suffering from strong interference significantly.

In Section 6 we focus on energy efficiency within the context of SON where an admission control and resource allocation scheme are proposed, which aims at balancing the energy usage by femto cell users between the signalling and the data transmission. Finally, RF front-end functionalities for SON are presented including an implementation of power control for downlink that combines both open-loop and closed-loop.

Section 7 looks at the issue of fixed and mobile femtocell relays, in which a novel full-duplex transmission scheme is proposed for femtocell base stations, which extends the coverage of indoor users. Mobile femtocell relays are studied next with a set of preliminary results.

Finally, conclusions are drawn in Section 8.

2. Overview of SON Techniques

This section gives an overview of the notion of self-organization (SO) as well as self-organizing networking (SON) by providing an in-depth taxonomy. Furthermore activities from pioneering papers in literature are reviewed. In particular the existing state-of-the art on interference management in the context of SO, distributed machine learning and RF Front-end functionalities is discussed in more detail. Major research projects dedicated to self-organization are also discussed and how these works have contributed to evolving standards and activities in 3GPP.

2.1 Self-Organization Taxonomy

Self-organization is a very broad term which has received different connotations in the past. For the sake of building a coherent BeFEMTO-wide approach, we aim at building a sufficiently complete working taxonomy which is elaborated on subsequent sections.

2.1.1 SON Definition

Self-organization (SO) has been defined in various fields including biology, computer science and cybernetics [1]. Since its conception, the widespread use and misuse of the term SO has led to its drift from a technical issue to a philosophical debate, as different authors have different interpretation of this notion particularly when it comes to designing SO in man made systems. We do not aim to join this debate, but rather focus on establishing underlining principles and characteristics that should be designed and subsequently observed in systems to be considered as self-organized. Even in the context of Wireless Communications Systems (WCS) the concept of SO is not new, but a widely accepted definition is still not available.

For instance, Simon Haykin gave a visionary statement on the emergence of SO as a new discipline (he referred to as cognitive dynamic systems) for the next generation of WCS [3]. Such *intelligent* WCS would "*learn* from the environment and *adapt* to statistical variations in input stimuli to achieve highly reliable communications whenever and wherever needed" [5]. Spilling et al. [6] introduced the idea that SO should be seen as an **adaptive functionality** where the network can detect changes and based on them, it makes intelligent decisions to minimise or maximise the effect of the same changes. Yanmaz et al. studied it from a more biomimetic perspective and defined it as phenomenon where nodes work cooperatively in response to changes in the environment in order to achieve certain goals [7]. This notion further characterises the behaviour of individual entities of systems and identifies that individual behaviours should emerge on a system wide scale. Prehofer et al [8] further gave a detailed insight into the design principles and summarised self-organization as **emergent behaviour** of system-wide adaptive structures and functionalities based on the local interactions of entities in the system. It is emphasized in this definition that the localisation and **distributed control** are though not necessary and sufficient features, irrespective of most SO systems in nature, which result from an organized emergent pattern through interaction of those local entities.

W. Elmenreich [9] started with a premise on how best to cope with complexity issue with self-organization as a solution, thus clarifying the main idea, rather than giving another definition. This idea highlights self-organized systems as consisting of a set of entities that obtain a global system behaviour, due to **local interactions** among these entities, without the need for a centralised control. They also emphasized that self-organized systems are neither a new class of systems nor always have emerging structure as their primary property.

In summary, even if there are various notions of SO in literature, to the best of our knowledge there is not a generally accepted definition of SO that can be used to classify systems or their functionalities as self-organizing, because of gaps and differences among existing notions of SO and its inherent overlapping with conventional adaptation. We thus provide the BeFEMTO notion of self-organization that attempts to fill this gap, bridge up these differences, and aim to clarify the boundary between adaptation and self-organization. To this end, the following three aspects of notion of SO need to be clarified:

Firstly, SO should not be considered as a holistic feature of a monolithic system. Rather considering SO as feature of an individual functionality of a system is a more logical approach. This refinement is in line

with the perspective explained in [9] and [10] that wireless systems with some sort of SO do not form a new class of wireless systems, rather SO should be viewed as a feature of these systems. The tendency to approach SO as feature of a system as a whole comes from the fact, that in natural systems that are source of inspiration for SO, the SO functionalities become very prominent, e.g. V-shape formation of birds while flocking, shoaling of fish, synchronous flashing of fire flies. But same systems namely group of birds, fish or fire flies might have many other functionalities e.g. searching for food, or breeding etc that might not be self-organizing. Since these functionalities remain in background as they do not emerge as collective prominent behaviour, we tend to neglect them, and classify the whole system as SO or none self-organizing.

Secondly, contrary to the view point in [7] and [8], SO needs not be defined based on *how SO is achieved* rather on the basis of *what SO can achieve* is more relevant in engineering systems i.e., in spite of the emergence of the system-wide coherent behaviour, result of local behaviours is a key observation in the design of natural systems with SO, but it should not be seen as defining characteristic of SO.

The first rational behind this view point is that there are examples in nature, like homeostatic operational control in living beings, where such an emergence is not present or is hidden from the observer, but still SO exists [9]. Therefore, in order to have sustainable definition of SO it should be defined on the basis of its performance characteristics rather than on the basis of its design. The approach towards designing SO should be left open to invite a variety of different inspirations from natural and non natural systems as well.

The second rational behind the perspective of not using design based characterisation of SO is the fact that there are many non biological systems that have been observed to have SO, e.g. economy in a free market is one such examples. The success of game theory to devise adaptive and sometimes truly SO algorithms is proof of this fact.

Finally, SO should be clearly distinguished from adaptiveness but at the same time it should not be essentially considered only arising from high degree of intelligence in the system. Though assuming SO as an outcome of intelligence is a very intuitive notion, but it is equally vague and difficult to design from practical point of view, due to all the ambiguities associated with *intelligence* itself. We rather suggest, from a view point of design and operation of system, it is more pragmatic to think on the line that intelligence actually can emerge from SO.

Above observations show that self-organization manifests a certain degree of intelligence where no single member of the system is intelligent enough individually to control or lead the whole system. The members do not combine their aggregate intelligence to achieve self-organization as a whole as there is no central authority or global communication among all of them. Hence, it can be inferred from close observation of these and other similar natural systems that it is self-organization that emerges from certain characteristics of the system that in turn may manifest some degree of intelligence. Based on the observations in nature, these characteristics of self-organizing systems can be identified to be scalability, stability and agility. Hence, without limiting the freedom of the design approaches towards SO, a definition of SO taking into account what discussed above, could be: **An adaptive functionality in a system is said to be self-organizing if it is scalable, stable and agile enough to maintain its desired objective(s) in face of all potential dynamics of its operational environment.** Translated to the networking needs of BeFEMTO, it means that **SON facilitates operation, without or with negligible (in volume or time) global networking information, with local decision making processes.**

2.1.2 SON Taxonomies

To facilitate coherent work in BeFEMTO, the following working taxonomy is proposed.

- **Time scale based classification:** a WCS has a set of different time scale dynamics as explained in Figure 2-1 that make the achievement of optimal performance objective a challenging task and call for research in first place. Classic radio resources management (RRM) and physical layer research is mostly focused on the very short time scale dynamics e.g. adaptive modulation and coding scheme algorithms operates at micro second scale [11]. On the other hand SO is mostly concerned with short to long term dynamics. The different self-organizing algorithms designed to cope with these dynamics have to operate on respective time scales. For example a load balancing algorithm might have to operate at time scale of minutes and hours [12] whereas adaptive sectorization algorithms might operate at the scale of days and months [13]. This

different diversity of times scale can be used to classify SO, although, this is the simplest taxonomy and it does not describe much about the scope or objectives of the algorithms.

- **Objective or use case based classification:** Each SO algorithm can be classified using categories of use cases it aims for. But the problem with this approach is that one algorithm can have multiple use cases, e.g. same self-organizing algorithm that aims for load balancing can optimise as well capacity or QoS.
- **Phase based classification:** A wireless system has three clear phases in its life cycle i.e. deployment, operation, maintenance or redeployment. For a holistically self-organizing WCS, SO can be classified with respect to one of these phases. The algorithms that self-organize in these three phases can be classified into categories of self-configuration, self-optimization and self-healing, respectively.

From the classification types highlighted above the phase based classification is the most viable and has been adopted in various projects and standardisation activities.

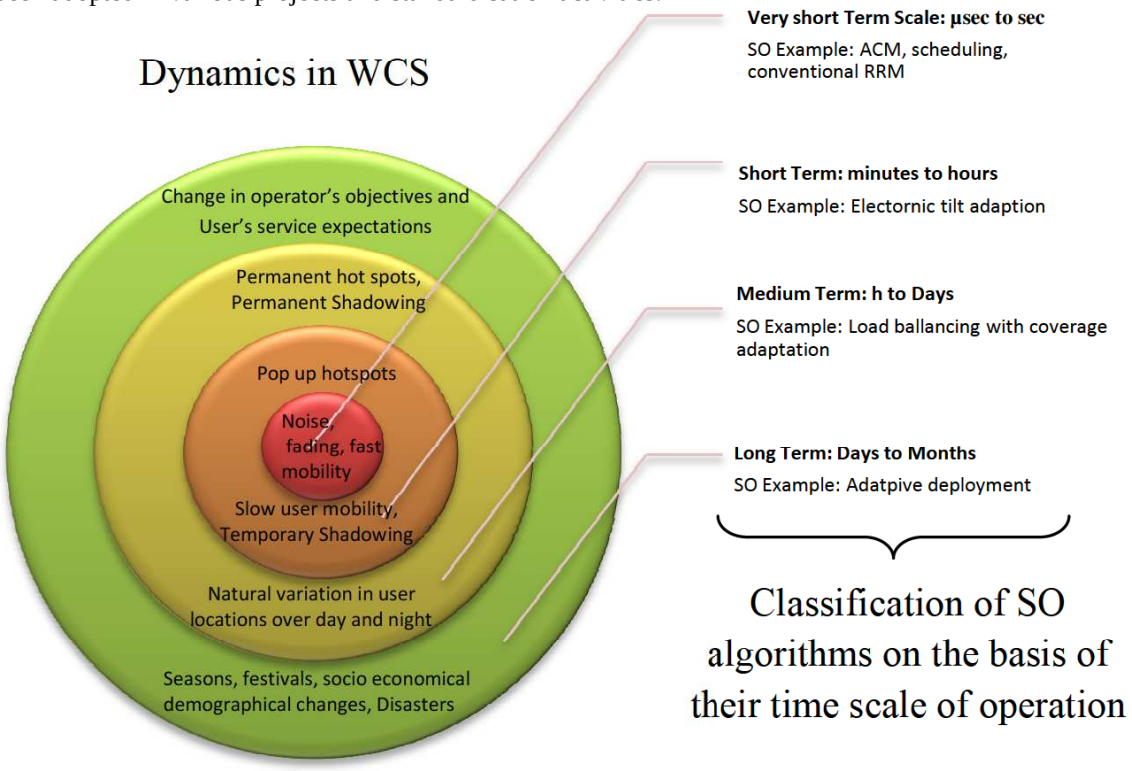

Figure 2-1: Time Scale based Classification of SO.

2.2 State-of-the-Art Technologies

In the context of WCS, the term self-organization has been first used by authors in [14] though in a limited sense of adaptiveness in the power control for GSM. Authors in [14] and [15] presented a simple adaptive power control algorithm to show how this kind of adaptability can mitigate the effect of BS positioning error. Works like [14] - [15] brought forth the need for the self-organization in cellular network and presented a number of adaptive algorithms under the umbrella self-organization but did not present an explicit design strategy to build real self-organization into cellular systems. A second generation of works in self-organization in cellular networks like [16] and [8] embarked on a holistic approach towards self-organization and postulated a set of germane principles and paradigms to be considered in the design process of self-organizing system but stood short of demonstrating these principles through a pragmatic application to specific problems in cellular systems. More recently, works like [19] ventured on designing self-organizing solutions for various problems in cellular system but some of the solutions presented, yield the useful level of adaptability at the cost of compromising one important feature or the other of SO, i.e. scalability, stability or agility. Furthermore, prelimniary works on self-organization can be found in [75][178] with an emphasis on automated diagnosis and troubleshooting

over 3G using bayesian networks, aiming at optimizing Quality of Service and overall systems performance in a multi-system environment.

2.2.1 Interference Management

Interference management is both mandatory and critical in the deployments scenarios considered within BeFEMTO, since macrocells and femtocells may share the same spectrum (co-channel) in a given geographical area (overlay). This can increase the capacity of the overall joint network manifold through high spatial frequency reuse. However, Macro users (MUEs) close to femtocells experience *femto-to-macro interference* that may impact the reliability of communications. A worst case scenario is that of closed subscriber group (CSG) femtocells, where radio conditions for MUEs in close vicinity of a femto BS could be highly unfavourable. Similarly, a user served by a femto BS located close to a macro base station may experience a very low signal to interference-plus-noise ratio (SINR). This will increase the outage probability in both the macro and femtocells where the outage probability is defined as the probability that a user does not reach the minimum effective SINR level required to connect to a service or to decode common control channel. In addition, neighbour femtocells belonging to the same operators may also interfere with each other thus creating *femto-to-femto interference (*also called *co-tier interference).*

Several researchers investigated techniques to avoid *cross-tier interference* (i.e. the *femto-to-macro* and *macro-to-femto interference*). Given the fact that the femto BS are to be managed and maintained by end home users, self-organized solutions to fight interference are highly desirable. In the following paragraph, we present some relevant literature that addresses the interference management issue with the help of different SON techniques.

Cognitive radio techniques can monitor the wireless environment and inform the resource allocation controller about local and temporal spectrum availability and quality [20], [21]. Thus, opportunistic access points can dynamically select available channels and adapt transmission parameters to avoid harmful interference between contending users.

Cho and al. compared orthogonal and co-channel frequency allocation schemes through simulations [22]. Bai and al. extended the analysis of the hybrid approach in [23] by considering both uplink and downlink scenarios [24]. The authors proposed to use the shared spectrum when it is favourable both to macro and femto users, otherwise, a partitioned approach is chosen.

Claussen defined a power control algorithm to limit the interference caused by femtocells in both uplink and downlink scenarios [25]. However, he neglected the impact of *co-tier interference*. To deal with the *co-tier interference*, Li and al. proposed a frequency scheduler that allows opportunistic reuse of the spectrum between each femto BS when the interference level is below a certain threshold [26].

The authors of [27] propose different spectrum allocation algorithms for femtocells based on channel quality measurements received from users. These are distributed algorithms and are based on channel quality measurements received by BS from users. The algorithm performance is evaluated in terms of femto/macro user throughput only.

A centralized solution for interference avoidance in femtocell network has also been discussed in [28]. However, the macrocell effect has not been taken into account.
A location based resource allocation scheme has been proposed in [29] for femtocells while considering reuse 1 in macro network. The proposed algorithm is dependent upon the information about the user's location and hence depends upon accuracy of this information.

The partial usage of subbands in femtocells has been proposed in [30][31][1] while considering reuse 1 and reuse 3 in overlay macro network. The selection of subbands out of a pool of subbands is carried out to avoid interference in [30]; the decision to select a subband for transmission is carried out by the femtocell in a distributed manner. Even though, the solution being suggested in [29] is distributed and self-organized, it assumes an exchange of information between femto and macro cells through X2 interface.

Guvenc and al. distinguished two coverage areas within a macrocell based on the distance between the femto BS and the Macro BS [23]. In the inner region, the femtocell coverage area is limited by the M-BS

interference hence a dedicated band is allocated to femto BSs while co-channel transmissions are allowed in the outer region.

Chandrasekhar and al. proposed to allocate a dedicated band to the femtocells within a macrocell [32] so that resource partitioning is optimized to meet both macrocell and femtocell users' rate constraints. Moreover, the authors defined a *blind round-robin* scheduler at each femtocell to limit the *co-tier interference*. Under this algorithm, femtocells access a random subset of their available channels, each channel being chosen with the same probability.

Su and al. presented a distributed resource allocation/power control algorithm to limit the *cross-tier interference* [33]. However, the complexity of the proposed algorithm grows linearly with the product of the number of femtocells and the number of available channels. Furthermore, this approach requires an information exchange between the M-BS and femto BSs. This coordination and limited availability of backhaul bandwidth result in scalability issues.

In [34], a comparison between co-channel and orthogonal channel deployment schemes in macro/femto network has been presented. It has been concluded that for co-channel deployment open access mode should be preferred over CSG in femtocells when MUEs are indoors.

2.2.2 RF Front-End Functionalities for Self-Optimization

Generally wireless communications systems use power control to reduce interference and increase system capacity while maintaining a minimum signal quality [35]. Implementation of power control in the downlink needs mechanisms that supervise the transmitted power, meaning the way the power amplifier (PA) works is controlled. The PA is the element that feeds the antenna in the transmitter part and provides the desired levels of the output signal. Femtocell requirements include both absolute and relative accurate transmit power requirements [36]. The absolute requirements define a lower and upper transmit power limit relative to a nominal transmit power. The relative requirements define a minimum and maximum transmit power differences between two transmitted slots, not necessarily adjacent time slots, as well as an aggregated transmit power difference over several time slots. There are two types of loops to implement the power control: closed-loop and open-loop.

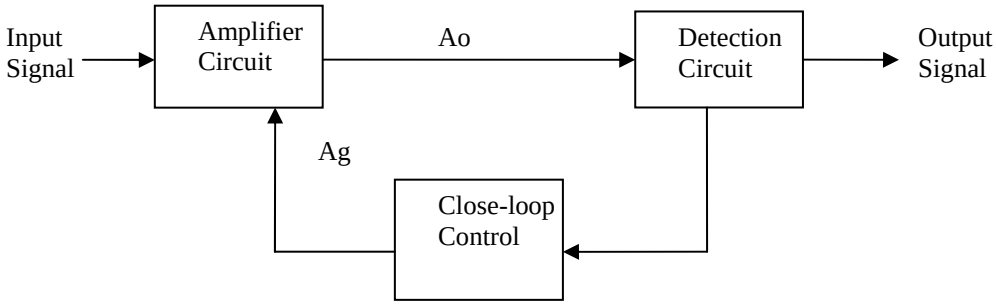

Figure 2-2: Closed-loop power control

Closed-loop power control Figure 2-2 represents one method for controlling the transmit power within the wireless communication device to comply with the relative and absolute transmit power requirements. Using a sample of the transmitted power, an error signal to a reference is calculated and with this signal the transmitted power signal is corrected. This type of control loop has the limitation of the power detector dynamic range.

Another type of power control loop is the open-loop power control. It adjusts the transmitted power in response to power control commands produced by operational parameters and/or environmental conditions instead of using a sample of the current transmitted power to calculate or correct the output power. These commands can be described as power commands produced by the Network Management,

the own unit detection of low traffic load (introducing an ECO-mode or dormant state) or user pushing a save energy mode.

Nowadays in mobile user equipment and other type of wireless communication systems like wireless sensor networks (WSN), the PA consumes approximately 40 % of the energy stored in the battery during one discharge cycle [37]. For this reason, the handset architect must be careful whilst selecting a PA that will provide the most efficient means of generating the required transmitted RF power while using the least amount of energy from the battery and using other functionalities to avoid wasting battery during low operation periods of time. Standard governance boards such as 3GPP set the requirements for over-the-air (OTA) requirements. These requirements are usually much more relaxed than typical carrier requirements as they require more stringent OTA performance. These OTA requirements are directly applicable to the 50 Ω (Ohm) power if RF front ends are benchmarked and compared with these requirements in mind [38].

The Sniffer Module is a real-time system that continuosly capture/monitors data or signal passing through the network. It is also called Network Listen Mode (NLM), Radio Environment Measurement (REM) or "HeNB Sniffer" in [39] and [40]. With it, the HeNB incorporates functionalities of user receiver, that is, a DownLink Receiver with special possibility of performance Reference Signal Received Power (RSRP), Reference Signal Received Quality (RSRQ) to obtain the power received from another femtocell and macrocells at FAP. With these measurements femtocell can calculate the best working point taking into account coverage and interference to both too close co-channel macrocell users and co-channel FAP. Other type of measurements described in [41] are performed in order to minimize interference to adjacent MUEs and macrocells, to detect victim UEs, obtain other cell ID, etc.

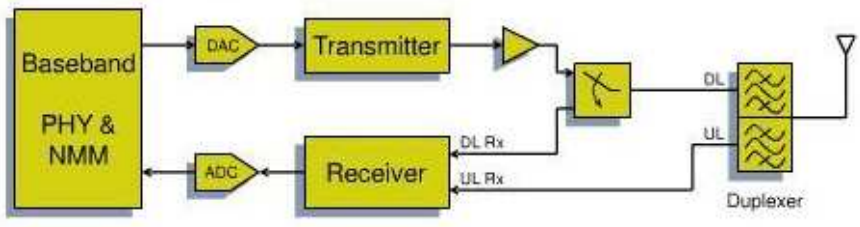

Figure 2-3: Sniffer Module.

2.2.3 Distributed Machine Learning

In this section we briefly discuss the state-of-the-art of distributed machine learning approaches, which can be used as a tool to implement self-organization in femto networks intelligent decision processes. The theory of learning in distributed environments has strong connections with Artificial Intelligence (AI) and Machine Learning (ML) concepts, applied to both single and multi node/agent settings, game theory and evolutionary computations.

An environment characterized by only one intelligent decision engine (as it is the case e.g. in traditional cellular networks) can be formulated in mathematical terms, as a Markov Decision Process (MDP). In the machine learning literature, two ways have been identified to solve MDPs. The first one is an analytical model-base8d approach, which relies on the knowledge of the state transition probability function of the environment. The second one, in turn, does not rely on this previous knowledge making it a model-free approach; it is based on reinforcement learning (RL). RL is a family of learning approaches which is mainly concerned with the development of algorithms that automatically learn the properties of the environment and adapt their behavior to them by means of trial and error [42]. At each time step, the agent perceives the state of the environment and takes an action to transit into a new state. A scalar reward is received, which evaluates the quality of this transition. On the other hand, in an environment characterized by multiple decision makers (as it is the case, e.g. in femtocell networks), we have to take advantage of the theory of learning in multi-agent and distributed systems. This topic has actually been studied in game theory since 1951 when Brown proposed the fictitious play algorithm [43]. In AI, the literature of single agent learning is extremely rich, while it is only in recent years that attention has been

focused on distributed learning aspects, in the context of multi-agent learning. It has been yielding some enticing results, being arguably a truly interdisciplinary area and the most significant interaction point between computer science and game theory communities.
The characteristics of the distributed learning systems are as follows: (1) the intelligent decisions are made by multiple intelligent and uncoordinated nodes; (2) the nodes partially observes the overall scenario; and (3) their inputs to the intelligent decision process are different from node to node since they come from spatially distributed sources of information. These characteristics can be easily mapped onto a multi-agent system, where each node is an independent intelligent agent. The theoretical framework for this mapping is found in stochastic games [42].

The applications of game theory to wireless communications mostly refer to static (stateless) games, which are stochastic games with no states. Since there is no state, the cost (reward) only depends on the joint actions, and the learning is associated to the adaptation to the other players' strategies. When played repeatedly by the same agents, the static game is called repeated game. The main difference from a one-shot game is that the agents can use some of the game's iterations (history) to gather information about other agents or their cost functions and make more informed decisions afterwards.

We distinguish in this context two different forms of learning. On the one hand, the agent can learn the opponent's strategies, so that it can then devise the best response. Alternatively, the agent can learn a strategy on his own that does well against the opponents, without explicitly learning the opponent's strategies. The first approach is sometimes referred to as model-based learning, and it requires at least some partial information of the other player's strategies. The second approach is referred to as model-free learning, and it does not necessarily require learning a model of the strategies played by the other players. We will discuss in the following a very partial sample of multi-agent learning techniques, which we consider are representative for this taxonomy:

- *Model-based approaches*: This approach, generally adopted in game theory literature, is based on building some model of the other agents' strategies, following which, the node can compute and play the best response. This model is then updated based on the observations of their actions. As a result, these approaches require knowledge or observability of the other agents' strategies, which may pose severe limits from the feasibility point of view. The best known instance of this scheme is fictitious play [43], which is a static game that simply counts the empirical plays of the other agents in the past. The other agents are assumed to be playing a stationary strategy, and the observed frequencies are considered to represent the other agents' mixed strategies. There exist different variations of the original schemes, for example those considering that the agent does not play the exact best response, but assigns a probability of playing each action. Other algorithms in the literature that can be classified into this group are the Metastrategy [44] and the Hyper-Q algorithms [45]. An example of a stochastic game approach in this category is the non-stationary converging policies (NSCP) game [47].
- *Model-free approaches*: A completely different approach, commonly considered in the AI literature, is the model-free one that avoids building explicit models of other agents' strategies. Instead, over time, each agent learns how properly the various available actions work in the different states. The algorithms in this category typically keep memory of the appropriateness of playing each action in a given state, by means of some representation mechanism, e.g., look-up tables, neural networks, etc [48]. This approach follows the general framework of RL and has its roots in the Bellman equations [49]. Particularly, the Q-learning algorithm, typically used in centralized settings, can be extended to the multi-agent stochastic game by having each agent simply ignore the other agents and pretend that the environment is stationary. We refer to this implementation of Q-learning as independent learning. Even if this approach has been shown to correctly behave in many applications [49], it lacks a strict proof of convergence, since it ignores the multi-agent nature of the environment and the Q-values are updated without regard for the actions selected by the other agents. A first step in addressing this problem is to define the Q-values as a function of all the agents' actions; however, the rule to update the Q-values is not easy to define in this more complicated case. For a two-player zero-sum repeated game, Littman in [50] suggests the minimax Q-learning algorithm. Later works, such as the Joint Action Learners (JAL) **[51]** and the Friend or Foe Q algorithm [52], propose other update rules for the particular case of common payoff games. More recent efforts can be found for the more general case of general-sum games [52]; however, the problem still remains not efficiently solved. Other algorithms falling in this category are the correlated equilibrium Q-learning (CE-Q) [69], the asymmetric Q-learning [70], the regret minimization approaches [71][72], etc.

To facilitate distributed and autonomous functioning of wireless networks, model-based learning approaches are considered not to be appropriate since they require each node/agent to acquire knowledge on the actions played by the other agents and thus yields prohibitive overheads. On the other hand, model-free approaches are adequate despite suffering prior mentioned shortcomings. Said shortcomings are essentially overcome by the docitive paradigm [73][74], which will be introduced in Section 5.
A summary of the taxonomy introduced in this section is given in Figure 2-4.

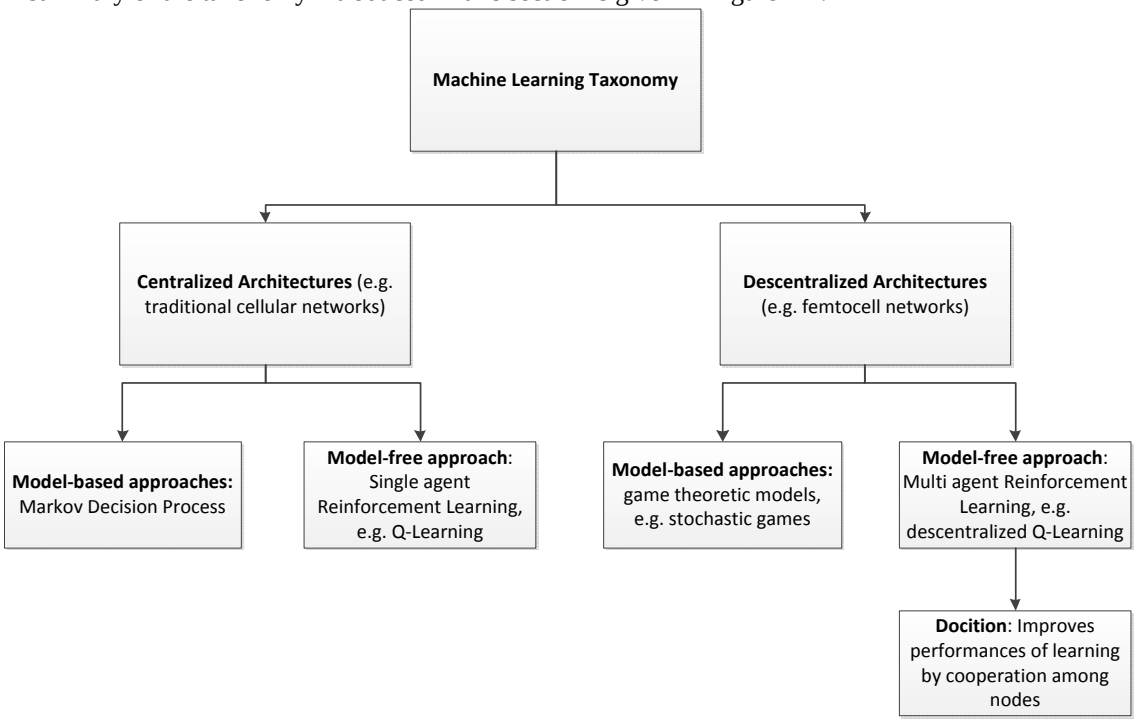

Figure 2-4 Taxonomy of learning approaches.

2.3 SON Projects & Standards

2.3.1 Major Research Projects on Self-Organization

The interesting research problems highlighted in the individual works and the increased understanding of need for self-organization in future WCSs has prompted research activities in a number of relevant projects in recent years dedicated to investigate, analyse and evaluate the possible usage of self-organization functionality in WCS. Here we present a summary of the aims and achievements of the major research projects in Europe on SO.

European CELTIC (Eureka Cluster) **Gandalf project** [75] identified the heterogeneous nature and increased complexity of future wireless networks, and studied SO as potential solution to overcome the complexity expected from concurrent operation of 2G, 2.5G, 3G and future network solutions. The project evaluated the effect of automation in network management and joint radio resource management in WLAN/UMTS networks with automated fault troubleshooting and diagnosis.

The European FP7 "end-to-end efficiency" **E^3 project** [76] focused on integrating current and future heterogeneous wireless systems into cognitive systems for self-management, self-optimization and self-healing (described as self-X systems). Focusing on autonomous cognitive radio functionalities, feasibility tests were performed for various schemes including autonomous Radio Access Technology (RAT) selection, acquiring and learning user information, self-configuration protocols and awareness signalling among the self-organizing network nodes. The tests validated that the proposed autonomous schemes were more efficient as feasible solutions for future networks.

Another major project dedicated to SO is the European FP7 **SOCRATES project** [77], which has identified some key objectives for which self-organization is required in WCS. These objectives are classified in the form of set of use cases. It is further concluded that most of the objectives SO has to deal

with in WCS are not independent from each other as the parameters controlling them are not mutually exclusive. SOCRATES has also gone in great details to describe a framework for the major tasks involved in self-organized wireless networks which include self-configuration, self-optimization and self-healing functionalities in future radio access networks.

2.3.2 Standardization Activities on Self-Organization

With the requirements of operators being identified and activities from various research projects being validated, it becomes necessary to have a common standard for multi-vendor compatibility and interoperability.

A consortium of major mobile communication operators and vendors came together under the working group of Next Generation Mobile Network (NGMN) and agreed that self-organizing functionalities would be required to improve operational expenditures (OPEX) and efficiency of wireless networks [78]. In fact, the need for automation (without human intervention on site) in some of the operation and maintenance (O&M) modules such as configuring, optimizing or repairing (healing) could lead to systematic organized behaviour that would improve network performance, its energy efficiency and reduce operational costs, thus in the good interest of operators.

The 3rd Generation partnership project (3GPP) has accepted work and study items on self-organization in Rel. 8 and 9, also based on NGMN inputs, with activities in the working groups RAN2, RAN3 and SA5 aimed at coming up with specification in the scope of self-optimization, self-configuration and self-healing for the identified use cases (see Figure 2-5).

The main specifications describe concepts and requirements for self-organizing networks [79] as well as detailed specifications on self-establishment of eNodeBs [80], automatic neighbour management [81], self-optimization [82] and self-healing [83].

In Rel. 8 the main focus of this specification work has been the macro eNodeB self-organization using centralized O&M-based solutions or distributed solutions with information exchange over the X2 interface. In Rel. 9, further additions to the SON functionalities have been made [84] and parameters and information models to provide self-configuration for HeNB have also been introduced [85].

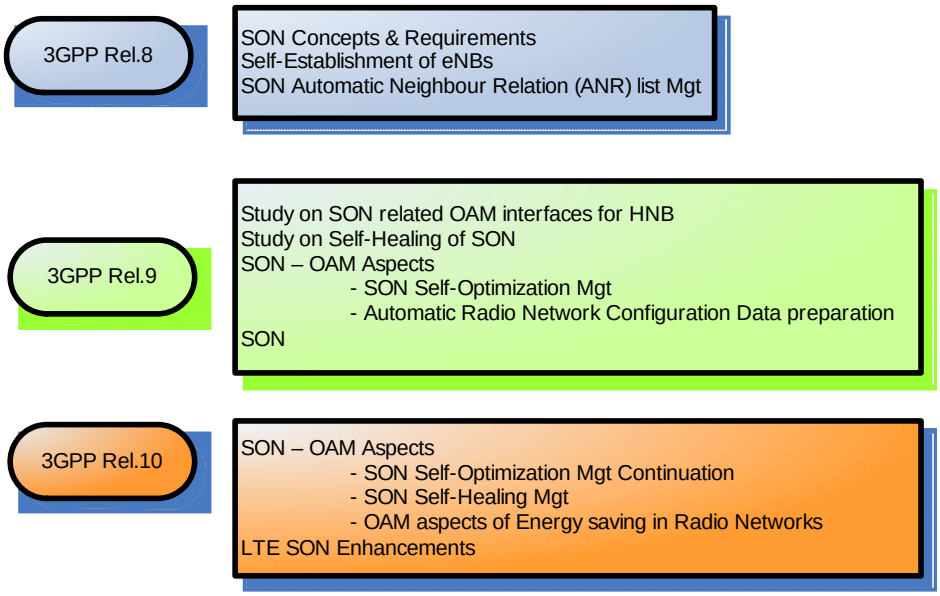

Figure 2-5: 3GPP SON Activities

In terms of 3GPP SO coordination aspects, in 3GPP Rel. 9 specifications, the X2 interface is (still) not applicable for HeNBs. This restriction has been partially relaxed in Rel. 10 as part of introduced mobility enhancements for femto nodes, whereby [84]:

"X2-based HO between HeNBs is allowed if no access control at the MME is needed, i.e. when the handover is between closed/hybrid access HeNBs having the same CSG ID or when the target HeNB is an open access HeNB"

In order to support such functionality, direct X2-connectivity between HeNBs has been introduced, independently of whether any of the involved HeNBs is connected to a HeNB GW. The resulting overall E-UTRAN architecture (with deployed HeNB GW) is depicted in Figure 2-6: with X2 interface added for HeNB.

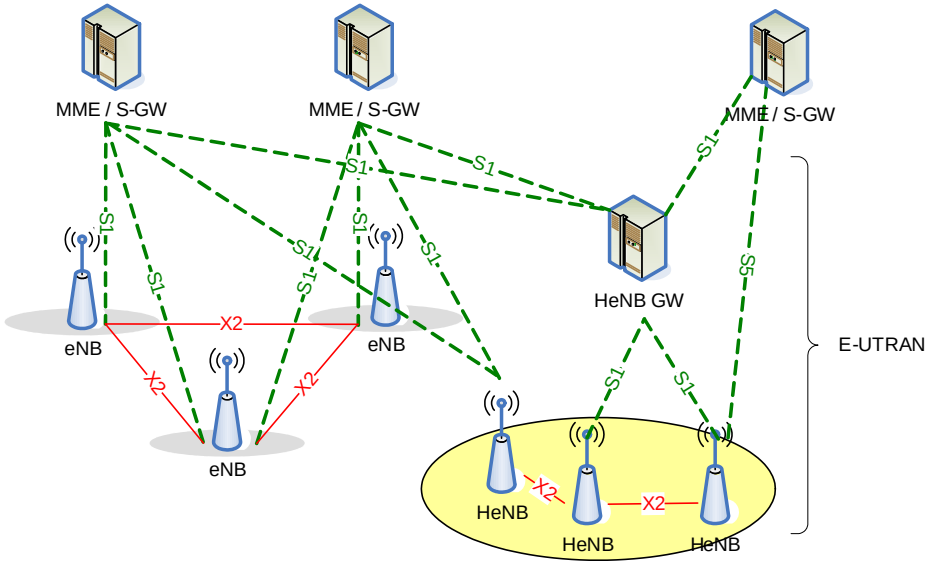

Figure 2-6: Overall E-UTRAN Architecture with deployed HeNB GW [84].

The introduction of the X2 interface for the above mentioned HeNB scenarios allows extending the possible support of HeNB also to additional functionalities currently relying on X2 application protocol design, including SON-related functionalities, like mobility robustness optimisation (MRO) and mobility load balancing (MLB). Such functionalities could be useful for example in case of HeNB clusters, like in enterprise environment or in open access HeNBs deployed under operator control. Figure 2-7 summarizes the possible cases, according to specification text [84].

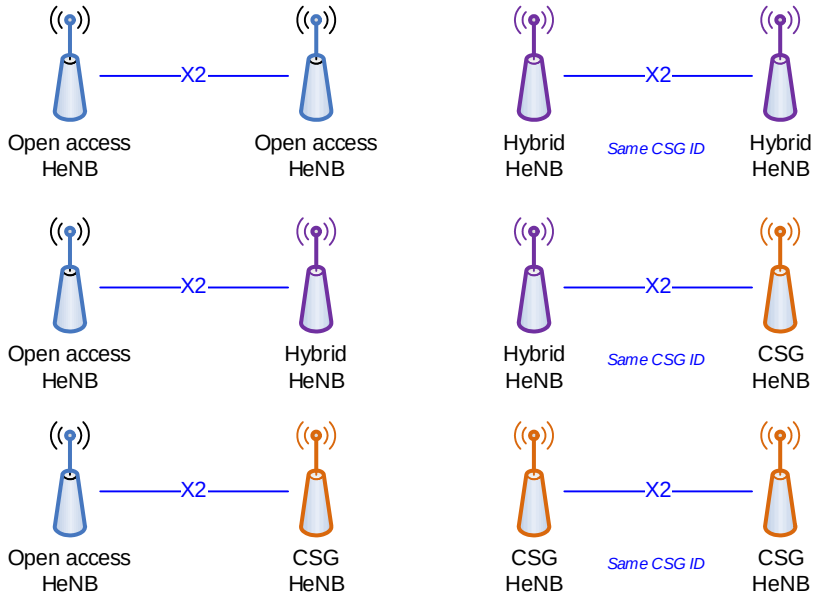

Figure 2-7: X2 Interface for HeNB use cases, according to Rel. 10 specification [84].

However the Rel. 10 enhancement do not include the possibility to have X2 interface setup between HeNBs and regular eNBs, thus limiting the possibilities of a closer cooperation between e.g. macro eNBs and femto nodes for tighter interference management or stronger protection of the macro eNB from interfering HeNBs because of their unplanned deployment.

3. Architectural Requirements of SON in 3GPP & BeFEMTO HeNB

In this section we recall the key use cases for SON functionalities for HeNB and provide a preliminary analysis of their relevance for the case of HeNB-HeNB as well as for the case of eNB-HeNB (see Figure 3-1). Besides 3GPP Rel. 8 and 9 SON functions and their support in the specification, a look into recent Rel. 10 additions to SON functions and to the extension to interference management case is also given. Finally, an overview of ongoing work for Rel. 11, where a new Work Item on SON has been opened, and recent trends is included.

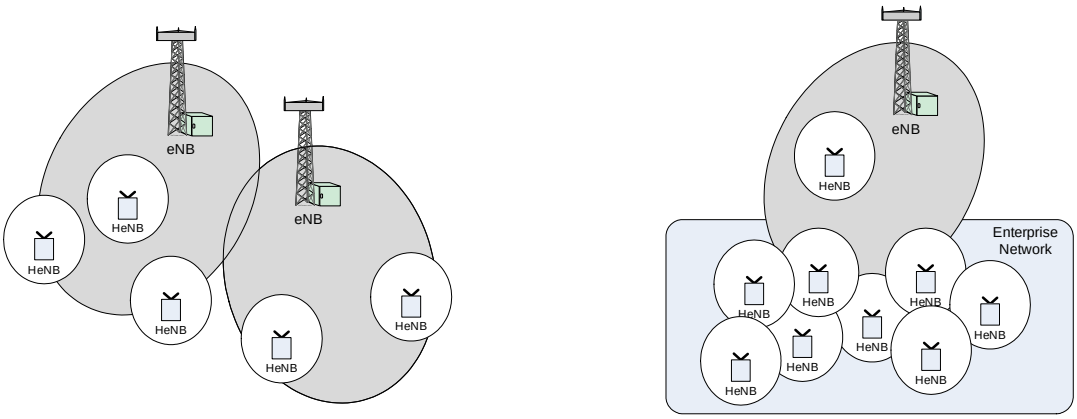

Figure 3-1: HeNB deployment: interaction with macro eNBs (left) and with other HeNBs (right)

3.1 HeNB use cases requiring a X2 Interface

Table 3-1 below summarizes the mapping between the different SON functionalities standardized in Rel. 8 and 9 and their extension and applicability for the two scenarios above, in case of HeNB (see [86] and [87]). These functionalities can be easily achieved by extending the X2 interface to the respective scenarios, thus also exploring synergies with other specification enhancements related to the X2 interface.

Table 3-1: SON use cases for HeNB and applicability to relevant scenarios

Functionality	**Use case**	**Applicability to eNB-HeNB case**	**Applicability to HeNB-HeNB case**
eNB Configuration Update	Automatic Configuration of Physical Cell Identity (PCI)	PCI split will ensure an appropriate choice of PCIs between eNB and HeNB.	Given the expected large number of HeNB e.g. in dense enterprise networks, automated configuration of PCIs is beneficial.
	Random Access Channel (RACH) Optimization	In scenarios where eNB and HeNB coexist, it is important to minimize interference among them and help for optimized coverage and access performance for setup and handover.	In scenarios where a large number of HeNB are present, it is important to minimize interference among them and help for optimized coverage and access performance for setup and handover.
	Automatic Neighbour Relation (ANR) Function	Providing ANR functionality in HeNB will be beneficial for mobility and help refining the neighbour relation of the macro eNB and HeNBs.	Given the expected large number of HeNB, and the fact they can be switched on/off, automatic neighbour relation function is beneficial for mobility.
Resource Status Update	Load Balancing	Load information exchange between eNB and HeNB could be beneficial in dense HeNB networks, to fairly distribute the traffic among nodes.	Load information exchange could be beneficial in dense HeNB networks, to fairly distribute the traffic among nodes.
Mobility Settings Change		Negotiation of parameters with HeNB helps optimizing the performance for scenarios where HeNB are present, for example to adjust user and resource distribution between the cells in case of highly loaded system or dense systems.	

Radio Link Failure (RLF) Indication	Mobility Robustness Optimization	Rel-9 introduced support for in-bound mobility to a HeNB either from another HeNB or from a macro eNB. Automated optimization of handover is beneficial. To support that, RLF Indication and Handover report are provided.

While the basic HeNB-HeNB case is partly covered by the Rel. 10 enhancements (see section [87]-[88] for more details), the eNB-HeNB case remains open and of interest. In fact some of the basic SON functionalities like Mobility Robustness Optimization (MRO) have been shown to be beneficial as there seems to be no significant difference between regular eNB or HeNB, as illustrated for example in [87] and [88] for HO-related call drop statistics. Such scenario can be addressed in the scope of Rel. 11 standardization work, where the introduction of possible X2 interface between macro eNB and HeNB is further considered. Higher priority use cases are interactions between macro eNB and open or hybrid HeNB, which are supposed to be more common in outdoor deployments or in typical low power node coverage provision in airports, shopping malls and enterprises. Interactions between macro eNB and closed subscriber group HeNBs (CSG cells) is also relevant but probably less appealing for optimization due to the nature of closed femto nodes, which are user-deployed and typically switched on/off more frequently. One of the case of interest is for enterprise deployments, where large number of employees arrives or leaves the building in a narrow time window (e.g. around office opening) and optimized mobility and coordination between eNB and CSG HeNB could be beneficial.

Looking at Rel. 10, some more functionalities based on X2 interface have been included in the system, as well as some enhancements of existing functions have been specified, as summarized inTable 3-2.

Table 3-2: Rel. 10 additional extensions to SON use cases and their applicability

Rel. 10 Extension	**Use case**	**Applicability to eNB-HeNB case**	**Applicability to HeNB-HeNB case**
Load Information	eICIC	Almost Blank Subframe (ABS) pattern signaling is included in the Load Information and the DL ABS status is added to the Resource Status Update message. eICIC enhancements are mainly targeting heterogeneous scenarios and extending the functionality to eNB-HeNB case could be beneficial.	eICIC enhancements are mainly targeting heterogeneous scenarios and less relevant for HeNB-HeNB
Resource Status Update			
RLF Indication	Mobility Robustness Optimization	Rel-10 has extended the scope of the RLF Report from the UE, including more information and allowing it to be sent also after fresh RRC establishment. This provides the means to further distinguish coverage problems (e.g. coverage holes) from HO optimization problems and can be beneficial for all scenarios.	
Handover Report			
SON Transfer Container		Another addition to MRO covers the optimization of unnecessary HO to another RAT (i.e. too early IRAT HO without connection failure), for which an extension to the SON Transfer Container for IRAT is specified. The extension is part of the S1-AP protocol and is available for all use cases.	
Cell Load Reporting	Load Balancing	Further additions to this functionality have been made for IRAT resource load reporting, with the introduction of event-triggered cell load reporting and of multi-cell load reporting. The extension is part of the S1-AP protocol and available for all use cases.	

In addition to further increase the value of extending MRO benefits with the provided enhancements, one of the cases of particular interest in Rel. 10 is the introduction of TDM ICIC (also known as eICIC), for advanced interference management in heterogeneous networks. The eICIC functionality is enabled by changes to the existing SON functions for load reporting in its basic version, and potentially motivates new SON functions for more advanced versions, which can be in the scope of future 3GPP releases.

Considering the use cases in Table 3-1 and additional functions in Table 3-2 like eICIC, the analysis shows that introducing X2 interface between eNB and HeNB is beneficial also for SON functionalities and will be considered for standardization for both open and hybrid/closed femto nodes. We will look into some more details about eICIC to further motivate such design.

Another aspect of interest in 3GPP, as part of the new Rel. 11 SON WI is to consider MRO solutions for heterogeneous deployments (HetNet), where large and small cells coexist in the same area. The current MRO solution is mainly designed having a homogeneous deployment in mind, while in case of HetNet it needs to be investigated if such solution still work and if further information like cell size and user speed might play a bigger role in optimizing handover parameters. In this view, problems already evaluated in the past like ping-pong and short-stay requires some more attention.

Mobile aspects of HeNBs (and of eNBs in general) are considered in Rel. 11 as part of the new Study Item on Mobile Relays. Relay functionalities have been introduced in Rel. 10 for fixed relay nodes, which consist in LTE eNBs with a LTE wireless backhaul: in Rel. 11 an extension of the relay is under investigation, looking for example at scenarios like high-speed train in-car coverage.

3.2 Carrier Aggregation at HeNBs

Carrier aggregation (CA) is not supported for Rel-10 HeNB and Rel-9 HeNB can serve only a single cell. At 3GPP RAN #51 meeting, work item (WI) on carrier-based HetNet ICIC was agreed, where enhancement on HeNB with CA is also considered. The support of only one cell was sufficient in typical use cases in Rel-9, however, higher peak throughput provided in Rel-10 and beyond can be achieved for home usage and for enterprise deployment scenarios only by enabling CA for HeNB. Additionally, CA could also be used for ICIC advanced mechanisms between macro cell and femto cells. Thus, HeNBs with CA (both for coordinated and uncoordinated deployments) has been proposed to be investigated in Rel-11.

3.2.1 Benefits of Carrier Aggregation at HeNBs

- Increase throughput: The deployment of fiber connections down to the home will provide high capacity backhaul link solutions for femto cells in the near future. Highest mobile data activity takes place within the user's home and new high-rate demanding multi-media applications have been appearing. As femto cells need to not be bottleneck they must provide datarates not less as backhaul link (broadband local network access link). Carrier Aggregation is one of the most important features (besides of enhanced MIMO scheme support) to meet the peak data rate requirements of International Telecommunication Union (ITU) for the IMT-Advanced .
- Similar user experience for indoor and outdoor users: A large change of total available bandwidth caused by a handover from a CA-capable macrocell to a non-CA-capable femtocell can cause an abrupt change of throughput in case if the femotocell will not be able to compensate throughput loss by the short distance.
  The CA-capable femtocell will be able to provide a similar user experience for indoor and outdoor users.
- Interference management: Carrier aggregation in HeNBs could facilitate interference mitigation between HeNBs and pico cell/macro cells. Interference management based on dynamic carrier selection, assignment of primary and secondary component carriers (PCC and SCC correspondingly) can be used for interference mitigation of control and data channels between different base station types. CA can be also used for ICIC in macro-femto scenarios. An example of handling the interference scenarios with cross-carrier scheduling with 2 component carriers is specified in [177] and illustrated in Figure 3.2. Downlink interference for control signalling is handled by partitioning component carriers in each cell layer into two sets, one set used for data and control and one set used mainly for data and possibly control signalling with reduced transmission power. For the data part, downlink interference coordination techniques can be used.

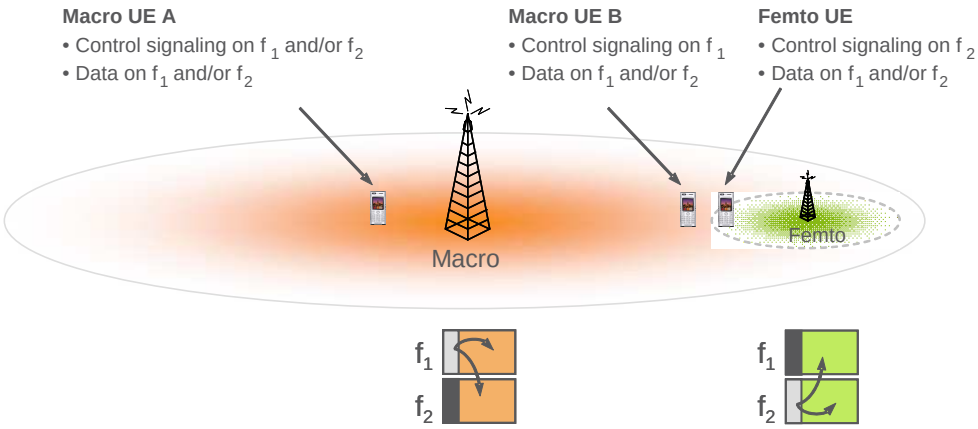

Figure 3-2: Example of interference management with carrier aggregation [177]

- Energy saving: Energy consumption of home user becomes an important issue. Carrier Aggregation is one of mechanisms to increase the flexibility for energy saving. HeNBs may switch off secondary carriers when high capacity is not used and switching them on only when additional throughput is required. UE power consumption may also be reduced when switching off non-required secondary carriers.

3.2.2 Scenarios with Carrier Aggregation/Multi-cell capable HeNBs

3.2.2.1 Macro UE Protection

Assuming both MeNB and/or HeNB support multiple carriers one of the carriers of HeNB interferes to Macro UE. Then, the HeNB recognizes which carrier interferes to the Macro UE and changes traffic load and/or power setting on this carrier.

As alternative, when MeNB (also multiple cells capable) detects interference from HeNB for a macro UE, it can handover Macro UE to other carrier which is not interfered from the HeNB.

3.2.2.2 Initial Carrier Selection

At power up, HeNB monitors MeNBs around by obtaining related information via network listening module or HeNB exchanges information with MeNB using X2 interface. Based on it, HeNB selects appropriate carrier(s) which will introduce less interference to MeNB around HeNB. The idea of the initial carrier selection is itself not new and is also applied for R8/R9 HeNBs, but with CA-capable HeNBs the scenario is extended for case of *multiple* carriers/cells selection.

In case of un-coordinated HeNBs, it is very challenging to predict how dynamic selection of any available cell carriers at HeNBs will impact robust and stable network function. Mobile operators avoid problems by limiting multiple carrier selection within a subset of carriers under O&M supervision.

3.2.2.3 CA-based ICIC Scenarios

3.2.2.3.1 CA-ICIC for Control Signaling Protection

PCCs and SCCs selection are managed by HeNBs and could be flexibly selected to mitigate interference. Despite of the fact that it is allowed in the strandard that different UE may have different carriers as their PCC, MeNB and HeNBs can use a single carrier as PCC for all its served UEs in challenging radio conditions in this scenario. SCC are, assigned per UE as needed. HeNBs choose their PCC on a component carrier different from the carrier chosen for UEs in challenging radio conditions by the strongest MeNB in the neighbourhood. In this case, control signalling of macro UEs in challenging radio conditions will be protected. The investigation should be performed how HeNB can determine the carrier reserved for control signalling protection of macro UEs.

3.2.2.3.2 Carrier Partitioning

Neighbouring HeNBs and the strongest MeNB coordinate carrier usage to avoid overlapping. The overlapping can be avoided for PCC or for both PCC and SCC. MeNB can reserve some carriers for the exclusive usage thus perfoming static carrier partioning between macro and femto networks. Dynamic

carrier partitioning is better suited between neighbouring HeNBs. It could be performed by a distributed algorithm to identify the carriers that are minimal from the surrounding interference. For enterprise femto cells, where the X2 support is supported, the dynamic partitioning may be done through X2 exchanging.

Carrier partitioning will significantly reduce interference but may result in lower spectral efficiency (especially when overlapping of both PCC and SCC is to be avoided). Here it is also assumed again the PCC is configured per node.

3.2.2.3.3 PCC/SCC Selection or Reselection for UE

PCC/SCC selection is done in generally per UE. This method could use report UE measurement configurations based on event-triggered reporting criteria(for possible events see [84]) which cause the UE to send a measurement report when ‘entry condition’ is met. Additionally, the statistical information about carrier usage and selected PCC/SCC for served UEs in the considered and the neighbouring cells could be taken into account.

4. SON for Interference Minimization

In this section, we introduce the main SON techniques which are mainly focused on the issue of interference arising in femtocell settings.

4.1 Interference study over a real network scenario

This section presents new results for the interference study from simulations over a real network scenario. This activity, already introduced in [97], aims to give a novel approach in the interference management framework, taking into account the peculiarities and heterogeneity inherent to real deployments. On this basis, this study expects to be a reference where to extract conclusions and guidelines that will be useful when applying RRM procedures and SON techniques. The effect of interference on system capacity should be quantified in order to address the interference management in most problematic scenarios with the help of the proper SON techniques.
The working scenario remains the same as in [97]. The aim is to assess performance in a real network scenario with a massive femto deployment. For that purpose, different alternative scenarios have been evaluated, varying the femto density per macro, starting from 10 to 40, which means increasing the number of femtos from 660 to 2640 in the whole scenario.

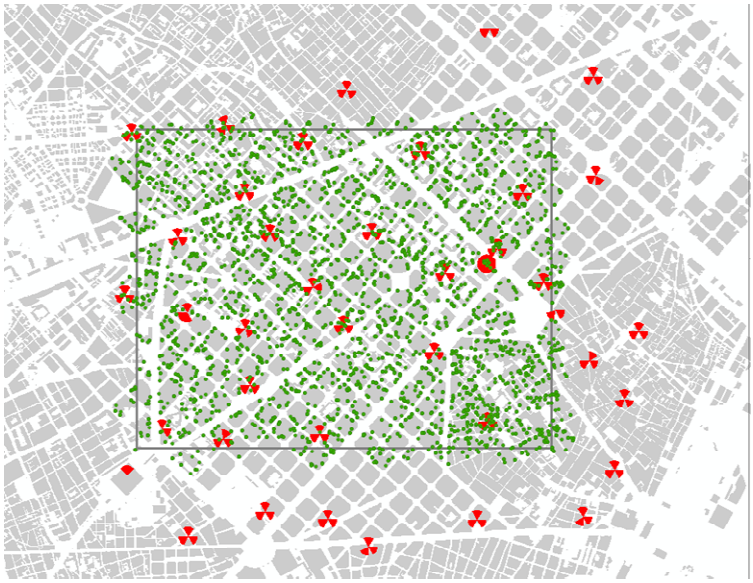

Figure 4-1: Real network scenario with 2640 femtos. Red dots (resp. green dots) represent 3 sectors macro BSs (resp. femto BSs)

The following table shows simulation assumptions considered for all studied scenarios.

Table 4-1: Simulation assumptions

UE connectivity restriction to femtocells	Open Access/Close Subscriber Group
Carrier Frequency	2600 MHz
Bandwidth	20 MHz
Frequency reuse	1
Max. macro BS power	46 dBm
Macro BS antenna gain	18 dB
Max. femtocell power	10 dBm
Femtocell antenna gain	2 dB
Power max. MS	23 dBm

The section is structured as follows. First, a performance analysis considering UE connectivity restriction to femtocells is presented. This analysis aims to assess the impact of dominant interference conditions in downlink when macro UEs are in close proximity of femtocells. Then, different spectrum allocation

strategies are analysed. This study evaluates the impact on capacity when available spectral resources for macros and femtos are not the same.
A new variable has been considered in simulations: the load factor. This parameter allows the evaluation of the same scenario under different load conditions. The effect of the load factor has been assessed for the open access situation. In the other two studies (close subscriber group impact and spectrum allocation strategies) a 75% load factor is assumed.

4.1.1 UE connectivity restriction to femtocells

Femtocells access can be open or closed depending on whether just a small group of users is authorised by the operator or the owner of the femtocell. In open access, UEs are connected to their best server anyway, either macro or femto, with no other restriction. The global capacity is expected to increase with the inclusion of femtocells but the interference level too. Nevertheless, this interference is less harmful with open access, as the results presented in [97] show.
Next figures verify the capacity enhancement experienced as the number of femtos is increased, under different load factors, considering open access. These results are for the whole scenario, including macros and femtos.

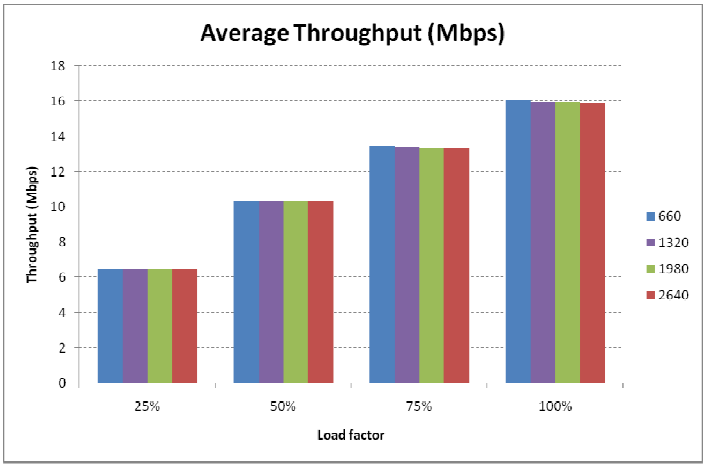

Figure 4-2: Average throughput in increasing femtos density scenarios, open access

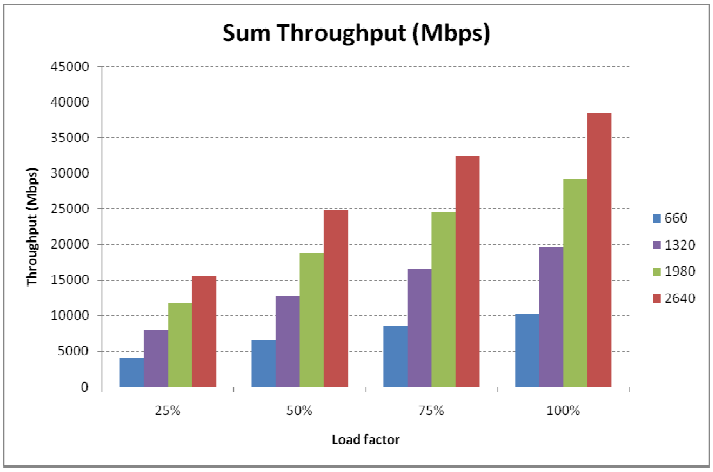

Figure 4-3: Sum throughput in increasing femtos density scenario, open access

The average throughput barely changes. The effect of increasing femtos density is better shown with the sum throughput, a magnitude that offers an accumulated throughput value for the whole scenario. The spectral efficiency also reflects the impact of increasing femtos density in the scenario. Values are calculated over the whole scenario and quantified per area unit.

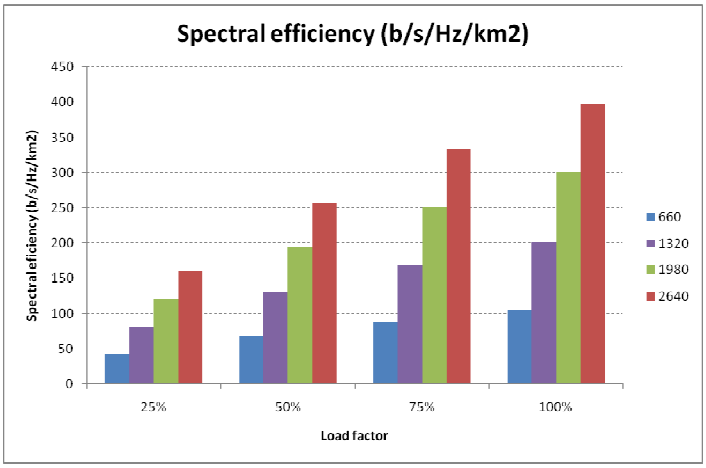

Figure 4-4: Spectral efficiency per km2 in increasing femtos density scenarios, open access

The spectral efficiency per femto cell is shown in the next figure. These values correspond to 75% load factor simulations.

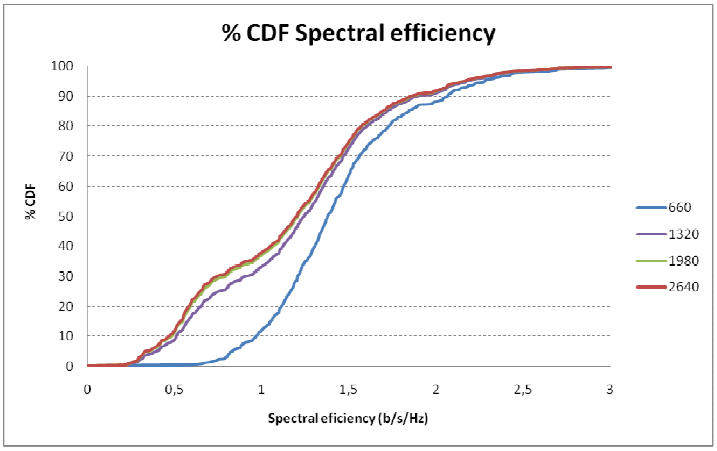

Figure 4-5: CDF Spectral efficiency per femto cell

This figure shows that there is still room until reaching the 8bps/Hz/cell Befemto target. It is important to remark that these results have been achieved in a scenario where no SON technique, that might have increased spectral efficiency, have been applied. However, the interference impact radically changes when considering UE connectivity restrictions to femtocells. When dealing with Close Subscriber Group (CSG) femtocells, radio conditions for macro UEs in close vicinity of a femto could be highly unfavourable. To assess the CSG retrictions, a parameter that represents the probability for the users located in the femto best server area to be connected to this femto is defined (CSG probability). A value of 25% for CSG probability means that just 25% of the users in the femto best server area are connected to this femto. The remaining 75% would be connected to their best macro server and hence, these 75% of users would experience a high degree of interference due to the former femto best server. Next figure shows how average throughput is degraded as the percentage of UEs connected to their best server femto decreases. The extreme cases have been also analysed. The 100% means that all UEs would be able to connect to the femto if this is the best server for them, so this means no restriction at all and is equivalent to open access. On the contrary, 0% simulates the worst case when no UEs could be connected to the desired femto.

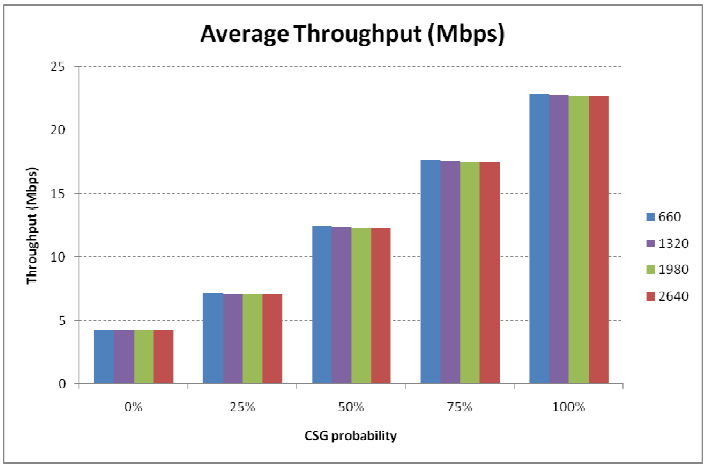

Figure 4-6: Average throughput in increasing femtos density scenarios, femto best server areas, CSG access

These throughput values average experienced throughput in zones where femtos are best server. However the following figure considers the whole simulation area. In such case, the degradation becomes softer, since zones where macros are best server are considered too, and in DL these points are not affected by the CSG condition (what are affected are macro UEs served in a femto best server area).

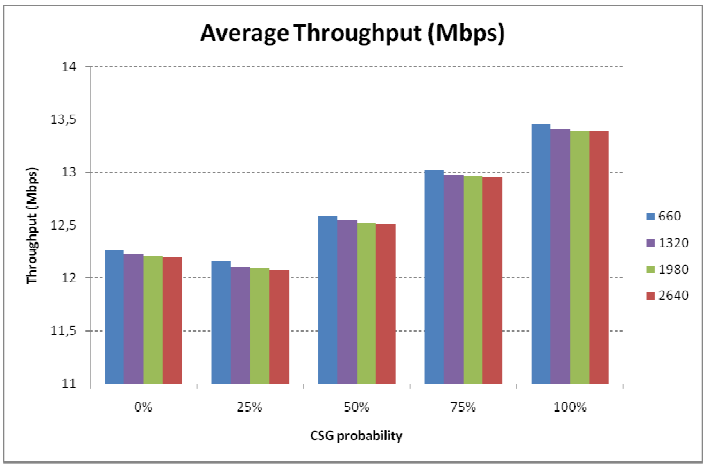

Figure 4-7: Average throughput in increasing femtos density scenarios, CSG access

For completing the analysis, figures with sum throughput and spectral efficiency are provided too.

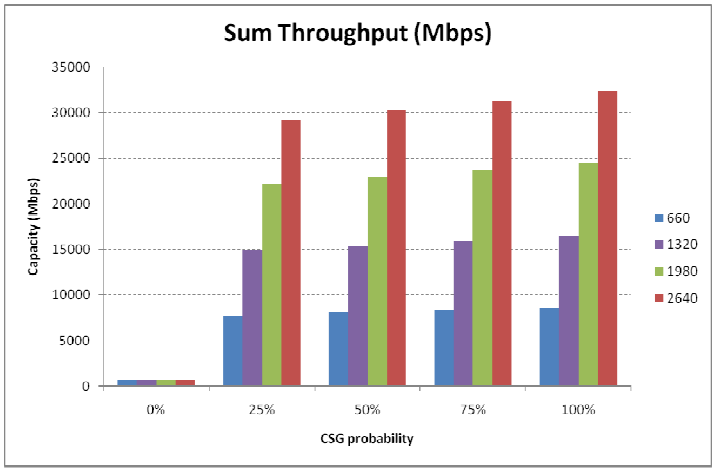

Figure 4-8: Sum throughput in increasing femtos density scenarios, CSG access

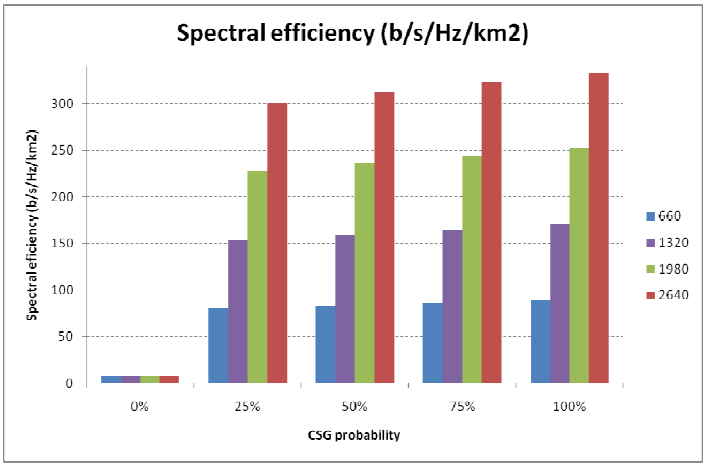

Figure 4-9: Spectral efficiency per km2 in increasing femtos density scenarios, CSG access

The following figures represent the cumulative distribution for DL SINR for all the considered scenarios with data processed only in femto best server areas. What is being compared are the two extreme situations, when there is no restriction, i.e. open access, and when no UE located in femto best server area can connect to the corresponding femto (curves named 0% CSG). As expected, the level of resulting interference is huge for the worst case: 0% CSG and a load factor of 100%. In this situation SINR value for 50th-percentile corresponds to -11 dB, which is indeed a very low value. In fact, the SINR vs. throughput look-up tables present available throughput values beyond -9 dB.

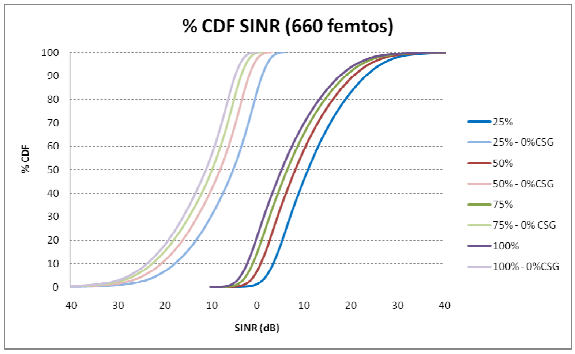

Figure 4-10: CDF SINR 660 femtos scenario

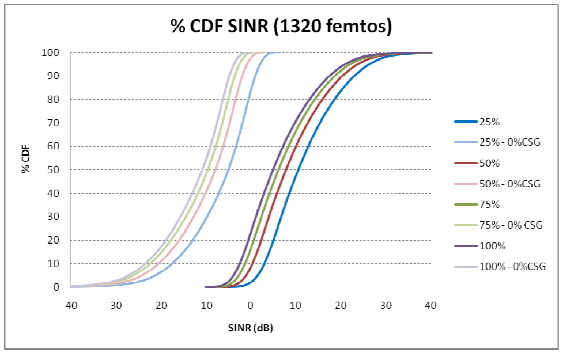

Figure 4-11: CDF SINR 1320 femtos scenario

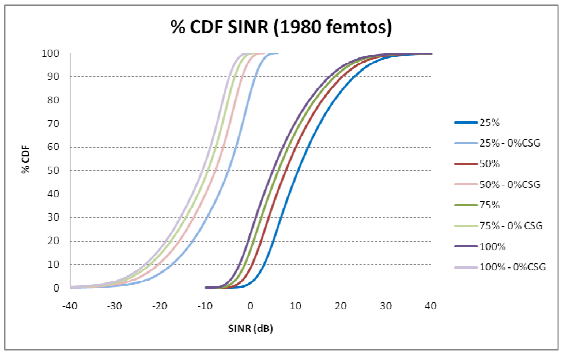

Figure 4-12: CDF SINR 1980 femtos scenario

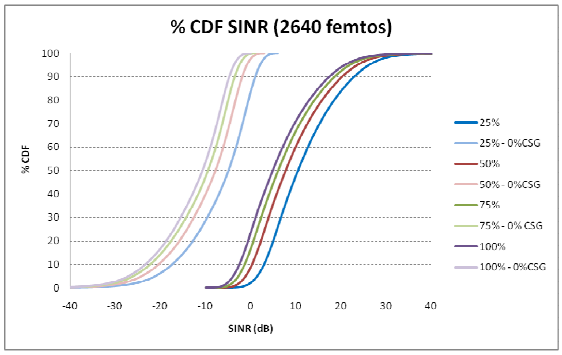

Figure 4-13: CDF SINR 2640 femtos scenario

4.1.2 Spectrum allocation strategies

In order to avoid cross-tier interference, operators may allocate different parts of the available spectral resource to macrocell and femtocell users. Simulations over real network scenario have been done in order to assess the impact on capacity. Three different strategies have been considered:
- the whole spectrum for macros (20MHz),
- macros and femtos share the spectrum (20 MHz)

- allocation of different parts of spectrum to each layer (10+10 MHz).
Provided results correspond to a 75% load factor, considering open access to femtos.
Next figures show values for average throughput in each of the studied strategies, and separating macro and femto areas.

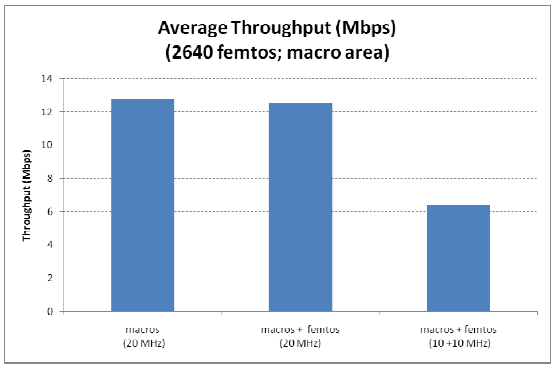

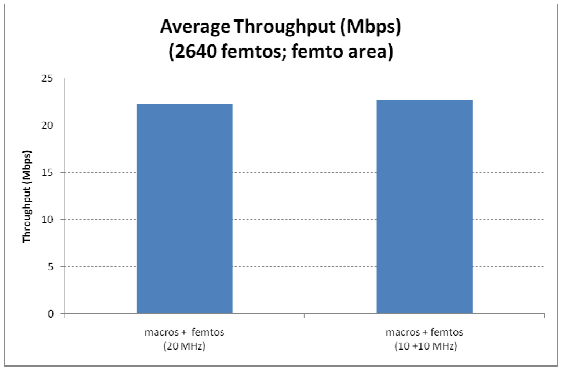

Figure 4-14: Average throughput in macro area **Figure 4-15: Average throughput in femto area**

It is verified that allocating different parts of spectrum for each layer, although potentially beneficial from an interference point of view, degrades macro capacity.
The following figures sum up all the results for the considered scenarios, in the whole simulation area.

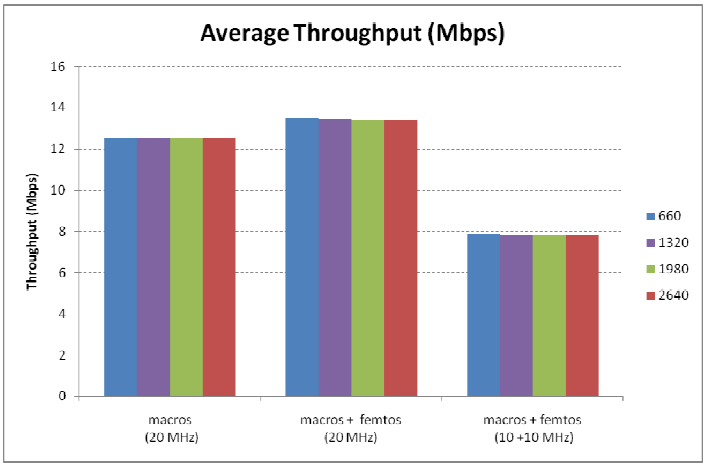

Figure 4-16: Average throughput for spectrum allocation strategies in increasing femtos density scenarios

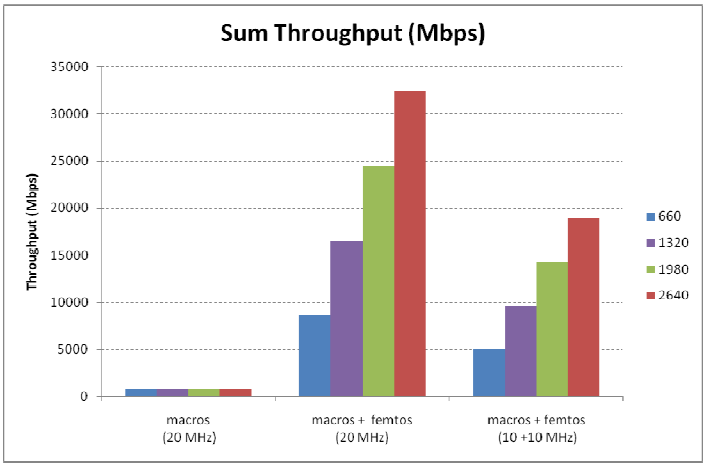

Figure 4-17: Sum throughput for spectrum allocation strategies in increasing femtos density scenarios

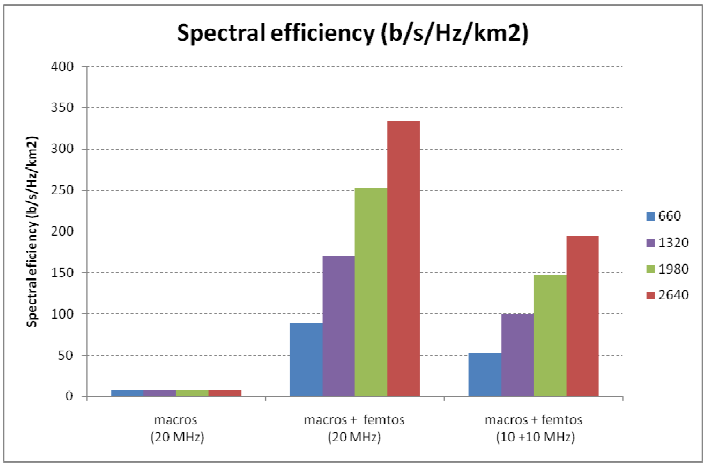

Figure 4-18: Spectral efficiency per km2 for spectrum allocation strategies in increasing femtos density scenarios

4.1.3 Conclusions

This section has presented results from two different studies carried out over a real network scenario. The first one has assessed the impact of dominant interference conditions in the downlink when macro UEs are in close proximity of femtocells. For that purpose, it has been defined a parameter, CSG probability, that represents the probability for the users located in the femto best server are to be connected to this femto. Results conclude that average throughput is degraded as the percentage of UEs connected to their femto best server decreases. It means that more macro UEs will experience a higher level of interference and hence will worse their throughput. This degradation is confirmed for any of the simulated scenarios, no matter if the number of femtos is higher of lower. The CSG probability could be a candidate parameter to be monitored in order to trigger a SON mechanism to deal with such harmful interference situation.
The second study analyse the impact on capacity when available spectral resources for macros and femtos are not the same. Simulations conclude that degradation in macro capacity can make this allocation strategy no worthy.

4.2 Cell Association for Interference Management

With the introduction of interference management and the related enhancements for heterogeneous networks (HetNet), the coordination between different eNBs also evolves from the pure peer-to-peer relation in homogeneous networks to a hierarchical relation, as depicted in Figure 4-26. While large (macro) cells provide the main coverage and basic capacity (hereafter called *coverage cell* or *macro cell*), a set of smaller (pico/femto) cells are deployed as overlay in the same spectrum to boost the system capacity (hereafter called *hotspot cell* or low power *cell*) and improve the user throughput and QoS.

We note that in order to fully benefit from the capacity boosting, the low power cells need to be able to capture enough traffic. This can be achieved by expanding the coverage range of those cells by making them looking larger for the surrounding UEs, compared to what they would be in normal conditions (*cell range expansion*). This can be obtained by silencing the macro cell in certain sub-frames and, in a coordinated manner, having the low power cells serving the UEs in those sub-frames (see [4], section 16.1.5).

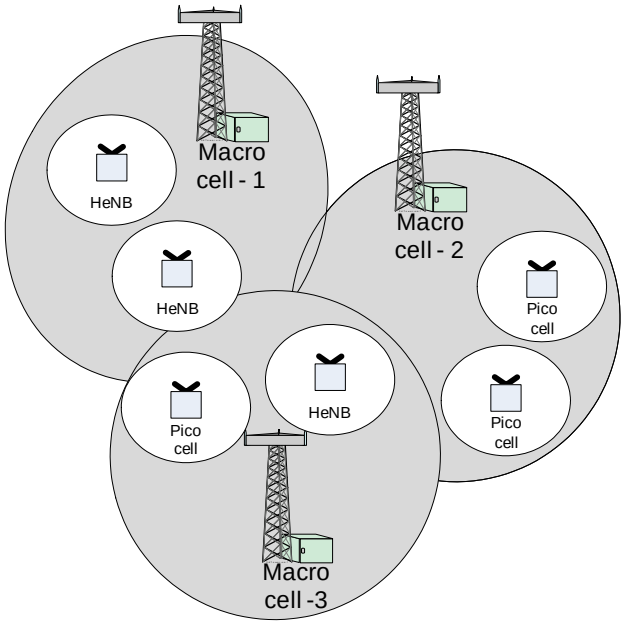

Figure 4-19: Heterogeneous network deployment, with macro and low power (pico/femto) cells

In order to manage the interference in such scenarios, some level of coordination between nodes overlapping in coverage is needed, in particular between a macro cell and the low power cells which are overlaid to the area covered by the macro cell.

4.2.1 The Need for Cell Association

The relation between nodes in a LTE network is naturally managed via the X2 interface, which is a peer-to-peer interface with both connected nodes at the same level of importance. However, recalling the scenario in Figure 4-19 for heterogeneous networks, it is evident that the role of the coverage cell is different than the one of low power cells. In fact the macro cell is strongly interfering (aggressor) one or more low power nodes (victims) overlapping its coverage, resulting in a position of higher hierarchy between the nodes. In order to create some degree of hierarchy and capture such difference, the concept of *Cell Association* is introduced:

> *Cell Association defines a relation between two overlaid cells (typically a macro cell and a low power cell in HetNet scenario) that can use eICIC as a method to counteract interference.*

By means of cell association, each node part of the HetNet deployment is able to exchange the appropriate information with its most relevant neighbours and use eICIC to counteract interference, while coordinated with those neighbors. A macro cell is generally associated to several low power cells overlapping its coverage, and therefore maintaining several cell associations. On the other hand each low power cell is associated with typically one macro cell and maintains one cell association (exception: low power cells deployed at the border between two or more macro cells may need to maintain few cell associations). It is worth noting that associating a pico cell with several macro cells may pose a challenge in coordinating the system and could potentially result in ineffective usage of resources; cell association therefore shall primarily be done with neighbours relevant for interference control.

4.2.2 Information needed in the eNB

In order to setup a cell association, the macro cell shall be aware of which low power cells are overlapping with its coverage. At the same time, each low power cell shall be aware of which macro cell is providing the basic coverage in the area where it is deployed - those are in fact the potential cells interfering with the low power cells that could strongly limit the performance of the capacity boost. In addition, the cells shall be aware of the eICIC capabilities of the other cells they may associate with, for the association to work properly.

This information could for example be determined during network planning, e.g. based on the location of the macro and low power cells: typically the low power cells are deployed in a second phase, to increase the capacity of the basic coverage layer, and during planning and installation it is possible to identify what macro cell they should be associated with. Once the information is available at the eNBs parenting the associated cells, those nodes could activate interference management via eICIC and coordinate with each other.

4.2.3 Scenarios for eICIC Cell Association

Different scenarios can be possible as part of a HetNet deployment, hereafter we consider the most relevant ones, i.e. a low power cell interfered by either a single macro cell or multiple macro cells.

4.2.3.1 Cell-to-cell Association

Given the much smaller radius of a low power cell compared to a macro cell, the general case where cell-to-cell association is considered when a low power cell is interfered by a single macro cell, is depicted in Figure 4-20

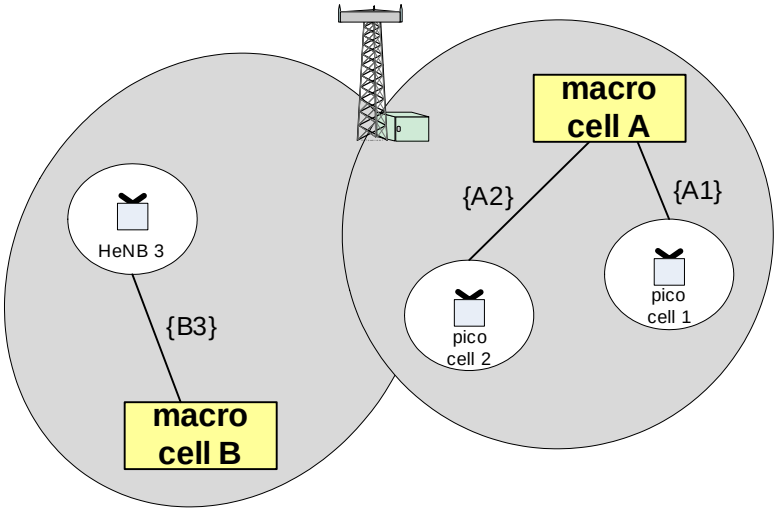

Figure 4-20: Cell-to- cell association: low power cell interfered by single macro cell.

In this case, for example low power cell 3 is deployed well within the coverage of the macro cell B and it is mainly interfered by it: Association {B3} enables interference management between these two cells. At this point the eNBs parenting macro cell B and low power cell 3 can exchange information about ABS pattern and related loading via X2 interface, as summarized in Table 3-2 for eICIC, and adjust the resource partition in a dynamic way based on the actual traffic demand. Coordination is limited to these two cells for this example, and similarly will happen for Associations {A1} and {A2} when considering macro cell A and low power cells 1 and 2.

4.2.3.2 Multiple Cell Association

Due to the particular deployment situation, it could happen that a low power cell is interfered by multiple macro cells, e.g. in the case it is located at the border of the coverage areas, as shown in Figure 4-21
In this case, while for low power cells 1 and 3 cell-to-cell association applies like before, for low power cell 2 there are two cell associations allowing coordination with both macro cells A and B : {A2} and {B2}, which could make the interference management more complex. In fact, while on one hand the performance of low power cell 2 may still be very limited if coordination is only explored with one of the two interferers, on the other hand the coordination based on cell association {A2} cannot be fully independent from the one based on cell association {B2} and a multiple cell association needs to be established.

Again the eNBs parenting macro cells A and B will exchange information about ABS pattern and related loading with the eNB parenting low power cell 2 via X2 interface. However, due to the multiple cell association, the low power cell 2 will have to match the ABS patterns of both the macro interfering cells,

calling for additional complexity of the system to properly setup and adjust the resource partition based on the actual traffic demand. Coordination in this case is de-facto among three cells and similar scenarios where even more cells are involved could also be possible.

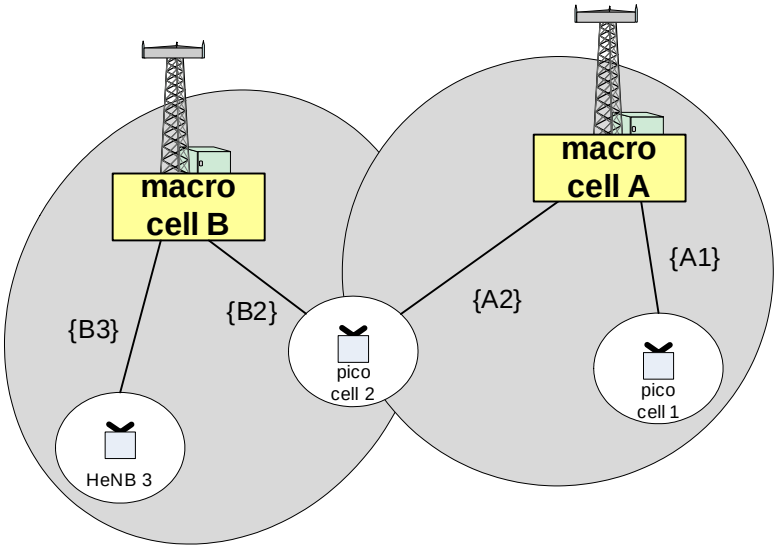

Figure 4-21: Multiple cell association: low power cell interfered by two macro cells

4.2.4 Cell Association Approaches

In this section we briefly illustrate different possible approaches to realize cell association in HetNet, starting from a basic configuration and including some enhancements for more advanced solutions.

4.2.4.1 Manual configuration via O&M

The basic approach for the establishment of cell association is to configure it manually via O&M, e.g. considering the cell location and coverage estimate (from network planning tools or coverage maps). This approach is manual, simple and does not require any assistance from other devices, and can be considered as the baseline solution to provide minimal functions for cell association. However, this brings also some disadvantages that can be overcome by other approaches, where the amount of manual work necessary is gradually reduced and more automation is included to facilitate cell association establishment and its usage.

4.2.4.2 Automatic Configuration without UE Assistance

One simple enhancement to provide some degree of automation is to let the eNBs involved in cell associations to exchange information between them via X2 interface. For example one could think of including in the low power cells a simple receiver to monitor the downlink spectrum and to identify the macro cells that are causing major interference, so that they can be associated to that low power cell. Also in this case the cell association is of static nature (low power cells could monitor the spectrum at activation for example, or after reset), while a reasonable degree of automation is added with operations executed directly at the eNB, embedding the necessary intelligence as possible SON functionality. One possible drawback of this approach is that it does not account for the user conditions, i.e. the association may be not optimal with respect to what users required in terms of assistance.

4.2.4.3 Automatic Configuration with UE Assistance

To further increase the automation possibility and to better consider the UE perception, the automatic configuration could be executed with UE assistance, whereby UE measurements are collected at the eNB and processed to determine what cell association is relevant.
The process is an increase of complexity of SON functionality and can for example be built in a similar way as the Automatic Neighbour Relation (ANR) function or embedded as an extension of it. This way a dependency from the UE received signal is introduced, and the needed mechanisms can be based on X2 interface, which may require further functional extensions. Considering that the eICIC is mainly helpful if able to correctly provide the instruments to reduce interference (at the UE receiver side) and to boost the UE throughput, including UE assistance is expected to help to select and adjust the associations.

4.2.5 Cell Association Evaluation

In this section we evaluate the three different approaches presented in section 4.2.4 with respect to capability to pair the right cells for interference management. The first part describes the evaluation method, the simulator platform and related assumptions, then results are presented and analyzed and finally some conclusions are drawn. Both single associations (one low power node associated with one macro) and multiple associations (one low power node associated with more than one macro) are considered in the comparative analysis.

4.2.5.1 Evaluation methodology and tools

For the evaluation and comparison of the different association approaches, a heterogeneous network deployment scenario is modelled in a system simulator. The simulation setup is described in Figure 4-22 and corresponds to the recommended layout described in 3GPP TS 36.814 [177]for heterogeneous network investigations. The macro deployment consists of a regular hexagonal cluster of 19 three-sector base stations for a total of 57 cells. In addition, low power nodes (e.g. HeNBs) with omnidirectional antennas are deployed each in a random position within the corresponding macro cell coverage area. The characteristics of the analyzed deployment are summarized in Table 4-2, for a LTE system with 10 MHz spectrum and using the channel model referenced in [177], derived from ITU-R M.2135 recommendation.

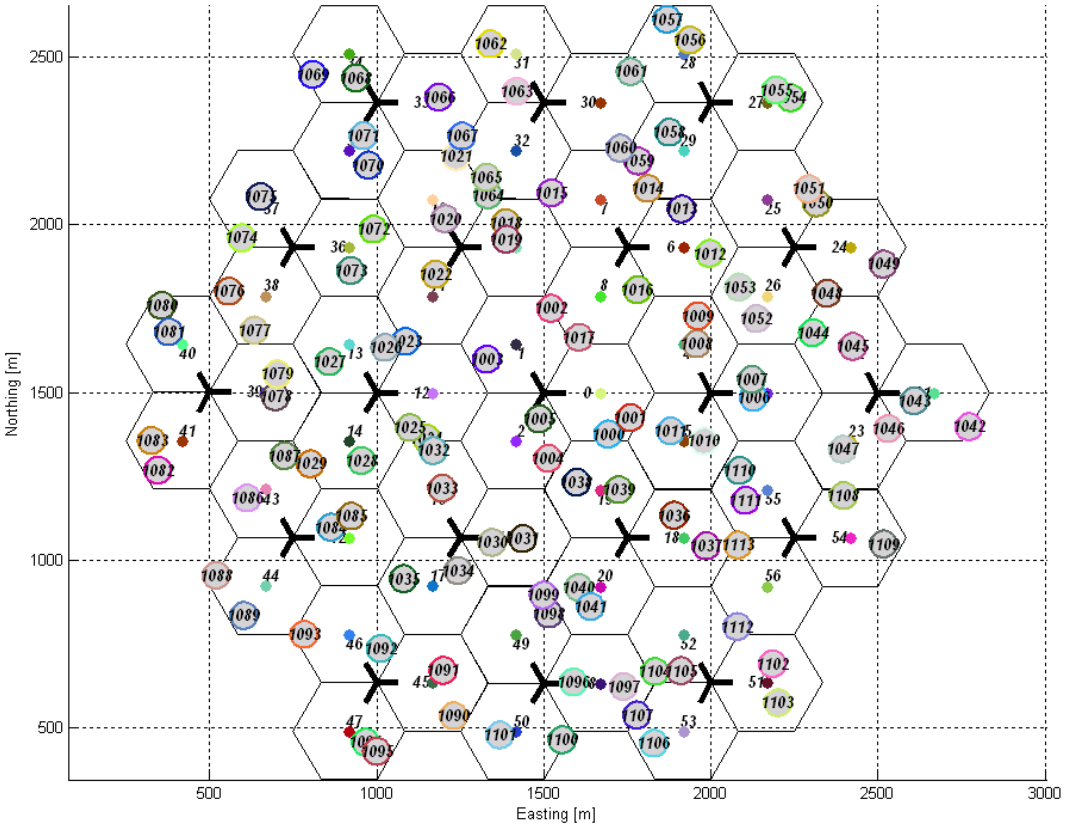

Figure 4-22: Cell association simulation layout with macro and low power cells.

Table 4-2: LTE system parameter for cell association simulations

System Parameters	**Value**
Carrier	2 GHz
Bandwidth	10 MHz
Subcarrier spacing	15 kHz
Number of subcarriers N	600
System Loading	Fully loaded
Number of users	30 users/macro cell
User distribution	Uniform in macro cell
Thermal noise density N0	-174 dBm/Hz
Macro Cell Parameters	**Value**
Layout	57 cells, sectorized
Inter-site distance	500 m
Transmission power	46 dBm
Antenna gain	17 dBi
Channel model	Uma, cfr. [177]
Shadowing std dev	4 (LOS) and 6 (NLOS) dB
Decorrelation distance	37 (LOS) and 50 (NLOS) m
UE Spatial Distribution	Uniform random
LPN Cell Parameters	**Value**
Number of LPNs dropped	2 nodes per macro cell
Transmission power	10 dBm
Antenna gain	5 dBi
Channel model	Umi, cfr. [177]
Shadowing std dev	3 (LOS) and 4 (NLOS) dB
Decorrelation distance	10 (LOS) and 13 (NLOS) m
CRE handover bias	12 dB

Performance results are collected by means of snapshot simulations, according to the following steps:

- Users are dropped uniformly in macro cell coverage areas at each drop
- Channel model towards macro cells and low power cells is calculated
- A serving cell is assigned to each user, based on strongest received signal strength and considering handover threshold bias for Cell Range Expansion (CRE)
- Cell association is performed according to the respective approaches described above
- Performance metrics, in term of UE geometry (SINR), are collected over several drops

Results are processed with main focus on users served by low power nodes in CRE region, which are the primary target of interference mitigation. For the evaluation of the user SINR, it is assumed that the associated macro aggressor(s) to each low power node is blanked for interference management when the low power node schedules such a user, to model eICIC technique with *Almost Blank Subframes* (ABS) [4]. This translates in considering null interference from the blanked cell when SINR is computed for the user, as captured in equation (4.1).

$$SINR = \frac{I_{or_S}}{N_{th} + \sum_{k \neq s, k \notin S_s} I_{or_k}} \tag{4.1}$$

where I_{or} is the received power at the user for each cell (s = serving cell, k = other cells), N_{th} is the thermal noise and S_s is the set of cells associated with the low power node server.

4.2.5.2 Simulation Results

In this section simulation results for cell association evaluation are presented, collected over 10 drops for each of the simulation case analyzed. All three different approaches for cell association have been modelled and contrasted towards an ideal cell association, where for each user, the strongest interferers are blanked.

In case of manual association via O&M approach (see 4.2.4.1), low power node cells are associated based on their location to the macro cell providing the underlying coverage. For the automated approach without UE assistance (see 4.2.4.2), a Radio Environment Monitoring (REM) unit consisting in a receiver at the low power node is used to detect the strongest macro cell interferers. For the automated approach with UE assistance (see 4.2.4.3), UE measurements are collected at the low power node and processed to assess the interferers that mostly causes problem to the served users.

Figure 4-23 shows the results in terms of UE geometry distribution for the three different cases, as well as the ideal case used as reference, which corresponds to having at each point of time the strongest interferers for the particular UE being scheduled silenced in neighbour macro cell aggressors. In addition, also the geometry of users served by low power node not in CRE (center cell users), for which ABS is not applied, is included. As can be seen, the approach with UE assistance is performing better: this is somehow expected as the approach tends to reduce interference that mostly matters from the user performance perspective. The other two approaches have slightly worse performance, whereby the REM assisted method seems slightly better than the manual configuration: this is somehow expected as signal measurements are considered.

.

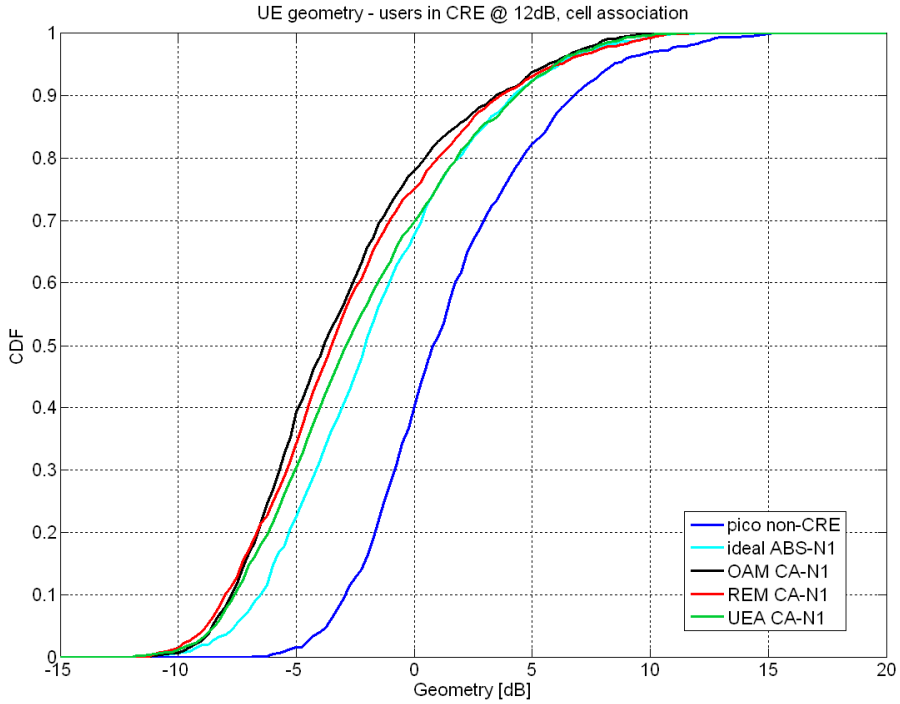

Figure 4-23: Cell association simulation results: UE geometry distribution.

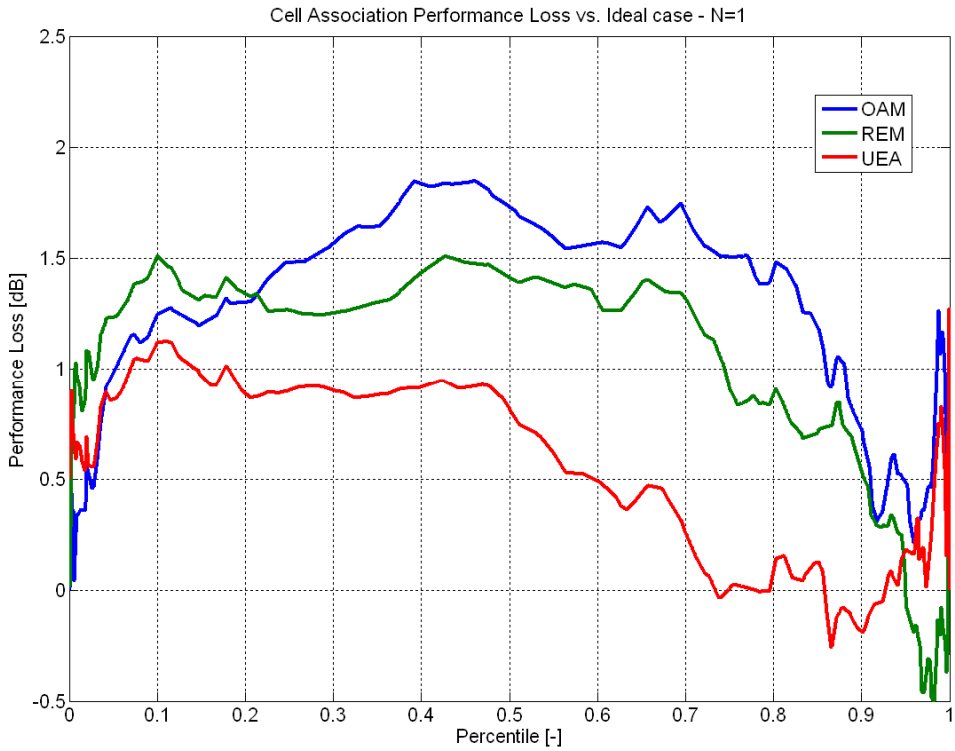

Figure 4-24: Cell association simulation results: performance loss compared to ideal case.

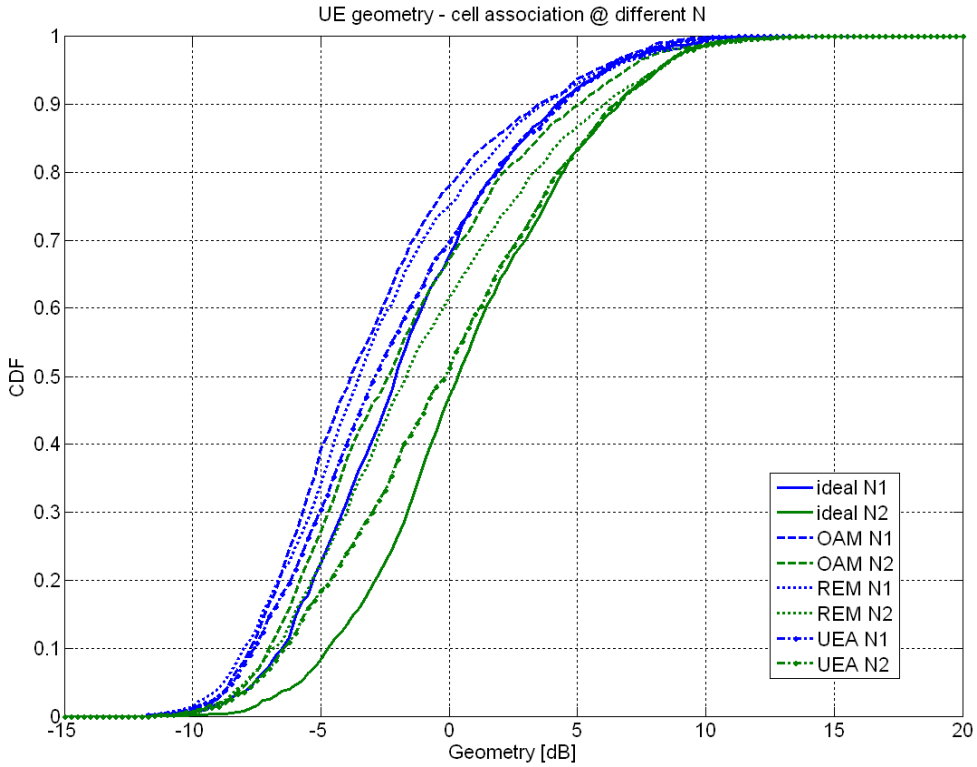

Figure 4-25: Single cell association vs. multiple cell association results.

Figure 4-24 represents the same results in terms of potential loss compared to the ideal case, for each percentile of distribution. As can be seen, the losses are within 1 dB for entire percentile range for UE assisted approach with almost no losses for the top 30 %-tile, while the baseline method and the REM assistance method shows losses of about 1.5 to 2.0 dB and a tendency to perform somewhat worse for upper 50%-tile of the users.

Analysis has been done also for the case where multiple aggressors are identified and blanked, by contrasting the case of single cell association and association with two cells (N = 1, 2). Figure 4-25 shows the results for both cases for all three cell association approaches, in terms of geometry distribution. What can be observed is that the advantages achieved by the cell association with UE assistance compared to other methods increases with more aggressors being blanked. In this case in fact, the information provided by the UE has higher value in case of dense deployments, whilst using pure planning consideration with OAM assistance may be more challenging.

4.2.5.3 Conclusions

Cell association has been evaluated by means of numerical simulations, comparing different approaches to the ideal association case. The baseline approach of OAM assistance and manual configuration provides a good basis for association with simple algorithms but requires more manual work and is in nature fully static. Providing assistance helps automating the configuration of the systems in general, though no benefits could be seen in case UE measurements are not used for the scope. Overall assisting the association by means of collected UE measurements has proved to be the best approach in terms of performance, reduction of manual configuration and adaptivity possibility, while using low power node receiver seems not providing any particular performance increase.

4.3 Achieving an Average Spectral Efficiency of 8 bps/Hz for Femto cells

Spatial multiplexing is a prominent feature of multiple input multiple output (MIMO) systems in 3GPP LTE networks. In order to achieve higher number of spatial layers (for a given antenna configuration), higher SINR (signal to interference-plus-noise ratio) values are required. With reuse 1 in the network, interference may become more significant and hence could reduce the SINR values. In this section, we study the performance of heterogeneous femto/macro network characterized by a MIMO spatial multiplexing. We present the values of two key performance indicators (KPIs), namely average cell throughput and average spectral efficiency with full frequency reuse in both the macro and femto networks. Then, we demonstrate the impact of a partial bandwidth utilization framework on the system performance. We show how the objective of 8 bps/Hz average spectral efficiency could be achieved in femto network by exploiting MIMO spatial multiplexing and employing a self-organized bandwidth allocation scheme for interference management.

The enhancement in performance as a result of spatial multiplexing in macro LTE networks has already been demonstrated in existing literature. Few references on the subject are: [147]–[150]. As for the performance analysis of spatial multiplexing in heterogeneous macro-femto network, some recent articles could be spotted. For example in [151], results for SU-MIMO (single user-MIMO) mode of LTE (which is one of the spatial multiplexing modes of LTE) are given. Authors have assumed reuse 1 in both macro and femto networks and have considered maximum of two femto cells per macro cell area. Authors of [152] have developed analytical models for the coverage evaluation in a two tier macro/femto network. Two spatial multiplexing modes, SU-MIMO and MU-MIMO, have been considered in this study. However, to simplify the analytical approach, authors have not considered shadowing in their model. Furthermore, they consider flat Rayleigh fading per subband.

The gain brought by spatial multiplexing is very promising but is greatly affected by other cell interference as has been discussed in [153]. Considering a co-channel deployment of macro-femto, interference will be a critical factor that will affect the spatial multiplexing. Hence it is necessary to study the effect of interference mitigation in this case. Interference management in a macro/femto network is an active topic of research at the moment. Different solutions based on power control and frequency reuse are for example presented in [30][31][34][89],[154]-[156]. In this article we rely on Monte Carlo simulations to first analyze the performance of spatial multiplexing mode (SU-MIMO) of LTE in a reuse

1 macro network with underlay femto network for different antenna configurations. Then we show the improvement in performance parameters because of a frequency mitigation framework. Our simulation results highlight that gain in performance because of the frequency mitigation mechanism is more pronounced in MIMO networks as compared to the ones with SISO.

The rest of this section is structured as follows. A brief introduction of closed loop spatial multiplexing mode of LTE (Rel. 8,9) is given in subsection 4.3.1. Details about wireless channel model, interference calculation and effective SINR computation are presented in section 4.3.2. In subsection 4.3.3, overall system description and simulation campaign parameters are introduced. Monte Carlo simulation results are discussed in subsection 4.3.4 followed by conclusion in subsection 4.4.6.

4.3.1 Close-Loop Spatial Multiplexing (CLSM)

Among the multiple spatial multiplexing modes specified in LTE (Rel. 8,9) [109], we focus on CLSM which is transmission mode 4 of LTE. In this transmission mode, independent data streams could be transmitted from each transmitting antenna. The maximum number of spatial streams is defined by $\min(N_t,N_r)$ where N_t and N_r are the number of transmit and receive antennas respectively. The UE sends the following three feedbacks (reflecting its radio environment) to the BS :

- CQI (channel quality indication)
- PMI (precoding matrix indicator)
- RI (rank indication)

where CQI specifies the modulation and coding scheme, PMI refers to the index of the codebook (a set of precoding matrices [107]) and RI indicates the maximum number of spatial layers that the UE could support. CQI and PMI are sent by the UE with the same periodicity, whilst RI is fed back with a period which is multiple of that of CQI/PMI. Furthermore, the CQI and PMI both could be frequency selective with a possible granularity to the level of a subband whereas RI is measured over wideband [107]. The elements of the transmission chain that involve CQI, PMI and RI feedbacks are shown in Figure 4-26:. According to [107], whatever the antenna configuration may be, the maximum of two codewords can be transmitted simultaneously.

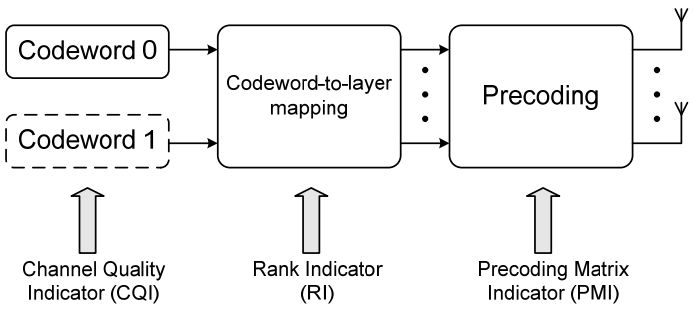

Figure 4-26: The elements in the transmission chain that implicate CQI, PMI andRI feedbacks at different stages.

4.3.2 Interference and Channel Model

4.3.2.1 Channel Realization

The radio channel between a UE *u* and a (H)eNB *b* suffers from long-term as well as short-term variations. The long-term propagation loss encompass the path loss $l_p^{(b,u)}$ and the lognormal shadowing $l_{Sh}^{(b,u)} \sim \tilde{\mathcal{N}}\left(0,\sigma^{(b)}\right)$. These components are computed according to the model 1 of [114]. Since the antenna gain of the UE $g^{(u)}$ and that of (H)eNB $g^{(b)}$ are also fixed entities, we subtract the two from the propagation loss and the resultant long-term variations loss $L^{(b,u)}$ can be written as:

$$10\log_{10}(L^{(b,u)}) = g^{(u)} + g^{(b)} - l_p^{(b,u)} - l_{sh}^{(b,u)} \quad (4.2)$$

where all the terms on the right hand side of the equation above are in dBs. The short-term part represents the fast fading. It is generated by using the MIMO SCME (spatial channel model extended) channel introduced in [157] which supports bandwidths higher than 5 MHz (since the bandwidth used in our system simulations is 10 MHz). For Doppler effect, a velocity of 3 km/h has been considered. As for power and delay profile, the urban macro (UMa) model has been taken into account. From the temporal representation, the frequency domain response is derived using FFT of size N_{FFT}. The number of useful subcarriers N is bandwidth specific and can be referred from [41].

4.3.2.2 Subcarrier SINR

Minimum mean square error (MMSE) receiver is applied on each subcarrier to detect each layer. Ignoring the fast fading gain associated with interfering (H)eNB, post-receiver SINR of subcarrier *n* for a UE *u* is calculated over every spatial layer transmitted.

4.3.2.3 Effective SINR

Channel gains experienced by subcarriers are likely to be different over the whole band due to the small coherence bandwidth (inversely proportional to the delay spread) of the multipath channel. Hence, different subcarriers (and subbands) may suffer from different SINR and the error rates on these subcarriers may not be the same. Therefore, block error rate (BLER) of the coded block (transmitted over multiple subcarriers) cannot be obtained through direct averaging of these error rates. In order to obtain a single SINR value of multiple subcarriers that could correspond to this BLER, certain physical abstraction models are used. The resultant single value is called the effective SINR. In our System Level Simulations (SLS), we have used the physical abstraction model Mean Instantaneous Capacity (MIC) [158]. As for CQI, we have chosen ”higher layer configured subband” reporting [107], so that the CQI for subband s is computed based on effective SINR. Each subband is comprised of N_{Sc} subcarriers. The set S_s of subbands for which a UE has to send CQI reports back to (H)eNB is configured by Radio Resource Control (RRC). While considering FFR, RRC only asks for reports on the subbands that are used by a particular (H)eNB. The instant of these reports is also set by RRC. In our simulations, we have considered a periodic reporting every Transmission Time Interval (TTI = 5ms).

4.3.3 System Model and Simulation Details

We have carried out simulations with four different antenna configurations: 1x1, 2x2, 4x2 and 4x4. To study the effect of interference mitigation in MIMO networks, we have considered four different scenarios (for every antenna configuration) of the frequency reuse framework that we have presented in [159]. These four scenarios are as follows:

- Reuse 1 in both the macro and femto networks
- Reuse 1 in macro and partial resource utilization in the femto
- FFR in the macro and reuse 1 in the femto networks
- FFR in the macro and partial resource utilization in the femto

For a brief recall, with FFR (see Figure 4-27:) in the macro network there are $\mathbf{S_0}$ subbands used in the inner region and $\mathbf{S_m}$ (where m $\in$ {1, 2, 3}) used in the outer region. If **S** represents the total subbands associated with system bandwidth *W*, then in every macro cell there will be $|\mathbf{S}|-|\mathbf{S_0}|-|\mathbf{S_m}|$ orthogonal subbands that could be exploited by the underlay femto cells. The least interfered subbands are found by a femto cell through sniffing process.

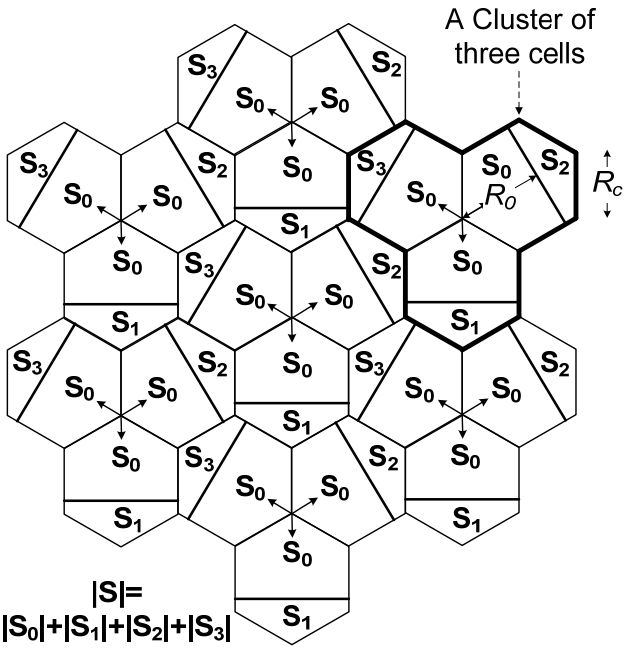

Figure 4-27: Fractional Frequency Reuse (FFR) case. Subbands S_0 are deployed with reuse 1 in the inner regions, while S_1, S_2 and S_3 are deployed with reuse 3 in the outer regions.

Simulation parameters are summarized in Table 4-3. Monte Carlo approach is used with a significant number of runs where in each run (lasting several TTIs) UEs are randomly dropped across a macro cellular network of 7 sites with 3 sectors per site. No macro UE is dropped inside the clusters that host femto cells. Deployment of femto cells is carried out with the help of dual-stripe model [114]. A bird view of a dual-stripe cluster is shown in Figure 4-28:. A femto cell is hosted by a 10 m× 10 m block inside the cluster. On each floor there are 40 blocks and a total of 6 floors have been considered in the simulation.

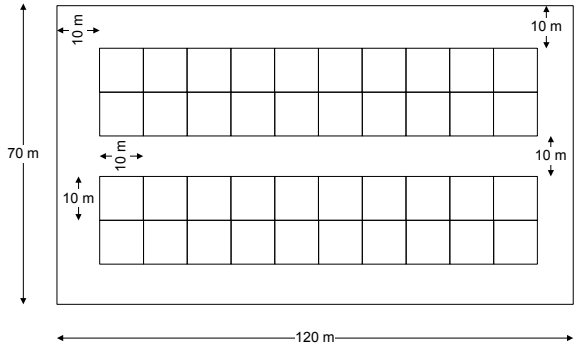

Figure 4-28: Dual-stripe model

The presence of HeNB in a block is governed by the probability of femto cell deployment. The position of HeNBs inside a block follows uniform random distribution. The transmission power per subcarrier is different for an eNB and HeNB. However, within the macro and femto networks themselves, this value is kept constant. To obtain the value of the subcarrier transmission power, the total transmission power of (H)eNB is divided by the number of useful subcarriers per (H)eNB.

In context of FFR, the size of the inner/outer region depends upon the division of resources (subbands in our case) between the inner and the outer regions. It is done in a way that the ratio of the surface area of the inner and outer regions is proportional to the ratio of the resources being allocated to the two regions. This is in coherence with the equal resource allocation scheme used for assignment of resources to UE. MUEs are dropped into a macro cell using uniform random distribution such that a certain number of MUEs are attached to the serving eNB according to the best link criteria.

Table 4-3 Simulation Parameters For Macro/Femto Network

LTE Parameter	**Value**
Carrier frequency	2 GHz
Bandwidth W	10 MHz
Subcarrier spacing	15 kHz
Number of subcarriers N	600
Number of subbands $\|\mathbf{S}\|$ associated with W	9
Number of subbands in the inner region per cell $\|\mathbf{S_0}\|$	6
Number of subbands in the outer region per cell $\|\mathbf{S_m}\|$	1
Thermal noise density N_0	-174 dBm/Hz
eNB Parameter	**Value**
Inter-site distance	500 m
Transmission power	46 dBm
Antenna gain $g^{(b)}$	14 dBi
Antenna pattern	$-\min\left\{12\left(\frac{\theta}{70}\right)^2, 20\right\}$ dB where θ is in degrees.
Shadowing standerd deviation	8 dB
Shadowing correlation	0.5 inter-site
	1 intra-site
HeNB Parameter	**Value**
Model	Dual-Stripes
Number of clusters dropped per macro cell	1
External wall attenuation	20dB
Internal wall attenuation	5dB
Number of floors	6
Number of blocks per floor	40 (20 per stripe)
Deployment probability inside a block	0.1
Transmission power	10 dBm
Antenna gain $g^{(b)}$	0 dBi
Shadowing standerd deviation	4 dB
Shadowing correlation	0
Number of UEs dropped per HeNB	1

The number of MUEs dropped per macro cell varies for reuse 1 and FFR cases. In either case, this number is equal to the number of subbands assigned to each cell. As per the parameter values listed in Table 4-3, 7 and 9 MUEs are dropped per cell for FFR and reuse 1 respectively. This is done to have equal number of subbands (one in this case) to be allocated per MUE. For HeNB deployment, on average, one dual-stripes cluster is randomly dropped per macro cell. HUEs are uniformly dropped inside the block near their serving HeNB and attachment is forced toward it. The drop is performed until all HeNB have a given number (one in our case) of HUEs. It is considered that there is no MUE present inside a cluster.

Attached UEs report their CQIs/PMIs every 5 TTIs of all subbands configured by their serving (H)eNB. The reporting period of RI is twice (i.e. 10 TTIs) that of PMI/CQI (as mentioned in section III, the reporting period of RI is a multiple of that CQI/PMI). The RI is reported over wideband. The selection of PMI and RI is carried out through an exhaustive search. The combination of PMI and RI that delivers maximum throughput is fed back by the UE. Based on these received reports, the (H)eNB allocates its resource to the users based on equal resource allocation scheduling scheme for the next TTI. The minimum scheduling unit is one subband. The scheduling of MUEs is carried out in a way that a subband is allocated to a UE which has the best channel quality on that subband while satisfying the condition that every UE gets equal number of subbands. However, equal resource allocation is not of that importance for the femto cells given the fact that each HeNB serves only one HUE at an instance and allocates all available subbands to it. We consider full buffer traffic model for both the HUE and MUE. The throughput calculation is derived from the effective SINR for each scheduled UE by using truncated Shannon bound, in adequation with the approach adopted in [160].

4.3.4 Analysis of Numerical Results

In this section, we present and discuss the results obtained through simulations. Since the amount of resources allocated per user is different for femto and macro networks, user throughput cannot be used as a metric of comparison. In order to fairly compare all the scenarios, in Figure 4-29:, we have presented the average spectral efficiency in bps/Hz that does not depend upon the amount of allocated resources per user. For the sake of clarity, we have included only two antenna configurations (1x1 and 4x4) in Figure 4-29: (a). The curves for the other two antenna configurations can be found in Figure 4-29: (b). All the curves in these figures correspond to the scenarios with 2 subbands allocated per femto cell through sniffing process. It can be observed that the gain realized by interference mitigation scheme FFR in the macro increases with higher antenna configurations.

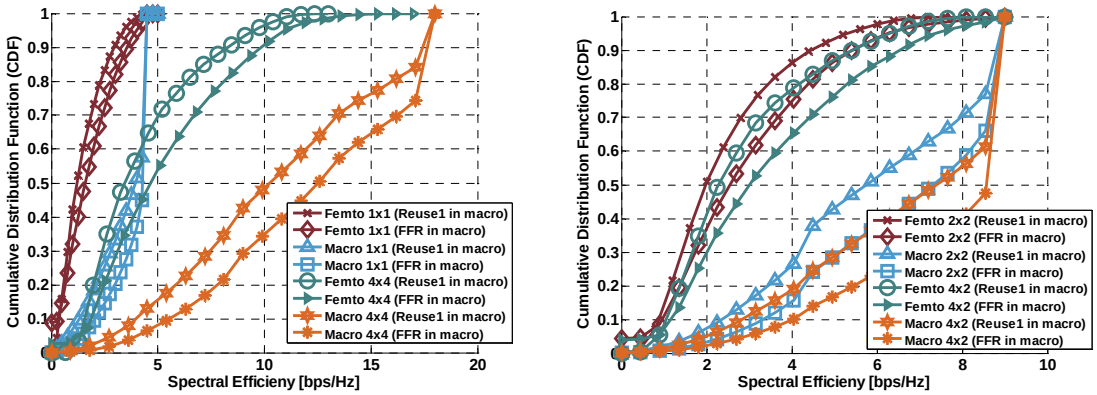

(a) (b)

Figure 4-29: CDF of spectral efficiency (bps/Hz) of both the macro and the femto

The average values of spectral efficiency for different antenna configurations are given in Table 4-4. It can be observed that partial subband usage by femto network and CLSM with 4x4 MIMO results into an average spectral efficiency of more than 8 bps/Hz. Spectral efficiency is an important parameter to gage the radio quality but from the point of view of operator, cell throughput has its own significance.

Table 4-4 Comparison of Average Values of Different Key Performance Indicators (KPIs)

Parameter	Antenna configuration	Subband usage per femto	Reuse 1 in macro		FFR in macro	
			Macro cell	Femto cell	Macro cell	Femto cell
Average cell throughput (Mbps)	1x1	Reuse 1	13.8	21	13.9	22.8
		2 subbands	16.1	6.7	14	8
	2x2	Reuse 1	22.1	35	21.8	38.1
		2 subbands	25.1	11.6	22	14.1
	4x2	Reuse 1	26.1	40.7	26	44.1
		2 subbands	29.8	13.2	26.1	15.7
	4x4	Reuse 1	39.2	62.7	38.5	68.1
		2 subbands	43	21	38.9	26
Average spatial spectral efficiency (bps/Hz)	1x1	Reuse 1	1.4	2.3	1.7	2.5
		2 subbands	1.4	3.3	1.7	3.7
	2x2	Reuse 1	2.3	3.9	2.9	4.2
		2 subbands	2.4	5.8	2.9	6.6
	4x2	Reuse 1	2.8	4.5	3.4	4.9
		2 subbands	2.8	6.6	3.4	7.3
	4x4	Reuse 1	4.2	7	5.2	7.6
		2 subbands	4.2	10.5	5.2	12.1

In presence of reduced usage of resources in femto, it is important to analyze its effect on the values of cell throughput. Thus CDFs of average cell throughput for all antenna configurations are given in Figure 4-30:.

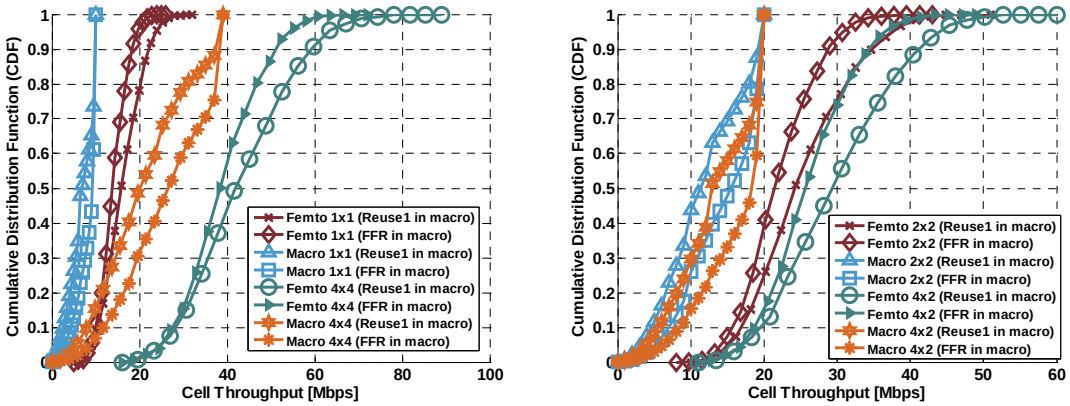

(a) (b)

Figure 4-30: CDF of cell throughput (Mbps) of both the macro and the femto

The average values of cell throughput for all studied scenarios are given in Table 4-4. Though 25% resource utilization (through sniffing process) per femto cell results into an average spectral efficiency of 8bps/Hz , but as compared to reuse 1 it suffers from almost 61% decrease in average cell throughput while considering FFR in macro network. However, the same value with reuse 1 in the macro network is about 66%. Hence frequency mitigation has earned us a gain of 5%.

4.3.5 Conclusion

We have shown the performance of a macro/femto network equipped with MIMO spatial multiplexing mode. We have shown that by combining spatial multiplexing characterized by 4x4 antenna configuration and interference mitigation, a target of 8bps/Hz is attainable. However, as compared to reuse 1, the average cell throughput is lesser. In future, we intend to work upon interference mitigation techniques that could further increase the value of average cell throughput while maintaining average spectral efficiency.

4.4 SON for Interference Minimization

4.4.1 Problem Statement

Fractional frequency reuse FFR, where interfering neighbors transmit data on orthogonal subbands (subbands are contiguous collections of frequency resources) is widely used in wireless cellular networks to enhance the throughput of cell-edge users. Access to the remaining subbands is restricted (possibly via power reduction) or even forbidden, so as to avoid detrimental interference with neighboring base stations (BSs). Thus, via the use of FFR, user equipments (UEs) located near the boundary of two or more BSs face less interference and enjoy better service quality. However, the disadvantage of using FFR is that it drastically decreases the spatial reuse of resources and hence decreases the system capacity. Additionally, the unpredictable variations in the interference caused by the uncoordinated deployment of small cells, indicates the necessity for dynamic frequency reuse approaches that aim at adapting the spatial reuse of resources to the observed interference conditions.

In [101], we have developed a centralized subband assignment scheme for uncoordinated networks coined Graph Based Dynamic Frequency reuse (GB-DFR). In GB-DFR, a central controller collects the identity (ID) of the interfering neighbors observed by each BS and maps this information onto an interference graph. It then assigns subbands to BSs by applying a modified graph coloring algorithm that takes into account the efficient spatial reuse of subbands. The novelty of GB-DFR stems from the flexibility in the number of subbands that can be assigned depending on the interference conditions observed by each BS. Those BSs facing low interference are assigned more subbands and vice versa. However, GB-DFR is suitable only for single user deployments where each BS serves just one UE. As the number of UEs served by the BS increases, the utilization of subbands decreases. For this purpose, an extended GB-DFR (eGB-DFR) is investigated that is better suited to serve multi-user scenarios with the objective of increasing the cell-edge capacity whilst maintaining high subband utilization. In order to enable this, we define two classes of subbands depending on their foreseen usage by a BS: primary subbands (PSs) and secondary subbands (SSs). The PSs are assigned by a central controller similar to

GB-DFR [101], so as to protect cell-edge UEs facing high interference. The PSs belonging to a particular BS cannot be used by their interfering neighboring BSs because such neighbors can cause high interference to UEs of the BS in question. In order to ban/block subbands at the interfering BSs, BSs send a PS indicator to their interfering neighbors. When a BS receives such an indicator, it cannot use the indicated subband and this way cell-edge UEs allocated resources from within the set of PSs experience low interference. Secondly, the SSs, belonging to the set of all unblocked (in other words, non-PS) subbands are assigned autonomously by BSs after PSs are assigned. SSs can be used by a BS depending on the prevailing interference conditions; but, enjoying no privileges, these subbands cannot be blocked at interfering neighboring BSs. Resources of SSs can therefore be allocated to cell-center UEs facing less interference as long as they do not cause high interference to neighboring BSs. Consequently, the usage of the PSs boosts cell-edge capacity, whereas the SSs increase the spatial reuse of resources especially for multi-user deployments. This is therefore a hybrid method comprising a centralized and a decentralized component.

4.4.2 System Model

We consider the downlink of a long term evolution (LTE) system where the system bandwidth consists of multiple subbands. Each subband consists of a fixed number of resource blocks (RBs) which are the most basic downlink resource allocation units for data transmission. A BS can allocate RBs of the same subband to multiple UEs; however, a RB can be allocated to only one UE in any given cell.

Owing to the cluttered deployment of BSs, it is impossible for a UE to identify the list of interfering BSs in advance. Instead, a global, pre-defined signal-to-interference-plus-noise ratio (SINR) threshold, γ_{th}, is defined which represents the minimum tolerated SINR for each UE. In LTE, UEs can differentiate between the received signals from various BSs in their vicinity with the help of BS-specific reference signals termed as common reference signals (CRSs). The received signal strength observed by UE_u from BS_n is determined by:

$$R_{u,n} = T_{CRS} G_{u,n} \tag{4.3}$$

where T_{CRS} is the constant CRS transmit power across all BSs and $G_{u,n}$ $G_{u,n}$ is the channel gain comprising the combined effect of path loss and shadowing between BS_n and UE_u. Based on the received signal strengths from the serving BS, BS_b, and from the set of all interfering BSs, I_u, a UE_u experiences a worst-case SINR of γ_u. If $\gamma_u < \gamma_{th}$, then from I_u, the largest interfering BS is removed and γ_u is recalculated. This process continues iteratively until

$$\gamma_u = \frac{R_{u,b}}{\sum_{i \in \overline{I_u}} R_{u,i} + \eta} \geq \gamma_{th} \tag{4.4}$$

where η accounts for thermal noise and $\overline{I_u}$ is the set of tolerable interfering neighbors defined using set notation

$$\overline{I_u} = I_u - I_{u,rem} \tag{4.5}$$

where $I_{u,rem}$ is the set of removed interfering BSs. The set of BSs belonging to $I_{u,rem}$ must not use the same subband from which RBs are allocated to UE_u, so that UE_u may achieve an SINR of at least γ_{th}. Based on the feedback received from its served UEs, a BS constructs the union set $I_{b,rem}$. This set becomes the neighbor list with regards to the BS in question.
Furthermore, in LTE, a UE is also capable of calculating the SINR at each subband. Then, it feeds this information back to its serving BS. The signaling of SINR levels is achieved in LTE by using the channel quality indicator (CQI) [107].

4.4.3 Extended GB-DFR

The eGB-DFR scheme consists of two parts: central assignment of PSs and autonomous assignment of SSs. Subband assignment is done on an event triggered basis which means subbands are updated only if there is a change in the interference environment. This will be described in detail in the following subsection. Additionally, all BSs are synchronized with a time duration equal to that of a so-called *time slot*. Between the starting instances of two time slots, the subband configuration remains undisturbed, *i.e.*, changes in the subband assignment are only made at the start of the time slots.

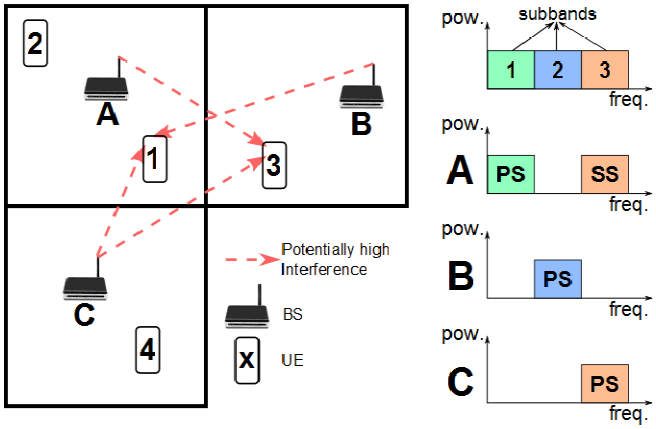

Figure 4-31: An example of subband assignment where the system bandwidth consists of 3 subbands.

A toy example of the allocation of subbands to the various users of various BSs is depicted in Figure 4-31. According to this figure, BS_C causes high interference to some UEs served by BS_A and BS_B. Since these UEs are allocated RBs from subbands 1 and 2, respectively, these subbands are blocked at BS_C. Likewise, BS_A cannot use subband 2 and BS_B cannot use 1. Therefore, subband 1 is declared the PS for cell A, subband 2 the PS for cell B and subband 3 for cell C. On the other hand, UE_2 served by BS_A does not face high interference from BS_B and BS_C, therefore BS_A may allocate subband 3 RBs to UE_2 without causing high interference to UE_4 served by BS_C.
A BS allocates RBs from PSs and SSs to UEs depending on the UEs' perceived interference conditions. Cell-edge UEs are prioritized for being allocated PS RBs, while the cell-center UEs can be allocated RBs from SS. This results in a fair allocation of resources among UEs in the same cell. For instance, BS_A in Figure 4-31, serves UE_1 and UE_2 and can transmit data on subband 1 and subband 3 as PS and SS respectively. As UE_1 faces high interference from BS_C on the SS, only RBs from the PS can be allocated to it. On the other hand, RBs from both PS and SS can be allocated to UE_2. In such a situation, for the sake of fairness, UE_1 gets all resources from the PS and all resources from the SS are allocated to UE_2.

4.4.3.1 Primary Subband Assignment

In order to assign PSs to BSs, the central controller uses an interference graph which is constructed according to the feedback from the BSs. In order to implement this, each BS reports its neighbor list to the central controller when a change (such as the introduction of a new BS to the network) is detected. The central controller then builds an interference graph based on this feedback. If the feedback from BSs causes a change in the interference graph, the central controller updates the PS assignment of all BSs and informs them.
After the PS is assigned, the BS in question can inform the (potential) interfering BSs of its served UEs via a PS indicator. In this way, the serving BS blocks the interfering BSs for using its PS and the desired γ_{th} can be achieved at the given UEs. The serving BS sends PS indicator only for those UEs to which RBs from the PS are allocated, *i.e.*, cell-edge UEs.

1) Construction of the Interference Graph: In the interference graph, each node corresponds to a BS and the edge connecting two nodes represents the interference between two BSs, if this interference exceeds the pre-defined threshold. One important point here is that the edges in the graph are assumed to be undirected, which means that if BS_A reports BS_B as its neighbor, then BS_B automatically becomes the neighbor of BS_A, whether BS_B reports BS_A as its neighbor or not.
Similar procedures are adopted in [102], [103] and [104], but neighboring relations are constructed between UEs meaning each node represents a UE in the interference graph. The main advantage of constructing the interference graph based on BSs instead of UEs is that it can remain unchanged for longer periods of time. This way, the update frequency of the PS assignment by the central controller decreases, and hence, so does the signaling overhead. There are two reasons why the proposed interference graph is stable. Firstly, locations of the BSs do not change frequently. As long as a new BS does not enter the network or the active one does not leave, the nodes in the graph remain same. Secondly, since the BS accumulates feedback from all its served UEs to construct the interference graph, the edges reflect the overall interference conditions experienced by the geographically diverse UEs. Therefore, the movement of one UE does not cause an adverse change to the interference graph, leading to stability. For instance, referring back to Figure 4-31, assume UE_2 served by BS_A changes its location

such that it starts to face high interference from BS_B. This, however, does not affect the interference graph since UE_1 already faces high interference from BS_B which in turn does not change the relation between BS_A and BS_B in the interference graph.
As a final remark, increasing γ_{th} results in a graph with higher connectivity, since this increases the number of the neighbors, and hence, the number of edges in the graph. This way, higher SINRs are achieved, but this is traded off with a reduced spatial reuse of subbands.

2) Graph Coloring Algorithm: Conventional graph coloring algorithms, such as the one given in [105], color the nodes of a graph with the minimum number of colors such that no two connected nodes (in this context, neighbor nodes) have the same color. By assuming that each color represents a different subband, graph coloring facilitates subband assignment, where two BSs connected via an edge in the interference graph cannot use the same subband.
The drawback of conventional graph coloring is the inefficient usage of the subbands since each BS is assigned only one subband. In order to increase the spatial reuse of subbands, a BS in a less interfering environment should be able to use more subbands without causing high interference to its neighbors. Shortcomings of conventional graph coloring are addressed in [101] with the proposed GB-DFR scheme, where the subbands are assigned to BSs in three steps and a cost function is introduced to maximize the spatial reuse of subbands. Additionally, in order to increase the fairness for situations where the number of subbands is high, a parameter s_{min} is introduced. It indicates the minimum number of subbands that should be assigned to each BS. The GB-DFR can be summarized as (for more details, the reader may refer to [101]):

- **Step 1:** Assigning s_{min} subbands to BSs
  - – Apply the graph coloring algorithm s_{min} times to the interference graph.
  - – For each visited BS assign the optimal subband in terms of utilization of subbands.
- **Step 2:** Assigning the remaining subbands to BSs
  - – For each subband, find out the BSs to which the given subband can be assigned.
  - – Choose the optimal BS in terms of utilization of subbands.
- **Step 3:** Find out BSs without any assigned subband
  - – If there is any BS which is not assigned any subband because of intense interference, assign a subband causing minimum interference to its neighbors.

The GB-DFR method efficiently solves the issue of assignment of subbands for the dynamic environment arising from the cluttered deployment of BSs and allows for UE movement. Also, since the number of nodes is relatively small, the proposed algorithm has low time complexity for the given interference graph and hence the central controller can update the subband assignment with a bearable delay. Note that the complexity does not increase as the number of served UEs increases. Consequently, applying the GB-DFR by a central controller is a convenient approach for assigning PSs to BSs. It is guaranteed that the interfering BSs use different PSs as long as the interference graph remains unchanged. However, assigning all subbands as a PS and restricting all potential interfering neighbors decreases the spatial reuse of subbands for multi-user deployments. For example, assume some BS_b is assigned multiple subbands, say subbands 1 and 2, after applying the GB-DFR. This forbids all its neighbors in the interference graph from using these subbands which protects the cell-edge UEs of BS_b. However, for cell-center UEs that do not need protection, BS_b does not need to restrict its neighbors. So that if BS_b uses subband 1 for cell-edge UEs and subband 2 for the cell-center UEs, then the neighbors of BS_b are not blocked for using subband 2. In this way, more subbands can be utilized. This gives an indication as to why we need to classify subbands as PSs and SSs. For this purpose in eGBDFR, we apply only the first and third steps of the GB-DFR for assigning PSs by setting s_{min} as the number of PS per BS. The rest of the subbands are assigned as a SS autonomously by BSs, the procedure of which is explained in the sequel.

4.4.3.2 Secondary Subband Assignment

Similar to PSs, the same γ_{th} is set for SSs which means a BS can assign a subband as a SS if any of its served UEs experiences an SINR higher than γ_{th} on the given subband. For the SS assignment, a BS gets feedback from the central controller (if its PS is updated), its neighboring BSs and its served UEs. When the BS receives an updated PS information from the central controller, it gives up its assigned SSs. This is because, the central controller updates the PS assignment without knowing the SS assignment. So, the BS should reassign SSs according to the updated PS assignment. However, as explained in the previous subsection, the PS assignment remains the same for longer periods of time, which means that the BS does not need to reset all its assigned subbands frequently.

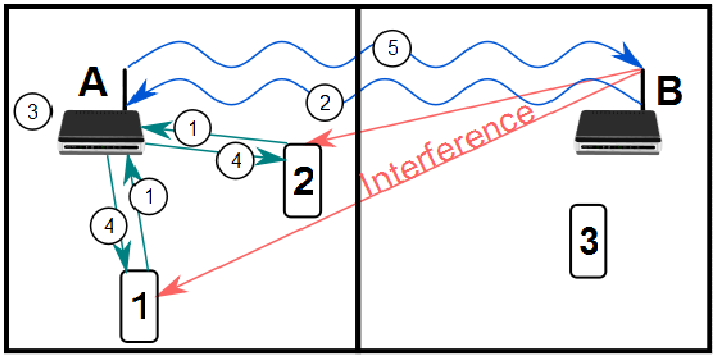

Figure 4-32: Overview of the autonomous assignment of SSs applied by BS_A. The arrows are numbered to indicate the order of the procedures.

For the time slots when the BS does not receive a PS update from the central controller, it computes the SS assignment for the next time slot, based on the feedback received by it from its served UEs and neighboring BSs in the previous time slot. This procedure is clarified via Figure 4-32 which shows an overview of the autonomous assignment of SSs applied by BS_A at the start of a time slot *t+1* (assuming that feedback has been received in time slot *t*). According to the figure, BS_A acts as a sink for collecting SINR levels on every subband from its associated UEs (1), and PS indicators from neighboring BSs, which is used for signaling the PS information to the interfering neighbors (2). Depending on the reported feedback from the time slot *t*, BS_A updates its subband assignment for the time slot *t + 1* (3), and from this allotment of subbands, downlink RBs are allocated to the served UEs (4), and a PS indicator is sent to the corresponding interfering BSs (5). The same procedure is followed by all BSs in the network. All subband selection processes are explained in the following subsections.

1) Set of Available Subbands for Transmission: A BS needs to use a metric to choose the most efficient subband in terms of a desired performance criterion. For this purpose, a metric termed as *subband availability* is introduced. The availability of a subband indicates how many UEs experience an SINR higher than γ_{th} on that subband in a given cell. However, if a BS receives a PS indicator from its neighbor(s), the given BS cannot use that subband. Therefore, in this case, the availability of the subband becomes 0 independent of the SINR levels reported by UEs. The calculation of the availability of subband *s* in BS_b is as

$$A_{s,b} = \begin{cases} \sum_{u \in U_b} 1(\gamma_u^s \geq \gamma_u^s) & \text{if } \mathbf{s} \text{ is not blocked} \\ 0 & \text{if } \mathbf{s} \text{ is blocked} \end{cases} \quad (4.6)$$

where 1 is a conditional binary function whose output is 1 if its argument holds true and 0 otherwise. Here, γ_u^s is the SINR at subband s measured by UE_u and U_b is the set of all UEs served by BS_b.

2) Assignment of Idle Subbands: Since the SS assignment is determined by a BS based on UE feedback, which inherently induces latency, it is possible that multiple BSs access the same subband giving rise to destructive interference. The occurrence of such failed subband assignments decreases as BSs learn the nature of their environment and the network reaches a stable point where BSs no longer need to update their subband assignments. Moreover, frequent changes in subband assignments creates a cascading effect whereby neighboring BSs are to update their subband selection, which increases the time required to reach a stable resource assignment. Therefore, we introduce a modified *p*-persistent slot allocation in SS assignment. In *p*-persistent slot allocation policy [106], when a channel is sensed idle by a transmitter, meaning no other transmitters send any packet, the transmitter sends the packet with a probability of *p*. In a similar manner, in eGB-DFR, an idle subband may be assigned with a certain probability depending on the subband's availability. For a given subband *s*, if a UE reports an SINR higher than γ_{th}, then BS_b assigns *s* with a probability of *p*. If multiple UEs experience an SINR higher than γ_{th}, which means availability of *s*, $A_{s,b}$, is greater than 1, then BS_b applies the *p*-persistent protocol $A_{s,b}$ times. The probability of the assigning *s* by BS_b for the next time slot *t+1* can be formulated as:

$$P_{s,b}(t+1) = 1-(1-p)^{A_{s,b}} \quad P_{s,b}(t+1) = 1-(1-p)^{A_{s,b}} \quad (4.7)$$

A BS updates its subband assignment only if the probability condition in (4.7) holds, so that simultaneous assignment of the same subband by interfering BSs becomes less likely. The subband selection therefore converges quicker to a stable state. In (4.7), it is obvious that the probability of assigning a subband increases as subband's availability increases. This favors the selection of a subband that can be allocated to more users with high SINRs.

3) SS Selection Algorithm: The idea of using SSs is to allocate more resources to cell-center UEs as has already been mentioned. Therefore, a BS searches for subbands on which cell-center UEs experience high SINR. This gives a BS the freedom to use more subbands for UEs facing less interference. However, the assigned subband should not interfere with the PSs of neighboring BSs. The SS selection algorithm applied by BS_b for time slot $t+1$ is given in Algorithm 4-1, where SS(t) is the set of SSs used in the previous time slot t, PS is the primary subband assigned by the central controller and S is the set of all subbands.

1: Calculate the availability of all subbands
2: $S \setminus \{SS(t) \cup PS\} \leftarrow S'$
3: $SS(t) \setminus \{s \in SS(t) \mid A_{s,b} = 0\} \leftarrow SS(t+1)$
4: **for** $i = 1 \rightarrow |S'|$ **do**
5: $s = S'(i)$
6: **if** $A_{s,b} > 0$ **then**
7: with a prob. of $P_{s,b}(t+1)$: add s to $SS(t+1)$
8: **end if**
9: **end for**

Algorithm 4-1: SS Selection

The SS selection algorithm first calculates the availability of all subbands using Algorithm 4.1. Additionally, before selecting any SS, the BS discards the subbands having zero availability from the SS set, SS($t+1$), because either these subbands are banned by the neighboring BSs via a PS indicator or all UEs in the cell experience SINRs lower than γ_{th} over these subbands. Therefore, such subbands cannot be used for the next time slot $t+1$. Then, in the set of subbands which are not assigned as a PS or SS, S', the subbands having an availability higher than 0 are assigned as a SS with a probability that is calculated using (4.7)

4.4.4 Simulation Setup

The simulated scenario consists of a single one-story building, modeled by a 5×5 grid, according to 3GPP specifications [113]. The 5×5 grid represents a square building consisting of 25 regularly arranged square-shaped apartments. Every apartment hosts a femto BS with a certain activation probability. If an apartment contains an active femto BS, it serves a certain number of UEs which are randomly distributed within the confines of the apartment. Full-buffer transmission is assumed such that every BS assigns all available resources from all available subbands to their served UEs. For the sake of simplicity, interference from the macrocell network is neglected, which may be accomplished by allocating different frequency bands to macro and femto BSs. The system parameters summarized in Table 4-5 are based on LTE specifications [113].

Table 4-5: Simulation Parameters

Parameter	Value
System bandwidth	20 MHz
Number of Subbands	4
Min. Sep. between UE and BS	20 cm
BS Antenna Gain	0 dBi
Antenna Pattern (Horizontal)	$A(\Theta) = 0$ dB (omnidirectional)
Interior Path Loss	$L=127 + 30\log_{10}d$ [km] where d is the distance between UE and BS
Shadowing Std. Dev.	10 dB
Max BS Tx power	10 dBm
Thermal Noise Density	η = -174 dBm/Hz
UE Noise Figure	9 dB

Apartment Dimensions	10m x 10m
Number of UEs per Femto BS	4
Femto BS Activation Prob.	0.2
SINR Threshold	γ_{th} =5 dB
Prob. *p* in (4.7)	0.25

For throughput calculations, the attenuated and truncated Shannon bound is applied, which approximates the spectral efficiency of appropriately selected modulation and coding schemes subject to the achieved SINR. Detailed information on throughput calculations can be found in [101]. As a final remark, each snapshot of the simulator lasts for 10 time slots. During the snapshot, positions and shadowing values of BSs and UEs are assumed to remain unchanged. This is reasonable since indoors, the mobility of users is not as high as would be the case for outdoors. The statistics, such as SINR and capacity, are calculated at the end of the 10th time slot, *i.e.*, when a stable resource allocation is achieved.

4.4.5 Results

The performance of eGB-DFR is compared to FFR and GB-DFR. We use two FFR schemes: FFR 1/4 and FFR 2/4 where each BS is centrally assigned one and two subbands out of four available subbands respectively. For eGB-DFR, the number of PS per BS is set as 1.

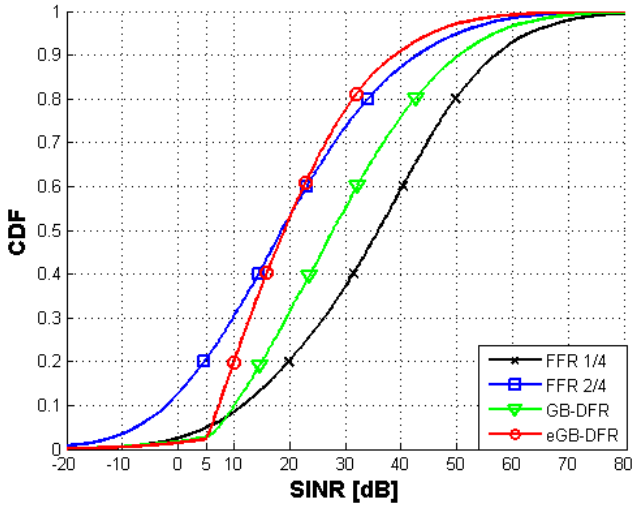

Figure 4-33: CDF of SINR

Figure 4-33 shows the cumulative distribution function (CDF) of the achieved SINR. With eGB-DFR and GB-DFR, nearly all UEs achieve an SINR exceeding γ_{th} =5 dB. It is seen that the best SINR performance is achieved by the system where each femto BS only uses one out of four available subbands.

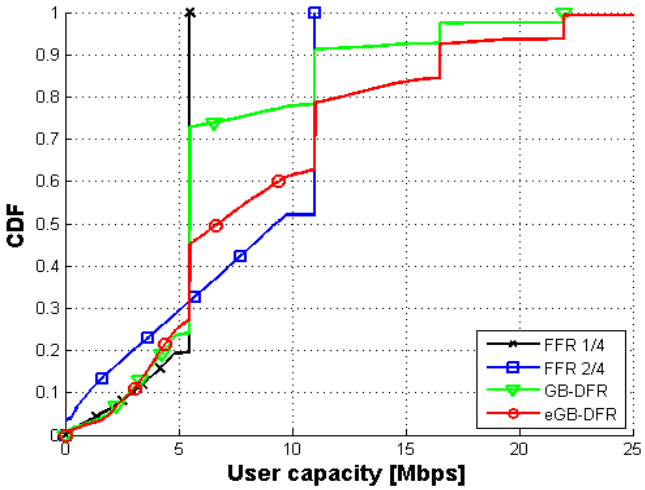

Figure 4-34: CDF of User Capacity

Figure 4-34 compares the CDFs of user capacity of the four methods. Due to the truncated Shannon bound, spectral efficiencies saturate at the SINR of 19.5 dB which is the maximum SINR value that can be used by the available modulation and coding schemes. Additionally, the value at which the saturation occurs depends on the number of resources available for allocation. As a result, despite the encouraging SINR performance exhibited by the system employing FFR 1/4, the capacity saturates at a mere 5.5Mbps, implying that a high proportion of resources remain unused. While the saturation capacity of FFR 1/4 is doubled with FFR 2/4, occasionally idle resources remain unused. Moreover, the cell-edge user throughput (given by the low percentiles of the user capacity CDF) substantially degrades. eGB-DFR, like the FFR 1/4 system shows very good cell-edge performance (at the low capacity regime), but also shows very promising cell-center performance at the high capacity regime. These improvements come at a loss of capacity approximately between the 30^{th} and 60^{th} percentiles compared to FFR 2/4. However, this loss is compensated by the cell-edge improvements and increase in capacity beyond the 80^{th} percentile. Figure 4-34 also shows the superiority of eGB-DFR over GB-DFR at high capacity regions. Since SSs are not blocked, more subbands are utilized with eGB-DFR, and hence, cell-center UEs can be allocated more resources.

Table 4-6: Performances of the Compared Methods

Method	Cell-edge Cap.	Average Cell Cap.
FFR 1/4	1.57 Mbps	19.82 Mbps
FFR 2/4	0.35 Mbps	30.23 Mbps
GB-DFR	1.90 Mbps	27.15 Mbps
eGB-DFR	1.96 Mbps	35.17 Mbps

The improvements in overall performance are summarized in Table 4-6, which compares the cell-edge capacity (defined as the 5% of the CDF of user capacity) and the average cell capacity. The results demonstrate that eGB-DFR significantly outperforms FFR and GB-DFR in terms of cell-edge and average cell capacity. Therefore, eGB-DFR boosts cell-edge capacity without compromising the system capacity.

4.4.6 Conclusion

The main contribution of this work is to assign resources in unplanned wireless networks that are characterized by varying interference conditions. The proposed eGB-DFR method takes the advantages of both central and autonomous resource assignment approaches. By assigning the PSs centrally, the system reaches a stable resource assignment in a short time and the cell-edge UEs are well-protected. Additionally, by assigning SSs autonomously, a BS gets more flexibility in choosing subbands available for transmission which increases the utilization of subbands. Simulation results demonstrate that eGB-DFR attains a significant improvement for both cell-edge as well as system capacities, compared to conventional centralized frequency reuse methods and GB-DFR. As the method relies on the measurements of UEs, it is able to dynamically adapt to the interference conditions faced in random deployments, thus balancing high spatial reuse of subbands with interference protection for cell-edge users. Furthermore, the method has less signaling overhead as existing LTE signaling procedures are used. Finally, it is worth mentioning that the use of eGB-DFR is not limited to the frequency-domain as shown in this paper, but can be used with any other domain such as the time- or code-domains.

4.5 Ghost Femtocells

The goal of this method is to achieve effective spectral reuse between macrocells and femtocells while guaranteeing the QoS of users served by both macro and femto base stations. We propose a novel resource management scheme that limits the overall interference per RB generated outside the coverage

range of a femtocell while reducing the transmission power in each Resource Block (RB). This method does not involve any message exchange between Femto and Macro BSs.

4.5.1 System Model

We concentrate on femto-to-femto and femto-to-macro interference in LTE downlink scenarios. We consider a mobile wireless cellular network in which mobile terminals and base stations implement an OFDMA air interface based on 3GPP/LTE downlink specifications [114]. OFDM symbols are organized into a number of physical RBs consisting of 12 contiguous sub-carriers for 7 consecutive OFDM symbols. With a bandwidth of 10 MHz, 50 RBs are available for data transmission. Each user is allocated one or several RBs in two consecutive slots, i.e., the Time Transmission Interval (TTI) is equal to two slots and its duration is 1 ms.

We assume that femtocells are deployed according to the 3GPP grid urban deployment model [115]. This model represents a single floor building with 10 m x 10 m apartments placed next to each other in a 5 x 5 grid. The block of apartments belongs to the same region of a macrocell. Each femto BS can simultaneously serve up to 4 users. To consider a realistic case in which some apartments do not have femtocells, we use a system parameter ρ_d called a deployment ratio that indicates the percentage of apartments with a femtocell. Furthermore, the 3GPP model includes ρ_a, another parameter called an activation ratio defined as the percentage of active femtocells. If a femtocell is active, it will transmit with a certain power over data channels. Otherwise, it will transmit over the control channel.

Information Theoretic Limits in Non-Ergodic Block Fading Channels

We can characterize many delay-constrained communication systems such as OFDM systems as instances of a block fading channel. Since the momentary instance of the wireless channel has a finite number of states, the channel is non-ergodic and it admits a null Shannon capacity [116]. The information theoretical limit is established by defining an outage probability P_{out} defined as the probability that the instantaneous mutual information for a given fading instance is smaller than the spectral efficiency R associated with the transmitted packet:

$$P_{out} = P_r(I(\gamma,\alpha) < R), \tag{4.8}$$

where $I(\gamma,\alpha)$ is a random variable representing the instantaneous mutual information for a given fading instance α and γ is the instantaneous Signal to Noise plus Interference Ratio (SINR). For an infinitely large block length, P_{out} is the lowest error probability that can be achieved by a channel encoder and decoder pair. Therefore, when an outage occurs, the correct packet decoding is not possible, hence P_{out} is information theoretical bound on the packet error rate. To obtain P_{out}, it is necessary to compute $I(\gamma,\alpha)$ associated with the current channel measurement on each group of RBs (M OFDM symbols x N subcarriers):

$$I(\gamma,\alpha) = \frac{1}{M \cdot N} \sum_{i=1}^{M} \sum_{j=1}^{N} I_{ij}\left(\left|\alpha_{i,k}\right|^2, {\sigma_k}^2\right) \tag{4.9}$$

where

$$I_{ij}\left(\left|\alpha_{i,k}\right|^2, {\sigma_k}^2\right) = \log_2(A) - \frac{1}{A} \sum_{k=1}^{A} E_z\left[\log_2\left(\sum_{q=1}^{A} A_{i,j,k,q}\right)\right] \tag{4.10}$$

and

$$A_{i,j,k,q} = \exp\left[-\frac{\left|\alpha_{ij} a_k + z - \alpha_{ij} a_q\right|^2 - |z|^2}{2\sigma^2}\right] \tag{4.11}$$

Note that Eq. (4.10) is derived from the work of Ungerboeck [117], where S is the size of the M-QAM modulation alphabet, **a** is the real or complex discrete signal transmitted vector, **z** are the Gaussian noise samples with variance σ^2 and E_z denotes expectation w.r.t. **z**.

4.5.2 Ghost Femtocells: the Proposed Resource Allocation Algorithm

In our vision, femtocells should be invisible in terms of interference generated to neighbour cellular users. Nevertheless, femtocells deployment presents a very challenging issue: while femto BSs power consumption and *interference range* should be *small*, the *coverage range* at which UEs can meet their QoS constraints should be *large*. Based on this observation, we propose a novel RRM algorithm designed to strongly lower femto BSs downlink transmission power. In our proposal, we take advantage of the unusual communication context of femtocells for which locally few UEs compete for a large amount of resources. We come out with a 9 step RRM algorithm, the *Ghost Femtocells* (RRM_{ghost}) that reduces transmission energy by using available frequency resources. The detailed description of the proposed algorithm is as follows:

Step 1: [Classification of Interferers] Femto UEs overhear the broadcast channel (BCH) and estimate which neighbour femto BSs are currently *strong* interferers. An interferer is *strong*, if its sensed power level is larger than a predefined threshold.

Step 2: [Feedback to femto BS] Femto UE feedbacks to the femto BS its QoS constraints, the momentary Channel State Indicator (CSI) measurements, and the cell-IDs of the femto BSs perceived as *strong* interferers.

Step 3: [Feedback to Control Unit] Each femto BS within the femtocell network (i.e. the group of femtocells placed in a block of apartments) reports this information to the Control Unit (CU). For each user *i* in the network, the CU stores the set of its neighbours V_i . The elements of this set are the users that are served by the femto BS of user *i* (HeNB^i) and the users that are served by the femto BSs that are indicated as strong interferers by HeNB^i.

Step 4: [Computing Scheduling Matrices] According to the CSI measurements and the selected scheduler algorithm, the CU computes scheduling metrics λ_i^j for every user *i* on every RB *j*. We assume that RRM_{ghost} implements a Proportional Fair based scheduler, that is

$$\lambda_i^j = SINR_i^j / \sum_{k=1}^{K} SINR_i^k , \tag{4.12}$$

where $SINR_i^j$ represents the instantaneous channel condition of the RB *j* observed at user *i* and $\sum_{k=1}^{K} SINR_i^k$ is the sum of SINRs of *K* RBs that have been already allocated to user *i*. RRM_{ghost} uses the values of this metric as the entries of the scheduling matrices M^{Tx} and M^{Rep} of dimensions $\sum_{k=1}^{N_f} N_k \times N_{RB}$ where N_f is the number of active femto BSs in the network, N_k is the number of users served by the femtocell k , and N_{RB} is the number of available RBs. In a first phase, based on M^{Tx} , the scheduler allocates to each user the minimum number of RBs that meets QoS and power constraints. Then, in a second phase, the proposed scheduler sorts matrix M^{Rep} to allocate to the served users additional available RBs. These two phases are described below in Steps 5 and 7.

Step 5: [Scheduling] For each user to serve, the CU selects the minimum number of RBs that meets QoS and power constraints. It schedules in three iterative steps:

Step 5-a: The controller selects the best user-available RB pair *(i,j)* with the best metric in M^{Tx} .

Step 5-b: The overall available power at user *i* served by the femto BS *k* is $\hat{P}_i = P^T / N_k$, where P^T and N_k are the power budget and the number of users of the femto BS *k*, respectively. The controller equally splits $\hat{P}_i$ in the set of RBs allotted to user *i* $\hat{RB}_i$. Then, according to ($\hat{RB}_i$) and $\hat{P}_i$ the algorithm selects the highest possible Modulation and Coding Scheme ($\hat{MCS}_i$).

Step 5-c: Then, the controller estimates the sum of the Mutual Information *I* given by set $\hat{RB}_i$ and $\hat{MCS}_i$.

• When $I = 0$, the selected user-RB pair cannot be served in this scheduling period so the values of the *i-rows* in both M^{Tx} and M^{Rep} are set to zero.

• When $I \geq R_{tg}$, user i is served. The values of the *i-row* in M^{Tx} and $M^{Rep}(i, j)$ are set to zero and the values of the *i-row* in M^{Rep} are updated according to the scheduler rule (cf. Eq. (4.12)) Moreover, $M^{Tx}(k, j)$ and $M^{Rep}(k, j)$, where $k \in V_i$, are set to zero.

• If $I < R_{tg}$, the user i is not served yet. The values $M^{Tx}(i, j)$ and $M^{Rep}(i, j)$ are set to zero and the values of the *i-rows* in M^{Rep} and M^{Tx} are updated according to the scheduler rule (cf. Eq. (4.12)). Moreover, $M^{Tx}(k, j)$ and $M^{Rep}(k, j)$, where $k \in V_i$, are set to zero.

Step 6: [MCS Scaling] Given the set of RBs ($\hat{RB}_i$) allocated to each served user i, the algorithm finds the MCS^* of the minimum order that meets the QoS target. If MCS^* is different from $\hat{MCS}_i$, the MCS of user i (MCS_i) is set equal to MCS^*. The goal of this process is threefold. First, it improves the transmission robustness. Second, it reduces the padding thus improving the spectral efficiency. Third, it increases the number of possible RBs to repeat the original message.

Step 7: [Repetition] The CU allocates unused RBs to repeat the original message and improve the transmission robustness. Scheduling is done in three iterative steps:

Step 7-a: The scheduler selects the user-available RB pair *(i,j)* that has the best metric in M^{Rep}.

Step 7-b: For each user-available RB pair *(i,j)*, the algorithm checks the Mutual Information I given by the entire set of RBs allocated to user i and MCS_i:

• If $I < R_{tg}$, repetitions would cause outage, hence the values of the row corresponding to user I in M^{Rep} are set to zero.

• When $I \geq R_{tg}$, the original message is repeated in the additional RB and $M^{Rep}(i, j)$ as well as $M^{Rep}(k, j)$, where $k \in V_i$, are set to zero.

Moreover the values of the *i-row* in M^{Rep} are updated according to the scheduler rule.

Step 7-c: The scheduler process terminates when no more user-RB pairs are available.

Step 8: [Power Scaling] The algorithm estimates the SINR perceived at each served user and reduces the allocated transmission power to meet the SINR threshold given by the target packet error rate (PER) and the selected MCS.

Step 9: [Message Reception] Finally, each user collects the information received in each of its allotted RBs and combines these RBs using the Chase combining scheme [118].

4.5.3 Simulation Results

In this section, we assess the effectiveness of the proposed scheme by comparing its performance with a reference algorithm ($RRM_{classic}$). In $RRM_{classic}$, there is no coordination within the femtocell network so HeNBs are not aware of the presence and allocation strategy of neighbour HeNBs. Moreover, $RRM_{classic}$ algorithm does not implement MCS and Power scaling (Steps 6 and 8 in RRM_{ghost} algorithm). We present simulation results for the system model and its parameters presented in Section 4.5.1. The results are averaged over 10^5 runs. At the beginning of each run, we independently generate the channel Rayleigh fading coefficients and randomly place HeNBs and femto UEs on the deployment grid. Moreover, indoor M-UEs are randomly distributed in the apartments where HeNBs are not deployed. Note that in the presented simulations, we consider that all deployed HeNBs are active ($\rho_a = 1$) with four femto UEs per HeNB. The block of apartments is located at 250 meters from the central M-BS.

Figure 4-35 shows the indoor M-UE performance as the normalized throughput versus the power budget P^T at each femtocell. In the co-channel femtocell deployment, indoor MUE performance is limited by femto-to-macro interference. Some recent research introduced cooperation within M-BSs and HeNBs in order to coordinate the access to the radio medium and avoid the cross-tier interference [98]. However, following the 3GPP Release 10 baseline [99], we do not implement this coordination in our system. Hence, the M-BS scheduler is not aware of the RBs exploited by the interfering HeNBs. When the M-BS assigns to an indoor user a RB that is used by a neighbour HeNB, this M-UE can be exposed to a high

level of interference. We aim to evaluate the effect of this interference on M-UE when femtocells use the reference $RRM_{classic}$ and the proposed RRM_{ghost}.
To compare these algorithms, we have set the M-UE throughput target (T_{tg}) equal to 600 kbit/s and considered three different femtocell deployment scenarios:

Scenario δ_L: low density — $\rho_d = 0.3$, star marked curves.
Scenario δ_A: medium density — $\rho_d = 0.5$, square marked curves.
Scenario δ_H: high density — $\rho_d = 0.8$, circle marked curves.

Solid and dashed lines, respectively, correspond to the throughput of $RRM_{classic}$ and RRM_{ghost} schemes. The results show how RRM_{ghost} strongly limits the impact of the femto-to-macro interference in all scenarios. For instance, under $RRM_{classic}$ and considering a HeNB power budget of 10 mW, M-UE achieves 15% of T_{tg} in Scenario $\boldsymbol{\delta_H}$, 40% of T_{tg} in Scenario $\boldsymbol{\delta_A}$, and 53% of T_{tg} in Scenario $\boldsymbol{\delta_L}$. Under RRM_{ghost}, M-UE achieves 63%, 78%, and 84% of T_{tg}, respectively. In fact, the M-UE performance under RRM_{ghost} almost does not depend on the HeNB power budget. This improvement comes from steps 6, 7, and 8 of the proposed scheme (MCS scaling, Repetition, and Power Scaling) that reduce the level of interference experienced in each RB by the M-UE.

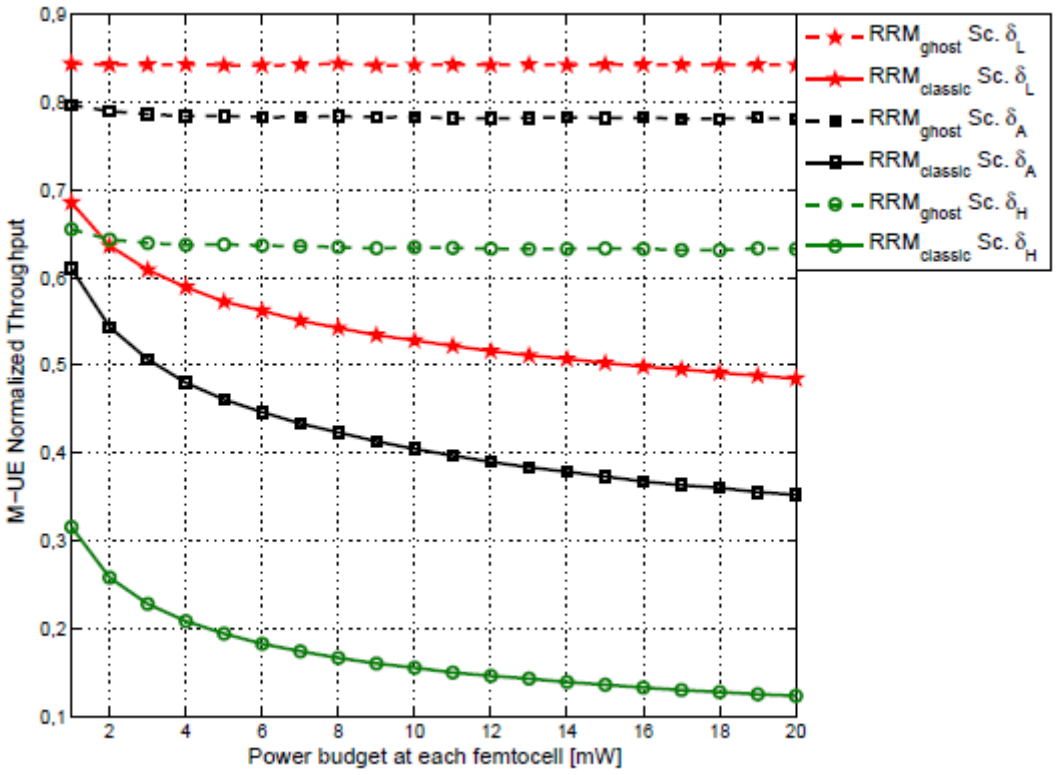

Figure 4-35 Average indoor M-UE normalized throughput versus power budget at each HeNB in different femtocell deployment scenarios.

Figure 4-36 shows the improvement in femtocell performance under RRM_{ghost}. We consider five different traffic scenarios:

Scenario Traf 1: Femto UE throughput target T_{tg} = 200 kbit/s, circle marked curves.
Scenario Traf 2: Femto UE throughput target T_{tg} = 400 kbit/s, square marked curves.
Scenario Traf 3: Femto UE throughput target T_{tg} = 600 kbit/s, diamond marked curves.
Scenario Traf 4: Femto UE throughput target T_{tg} = 1 Mbit/s, star marked curves.
Scenario Traf 5: Femto UE throughput target T_{tg} = 2 Mbit/s, triangle marked curves.

Figure 4-36 shows the average Femto UE throughput versus the femtocell power budget P^T. We investigate the *femto-to-femto interference* when the HeNBs implement the reference $RRM_{classic}$ and the proposed RRM_{ghost}. We can observe that RRM_{ghost} always provides better throughput, but to different extent depending on scenario. Under $RRM_{classic}$, there is no coordination between neighbours HeNBs, thus schedulers are not aware of the RBs used by neighbour HeNBs. Hence, when a femtocell scheduler assigns to one of its serving user a RB used by a neighbour user, both the femto UEs can be exposed to a high level of interference. In Scenarios Traf 1 and Traf 2, the probability that neighbour HeNBs allocate the same RBs is fairly small under $RRM_{classic}$. Hence, RRM_{ghost} results in an improvement. In Scenarios Traf 3, Traf 4 and Traf 5, the *femto-to-femto interference* grows under the $RRM_{classic}$ scheme and the femto UEs performance decrease. On the contrary, in Scenarios Traf 3 and Traf 4 under RRM_{ghost}, femto UEs achieve performance beyond 90% of *Ttg*. In Scenarios Traf 5, femto UEs need several RBs to achieve T_{tg}, hence the probability that neighbour HeNBs allocate the same RBs is very high so both RRM_{ghost} and $RRM_{classic}$ are far away from T_{tg}. This effect comes from some concurrent effects. With higher T_{tg}, a larger number of RBs and/or a higher order of spectral efficiency are needed for each user to meet his/her QoS constraints. This translates in either larger interference generated to neighbour cells on some RBs and/or a need to transmit on the same number of RBs, but with a higher spectral efficiency. Transmission is thus more sensitive to both noise and interference generated by close interferers. As a result, the proposed scheme strongly limits the impact of the *femto-to-femto interference*.

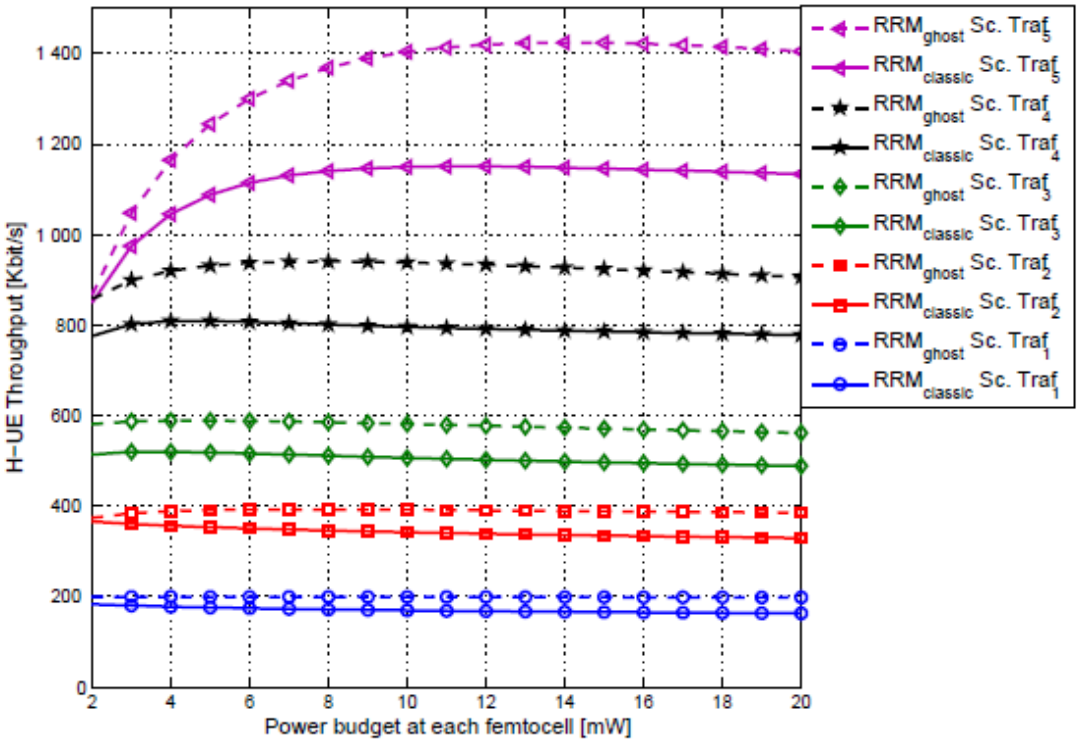

Figure 4-36 Average femto-UE throughput in function of the power budget at each HeNB in different traffic scenarios

4.5.4 Conclusions and future work

The future 3GPP/LTE femtocells deployment is expected to be dense: a large population of potential interferers will need to share scarce common frequency resources while few users will locally have access to a large amount of resources. Classical resource allocation and interference mitigation techniques cannot address the challenge of limiting interference between neighbour femtocells and maintaining a high level of reliability for macro UE communications. Even if we have not completely made femtocells *invisible* so that the communications in neighbour femtocells do not harm any user in the network, we have obtained some important results. We have designed RRM_{ghost}, a novel radio resource management scheme that efficiently uses the available wireless spectrum in a two-tier network. It limits the undesired effects of interference by reducing the radiated power P^T required at femtocells to meet target QoS constraints. We have evaluated the effectiveness of the proposed scheme for different femtocells loads

and for different dense urban deployment scenarios based on the 3GPP/LTE specifications. Our simulation results show that RRM_{ghost} significantly improves communication reliability for user equipment associated with both the macro base station and femtocells.

4.6 Self-Optimization of Antenna Tilt

The scope of this contribution is focused on Spectral Efficiency (SE) enhancement on the access link of Outdoor Fixed Relay femtocells (OFR) through SO of eNB antennas tilt.

OFR are different from conventional femtocells as, unlike femtocells, OFR generally have an over the air inband back haul link called access link, to relay the traffic data to and from their donor eNB. This access link requires radio resource partitioning between the eNB and OFR to avoid mutual interference. Such additional partitioning of resources is bound to have negative impact on the spectrum reuse efficiency of the system and hence capacity. Therefore, it is very desirable to optimise the spectral efficiency of the access link so that less fraction of radio resources have to be allocated to OFR access link and more resources can be used to provide service to users then back hauling. In this contribution we present a novel framework and the preliminary results of SE enhancement on the access link through SO of eNB antenna tilts. To the best of our knowledge, this concept is novel and the solution presented here is a first attempt in this particular direction.
The rest of this section is organized as follows. First we present system model and assumptions, and than we present a novel concept of *triplet* of adjacent sectors to decompose the system wide tilt optimization problem into sub optimal but locally achievable solution. It is followed by preliminary numerical results to demonstrate the potential of the proposed solution. Finally, pragmatic implementation aspects and future work of the presented framework are highlighted.

4.6.1 System Model and Assumptions

We consider a sectorized multi cellular network with each base station having three sectors and each sector containing one OFR, as shown in Figure 4-37.

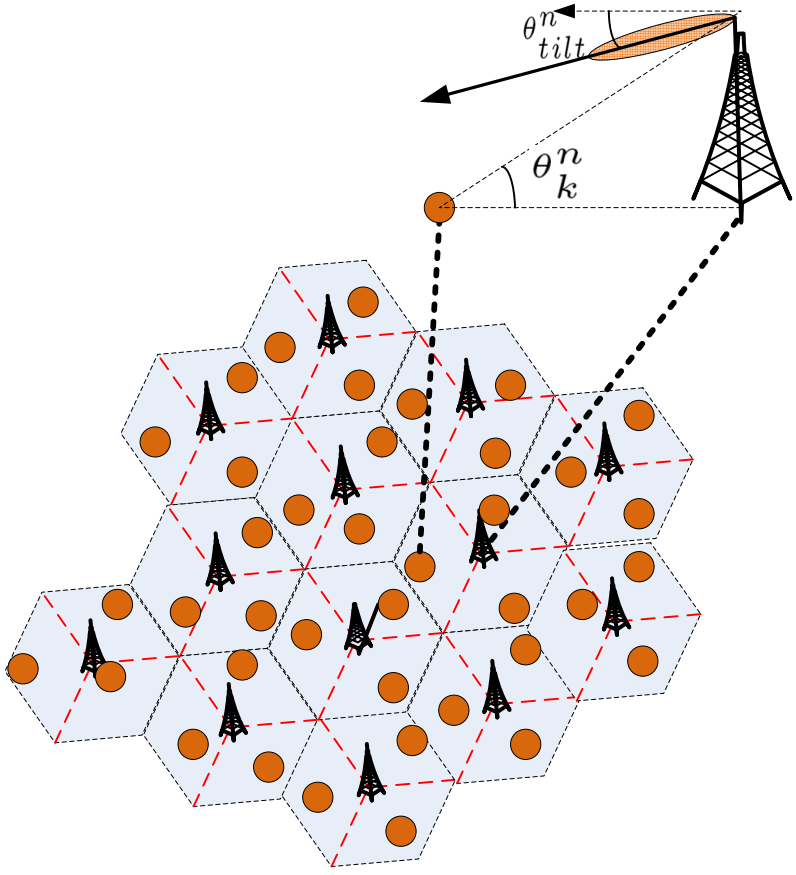

Figure 4-37: System model for problem formulation. Small circles show randomly located OFR's

Let N denote the set of points corresponding to the transmission antenna location of all sectors and K denote the set of location points (e.g. representing location of RS) in the system. The geometric Signal to Interference Ratio i.e. SIR perceived at a location k being served by n^{th} sector can be given a

$$\gamma_k^n = \frac{P^n G_k^n \alpha\left(d_k^n\right)^{-\beta}}{\sum_{\forall m \in \mathsf{N} \setminus n}\left(P^m G_k^m \alpha\left(d_k^m\right)^{-\beta}\right)} \qquad m, n \in \mathsf{N}, k \in \mathsf{K} \tag{4.13}$$

where P is transmission power, d is distance α and β are pathloss model coefficient and exponent respectively. G is the antenna gain and for 3GPP and LTE and LTE-A it can be modelled as [143]

$$G_k^n = 10^{0.1\left(\lambda_v\left(G_{max} - \min\left(12\left(\frac{\theta_k^n - \theta_{tilt}^n}{B_v}\right)^2, A_{max}\right)\right) + \lambda_h\left(G_{max} - \min\left(12\left(\frac{\phi_k^n - \phi_a^n}{B_h}\right)^2, A_{max}\right)\right)\right)}, \quad \forall n \in \mathsf{N} \tag{4.14}$$

where θ and ϕ are vertical and horizontal angles, from n^{th} sector to k^{th} location. Subscripts h, a and v denote horizontal, azimuth and vertical respectively. Subscript denotes the tilt angle of particular sector antenna as shown in the Figure 4-37. B represents beamwidth and λ is weighting factor to weight horizontal and vertical beam pattern of the antenna in 3D antenna model [143]. For the sake of simplicity we can neglect the maximum attenuation factor A_{max} in (4.14).

Without this clamping, antennas will have continuously increasing attenuation as a function of angular distance from their bore site instead of flat attenuation after a certain angular distance from boresight. The angular distance beyond which the flat attenuation occurs is 90^0 in case of a three sector antenna with 70^0 beam width. Since the clamping factor only plays a role in determining antenna attenuation for users almost behind the antenna, in sectorized deployments with hexagonal topology the effect of this simplification is negligible. Without loss of generality we assume maximum gain of 0 dB. Thus by neglecting clamping effect A_{max} and putting $G_{max} = 0$ in (4.14) it can be simplified as

$$G_k^n = 10^{-1.2\left(\lambda_v\left(\frac{\theta_k^n - \theta_{tilt}^n}{B_v}\right)^2 + \lambda_h\left(\frac{\phi_k^n - \phi_a^n}{B_h}\right)^2\right)} \tag{4.15}$$

We assume that all the base stations transmit with the same power. This assumption is in line with LTE where no power control is applied to downlink. For such a scenario, by using (4.15) in (4.13) the SIR at location of k^{th} user can be determined as

$$\gamma_k^n = \frac{\left(d_k^n\right)^{-\beta} 10^{-1.2\left(\lambda_v\left(\frac{\theta_k^n - \theta_{tilt}^n}{B_v}\right)^2 + \lambda_h\left(\frac{\phi_k^n - \phi_a^n}{B_h}\right)^2\right)}}{\sum_{\forall m \in \mathsf{N} \setminus n}\left(\left(d_k^m\right)^{-\beta} 10^{-1.2\left(\lambda_v\left(\frac{\theta_k^m - \theta_{tilt}^m}{B_v}\right)^2 + \lambda_h\left(\frac{\phi_k^m - \phi_a^m}{B_h}\right)^2\right)}\right)} \tag{4.16}$$

For the sake of simplicity, we use the following substitutions

$$c_k^l = \frac{B_v^2 \lambda_h}{\lambda_v}\left(\frac{\phi_k^l - \phi_a^l}{B_h}\right)^2 \tag{4.17}$$

$$h_k^m = \alpha\left(d_k^m\right)^{-\beta} \tag{4.18}$$

$$\mu = \frac{-1.2\lambda_v}{B_v^2} \tag{4.19}$$

Using the substitutions in (4.17)-(4.19), the SIR in (4.16) can be written as

$$\gamma_k^n = \frac{h_k^n 10^{\mu\left(\left(\theta_k^n - \theta_{tilt}^n\right)^2 + c_k^n\right)}}{\sum_{\forall m \in \mathsf{N} \setminus n} \left(h_k^m 10^{\mu\left(\left(\theta_k^m - \theta_{tilt}^m\right)^2 + c_k^m\right)} \right)} \tag{4.20}$$

Note that it can be seen that γ is function of vector of tilt angles of all sectors i.e. θ_{tilt}^N where $N = |\mathsf{N}|$, but for the sake of simplicity of expression we will show this dependency only where necessary.

Given the small sector size, we safely assume that a sector at most can have one OFR within it at random location.

4.6.2 Problem Formulation

Given the system model and assumption, the problem is to *optimize system wide antenna tilts to maximize the aggregate throughput* η *at access link of all the OFRs*. Mathematically

$$\max_{\theta_{tilt}^N} \eta\left(\theta_{tilt}^N\right) = \max_{\theta_{tilt}^N} \sum_{\forall s \in \mathsf{S}} \log_2\left(1 + \gamma_s^n\left(\theta_{tilt}^N\right)\right) \tag{4.21}$$

where S is set of all points identifying locations of all OFR's in the system.

4.6.3 Design SO solution

The formulation in (4.21) is a complex nonlinear multivariable optimization problem. Even if it could be solved easily, its solution would require global cooperation among all eNB's in the WCS and hence would not be scalable and agile as explained in introductory sections, and therefore would lack SO. In order to achieve a SO solution the complexity of the problem needs to be reduced, such that its solution can be executed locally in a distributed manner. There are two main reasons of complexity in this problem; firstly the large scale vector optimization over vector θ_{tilt}^N that has as many components as number of sectors in the system i.e. $|\mathsf{N}|$ which prevents scalability. Secondly the mutual coupling between these variables that requires global cooperation is another reason of complexity of the problem. In order to disintegrate this complex global problem into simpler local problem, we propose to aim for sub optimal solution as suggested in [8]. By not aiming for optimal solution, the tilt optimization can be done locally. To enable this localisation, we propose the concept of *triplet*. The triplet is a fixed cluster of three adjacent and hence most interfering sectors as shown in Figure 4-38. In the next section we show how this concept of triplet can be used to decompose our problem and hence make the solution distributed to achieve SO.

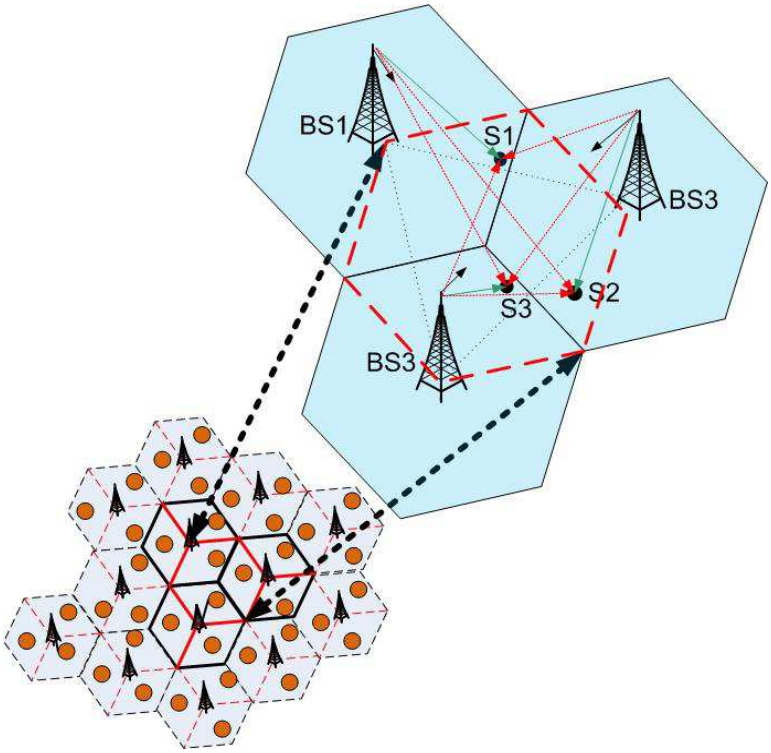

Figure 4-38: Illustration of the concept of triplet of most interfering sectors. Tilts are organized within each triplet independently leading to near optimal throughput at access links in distributed manner.

4.6.4 Solving the Tilt Optimization Problem within a Triplet

Let $\theta_{tilt}^{T_i}$ denote a vector of tilt angle of sectors within i^{th} triplet, now the local optimization problem to be solved and executed within i^{th} triplet is given as

$$\max_{\theta_{tilt}^{T_i}} \sum_{\forall s \in S_i} \log_2\left(1+\hat{\gamma}_s^n\left(\theta_{tilt}^{T_i}\right)\right) \tag{4.22}$$

where S_i is the set of locations of the three OFR within i^{th} triplet. The symbol ^ shows that SIR here is approximate SIR as it considers interference from the two most interring adjacent sectors only. It is because of this approximation that it can be written as function of tilts within the triplet only. To enable SO of tilts within in each triplet the optimization problem in (4.22)**Erreur ! Source du renvoi introuvable.** need to be solved. Below we present a solution methodology for solving the problem in (4.22)**Erreur ! Source du renvoi introuvable.**.

If C is the total achievable throughput in a given triplet (subscript *i* is dropped for simplicity of expression), then

$$C = \log_2\left(1+\hat{\gamma}_1^1\right)+\log_2\left(1+\hat{\gamma}_2^2\right)+\log_2\left(1+\hat{\gamma}_3^3\right) \tag{4.23}$$

where postscripts denote sector number and subscripts denote OFR within a triplet, as shown in Figure 4-38. By substituting (4.20) in (4.23) we get

$$C = \log_2\left(1+\left(\frac{h_1^1 10^{-1.2\mu\left(\left(\theta_1^1-\theta_{tilt}^1\right)^2+c_1^1\right)}}{\left(h_1^2 10^{-1.2\mu\left(\left(\theta_1^2-\theta_{tilt}^2\right)^2+c_1^2\right)}\right)+\left(h_1^3 10^{-1.2\mu\left(\left(\theta_1^3-\theta_{tilt}^3\right)^2+c_1^3\right)}\right)}\right)\right)+$$

$$\log_2\left(1+\left(\frac{h_2^2 10^{-1.2\mu\left(\left(\theta_2^2-\theta_{tilt}^2\right)^2+c_2^2\right)}}{\left(h_2^1 10^{-1.2\mu\left(\left(\theta_2^1-\theta_{tilt}^1\right)^2+c_2^1\right)}\right)+\left(h_2^3 10^{-1.2\mu\left(\left(\theta_2^3-\theta_{tilt}^3\right)^2+c_2^3\right)}\right)}\right)\right)+$$

$$\log_2\left(1+\left(\frac{h_3^3 10^{-1.2\mu\left(\left(\theta_3^3-\theta_{tilt}^2\right)^2+c_3^3\right)}}{\left(h_3^1 10^{-1.2\mu\left(\left(\theta_3^1-\theta_{tilt}^1\right)^2+c_3^1\right)}\right)+\left(h_3^2 10^{-1.2\mu\left(\left(\theta_3^2-\theta_{tilt}^2\right)^2+c_3^2\right)}\right)}\right)\right) \quad (4.24)$$

in order to maximize C as function of tilt angles , the optimization problem can be written as

$$\max_{\theta_{tilt}^1,\theta_{tilt}^2,\theta_{tilt}^3} C\left(\theta_{tilt}^1,\theta_{tilt}^2,\theta_{tilt}^3\right) \quad (4.25)$$

$$\theta_{tilt}^1,\theta_{tilt}^2,\theta_{tilt}^3 < \frac{\pi}{2} \quad (4.26)$$

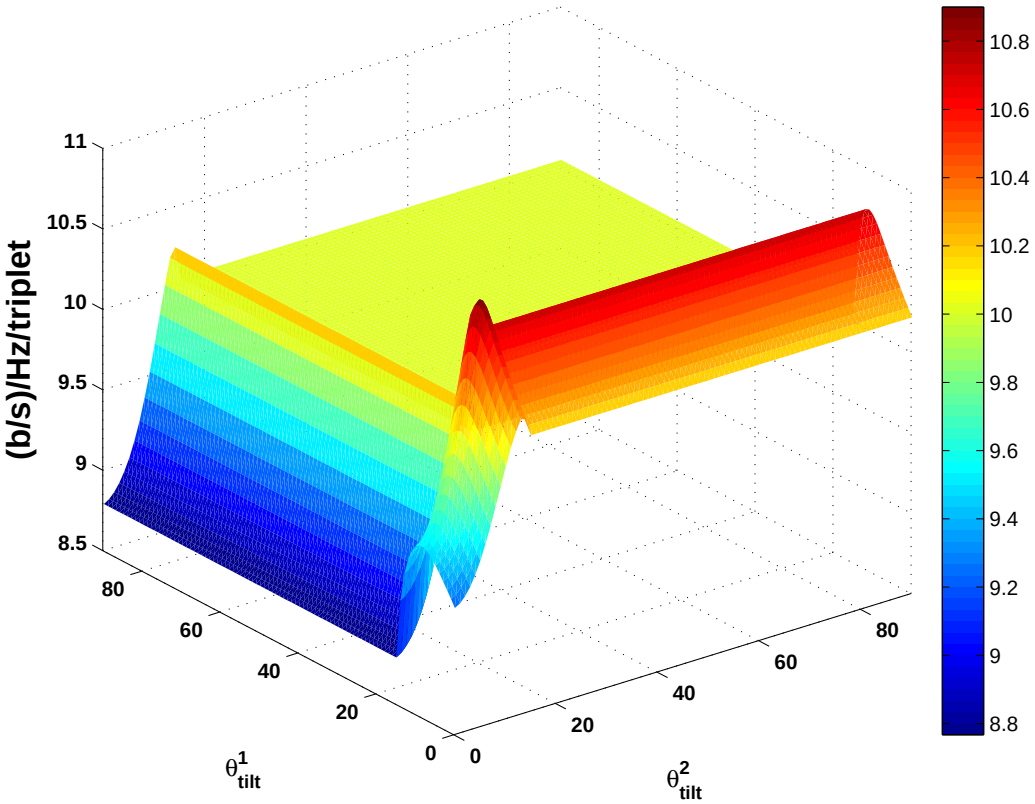

Figure 4-39: Aggregate throughput C plotted for the three access links in a triplet of sectors as function of tilt angles of the two sectors in the triplet. Tilt angle of third sector is fixed at 13^0 degree for ease of plotting. Though there is a clear global optimum it can be seen that C is not a convex function.

Figure 4-39 plots C versus θ^1_{tilt} and θ^2_{tilt} for fixed value of θ^3_{tilt}. It can be seen that C is not a convex function of θ but it has a clear global optimum. Since the number of optimization parameters is only three and their range is also limited i.e. $0 < \theta < 90$, the solution of (4.25) can be easily determined using non linear optimization techniques that can tackle a non convex optimization objective. Since degrees of optimization variables higher than 2 are involved in the optimization function, we solve it using sequential quadratic programming (SQP). For sake of clarity, we drop the subscript 'tilt'. Instead we use subscript to present the association with a sector in the triplet. Then the problem can be written in the standard form as

$$\min_{\boldsymbol{\theta}} \; -C(\boldsymbol{\theta}) \tag{4.27}$$

subject to:

$$g_j(\theta) < 0 \quad , j = 1,2,3 \tag{4.28}$$

where $\boldsymbol{\theta} = [\theta_1, \theta_2, \theta_3]$ and $g_j(\theta) = \theta_j - \frac{\pi}{2}$. The Lagrangian of above problem can be written as

$$\mathsf{L}(\boldsymbol{\theta}, \boldsymbol{\lambda}) = C(\boldsymbol{\theta}) - \boldsymbol{\lambda}^T \mathbf{g} \tag{4.29}$$

$$\mathsf{L}(\boldsymbol{\theta}, \boldsymbol{\lambda}) = C(\boldsymbol{\theta}) - \sum_{j=1}^{3} \lambda_j (\theta_j - \frac{\pi}{2}) \tag{4.30}$$

If $\hat{H}$ denotes the approximate of the Hessian matrix H, then we can define quadratic subproblem to be solved at rth iteration of SQP as follows

$$\min_{\mathbf{w} \in R^J} \quad \frac{1}{2} \mathbf{w}^T \hat{\mathbf{H}}(\mathsf{L}(\boldsymbol{\theta}, \boldsymbol{\lambda}))_r \mathbf{w} + \nabla C(\theta)_r \mathbf{w} \tag{4.31}$$

subject to:

$$w_j + \theta_{j_r} - \frac{\pi}{2} < 0 \quad j = 1,2,3 \tag{4.32}$$

where Hessian is given as

$$\mathbf{H}(\mathsf{L}) = \begin{bmatrix} \frac{\partial^2 \mathsf{L}}{\partial \theta_1^2} & \frac{\partial^2 \mathsf{L}}{\partial \theta_1 \theta_2} & \frac{\partial^2 \mathsf{L}}{\partial \theta_1 \theta_3} \\ \frac{\partial^2 \mathsf{L}}{\partial \theta_2 \theta_1} & \frac{\partial^2 \mathsf{L}}{\partial \theta_2^2} & \frac{\partial^2 \mathsf{L}}{\partial \theta_2 \theta_3} \\ \frac{\partial^2 \mathsf{L}}{\partial \theta_3 \theta_1} & \frac{\partial^2 \mathsf{L}}{\partial \theta_3 \theta_2} & \frac{\partial^2 \mathsf{L}}{\partial \theta_3^2} \end{bmatrix} \tag{4.33}$$

Below we briefly describe the three main steps taken to solve the above problem through SQP:

1. **Updating $\hat{\mathbf{H}}$:** At each iteration the value of $\hat{\mathbf{H}}$ is updated using the Broyden-Fletcher-Goldfarb-Shanno (BFGS) approximation method i.e.

$$\hat{\mathbf{H}}_{r+1} = \hat{\mathbf{H}}_r + \frac{\mathbf{b}_r \mathbf{b}_r^T}{\mathbf{b}_r^T \mathbf{a}_r} - \frac{\hat{\mathbf{H}}_r^T \mathbf{a}_r^T \mathbf{a}_r \hat{\mathbf{H}}_r}{\mathbf{a}_r^T \hat{\mathbf{H}}_r \mathbf{a}_r} \tag{4.34}$$

where

$$\mathbf{a}_r = \boldsymbol{\theta}_{r+1} - \boldsymbol{\theta}_r \tag{4.35}$$

$$\mathbf{b}_r = \left(\nabla C(\boldsymbol{\theta})_{(r+1)} - \sum_{j=1}^{3} \lambda_{j\nabla} g_{j,(r+1)} \right) - \left(\nabla C(\boldsymbol{\theta})_{(r)} - \sum_{j=1}^{3} \lambda_{j\nabla} g_{j,(r)} \right) \tag{4.36}$$

2. **Solution of Quadratic subproblem:** Once the Hessian is known the problem.The quadratic programming problem can be solved using standard methods. We use gradient projection method as described in [144].

3. **Line search and Merit function:** The solution of quadratic subproblem in the r^{th} iteration of SQP algorithm returns the vector $\mathbf{w}_r$ that provides the locus for the next iteration as follows

$$\boldsymbol{\theta}_{r+1} = \boldsymbol{\theta}_r + \alpha \mathbf{w}_r \tag{4.37}$$

where α is set such that sufficient decrease in the merit function is achieved. We use the merit function defined in [145] i.e. given as

$$\psi(\theta) = C(\theta) + \sum_{j=1}^{3} \mu_j . \max\left(0, g_j(\theta)\right) \tag{4.38}$$

where μ is a penalty parameter which we set as recommended in [145] i.e.

$$\mu_{j,(r)} = \mu_{j,(r+1)} = \max_j \left\{ \lambda_j , \frac{\mu_{j,(r)} + \lambda_j}{2} \right\}, \quad j = 1,2,3 \tag{4.39}$$

Through the above steps of SQP, the problem in (4.25) can be solved within each triplet independently to determine the optimal tilt angle to be adapted and maintained by each triplet for given locations of OFR within that triplet.

The execution of this solution in each triplet in the WCS independently, results in achievement of the system-wide objective in (4.21), approximately. We call this framework TO-BSOF (Tilt Optimization through bio-mimetic SO Framework), as the basic idea of decomposing global objective into local objective is inspired from SO systems in nature. In next section we present preliminary numerical results to demonstrate the potential of TO-BSOF.

4.6.5 Numerical Results

A full scale evaluation of TO-BSOF requires multi cell system level simulator with OFR and macro cell overlay modelling capabilities. Development of such simulator is a work in progress. Nevertheless, in order to assess the potential gain TO-BSOF can yield, numerical results for two different set of location of OFRs in triplet are obtained, as shown in Figure 4-40.

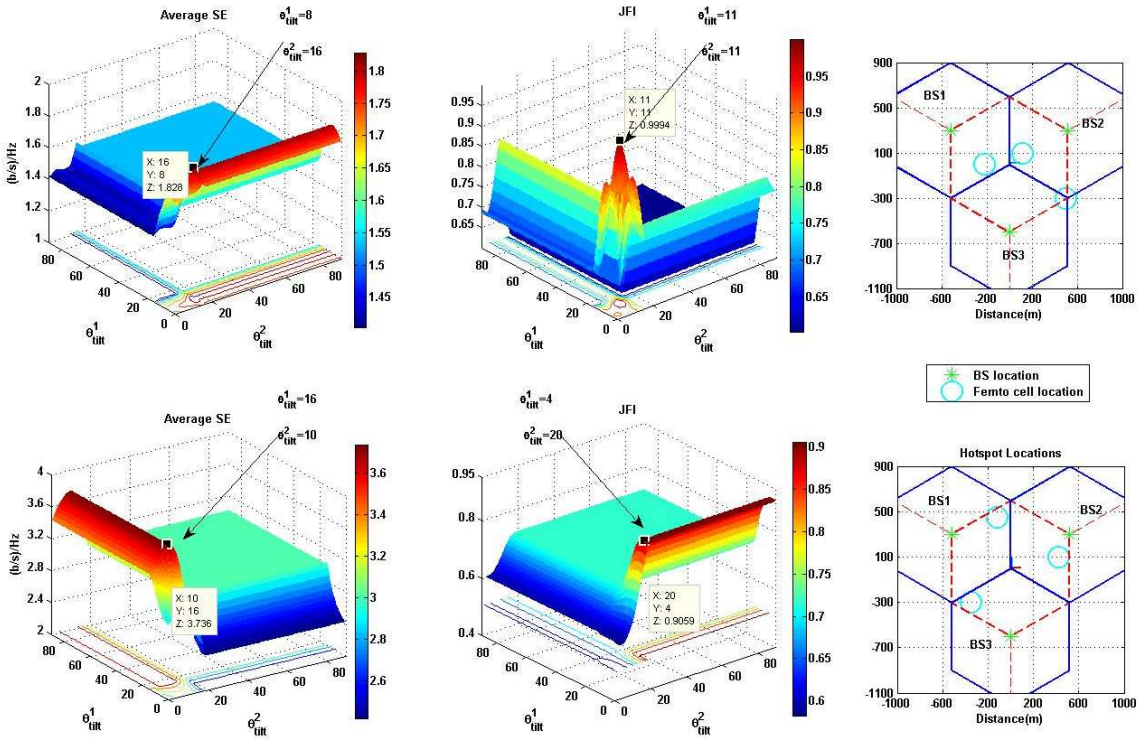

Figure 4-40: Average spectral efficiency per link and the Jain's fairness index among the access links within a triplet are plotted as function of tilt angle of two sectors while third is fixed at 13^0 degree.

It can be seen that depending on the location of OFRs, a gain in spectral efficiency from 1bps/Hz to 2bps/Hz can be achieved on average within each triplet, and hence system wide, through TO-BSOF. To investigate the impact of TO-BSOF on fairness, Jain's Fairness Index (JFI) is also plotted. It is interesting to note that optimal tilt angle for maximum fairness among access links throughput are different than the optimal tilt for maximum spectral efficiency. Nevertheless it is anticipated that fairness among access link

is not an important performance objective as long as significant gain in spectral efficiency can be achieved. TO-BSOF seems promising in this regard; however a thorough investigation is required to evaluate system level performance gain and impact on macro cell users. These issues are the scope of future work and are discussed in details in next section that concludes this contribution.

4.6.6 Practical Implementation of TO-BSOF

TO-BSOF is implementable in a distributed and self-organizing manner and performance close to optimal can be achieved. The main advantage of TO-BSOF is that it does not have heavy signalling overheads associated with it. A negligible amount of signalling among the sectors within triplet is required to determine the location of OFRs. This signalling can be done through X2 interface and needs to be done only when location of OFR is changed.

Although the globally optimal performance is not aimed for by TO-BSOF, however it is just like what is observed in nature, where no SO aims for perfectly optimal objective e.g. common cranes never fly in perfect V shape, but even maintaining a near V-Shape increases their flight efficiency significantly [146]. Furthermore, as postulated in [8] one of the four main paradigms for designing self-organization into system is that, for perfect self-organization perfect objectives should not be aimed for. So here the self-organizing nature of the proposed solution is perfect but at cost of sub-optimal global objective.

Another advantage of TO-BSOF that makes it pragmatic is that because of its highly localised nature it is very agile as it has no intrinsic delays caused by excessive global signalling or complex coordination. Therefore, TO-BSOF can be implemented in an online manner using event-based triggering mechanisms. The execution of TO-BSOF can also be periodic in an off-line manner. Such off-line execution will not require real time position information of OFR locations, rather it can rely on off-line information. In case of periodic execution the time period of re-execution can range from minutes to months and can be set based on the statistics of the long term variations of location of OFR in the area of interest.

4.6.7 Implications of TO-BSOF and Future work

While performance gain of TO-BSOF is promising and its practical implementation is simple and very little demanding in terms of hardware and software, a number of issues need to be addressed before practical realisation of this work. These issues are the scope of ongoing and future work and are briefly listed here.

1. TO-BSOF is based on the assumption that each sector contains one OFR. In real WCS, there can be scenarios where some sectors do not have OFR at all. In this case concept of triplet will not work. A solution with consideration of such heterogeneous scenario is being investigated in ongoing work.
2. TO-BSOF at the moment does not consider impact on macro sectors users, that impact need to be considered and minimised. It can be done by including an appropriate constraint in the problem formulation reflecting the interest of macro users. This issue is the focus of our work in progress
3. System level performance evaluation of TO-BSOF and improved version of TO-BSOF with point 1 and 2 taken care of is the scope of the future work based on this contribution.

5. SON for Radio Resource Management

This section only contains the innovative contribution of docition. In subsequent deliverables, the remaining technical contributions will be presented in greater depth.

5.1 Docition

In this activity, we focus on optimizing the self-organizing approach introduced in D4.1 to target coexistence in terms of downlink interference from femto-to-macro user and femto-to-femtouser. The approach that we propose is based on reinforcement learning. This algorithm is capable of finding optimal solutions in dynamic scenarios characterized by only one decision maker. In a wireless scenario, the one decision maker scheme could be applied in traditional cellular networks where a node like the Radio Network Controller (RNC) is in charge of making decisions that affect a whole area.

Reinforcement Learning does not require environmental models and allows nodes to take actions while they learn. Among RL techniques, Q-learning [42] has been especially well studied, and possesses a firm foundation in the theory of Markov decision processes (MDPs). Q-learning can still be applied to the distributed femtocell setting, in the form of the so called decentralized Q-learning. Here, each node learns independently from the other nodes, which are assumed to be part of the surrounding environment. This paradigm, known as independent learning, has been presented in D4.1.

However, when multiple decision makers intervene in the scenario, the environment is no longer stationary, since it consists of other agents who are similarly adapting. This may generate oscillating behaviours that not always reach equilibrium and that are not yet fully understood, even by machine learning experts. The dynamics of learning may thus be long and complex in terms of required operations and memory, with complexity increasing with an increasing observation space. A possible solution to mitigate this problem to speed up the learning process, to create rules for unseen situations, and to make the learning process more agile, is to facilitate expert knowledge exchange among learners [73][74].

Even as cognition and learning have received considerable attention from various communities in the past, the process of knowledge transfer, i.e., teaching over the wireless medium has received fairly little attention to date. We thus aim at introducing in this internal report an emerging framework for femtocells, referred to as docition, from “docere” = “to teach” in Latin, which relates to nodes teaching other nodes. The femto BSs are not (only) supposed to teach end-results, but rather elements of the methods of getting there. This concept perfectly fits a femtocell network scenario, where a femtocell is active only when the users are at home. When a femto BS is switched on, instead of starting a very energy expensive context awareness phase to sense the spectrum and learn the proper radio resource management (RRM) policy, it can take advantage of the decision policies learnt by the neighbour femtocells, which have been active during a longer time. This novel paradigm for femtocells will be shown to capitalize on the advantages but, most importantly, mitigate major parts of the drawbacks of purely self-organized and cognitive schemes, thus increasing their precision and accuracy and thereby speeding up the learning process.

5.1.1 Independent Learning

The distributed femtocell scenario can be mathematically formulated by means of a stochastic game defined by the quint-tuple $\{N, S, A, P, R\}$, where:

- N is the set of agents, i.e., the femto BSs, indexed 1, 2, $\cdots$,n;
- $S = \{s_1, s_2, \cdots, s_n\}$ is the set of possible states;
- A is the action space defined by the product $A = \{a_1, \cdots, a_n\}$ is the set of actions available to the i^{th} femto BS;
- P is a probabilistic transition function, defining the probability of migrating from one state to another provided the execution of a certain joint action;
- C is the cost function.

To achieve coexistence in terms of interference with the macro system, the objective of the N femto BSs is to distributively learn a joint optimal policy to achieve the common objective of maintaining the aggregated interference at the macro users below a threshold. Known as multi-agent learning problem, it can be solved by means of distributed RL approaches, when the probabilistic transition function cannot be deduced.
There exist several RL algorithms and for our particular problem, we consider the decentralized Q-learning algorithm. However, in this field many problems still remain open. The main challenge is how to ensure that individual decisions of the nodes result in jointly optimal decisions for the group, considering that the standard convergence proof for Q-learning does not hold in this case as the transition model depends on the unknown policy of the other learning femto BSs.

In principle, it is possible to treat the femtocell network as a centralized one, where each node has complete information about the other nodes and learns the optimal joint policy using standard RL techniques. However, both the state and action spaces scale exponentially with the number of nodes, rendering this approach infeasible for most problems, not to mention the signalling burden that this would generate over the backhaul network. Alternatively, we can let each node learn its policy independent of the other nodes, but then the transition model depends on the policy of the other learning nodes, which may result in oscillatory behaviours and in slow speed of convergence to prior set targets.

This paradigm of independent learning works by directly distributing the intelligence of the Q-learning algorithm, designed for single agent systems, to a multi-agent setting.

Decentralized Q-learning works by letting each femto BS *i* estimate its own Q-function, whose values, the Q-values $Q(s,a)$, for each state-action pair are uploaded in a Q-table. The value $Q(s,a)$ is defined to be the expected discounted sum of future cost obtained by taking action a ∈ A_i from state $s \in S$ and following an optimal policy thereafter.

Once these values have been learned, the optimal action from any state is the one with the lowest Q-value. After being initialized to arbitrary numbers, Q-values are estimated on the run, on the basis of experience. In the following we describe the algorithm in more details:

- The agent ♓ senses the state $s_t^{i,r} = s \in S$.
- Based on ♦, agent ♓ selects an action $a_t^{i,r} = a \in A$.
- As a result, the environment makes a transition to the new state $s_{t+1}^{i,r} = v \in S$.
- The transition to the state *v* generates a cost $c_t^{i,r} = c \in R$, for agent *i*.
- The cost ♍ is fed back to the agent and the process is repeated.

The objective of each agent is to find an optimal policy $\pi^*(s)$ for each *s*, to minimize some cumulative measure of the cost $c_t^{i,r} = c(s, a)$ received over time. For each agent *i* and learning process *r*, we define an evaluation function, denoted by $Q^{i,r}(s, a)$, as the expected total discount cost over an infinite time. To simplify the notation, in the following we refer to $Q^{i,r}(s, a)$ as Q(s, a):

$$Q(s,a) = \mathrm{E}\left\{\sum_{t=0}^{\infty} \gamma^t c\left(s_t, \pi(s)\right) \middle| s_0 = s\right\} \tag{5.1}$$

where $0 \le \gamma \le 1$ is a discount factor. If the selected action a at time t following the policy $\pi(s)$ corresponds to the optimal policy $\pi^*(s)$, the Q-function is minimized with respect to the current state. Let $P_{s,v}(a)$ be the transition probability from state *s* to state *v*, when action *a* is executed. Then, the above equation can be expressed as:

$$Q(s,a) = \mathrm{E}\{c(s,a)\} + \gamma \sum_{v \in S} P_{s,v}(a) Q(v,b) \tag{5.2}$$

where $\mathrm{E}\{c(s,a)\}$ denotes the expected value of $c(s,a)$. The above equation indicates that the Q-function of the current state-action pair, for each agent *i* and learning process *r*, can be represented in terms of the expected immediate cost of the current state-action pair and the Q-function of the next state-action pairs. The task of Q-learning is to determine an optimal stationary policy $\pi^*(s)$ without knowing $\mathrm{E}\{c(s,a)\}$ and $P_{s,v}(a)$, which makes it well suited for learning a power allocation policy in a femtocell systems. The principle of Bellman's optimality assures that, for single agent environments, there is at least one optimal stationary policy $\pi^*(s)$ which is such that:

$$V^*(s) = \min_{a \in A} \left[E\{c(s,a)\} + \gamma \sum_{v \in S} P_{s,v}(a) V^*(v) \right] \quad (5.3)$$

In multi-agent settings, where each agent learns independently from the other agents, we approximate the other agents as part of the environment, and we still can apply Bellman's criterion. In this case, the convergence to optimality proof does not hold strictly, but such an independent learning approach has been shown to correctly converge in multiple applications [53]. Applying Bellman's criterion [42], first we have to find an intermediate minimal of $Q(s,a)$, denoted by $Q^*(s,a)$, where the intermediate evaluation function for every possible next state-action pair (v, b) is minimized, and the optimal action is performed with respect to each next state v. $Q^*(s,a)$ is:

$$Q^*(s,a) = E\{c(s,a)\} + \gamma \sum_{v \in S} P_{s,v}(a) \min_{b \in A} Q^*(v,b) \quad (5.4)$$

This allows us to determine the optimal action *a** with respect to the current state *s*. In other words, we can determine $\pi^*(s)$. Therefore, $Q^*(s,a^*) =$ is minimal, and can be expressed as:

$$Q^*(s,a^*) = \min_{a \in A} Q^*(s,a) \quad (5.5)$$

As a result, the Q-value $Q(s,a)$ represents the expected discounted cost for executing action a at state s and then following policy π thereafter. The Q-learning process tries to find $Q^*(s,a)$ in a recursive manner using available information (*s, a, v, c*), where *s* and *v* are the states at time *t* and *t* + 1, respectively; and *a* and *c* are the action taken at time *t* and the immediate reward due to *a* at *s*, respectively. The Q-learning rule to update the Q-values relative to agent *i* and learning process *r* is:

$$Q(s,a) \leftarrow Q(s,a) + \alpha \left[c + \gamma \min_{a} Q(v,a) - Q(s,a) \right] \quad (5.6)$$

where α is the learning rate. For more details about RL and Q-learning the reader is referred to [49].

5.1.2 Docitive Femtocells

Some early contributions in machine learning literature [73][74] suggest that the performance of a multi-agent learning can be improved by using cooperation among learners in a variety of ways. In our scenario, for example, a femto BS which has recently been switched on can advantageously exchange information via a (backhaul) network, through a X2 interface between femtos, with other expert femto BSs in the neighbourhood, the so-called docitive femtocells. The agents select the most appropriate femto BS from which to learn, based on the level of expertness and the similiarity of the impact that their actions may have on the environment, which is captured by a gradient introduced in the next section. The rationale behind the definition of this gradient is that nodes should learn from nodes in similar situations, e.g., a femto BS which is located close to a macro user should learn the policies acquired by a femto BS operating under similar conditions. Depending on the degree of docition among nodes, we consider in this section the following cases:

- *Startup Docition*. Docitive femto BSs teach their policies to any newcomers joining the network. In this case, each node learns independently; however, when a new femtocell joins the network, instead of learning from scratch how to act in the surrounding environment, it learns the policies already acquired by more expert neighbours. Policies are shared by Q-table exchanges between femto BSs with similar gradients.
- *IQ-Driven Docition*. Docitive radios periodically share part of their policies with less expert nodes with a similar gradient, based on the reliability of their expert knowledge. More expert nodes share their expert knowledge periodically, by exchanging rows of the Q-table, corresponding to states that have been previously visited.

The degree of cooperation, and thus the overhead, augments with an increasing degree of docition. The optimum operating point hence depends on the system architecture, performance requirements, etc.

5.1.3 Simulation Scenario

The scenario considered to validate the proposed approach is based on 3GPP TSG (Technical Specification Group) RAN (Radio Access Network) WG4 (Working Group 4) simulation assumptions

and parameters [113]. It is deployed in an urban area, and it works at 1850 MHz. We consider L = 1 macrocells with radius R_M = 500 m and F = 1 blocks of apartments, randomly located inside the macrocell coverage area, as it is shown in Figure 5-1.

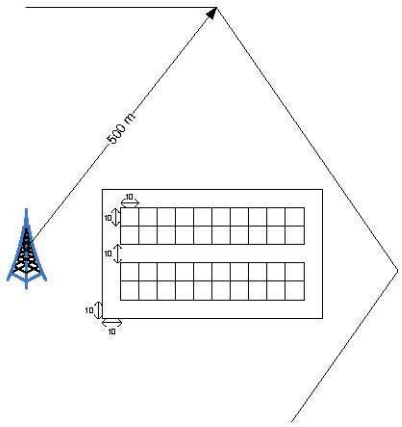

Figure 5-1: Femtocell system layout

Each block of apartments has two stripes, separated by a 10 m wide street, as it is represented in Figure 5-1. Each stripe has 2 rows of B = 10 apartments of size of 10 × 10 m. The total block size is 10 (B + 2) × 70 m. We introduce an occupation ratio which can vary from 0 to 1 and determines whether inside an apartment there is a femtocell or not. We set this parameter to 0.5. Femtocells switch on randomly and then start their learning process. Each femtocell provides service to its C = 2 associated femto users, which are randomly located inside the femtocell area. Macro users are also located randomly inside the femtocell block. We consider that macro users are always outdoors and femto users are always indoors.

We consider the macro and femto systems to be based on LTE; therefore, the frequency band is divided into resource blocks (RBs) of width 180 kHz in the frequency domain and 0.5 ms in the time domain. Those RBs are composed of 12 sub-carriers with a width of Δf = 15 kHz and 7 OFDM (orthogonal frequency division multiplexing) symbols. For simulations we consider 6 resource blocks, which correspond to an LTE implementation with a channel bandwidth of BW = 1.4 MHz. The antenna patterns for macro BS, femto BS and macro/femto users are omnidirectional, with 18 dBi, 0 dBi and 0 dBi antenna gains, respectively. The shadowing standard deviation is 8 dB and 4 dB, for macro and femto systems, respectively. The macro and femto BS noise figures are 5 dB and 8 dB, respectively. The transmission power of the macro BS is 46 dBm, whereas the femto BS adjusts its power through the learning scheme, with a maximum value of 10 dBm.

The considered pathloss (PL) models are for urban scenarios and are summarized in [113]. We also consider the 3GPP implementation of frequency-selective fading model specified in [46] (urban macro settings) for macro BS to user propagation, and a block fading model with coherence bandwidth 750 kHz for indoor propagation.

5.1.4 Results and discussions

The state, actions and cost of the decentralized Q-learning algorithm are defined as follows:

- *State*: At time *t* for femtocell *i* and RB *r* the state is defined as:

$$s = \{I_t^r, Pow_t^i\} \tag{5.7}$$

where I_t^r specifies the level of aggregated interference generated by the femtocell system. The set of possible values is based on:

$$I_t^r = \begin{cases} 0 \ if \ \ SINR_t < SINR_{Th} - 2dB \\ 1 \ \ if \ \ SINR_{Th} - 2dB \le SINR_t \le SINR_{Th} + 2dB \\ 2 \ \ otherwise \end{cases} \tag{5.8}$$

Where $SINR_t$ is the instantaneous SINR measured at the macro user for RB *r* and $SINR_{Th}$ = 20 dB represents the maximum value of SINR that can be perceived by the macro users.

$Pow_t^i = \sum_{r=1}^{r=R} p_t^r$ denotes the total transmission power by the femtocell *i* in all RBs at time *t*. The set of possible values is based on:

$$Pow_t^i = \begin{cases} 0 \; if \;\; Pow_t^i < Pow_{Th} - 6dB \\ 1 \;\; if \;\; Pow_{Th} - 6dB \le Pow_t^i \le Pow_{Th} \\ 2 \;\; otherwise \end{cases} \quad (5.9)$$

where Pow_{Th} = 10 dBm is the maximum transmission power that a femto BS can transmit.

- *Action*: The set of possible actions are the *l* = 60 power levels that femto BS can assign to RB *r*. Those power levels range from −80 to 10 dBm effective radiated power (ERP), with 1 dBm granularity from 10 dBm to −40 dBm and 4 dBm granularity from −40 dBm to −80 dBm.

- *Cost*: The cost c_r^t assesses the immediate return incurred due to the assignment of action *a* in state s. The considered cost function is:

$$c_t^r = \begin{cases} K \;\; if \;\; Pow_t^i > Pow_{Th} \\ \left(SINR_t - SINR_{Th}\right)^2 \end{cases} \quad (5.10)$$

where K = 500. The rational behind this cost function is that the total transmission power of each femtocell does not exceed the allowed Pow_{Th}, and the SINR at the macro user is below the selected threshold $SINR_{Th}$.

With respect to the Q-learning algorithm, the learning rate is α = 0.5 and a discount factor γ = 0.9. Also, we introduce a probability ε = 0.05 of visiting random states in the first half of the Q-learning iterations.

The gradient ∇_t^i for femtocell *i* is defined as: $\nabla_t^i = \sum_{r=1}^{r=RB} \frac{SINR_t^r - SINR_{t-1}^r}{a_r^t - a_t^{t-1}}$, where a_r^t and a_r^{t-1} represent the actions taken for RB *r* and time *t* and *t* − *1* respectively, and $SINR_t^r$ and $SINR_{t-1}^r$, represents the SINR at the macro user in RB *r* at time *t* and *t*−*1*, respectively.

In the following, we compare the performance of 1) independent learning; 2) startup docition; and 3) IQ driven docition. Figure 5-2 shows performances in terms of precision, i.e., oscillations around the target SINR. In particular, it represents the complementary cumulative distribution function (CCDF) of the variance of the average SINR at the control point with respect to the set target of $SINR_{Th}$ = 20 dB. It can be observed that due to the distribution of intelligence among interactive learners the docition stabilizes the oscillations by reducing the variance of the SINR with respect to the specified target. More precisely, at a target outage of 1 %, we observe that the IQ driven docition outperforms the startup docition by a factor of two, and the independent learning algorithm by at about an order of magnitude. Figure 5-3 shows the probability that the total power at a femtocell is higher than Pow_{Th} as a function of the learning time. It can be observed that the docitive approaches better satisfy the constraint in terms of total transmission power, and significantly speeds up the learning process.

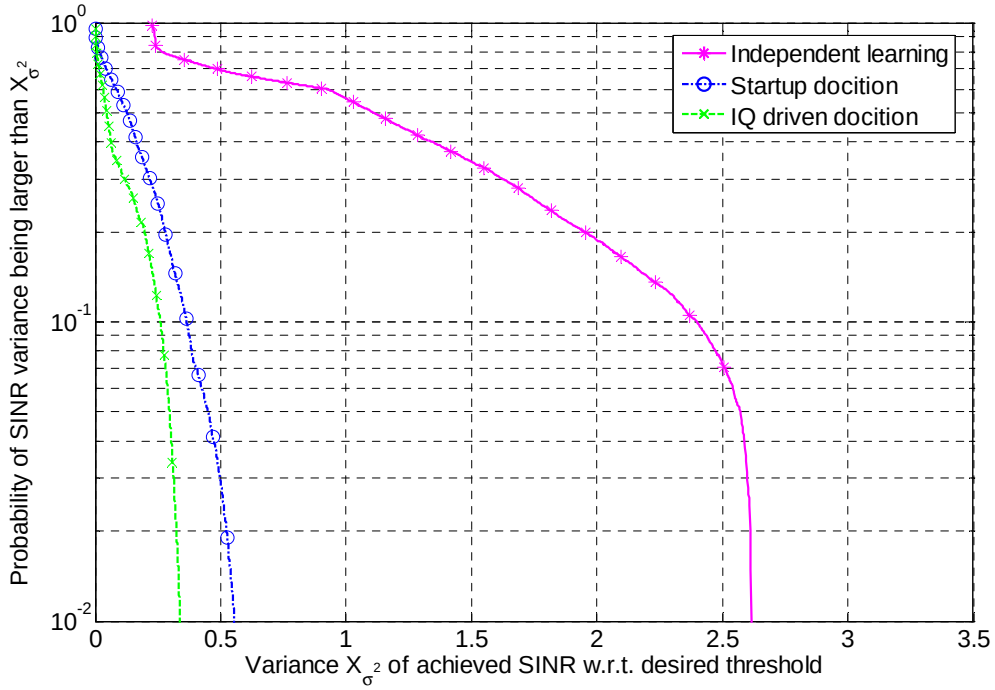

Figure 5-2: CCDF of the average SINR at macrouser.

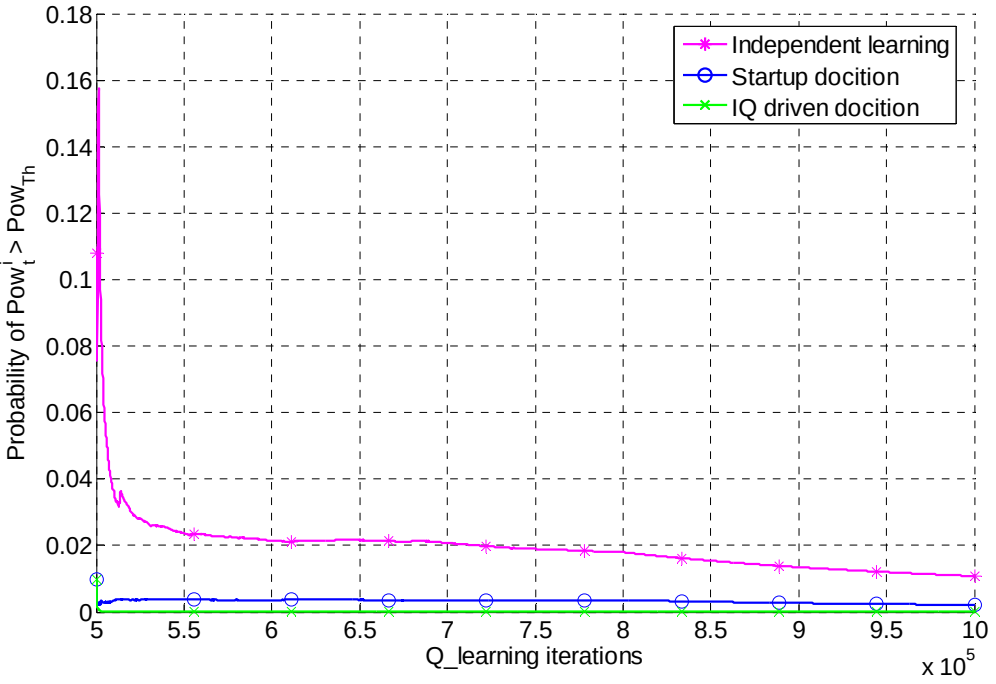

Figure 5-3: Probability that the total transmission power is higher than Pow_{Th}.

5.1.5 BeFEMTO 10dBm & 8bps/Hz/cell Target

The decentralized Q-learning scheme, following the independent learning or docitive paradigm, has been compared to two reference algorithms:

• **Distance-Based Non-Cognitive.** The rationale behind this reference algorithm is that femtocell i selects the transmission power of RB *r* based on its distance from the macrouser using that RB. The set of

possible values of power to assign is the same as for the decentralized Q-learning. Notice that this reference algorithm is only proposed as a non-cognitive benchmark for comparison purposes, and for its implementation we make the hypothesis that the femto network has at least some approximate knowledge of the position of the macrousers, which is a quite difficult hypothesis in a realistic cellular network.

• **Iterative Water-Filling.** It is a non-cooperative game where agents are selfish and compete against each other by choosing their transmit power to maximize their own capacity, subject to a total power constraint. The solution is given by the iterative waterfilling power allocation solution [54].

Figure 5-4 shows the macrocell capacity, for the case of 4x4 antennas, as a function of the femtocell density. It can be observed that learning techniques do not jeopardize the macrocell capacity, maintaining it at a desired level (above the BeFEMTO target of 8bps/hz/cell, independently of the number of femtocells. On the other hand, with the distance-based reference algorithm, the macrocell capacity decreases when the number of femtocells increases, since the reference algorithm does not adaptively consider the aggregated interference coming from the multiple femtocells in the power allocation process. Furthermore, the iterative WF algorithm dramatically reduces the macrocell capacity due to its selfish power allocation policy.

In the next deliverable, we will focus on achieving the BeFEMTO targets in terms of spectral efficiency, not only for the macrocell network, but also for the femtocell's.

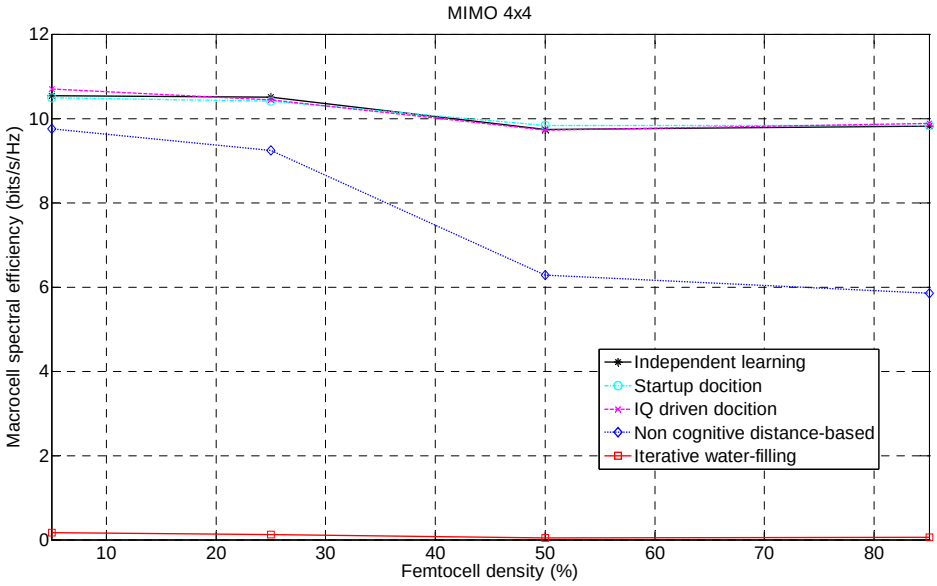

Figure 5-4: Macrocell spectral efficiency as a function of the femtocell density in the femtocell block.

5.1.6 Conclusion and Future Work

We have presented a decentralized Q-learning approach for interference management in a macro-femto network to improve the systems' coexistence. However, the main drawback of the proposed scheme is the length of the learning process. As a result, we have focused on the novel paradigm of docition, with which a femto BS can learn the interference control policy already acquired by a neighboring femtocell which has been active during a longer time, and thus saving significant energy during the startup and learning process. Notably, we have shown in a 3GPP compliant scenario that, with respect to decentralized Q-learning, docition applied at startup as well as continuously on the run yields significant gains in terms of convergence speed and precision. We have also presented spectral efficiency results of the macro network, showing that BeFEMTO target of 8bits/s/Hz/cell can be achieved by applying the proposed learning approaches, even when the density of femtocells in the femtocell block in the scenario is increasing.

5.2 Spectrum Leasing as an Incentive for Macro-Femtocell cooperation in the UL

5.2.1 Problem Statement

We propose a framework for macrocell-femtocell cooperation under a closed access policy, in which a FUE may act as a relay for MUEs. In return, each cooperative macrocell user grants the FUE a fraction of its super-frame. We formulate a coalitional game in which macrocell and femtocell users are the players, which can take individual and distributed decisions on whether to cooperate or not, while maximizing a utility function that captures the cooperative gains, in terms of throughput and delay. We show that the network can self-organize into a partition composed of disjoint coalitions which constitutes the recursive *core* of the game representing a key solution concept for coalition formation games in partition form.

5.2.2 System Model

Consider the *uplink* direction of an Orthogonal Frequency Division Multiple Access (OFDMA) macrocell network in which N FAPs are deployed. These FAPs are underlaid to the macrocell frequency spectrum, and, within the femtocell tier, FAPs are allocated over orthogonal frequency subchannels1. Let $N = \{1,...,N\}$ and $M = \{1,...,M\}$ denote, respectively, the sets of all FAPs and MUEs in the network. The packet generation process at each MUE-MBS link is modeled as an M/D/1 queuing system, in which packets of constant size are generated using a Poisson arrival process with an average arrival rate of λ_m, in packets/second. Similarly, the link between FUE l and its belonging FAP is modeled as an M/D/1 queuing system with Poisson arrival rate of λ_l. In the non-cooperative approach (N.C), the MBS offers MUE m a link transmission capacity (measured in bits/s/Hz) of:

$$\mu_m^{N.C} = \log\left(1 + \frac{|h_{m,0}|^2 P_m}{\sum_{l \in \Phi_l^0} |h_{l,0}|^2 P_l + \sigma^2}\right) \qquad (5.11)$$

where $|h_{m,0}|^2$ is the channel gain between MUE m and the MBS denoted by subscript 0, P_m is the power used at MUE m, Φ_l^0 is the set of FUEs operating on the same subchannel as MUE m, $|h_{l,0}|^2$ is the channel gain between FUE l and the MBS, P_l is the power used at FUE l and σ^2 is the noise variance of the symmetric additive white Gaussian noise (AWGN). Moreover, due to the nature of underlay spectrum access, FAPs are limited by the interference from nearby MUEs and by capacity in terms of number of available spectral resources. As a matter of fact, each FAP n provides a generic FUE l with a link transmission capacity of :

$$\mu_l^{N.C} = \log\left(1 + \frac{|h_{l,n}|^2 P_l}{\sum_{m \in \Phi_m^{n0}} |h_{m,n}|^2 P_m + \sigma^2}\right) \qquad (5.12)$$

where $|h_{l,n}|^2$ is the channel gain between FUE l and its belonging FAP n, Φ_m^n is the set of MUEs operating on the same subchannel as FUE l, $|h_{m,n}|^2$ is the channel gain between MUE m and FAP n.

The probability of successful transmission can be computed as the probability of maintaining the SINR above a target level γ_m and γ_l, respectively for a MUE or a FUE, and is expressed as:

$$P_{s_m} = \Pr\left(\frac{|h_{m,0}|^2 P_m}{\sum_{l \in \Phi_l^0} |h_{l,0}|^2 P_l + \sigma^2} \geq \gamma_m \right)$$
$$P_{s_l} = \Pr\left(\frac{|h_{l,n}|^2 P_l}{\sum_{m \in \Phi_{ml}^0} |h_{m,n}|^2 P_m + \sigma^2} \geq \gamma_l \right) \quad (5.13)$$

To reduce the outage in MUE-MBS transmissions, a Hybrid ARQ protocol is employed at the medium access control layer. Consequently, the effective input traffic $\tilde{\lambda}_m$ from an MUE m, accounting for a maximum of m retransmissions is given by:

$$\tilde{\lambda}_m = \lambda_m \sum_{d=1}^{D} P_{s_m} (1 - P_{s_m})^{d-1} \quad (5.14)$$

We consider M/D/1 queueing delay for the MUEs m, and thus the average waiting time can be expressed by Little‘s law as:

$$\tilde{\lambda}_m = \lambda_m \sum_{d=1}^{D} P_{s_m} (1 - P_{s_m})^{d-1} \quad (5.15)$$

Likewise, we consider M/D/1 queueing delay for the MUEs m, and thus the average waiting time can be expressed by Little‘s law as:

$$D_m^{N.C} = \frac{\tilde{\lambda}_m}{2\mu_m^{N.C}(\mu_m^{N.C} - \tilde{\lambda}_m)} \quad (5.16)$$

Note that once a transmission on a MUE-MBS link drops due to an outage event, it is reiterated up to D times (otherwise dropped), and the increased congestion produces an average higher delay at the end user.

5.2.3 Femtocell Cooperation

We formulate the problem of cooperation between FUEs and MUEs as a coalional game in partition form, whose solution is the concept of the recursive core. The aim of the proposed cooperative approach is to minimize the delay of the MUE transmissions through FUE assisted traffic relay, considering bandwidth exchange as a mechanism of reimbursement for the cooperating FUEs. In existing wireless networks adopting a closed access policy, FUEs and MUEs are typically scheduled independently. As a result, in the considered model, the objectives of the FAPs and the MUEs are intertwined from different viewpoints. At the FAP side, high interference level can be due to MUEs operating over the same subchannel which consequently limits the achievable rates. At the MUE side, poor signal strength reception may result in a high number of retransmissions and higher delays. To overcome this, we propose that upon retransmissions, an MUE delivers its packets to the core network by means of FUE acting as relay terminal. We model each relay FUE as an M/D/1 queue and use the Kleinrock independence approximation. For the relay FUE, cooperation incurs significant costs in terms of delay and spectral resources, since the FUE relays the combined traffic $\tilde{\lambda}_l$ over its originally assigned subchannels. Therefore, it is reasonable to assume that FUEs will willingly bear the cooperation cost only upon a reimbursement from the serviced MUEs. We propose that, upon cooperation, the MUE autonomously delegates a fraction $0 < \alpha \leq 1$ of its own superframe to the serving FUE l. At the relay

FUE l, the portion α is further decomposed into two subslots according to a parameter $0 < \beta_l \leq 1$. The first subslot $\alpha\beta$ is dedicated to relay MUE's traffic. The second subslot of duration $\alpha(1-\beta_l)$ represents a reward for the FUE granted by the serviced MUE, and it is used by the FUE for transmitting its own traffic. This method is known in the literature as spectrum leasing or bandwidth exchange and represents a natural choice for such kind of incentive mechanisms. Figure 5-5 illustrates the considered scenario compared to the traditional transmission paradigm.

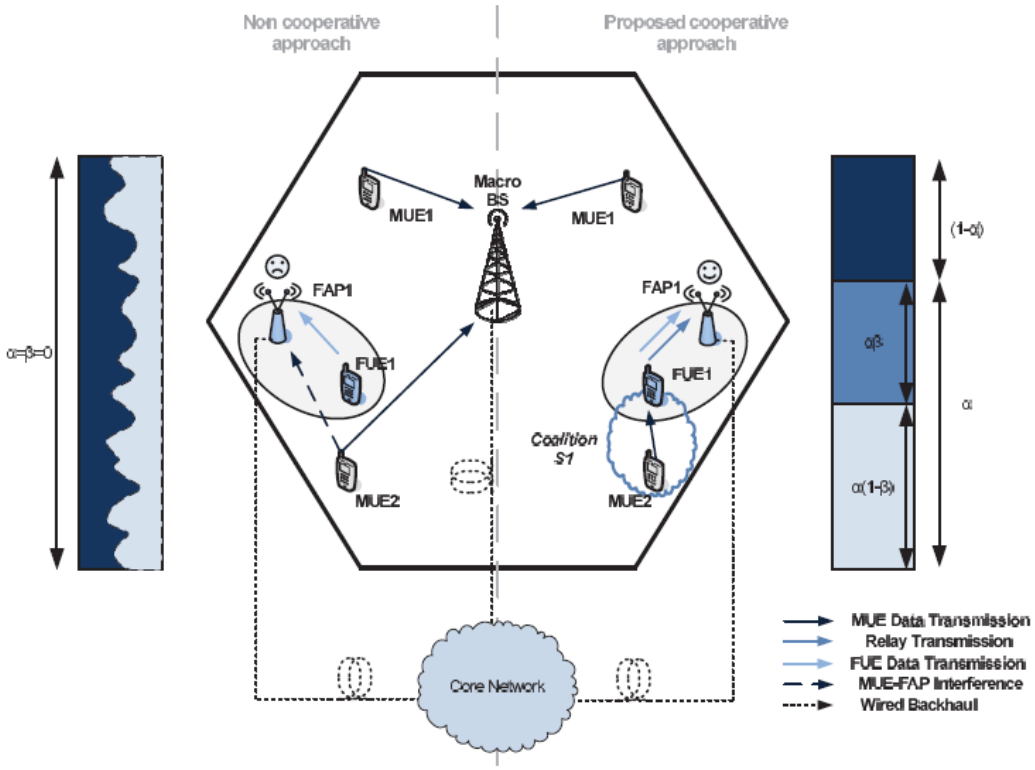

Figure 5-5: A concept model of the proposed solution compared to the traditional non-cooperative approach.

Note that this concept solution allows to align and separate in time the transmissions allowing avoiding interference at the FAP from the MUEs within the coalition. In order to do that, we assume that operations are synchronized. In order to increase their throughput and reduce MUE-to-FAP interference, the FAPs have an incentive to cooperate and relay the MUE's traffic. In this respect, FUEs may decide to service a group of MUEs, and thus form a coalition S_l in which transmissions from FUE l and MUEs within the same coalition are separated in time. The proposed cooperation scheme can accommodate any relaying scheme such as the decode-and-forward or compress-and-forward schemes. In this work, we use a decode and forward relay scheme, assuming that a packet is successfully received. Finally, the achievable service rates for MUEs and FUEs in the cooperative approach become:

$$\begin{cases} \mu_m^C(\alpha, \beta_l) = \min\left\{(1-\alpha)\mu_m^R, \alpha\beta_l\mu_l^R\right\} \\ \mu_l^C(\alpha, \beta_l) = \alpha(1-\beta_l)\mu_l^R \end{cases} \quad (5.17)$$

with

$$\mu_m^R = \log\left(1+\frac{|h_{m,l}|^2 P_m}{\sigma^2}\right)$$

$$\mu_l^R = \log\left(1+\frac{|h_{l,n}|^2 P_m}{\sum_{m\in\Phi_m^{n0}\neq S_l}|h_{m,n}|^2 P_m+\sigma^2}\right)$$

where $|h_{m,l}|^2$ denotes the channel gain of the relay link from MUE $m \in S_l$ and FUE l. Note that the factor $1-\alpha$ is due to the fraction of superframe occupied by the D2D transmission, while the second factor $\alpha\beta_l$ accounts for the fraction occupied by the forward transmission by the FUE. Due to the fact that MUEs are originally assigned orthogonal subchannels, the first hop of the relay transmission is not affected by interference. Moreover, note that by separating the transmissions from MUE and FUE within the superframe, the FUE forward transmissions are affected only by interference from non-cooperative MUEs, outside the coalition. At this point, since the FUE may have to transmit independent packets of its own, the input traffic generation (or the packet arrival at the queue of the FAP) has to account for the packets generated at the FUE and at the MUEs for which the FUEs is relaying. Consequently, the effective traffic $\tilde{\lambda}_l$ generated by FUE l, accounting for its own retransmissions becomes:

$$\tilde{\lambda}_m = (\lambda_l + \sum_m \tilde{\lambda}_m)\sum_{d=1}^{D} P_{s_m}(1-P_{s_m})^{d-1} \tag{5.18}$$

where D is the maximum number of retransmissions before the packet is dropped, $\tilde{\lambda}_m$ and P_{s_m} are computed considering that the SINR this time refers to the FUE-FAP link. Moreover, also in this case, we used the Kleinrock approximation to combine traffic arrival rates from queues in sequence. Furthermore, we model every D2D link as a M/D/1 queue system and investigate the average delay incurred per serviced MUE. For a given MUE m served by FUE l, we express the average delay as:

$$D_m^R = \frac{\tilde{\lambda}_m}{2\mu_m^R(\mu_m^R - \tilde{\lambda}_m)} \tag{5.19}$$

It is important to underline that, to guarantee the stability of the queues, for any MUE m serviced by a FUE in the network, the following condition must hold:

$$\tilde{\lambda}_m < \mu_m^R \tag{5.20}$$

In the event where this condition is violated, the system is considered unstable and the delay is considered as infinite. In this regard, the analysis presented in the remainder of this paper will take into account this condition and its impact on the coalition formation process (as see later, a coalition where $\tilde{\lambda}_m \geq \mu_m^R$ will never form). Having considered this, we now define $D_l^C = \frac{\tilde{\lambda}_l}{2\mu_l^C(\mu_l^C - \tilde{\lambda}_l)}$ as the delay at the FUE for transmitting the aggregated traffic. Finally, we can compute the average delay for an MUE as a sum over the MUE-FUE and FUE-FAP hops, as:

$$D_m^C = D_m^R + D_l^C \tag{5.21}$$

We assume that the relay FUEs performs half-duplex operations, i.e., they first receive the MUE's packets in a transmission window wide $1-\alpha$ in the subchannel originally utilized at the MUE. Successively, each FUE forwards the MUE's packets in the next transmission window wide $\alpha\beta_l$ in a FIFO policy.

5.2.4 Coalitional game concept

It appears clear that MUEs and FUEs have a strong incentive to cooperate to improve their performance using advanced techniques such as relaying and spectrum leasing. Since MUEs and FUEs exhibit a tradeoff between the achievable throughput and the transmission delay, we use a suitable metric to quantify the benefit of cooperation defined as power of the network. Indeed, the power is defined as the ratio of maximum achievable throughput and delay (or a power of the delay). Thus, given a coalition S_l, composed by a set of $|1-S_l|$ MUEs and a serving relay FUE l, we define a mapping function $U(S_l,\Pi_\Phi)$ as:

$$U(S_l,\Pi_\Phi)=\left\{x \mid x_i(S_l,\Pi_\Phi)=\frac{\mu_i^C(\alpha,\beta_l,\Pi_\Psi)^\delta}{D_i^{(C)(1-\delta)}},\forall i\in S_l\right\} \tag{5.22}$$

where δ is a transmission capacity-delay tradeoff parameter to model the service tolerance to the delay. The set $U(S_l,\Pi_\Phi)$ is a singleton set and, hence, closed and convex. Note that, the player's payoff denoted by $x_i(S_l,\Pi_\Phi)$ directly refers to a ratio between the achievable throughput and the average delay for player i in coalition S_l and quantifies the benefit of being a member of the coalition. In consequence, the game (Ψ,U) is an NTU game in partition form and, within each coalition, the utility of the players is univocally assigned.

In order to solve the proposed coalition formation game in partition form, we will use the concept of a recursive core as introduced in [119] and further investigated in [120]-[122]. The recursive core is one of the key solution concepts for coalitional games that have dependence on externalities, i.e., in partition form. Due to the challenging aspect of NTU games in partition form, as discussed in [120]-[122], the recursive core is often defined for games with transferable utility where the benefit of a coalition is captured by a real function rather than a mapping. By exploring the fact that, for the proposed game is a singleton set, then we can define an adjunct coalitional game (Ψ,U) in which we use, for any coalition S_l, the following function over the real line (i.e., similar to games with transferable utility) which represents the sum of the users' payoffs:

$$v(S_l,\Pi_\Phi)=\begin{cases}\sum_{i=1}^{|S_l|}x_i(S_l,\Pi_\Psi) & if \quad |S_l|>1,\quad \alpha>0\\ 0 \quad otherwise\end{cases} \tag{5.23}$$

as the value of the game. Essentially, the recursive core is a natural generalization of the well-know core solution for games in characteristic form, to games with externalities, i.e., in partition form [119], Lemma 10]. In fact, when applied to a game in characteristic function form, the recursive core coincides with the original characteristic form core. The recursive core is a suitable outcome of a coalition formation process that takes into account externalities across coalitions, which, in the considered game, are represented by effects of mutual interference between coalitions.

5.2.5 Distributed implementation of the recursive core

Once a coalition S_l has formed, the FUE l optimizes its own payoff by deciding upon β_l and the transmit power. At the FUEs side, to relay traffic for a set of MUEs incurs a cost that must be taken into account by the FUE before making any cooperation decision. In this paper, we consider a cost in terms of the transmit power that each FUE spends to transmit for the MUEs within the same coalition. Namely, a FUE spends $\beta_l P_l^{(R)}$ to relay MUEs traffic and $(1-\beta_l)P_l^{(R)}$ for its own transmissions, while the overall transmit power is limited by $P_{\max}$ as:

$$\begin{aligned} &\max \quad x_i(S_l, \Pi_N) \\ &s.t. \quad 0 < \alpha, \beta_l \le 1; \quad \beta_l P_l^{(R)} + (1-\beta_l)P_l^{(T)} < P_{\max} \end{aligned} \tag{5.24}$$

Mainly, the FUE is fed back with the estimated aggregated interference from the MUEs m outside the coalition (and included in Φ_m^n), which is practically measured by its own belonging FAP. To reach a partition in the recursive core, the players in Ψ use Algorithm 1 in [18]. This algorithm is composed mainly of three phases: Interferer discovery, recursive core coalition formation, and coalition-level cooperative transmission. Initially, the network is partitioned by $|\Psi|$ singleton coalitions (i.e., non-cooperating mobile users). The MBS periodically requests RSSIs measurements from the MUEs to identify the presence of femtocells which might cooperatively provide higher throughput and lower delays through D2D communication. A similar measurement campaign is carried out at the FUE, as requested by the respective FAP. Successively, for each of the potential coalitional partners, the potential payoffs are computed, considering the mechanisms of spectrum leasing captured. Ultimately, each MUE or FUE sends to the counterpart which ensures the highest payoff a request for cooperation. If both MUEs and FUEs mutually approve the cooperation request, they form a coalition, set up a D2D connection and the MUE acknowledges its MBS about the established a connection. Even during the D2D transmission, the MUEs still maintain a connection to the radio resource control of its original MBS. Being limited by interference, the most eligible partners for FUEs are dominant interfering MUEs, while, vice versa for a MUE, the higher utilities are granted by FUE in the vicinity or experiencing good channel gains. The recursive core is reached by considering that only the payoff-maximizing coalitions are formed. Clearly, this algorithm is distributed since the FUEs and MUEs can take their individual decisions to join or leave a coalition, while, ultimately reaching a stable partition, i.e., a partition where players have no incentive to leave the belonging coalition. Those stable coalitions are in the recursive core at the end of the second stage of the algorithm. Finally, once the coalitions have formed, the members of each coalition proceed to construct a D2D link and perform the operations described in Section III. As a result, intra-coalition uplink interference at the respective FAPs is suppressed and the MUEs achieve lower delays. In addition, by cooperatively solving the strongest interference, the FUEs achieve the maximum achievable payoff, and, therefore, have no incentives to break away from the belonging coalitions since it would lead to lower payoffs. Thus, the formed coalitions represent a stable network partition which lies in the recursive core.

5.2.6 Simulation Results

We consider a single hexagonal macrocell with a radius of 1 Km within which N FAPs are underlaid with M MUEs. Each FAP N serves $L_n = 1$ FUE scheduled over orthogonal subchannel, adopting a closed access policy. We set the maximum transmit power at MUEs and FUEs to $P_{\max} = 20$ dBm, which includes both the power for the serviced MUE's and its own transmissions. The considered macrocell has 500 available subcarriers, each one having a bandwidth of 180 KHz, and dedicates one OFDMA subchannel to femtocell transmissions. In Figure 5-6, we evaluate the performance of the proposed coalition formation game model by showing the average payoff achieved per MUE during the whole transmission time scale as a function of the number of MUEs M. We compare the performance of the proposed algorithm to that of the non-cooperative case, for a network with 50, 100, 200 FAPs using a closed access policy. The curves are normalized to the performance of the non-cooperative solution. For small network sizes, MUEs do not cooperate with FUEs due to spatial separation. Thus, the proposed

algorithm has a performance that is close to the non-cooperative case for M < 60. As the number of MUEs grows, the probability of being in proximity of an FUE gradually increases and forming coalitions becomes more desirable. Hence, the MUEs become connected to a nearby FUE which allows for a higher SINR, allowing for high values of payoff. For example, Figure 5-6 shows that cooperating MUE can gain up to 75% with respect than the non-cooperative case in a network with N = 200 FAPs and M = 160 MUEs. In fact, Figure 5-6 clearly shows that the average payoff per MUE increases in the cooperative case as the number of femtocells is large. It is also demonstrated that the proposed coalitional game model has a significant advantage over the non-cooperative case, which increases with the probability of having FUEs and MUEs in proximity, and resulting in an improvement of up to 205% for M = 200 MUEs.

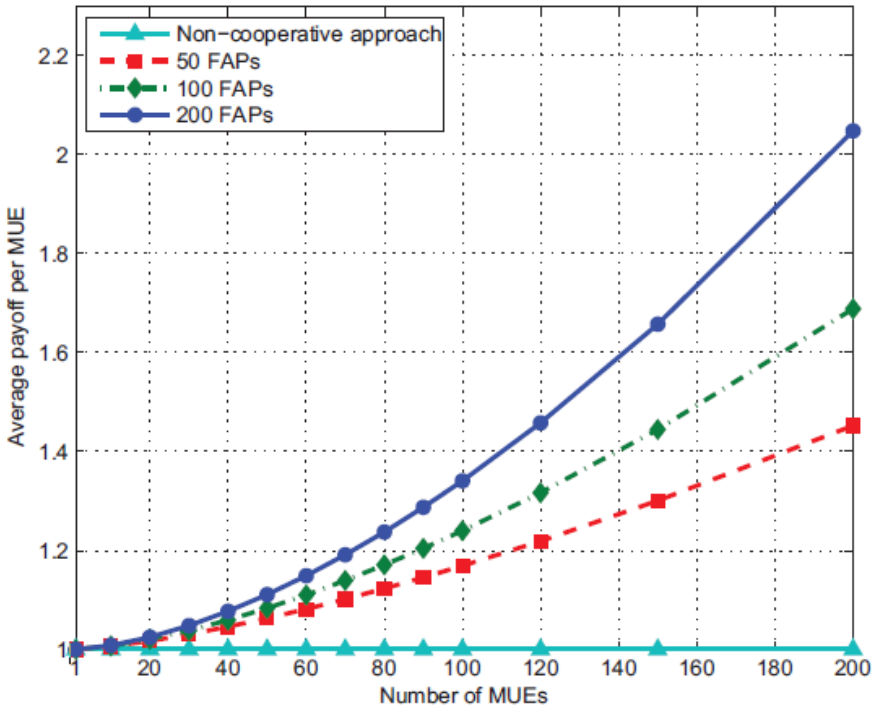

Figure 5-6: Average individual payoff per MUE, normalized to the average payoff in the non-cooperative approach, for a network having N = 50, 100, 200 FAPs, δ = 0.5, r = 20m.

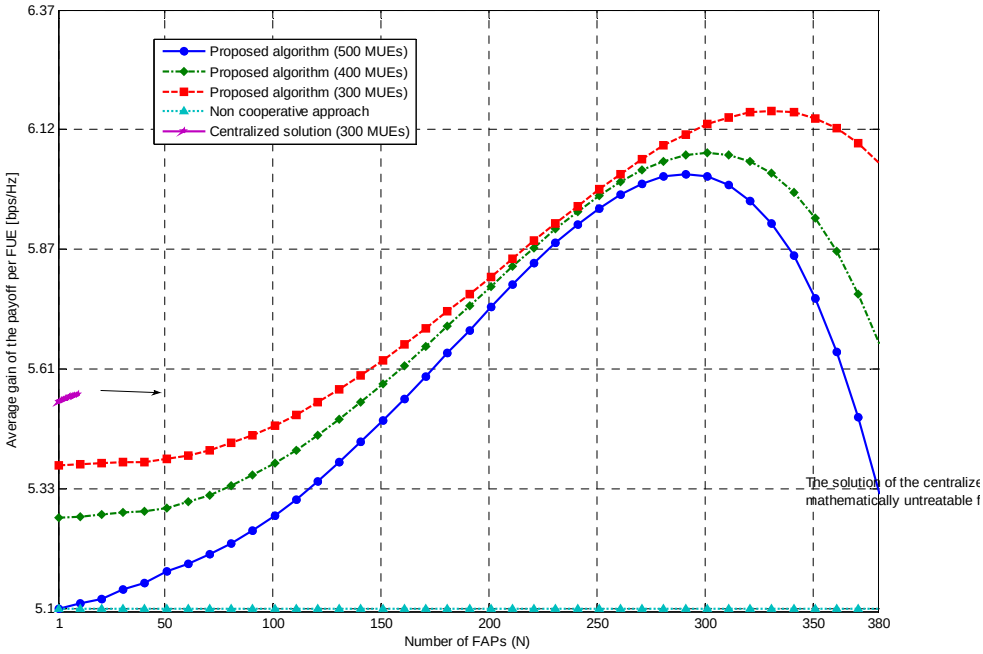

Figure 5-7: Average individual payoff per FUE, normalized to the average payoff in the non-cooperative approach, for a network having M = 300, 400, 500 MUEs, δ = 0.5, r = 20.

In Figure 5-7, we show the average payoff per FUE as a function of the number of FAPs in the network N, for different number of MUEs M = 300, 400, 500 and normalize the curves to the performance of the non-cooperative solution. As previously seen, cooperation seldom occurs in cases where MUEs and FUEs are spatially separated, as for low numbers of FUEs in the network. Nevertheless, as the density of FAPs increases, coalitions start to take place yielding to higher gains for the FUEs. For instance, Figure 5-7 shows that the average payoff per FUE resulting from the coalition formation can achieve an additional 15% gain with respect to the non-cooperative case, in a network with N = 200 FAPs and M = 500 MUEs. Therefore, we demonstrated how cooperation can be beneficial to the FUEs in highly populated areas where the density of interferers (i.e., potential coalitional partners) is high. Finally note that, since the femtocells are orthogonally scheduled, the performance of each FUE in the non cooperative approach is transparent to the density of femtocells in the network.

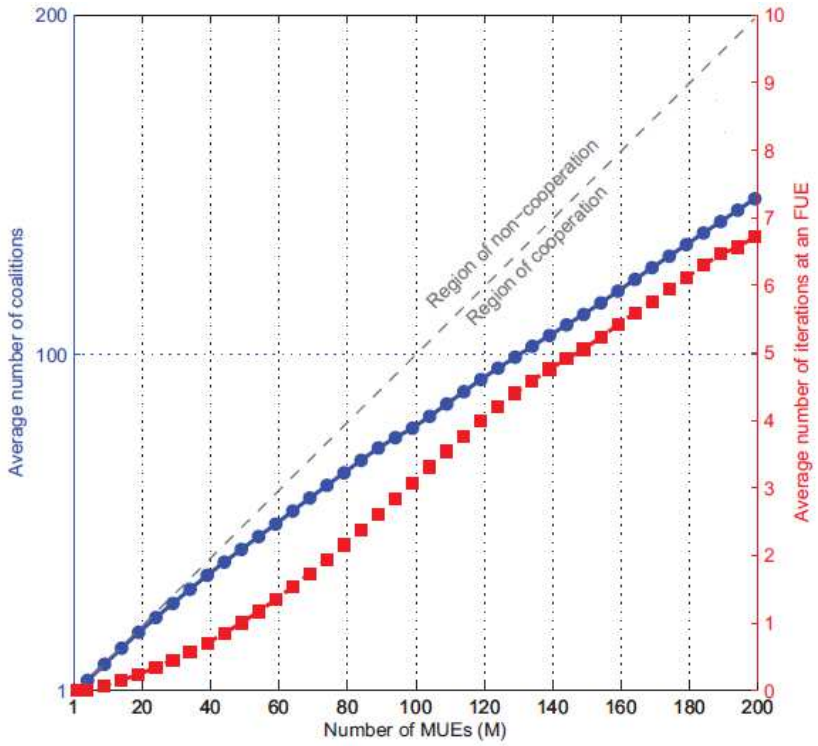

Figure 5-8: Average number of iterations till convergence and average number of coalitions as a function of the number of MUEs in the network. The bisectrix delimits the area of cooperation and non-cooperation, therefore, the points on the bisectrix represent full non-cooperative MUEs, denoted by singleton coalitions. N = 200, δ = 0.5.

Figure 5-8 shows the growth of the number of coalitions, i.e., the size of a partition in the recursive core, while the number of MUEs increases. Additionally, the average number of iteration in the proposed algorithm is observed. The network is initially organized in a non-cooperative structure where each player (i.e., MUE or FUE) represents a singleton coalition, therefore the number of coalitions equals the number of players in the network (grey dotted line) and, since interferers are out of range of cooperation, the number of iterations is minimum. Initially, for M < 40 cooperation seldom occurs, due to the large distance between potential coalitional partners. As M increases, the network topology changes with the emergence of new coalitions. For example, when N = 200 FAPs and M = 200 MUEs are deployed, 138 coalitions take place, requiring an average number of algorithm iterations of 6.9. Therefore, it can be seen that the incentive towards cooperation becomes significant when the femtocells' spectrum becomes more congested and femtocells are densely deployed in the network. Eventually, for larger M, the process of coalition formation is limited by the number of MUEs which a relay FUE can service, given the mechanism of reimbursement.

5.2.7 Conclusions and future work

We have introduced a novel framework of cooperation among FUEs and MUEs, which has a great potential for upgrading the performance of both classes of mobile users in next generation wireless femtocell systems. We formulated a coalitional game among the FUEs and MUEs in a network adopting a closed access policy at each femtocell. Further we have introduced a coalitional value function which accounts for the main utilities in a cellular network: transmission delay and achievable throughput. To form coalitions, we have proposed a distributed coalition formation algorithm that enables MUEs and FUEs to autonomously decide on whether to cooperate or not, based on the tradeoff between the cooperation gains, in form of increased throughput to delay ratio, and the costs in terms of leased spectrum and transmit power. We have shown that the proposed algorithm reaches a stable partition which lies in the recursive core of the studied game. Results have shown that the performance of MUEs and FUEs are respectively limited by delay and interference, therefore, the proposed cooperative strategy can provide significant gains, when compared to the non-cooperative case as well as to the closed access policy.

5.3 Spatial and Time Domain based Interference Coordination in Heterogeneous Networks

In [110] the concept of **B**ase **S**tation **C**oordinated **B**eam **S**election (BSCBS) has been introduced and preliminary simulation results were presented. In this contribution further analysis of BSCBS is provided including simulations for larger antenna configurations. The main idea of BSCBS is to coordinate selection of beams at neighboring cells to avoid beam 'collision' when two nearby cell-edge users in different cells are served using the same time-frequency resources. Currently, In LTE Rel-10, a time domain based interference management scheme, called **e**nhanced **I**nter **C**ell **I**nterference **C**oordination (eICIC) is specified [4], which aims to reduce interference by blanking subframes in time domain. A comparison between the proposed spatial domain scheme and the currently specified time domain interference coordination schemes is provided as well.

5.3.1 Coordinated Beam Selection based on Restriction Requests

The algorithmic description of BSCBS provided in **[110]** shall be briefly repeated here. The general idea of beamforming for transmitting data to mobile users in a wireless network with sectorized base station antennas is to radiate most of the power into the desired direction. A beam directed towards a cell-edge user may cause significant interference to a nearby user in an adjacent cell when both users are served at the same time-frequency resources. Performance gains can be expected when the selection of beams can be coordinated in neighbour cells in such a way that beam collisions between nearby cell-edge users can be avoided. An example situation is shown in Figure 5-9. Beam collisions can be avoided by coordinating the selection of precoding matrices in different cells. The coordination is based on feedback from UEs including not only CQI, Rank Indicator (RI) and Precoding Matrix Indicator (PMI), but also different types of additional messages to support the cooperation. For example, a RESTRICTION REQUEST (RR) feedback message from the UE contains information about unwanted precoding matrices. The users request in advance the restriction of the usage of certain precoding matrices in neighbour cells over the resources that could be used for data transmission at a later time instant. More details of the message design are provided in **[110]** and **[133]**.

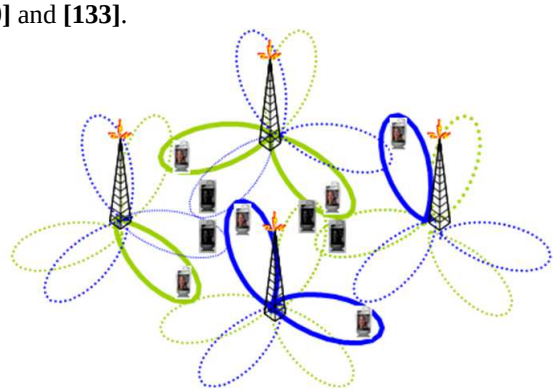

Figure 5-9: Avoidance of beam collisions

The overall goal of the coordination approach is then to maximize a network (cluster) wide utility metric over all the combinations of precoding matrices considering the restriction request from received from users. This requires the exchange of messages between base stations over the X2 interface that logically connects base stations with each other in LTE. In order to keep the information exchange acceptable both in delay and complexity, a scheduling design was chosen that can be added on top of the Rel. 8 scheduling functionality. The flow chart of the scheduling approach is shown in Figure 5-10.

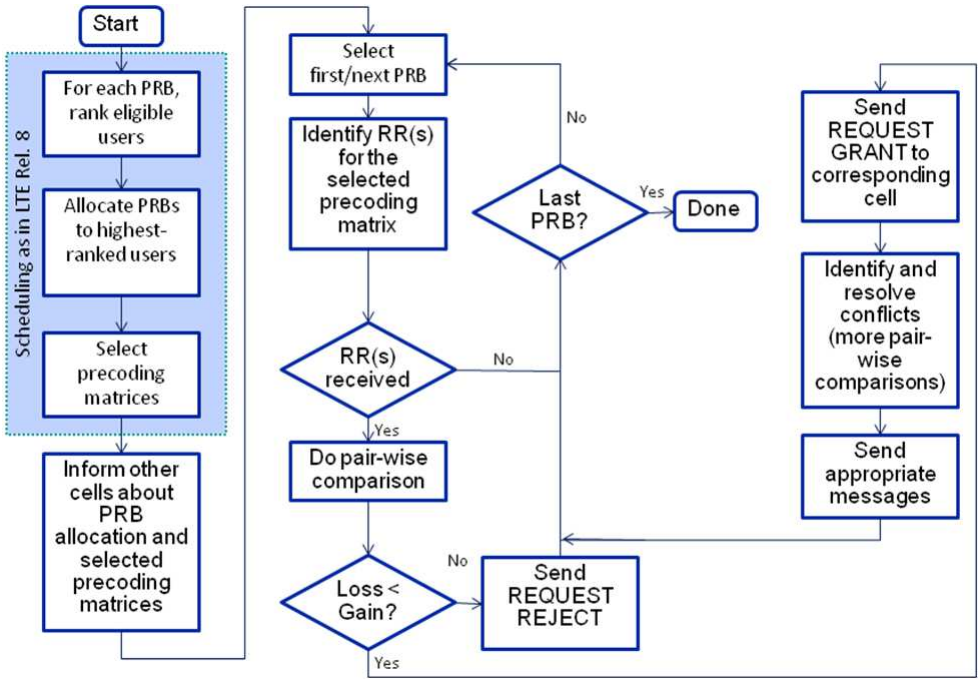

Figure 5-10: Flow chart of scheduling approach

The main steps of the coordination approach are as follows:

- As a first step, the coordinating cells make tentative scheduling decisions without considering any RR reports. This scheduling is then the same as would be done in an LTE Rel. 8 system.
- In the next step, the scheduler at each cell compares the precoding matrices identified in the received RR reports with the precoding matrices selected for tentatively scheduled UEs. In case of valid precoding matrix restrictions (explained later in detail), the scheduler decides about accepting or rejecting the requests after comparing a given UE utility metric. In case the precoding matrices are restricted at the cell, the UE(s) that requested the restriction in the first place should see a gain in their utility metrics (given the interference situation does not change much when the data is actually transmitted). On the other hand, the restriction of the preferred (or most suitable) precoding matrices might result in an utility loss for a UE when served by the cell. To compute utility gains, the required information is reported by the UEs in their respective RRs. Based on the result of a utility comparison, the following two cases are possible.
    a. If the overall utility gain in the other coordinating cells is larger than the utility loss in the own cell, the cell revises its tentative scheduling decision and restricts the precoding matrices in question. It informs the serving cells of the UEs from which it received the corresponding RESTRICTION REQUESTs by sending REQUEST GRANT messages.
    b. If the overall utility gain is smaller than the utility loss, REQUEST REJECT messages are sent to the serving cells. In this case, the scheduler keeps its tentative scheduling decisions.
- If the REQUEST GRANT messages sent and received by a cell contradict each other, conflict resolution is done based on a comparison of net utility gains of the contradicting grants. Depending on the result of this comparison, the cell either revokes it own grant and goes back to using the original scheduling decision or rejects the received grant by sending a GRANT REJECT message to the source cell.

5.3.2 Simulation results for Dual Stripe Femto Model

A time line for the message exchange has been provided in [110]. Preliminary simulation results for 2x2 antenna configurations have been presented in [110] as well. Since BSCBS coordinates a single interferer that is perceived by the UE as strongest, it is clear that BSCBS is most beneficial if a small number or, in particular, a single strong interferer is present that impairs the communication link between the UE and the serving cell. Such situations are likely to appear in scenarios where femto cells with closed subscriber group (CSG) functionality are deployed. If a UE outside the subscriber group is in the vicinity of a femto cell that is not serving it, the interference caused by this femto cell can cause degraded SINR at the out-of-CSG macro UE and possibly lead to outage. A model for such a situation is a hexagonal macro cell

layout and dual stripe clusters of femto cells. Each femto cell served at least a single UE within its CSG. In order to simulate the case that a macro user is in the vicinity of a femto cell, the placement of macro users is non-uniform. 80% of the macro users are placed within the dual stripe cluster and 20% are placed uniformly within the macro cell. Figure 5-11 shows the scenario where macro UEs are inside the dual stripe cluster.

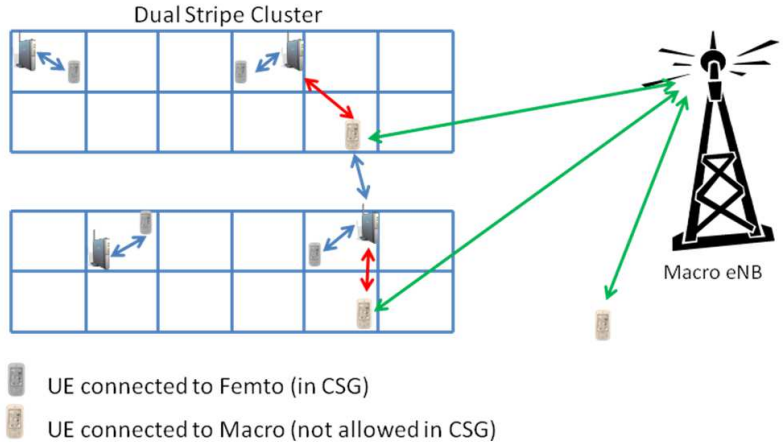

Figure 5-11: Impairment of macro UEs by CSG femto cells

Preliminary simulation results for 2x2 antenna configurations have been provided in [110]. These simulations have been extended to 4x2 antenna configuration. The simulation assumptions are provided in Table 5-1. In the simulations it is assumed that each RESTRICTION REQUEST message sent by the UE covers a frequency subband of 5 PRB (called frequency validity of 5 PRB in the following). The subband validity of such a message exploits the frequency dependency of the spatial domain.

Table 5-1: Simulation assumptions

Parameter	Setting
Channel Model	SCME urban macro, 1.4MHz bandwidth
Macro eNB antenna configuration	4 antennas. λ/2 spacing, vertically polarized, 3 sectors (cells) per eNB
Macro user distribution	10 UEs per macro cell
Scheduler, traffic model	Proportional fair, full buffer
UE equalizer	MRC
Coordination threshold	Only UEs below -3dB geometry use coordination
Link adaptation	Ideal, no HARQ (Hybrid Automatic Repeat Request)
CQI Feedback delay	7ms
X2 message delay	<< 1ms
Allowed codebook restriction:	Restrict 0 (0%), 16 (50%), 24 (75%), 28 (88%) or 32 (100%) PMIs from the LTE Rel. 8 codebook with 32 entries for 4 Tx antennas and 2 Rx antennas
Femto layout	Dual Strip, 1 cluster per macro cell, urban deployment
Node type	Femto (PL and SF according to 3GPP TR 36.814 urban deployment, closed access)
Femto antenna configuration	4 antennas, λ/2 spacing, vertically polarized, isotropic
UE antenna configuration	2 antennas, λ/2 spacing, vertically polarized, isotropic
Femto deployment ratio	0.05

Probability of indoor macro user (close to femto)	0.8
Femto user distribution	3 CSG users per femto
Frequency validity of a RR message	5 PRB
Algorithm version	a) w/o utility comparison (accepting all RRs) b) w/ utility comparison

Figure 5-12, Figure 5-13 and Figure 5-14 show the throughput CDFs for CSG femto UEs, macro UEs w/ and w/o sending RESTRICTION REQUEST messages.

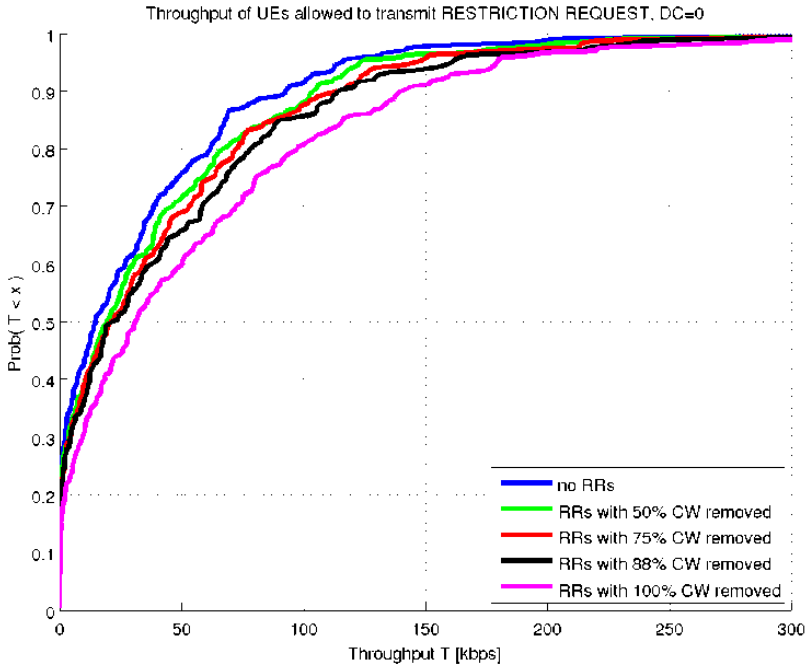

Figure 5-12: Throughput of Macro UEs sending RESTRICTION REQUEST Messages

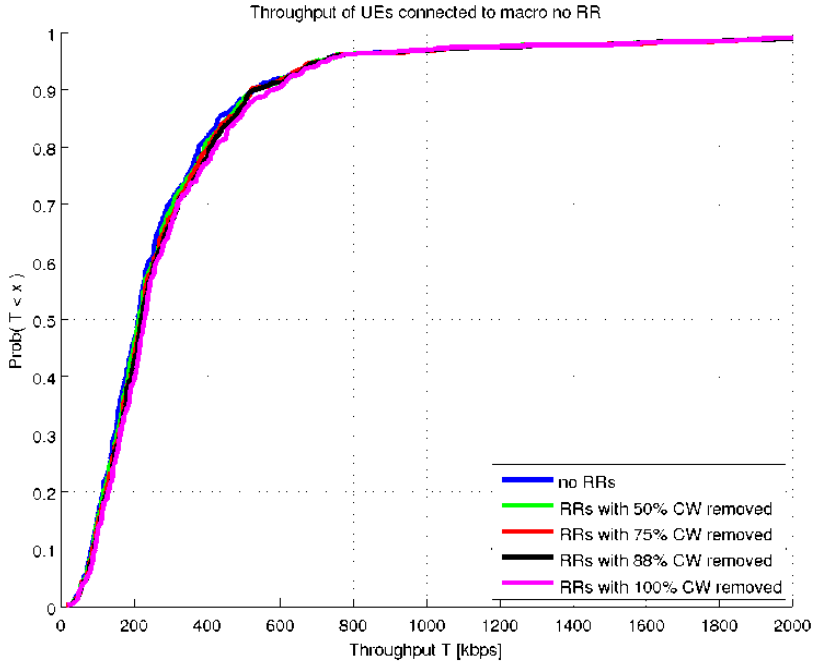

Figure 5-13: Throughput of Macro UEs not sending RESTRICTION REQUEST Messages

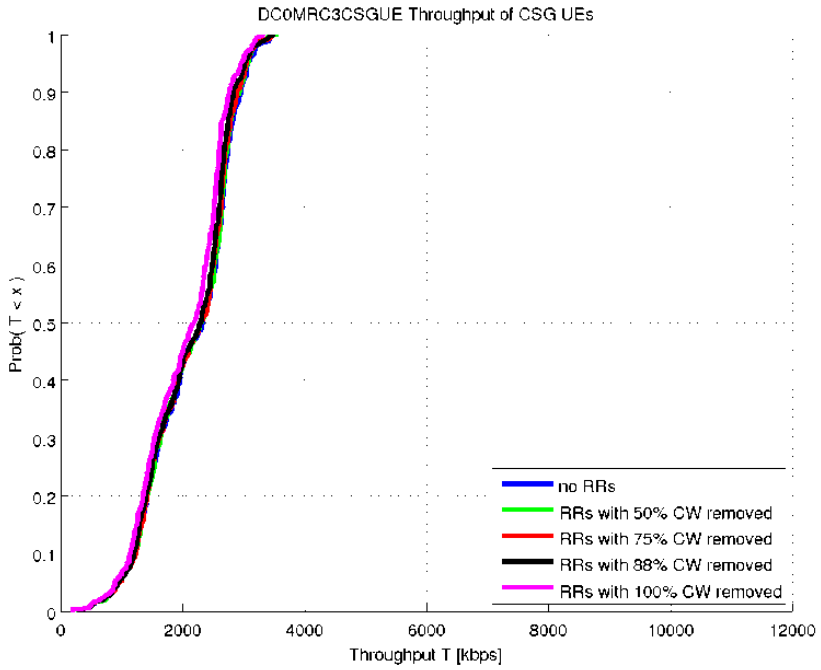

Figure 5-14: Throughput of CSG Femto UEs

It is seen in Figure 5-12 that the macro UEs that are allowed to send RR messages (i.e. whose geometry is below – 3 dB) benefit significantly from the reduction in interference by avoiding unfavourable beams in the femto cell. Obviously, the gains become the larger the more codebook entries are restricted. Figure 5-13 shows that even macro UEs better RF conditions (i.e. whose geometry is larger than -3 dB) benefit slightly from restricting beams in the femto cell. Gains are again largest, if the femto restricts all beams in the current subframe since then the femto does not generate interference at all.

Of course, restricting codebook entries in a subframe reduces the available resources in the femto cell and leads to a throughput reduction in the femto cell. However, Figure 5-14 reveals that throughput loss is not very significant. The reason for that is that the macro UE that demands restricting beams in the femto cell is scheduled only in certain subframes. In other subframes when the macro UE is not scheduled, no beams in the femto cell need to be restricted. Then all resources in the femto cell are available and instantaneously no throughput loss occurs. Again, as Figure 5-14 shows, the loss is the largest the more codebook entries are restricted. But even in the case of 100% codebook restriction the losses are negligible.

The absolute median user throughput for the femto UEs is about 2.1 Mbits/s. Since the bandwidth in the simulations is 1.4 MHz, the spectral efficiency that one user achieves is 1.5 bits/s/Hz. Since 3 users are active in each femto cell, the median spectral efficiency for the cell throughput of the femto cell is 4.5 bits/s/Hz/femto cell.

Figure 5-15 shows the mean relative gain in throughput for the macro and femto UEs compared to the reference system without codebook restrictions. It is seen that the macro UEs in close vicinity to the CSG femto UEs can benefit significantly by codebook restrictions. As already mentioned the throughput loss for femto UEs is small. Figure 5-15 shows that in average 5% throughput reduction for femto users needs to be taken into account by improving the throughput for macro users that suffer from strong interference by the femto cell.

However, due to the low load in a femto cell each femto user experiences a spectral efficiency of 1.5 bits/s/Hz. 5% throughput reduction still provides a spectral efficiency of 1.425 bits/s/Hz which corresponds to 14.25 Mbits/s in 10 MHz compared to 15 Mbits/s in the reference system. This loss seems to be acceptable for the femto users since absolute throughput is still tremendous.

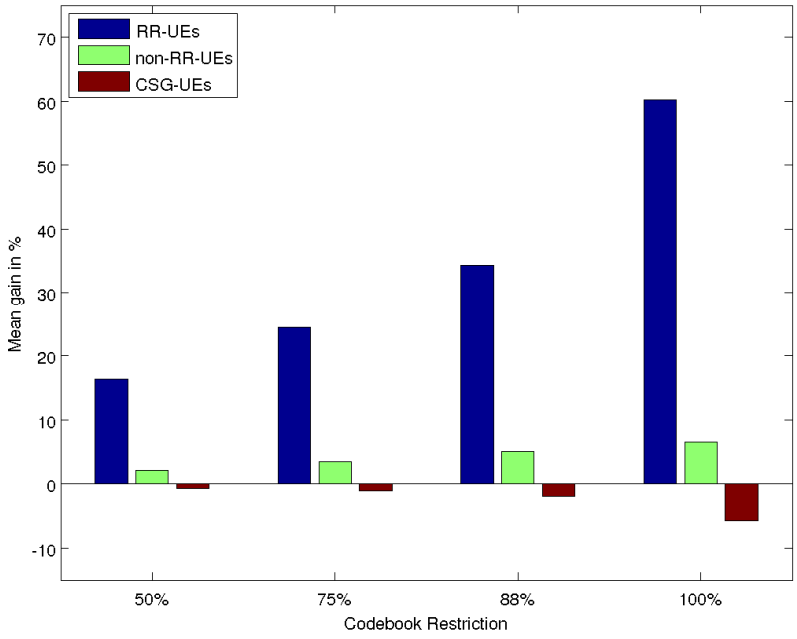

Figure 5-15: Mean Relative Gain of Macro and Femto UEs

5.3.3 Comparison with eICIC in LTE Rel-10/11

The interference coordination scheme described in the previous sections aims to control the interference in spatial domain by restricting codebook entries on a per subframe basis. The performance analysis revealed that the designed scheme performs best if the entire codebook is instantaneously restricted for the frequency validity of the RESTRICTION REQUEST message (5 PRBs in the analysis above). If no codebook entry is available for usage the femto cell does not transmit any data in this subframe over the indicated PRBs, i.e. the subframe is blanked in time domain over a frequency subband. In this sense the coordination scheme in spatial domain transforms to a coordination scheme in time domain. It can

therefore be concluded from the analysis presented here that coordination schemes in time domain provide a very efficient solution for coordinating interference in heterogeneous networks.

A pure time domain interference coordination scheme is currently specified in 3GPP LTE Rel-10 under the name eICIC [4]. Coordination of the interference is achieved by introducing so-called **A**lmost **B**lank **S**ubframes (ABS) as illustrated in Figure 5-16.

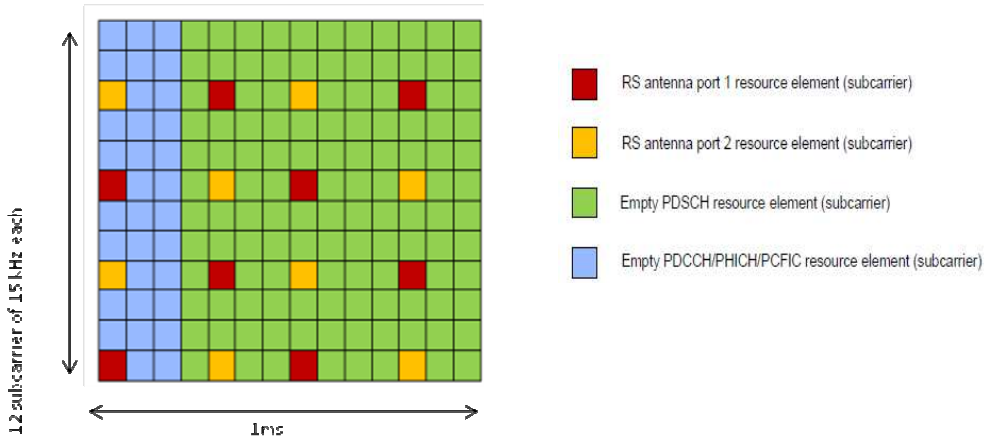

Figure 5-16: Almost Blank Subframes (ABS) in LTE Rel-10

In ABS no data and control channels (PDSCH/PDCCH) are transmitted in order to reduce interference to neighbour cells in those subframes. Only the cell-specific reference signals (CRS), synchronization signals and network information are sent to ensure backward compatibility. Comparing this approach to the spatial domain scheme of the previous section, it can also be seen as a scheme that restricts usage of all codebook entries in a ABS. Hence, time domain scheme is a special case of a spatial domain scheme if the entire codebook is restricted in a subframe.

In the spatial domain scheme of the previous section, the macro UE sent RESTRICTION REQUEST (RR) messages to its serving cell (i.e. the macro cell), which then forward the RESTRICTION REQUEST message over the X2 interface to the cell that causes strong interference to the macro UE (i.e. the CSG femto cell). In the designed scheme the X2 messages can be sent each subframe, i.e. each 1ms. Two different algorithms have been investigated:

a) The femto cell accepts all RR messages w/o utility comparison: This approach provides largest benefits to the macro UEs that sent RR messages

b) The femto cell only accepts RR messages if the utility metric is increased: This approach aims to maximize average cell throughput but may not significantly improve performance of cell edge macro UEs

In eICIC it was decided that the aggressor cell (i.e. the CSG femto cell) decides autonomously on its own how many subframes shall be configured as ABS. The victim cell (i.e. the macro cell) is only allowed to invoke the aggressor that more ABS are needed to ensure sufficient performance for the cell edge macro UEs. However, the CSG femto cell does not have to follow this invocation. This can be seen as a correspondence to algorithm b) above. The reason why a concept like algorithm a) above was not adopted in Rel-10 is that multiple victims invoking ABS may take away too many resources from the aggressor.

Figure 5-17 shows an macro – pico cell example how the aggressor cell informs the victim cell which subframes are configured as ABS. This knowledge is important for the victim cell since it needs to ensure that the suffering cell edge user is scheduled in this subframe that is declared as ABS in the aggressor. Note that this requires time synchronization at subframe level between aggressor and vitim cell. The X2 message in eICIC is a simple bitmap of length 40 bits where each bits indicates ABS or regular subframe. It has been decided in 3GPP that this bitmap can be updated with a granularity of 40ms compared to 1ms update rate of the designed scheme.

The codebook restrictions required in the designed spatial coordination scheme BSCBS can also be indicated over X2 by means of a bitmap, where each entry indicates whether the codebook entry is allowed or not. For a 4x2 antenna configuration a bitmap of length 32 bits is required. In case that the special case of full codebook restriction corresponding to time domain coordination is applied a single bit

is sufficient, results in the same X2 data rate for BSCBS and eICIC (1bit/1ms in BSCBS, 40bits/40ms in eICIC), if each RR message has a frequency validity of the entire system bandwidth.

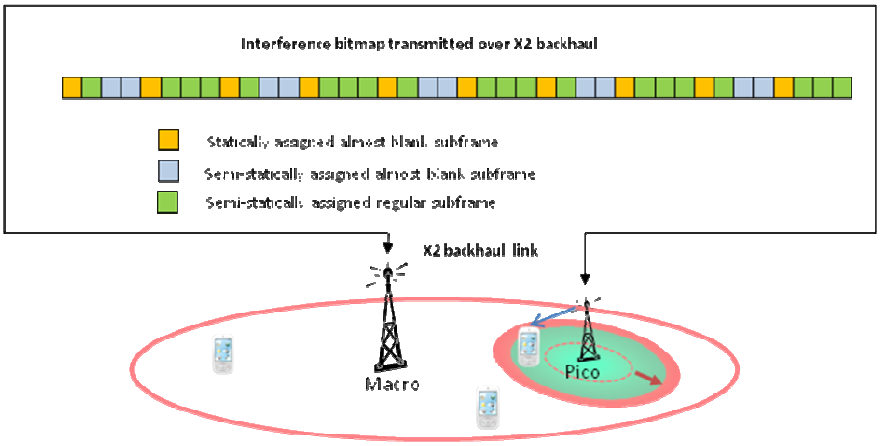

Figure 5-17: Information Exchange over the X2 Interface

The design of the RR messages in BSCBS allows that each message covers a subband of a certain length. In the simulations in the previous section it has been assumed that this frequency validity is 5 PRB. This means that the aggressor may apply codebook restrictions in a subframe for the indicated PRBs only. This offers another dimension in the coordination. In eICIC the frequency dimension is not exploited. Here a ABS applies for the entire system bandwidth in frequency domain. In this sense, BSCBS offers more flexibility than eICIC.

BSCBS relies on measurements conducted by the UE and sent over the uplink air interface to the serving cell. Therefore the specification in 3GPP of BSCBS would also impact the air interface since new messages are required to support the restriction of codebook entries. In eICIC, however, the uplink air interface is not impacted, since coordination is only done in time domain. In eICIC existing downlink measurements are sufficient to indicate the presence of a strong interferer.

System level performance evaluation of eICIC can be found in **[134]** and the references therein.

5.3.4 Conclusion

In this contribution the designed interference coordination scheme in spatial domain (BSCBS) has been analyzed further. It has been shown that BSCBS allows improving the performance of UEs suffering from strong interference significantly. In the considered macro – CSG femto cell deployment scenario the performance degradation of the femto users is marginal. The results indicate that the largest gains are achieved for full codebook restriction, which transforms the spatial coordination into time domain coordination. This verifies the efficiency of time domain interference coordination in heterogeneous scenarios. Such a time domain interference coordination scheme is currently specified in 3GPP LTE Rel-10 (eICIC). A design comparison between BSCBS and eICIC has been conducted revealing several similarities between both schemes but also some differences, e.g. the impact on the air interface in uplink and the availability of a frequency domain in BSCBS. From this comparison between BSCBS and eICIC it can be concluded that the main design goal of eICIC in LTE Rel-10 was simplicity, as less standard impact as possible and robustness. The system level results in [134] show that still large system capacities gains can be achieved by pure time domain coordination. BSCBS introduces a frequency component in the interference coordination which is not available in eICIC. It remains to be shown whether this additional feature enlarges the gains of time domain interference coordination even further. In near future Coordinated Multipoint (CoMP) will be introduced in LTE Rel-11. Such schemes are able to provide interference coordination jointly in time, frequency and spatial domain. It is an interesting area for further investigation, whether joint coordination in all domains provides further gains in heterogeneous networks compared to pure time domain coordination as eICIC does.

6. SON for Improving Energy Efficiency

The emphasis of this section is on energy efficiency within the context of SON.

6.1 Energy-Aware Self-Organized Networking Enabled Co-Channel Femtocell

In this section, we consider that a co-channel femto cell sharing the spectrum with the overlaid macrocell is randomly deployed within a service radius of the macrocell. With regard to the co-channel femto cell, we design a generic energy usage model in such a way that energy usage by femto cell users at both the signalling and the data phases is taken into consideration. Considering the worst-case scenario of interference when femto cell users are deployed in a corner of the femto cell nearest toward the macrocell, autonomously self-organizing techniques of the energy usage at the femto cell are proposed while satisfying constraints on both the interference toward the macrocell and the energy requirements.

6.1.1 System and channel models

Concern a co-channel femto cell network that supports a circularly serviced area with the radius r^{f_o} and opportunistically operates over the same spectrum as the overlaid macrocell network, serving a coverage radius r^{m_o}. The serviced area by the co-channel femto cell access point (FAP) is assumed to be randomly deployed within the coverage of the macrocell network. We assume that the distance (denoted by d_o) between the FAP and the MBS can be known at the FAP by using conventional positioning approaches (e.g., macrocell signals, enhanced cell identification, and global positioning system (GPS) [108]) and SON enabling techniques developed in D4.1 [110].

Consider uplink communications via orthogonal channels in the frequency domain (e.g., 3GPP's LTE [109]). Let $\overline{K}^f$ femto cell users (FUEs) each having a single antenna intend to communicate with the FAP having *d* receive antennas. Suppose that the wireless channel per antenna pair between each FUE to the FAP is flat Rayleigh fading and the channel coefficients are independent and known perfectly at the FAP. The corresponding received signal to the interference and the noise ratio (SINR) at the FAP from FUE i can be given as

$$\rho^{f_i} = \frac{\Theta_f x_{f_i} P_1^{f_i} / \mathrm{PL}_{f_i}}{I_o^f + \sigma^2}, \qquad \forall i \tag{6.1}$$

where x_{f_i} is a channel gain as a Chi-square distributed random random variable with *2d* degrees of freedom (i.e., $x_{f_i} \sim \chi^2_{2d}$), $P_1^{f_i}$ is the power of the data transmission, PL_{f_i} is a path loss toward its FAP, $I_o^f = \sum I_o^{mf_j}$ denotes the aggregated interference on average from both the neighbouring macrocell users (MUEs) and co-channel femtocell users, and σ^2 is the variance of the complex-valued zero-mean additive white Gaussian noise (AWGN). In this equation, notice that PL_{f_i} can be represented as

$$PL_{f_i} = L_1^f + L_2^f \log_{10} r^{f_i} \tag{6.2}$$

where L_1^f represents the penetration loss in the femto cell, mainly caused by indoor walls, L_2^f denotes the path loss exponent in the femto cell transmission, and r^{f_i} (m) is a random (but static) distance between the transmitter and the FAP.

Based on this path loss, FUE i, $\forall i$ transmitting at the distance r^{f_i} with respect to the FAP selects a transmit power level $P_1^{f_i} = P_1^f \Lambda_{f_i}$, where $\Lambda_{f_i} = \left(r^{f_i}\right)^{L_2^f/10} 10^{L_1^f/10}$ denotes a compensation component for the attenuation (i.e., a path loss) such that the FAP receives the desired power P_1^f on average.

Similarly, the j-th macrocell user equipment (MUE *j*) at a random distance r^{m_j} with respect to the MBS selects its transmit power level $P^{m_j} = P^m \Lambda_{m_j}$, where $\Lambda_{m_j} = \left(r^{m_j}\right)^{L_2^m/10} 10^{L_1^m/10}$ is the attenuation

compensation component in the macrocell network, and similarly to the femto cell transmission, L_1^m and L_2^m are the loss of the penetration and the path loss exponent in the macrocell transmission, respectively.

By transmitting at $P_1^{f_i}$ power, FUE i causes the cross-interference received at the MBS by

$$I_o^{fm_i} = \Theta_m P_1^{f_i} / \mathrm{PL}_{f_i^c} \qquad (6.3)$$

where $\mathrm{PL}_{f_i^c} = L_1^f + L_2^f \log_{10}\left(r^{f_i^c}\right)$, $r^{f_i^c}$ is the counterpart distance toward the MBS, and Θ_m is a log-normal distributed attenuation caused by shadowing from FUEs to the MBS.

Notice, as per our system model, that the FAP experiences interference caused by neighbouring macrocell UEs as well as co–channel femto cell UEs active in other FAPs. In particular, thelatter interference source is located far away from the victim FAP since these interferers from theco–channel femto cells are not from femto cells, who are near to the victim FAP and coordinatesto operate in orthogonal manner. While, the former interference source is from macrocell UEs
who are near to the victim FAP. Therefore, due to the fact that typically the transmission power
by macrocell UEs is stronger than that of the femto cell UEs, the interference is dominated
by the source of the neighbouring macrocell UEs and its expression is straightforward from the above equation and is omitted here.

In the above co-channel femto cell network, we address an energy-aware self-organizing technique on energy usage over the femto cell users. First, notice the fact that in conventional self-organizing mechanisms, there inevitably exist following two different main phases of energy usage:

i. Phase 0: is to represent signalling energy phase in which signalling information is exchanged,
ii. Phase 1: is to represent data-transmission energy phase in which data transmission occurs.

Particularly, we propose operations in the two phases as follows. In Phase 0, the FAP self-organizes only a subset of K^f FUEs randomly selected at every time slot. Here, the size of the subset is set to $K^f \le \overline{K}^f$ and the corresponding entries of the subset are random according to the uniform distribution such that FUE i for all i are equally likely activated. Moreover, the average power level of the activated FUEs is autonomously adjusted such that the sum cross-interference by all FUEs toward the MBS remains below the desired level. In Phase 1, we consider the opportunistic transmission in such a way that among the subset of K^f activated FUEs given at Phase 0, only the best FUE is admitted to access the femto cell network. Finally, the criterion of selecting the best FUE is to find the user whose index is defined as $f_{i^*} := \arg\max_{f_i} \rho^{f_i}$.

6.1.2 Problem Description

We study a self-organizing problem that in a given random deployment of the FAP the sum energy usage (E^f) by FUEs is maintained below the maximum allowance as well as the cross--interference (I_o^{fm}) is less than the tolerance level by the MBS. It is investigated how to self-organize the sum energy usage among FUEs in order to enhance the sum capacity of a femto cell-of-interest. Toward this end, we take into account following two constraints:

$$E^f \le E_o \qquad \text{and} \qquad I_o^{fm} \le I_o \qquad (6.4)$$

where E^f is the sum energy usage by all FUEs at Phases 0 and 1, its maximum is limited by E_o. $I_o^{fm} = \sum I_o^{fm_i}$ denotes the sum cross-interference on average at the MBS from FUEs, and its pre-defined maximum is I_o.

6.1.3 Energy-Aware Self-Organization

6.1.3.1 Sum energy usage in a co-channel femto cell

For a given $\overline{K}^f$, when randomly activating $K^f \le \overline{K}^f$ FUEs, the sum energy usage at both Phases 0 and 1 during a given time slot period T_s can be statistically represented as

$$E^f := \frac{1}{\overline{K}^f}\sum_{i=1}^{\overline{K}^f} P_1^{f_i} T_s + \frac{K^f}{\overline{K}^f}\sum_{i=1}^{\overline{K}^f} P_0^{f_i} T_s \quad (6.5)$$

$$= E_1^f + E_0^f \quad (6.6)$$

where $P_0^{f_i} = P_0^f \Lambda_{f_i}$ denotes the power for signalling and thereby the product of $P_0^{f_i} T_s$ represents the energy usage by FUE i at Phase 0. In, let us denote $P_0^f = \alpha^{-1}\hat{P}_1^f$, where α is a fixed system parameter and $\hat{P}_1^f$ denotes P_1^f when $K^f = \overline{K}^f$. As can be seen in (6.6), therefore, E^f consists of two terms, that is, E_1^f denotes the sum energy at Phase 1 while E_0^f at Phase 0.

It is worth mentioning that the amount of E_0^f in (6.6) is considerable, as compared to E_1^f. In the femto cell the signalling energy used by each FUE becomes large due to the presence of self-organizing operation, due to its random deployment. As a result, for a given $\hat{P}_1^f$, $\alpha = \hat{P}_1^f / P_0^f$ at each FUE results in less than the conventional case (e.g., $\alpha \le \hat{\alpha}$ where $\hat{\alpha}$ is for the conventional cellular case). When activating K^f FUEs, the energy usage E_0^f at Phase 0 depends on both P_0^f and the $K^f \le \overline{K}^f$ FUEs and thus its amount becomes notable. Therefore, taking into consideration both E_0^f and E_1^f is worthy for further investigation.

6.1.3.2 Case when $I_o^{fm} \le I_o$: Impact of K^f and P_0^f on P_1^f

Under the interference requirement, we now aim at analyzing how much P_0^f should be chosen to satisfy $I_o^{fm} \le I_o$. First, by using (6.3), (6.5) and (6.6), it can be shown that for a given $\overline{K}^f$, I_o^{fm} in (6.4) is written as

$$I_o^{fm} = \sum_{i=1}^{\overline{K}^f} I_o^{fm_i} = \frac{\Theta_m}{\overline{K}^f}\sum_{i=1}^{\overline{K}^f} P_1^{f_i} / \mathrm{PL}_{f_i^c} + \frac{\Theta_m K^f}{\overline{K}^f}\sum_{i=1}^{\overline{K}^f} P_0^{f_i} / \mathrm{PL}_{f_i^c} \quad (6.7)$$

$$= \frac{\Theta_m}{\overline{K}^f}\sum_{i=1}^{\overline{K}^f} P_1^f \Lambda_{f_i} / \mathrm{PL}_{f_i^c} + \frac{\Theta_m K^f}{\overline{K}^f}\sum_{i=1}^{\overline{K}^f} P_0^f \Lambda_{f_i} / \mathrm{PL}_{f_i^c} \quad (6.8)$$

where the two terms on the second right hand side of (6.7) represent the sum cross-interferences occurring at Phases 1 and 0, respectively. It is worth mentioning that in (6.7), the first term is related to E_1^f while the second term results from using E_0^f. Moreover, (6.8) can be obtained by inserting both $P_1^{f_i} = P_1^f \Lambda_{f_i}$ and $P_0^{f_i} = P_0^f \Lambda_{f_i}$ into (6.7).

Based on (6.8), we consider the worst scenario interference when all FUEs are deployed at a corner of a femto cell nearest to the MBS. This is in order to investigate the impact of the maximum I_o^{fm} on the MBS performance. Particularly, let $\Lambda_{f_i} = \Lambda_{f_o}$, $\forall$i in (6.8) be strongest by setting $r^{f_i} = r^{f_o}$, $\forall i$. This reveals that $P_0^{f_i} = P_0^{f_o}$. Meanwhile, it reveals that the minimum $\mathrm{PL}_{f_i^c} \approx \mathrm{PL}_{f_o^c}$, $\forall i$ are concerned since $r^{f_o} << r^{f_m}$ in practice. Therefore, it can be obtained that in the worst scenario, $\Lambda_{f_i} / \mathrm{PL}_{f_i^c} \approx \Lambda_{f_o} / \mathrm{PL}_{f_o^c}$ are maximized, in which I_o^{fm} becomes strongest.

By using the above consideration, it can be shown that in the worst scenario, (6.8) is simplified:

$$I_o^{fm} = \left(P_1^f + K^f P_0^f\right)\left(\frac{r^{f_o}}{r^{f_o^c}}\right)^{L_2^f/10}\Theta_m . \qquad (6.9)$$

Inserting (6.9) into the constraint $I_o^{fm} \le I_o$ in (6.4), it can be presented that in the worst scenario, we have

$$I_o^{fm} \le I_o \quad \Rightarrow \quad \left(P_1^f + K^f P_0^f\right)\left(\frac{r^{f_o}}{r^{f_o^c}}\right)^{L_2^f/10} \le \eta \mathrm{P}_r^m \qquad (6.10)$$

In (6.10), let $I_o = \eta\Theta_m \mathrm{P}_r^m$ denote the maximum toleration threshold by the MBS, where $\Theta_m \mathrm{P}_r^m$ is the receive power on average requested at the MBS from its own MUEs, and $\eta \in [0,1]$ is a given constant.

Therefore, it can be obtained from (6.10) that P_0^f satisfying $I_o^{fm} \le I_o$ should be with respect to K^f, P_1^f, and $\eta \mathrm{P}_r^m$

$$P_0^f \le K^{f\,-1}\left(\eta \mathrm{P}_r^m \left(r^{f_o^c}/r^{f_o}\right)^{L_2^f/10} - P_1^f\right) \qquad (6.11)$$

It can be analytically seen in (6.11) that for given parameters such as $\eta \mathrm{P}_r^m$, r^{f_o}, and L_2^f, P_0^f decreases with respect to both K^f and P_1^f while maintaining $I_o^{fm} \le I_o$. Particularly, P_0^f scales inversely with the order of K^f in a given P_1^f while for a given K^f, P_0^f linearly decreases with respect to P_1^f. Therefore, it is worth mentioning that the femto cell network should autonomously select P_0^f, P_1^f, and K^f so that the maximum interference tolerated by the MBS can remain less than or equal to I_o.

6.1.3.3 Case when $E^f \le E_o$: Impact of K^f and P_0^f on P_1^f

Let $E_o = E^f$ in the extreme case when $K^f = \overline{K}^f$. In order to maintain $E^f \le E_o$ for a given $K^f < \overline{K}^f$, then, we can obtain

$$P_1^f \le \left(\overline{K}^f \alpha^{-1} - K^f \alpha^{-1} + 1\right)\hat{P}_1^f .$$

It can be seen from this equation that when satisfying $E^f \le E_o$, P_1^f is represented with respect to both K^f and $P_0^f = \alpha^{-1}\hat{P}_1^f$. For a given P_0^f, this equation shows that the transmit power for the data decreases with K^f. Therefore, for a given K^f, the use of P_1^f satisfying the energy requirement provides the power gain of, at most, $\left(\overline{K}^f \alpha^{-1} - K^f \alpha^{-1} + 1\right)$, as compared to the extreme case when $K^f = \overline{K}^f$ (i.e., $P_1^f = \hat{P}_1^f$).

6.1.3.4 Case when both $I_o^{fm} \le I_o$ and $E^f \le E_o$: Selection of K^f and P_0^f

Now we consider the case when both $I_o^{fm} \le I_o$ and $E^f \le E_o$ are maintained simultaneously. Then we investigate the impact of this constraint on selection of both P_0^f and P_1^f and it will be shown how the ergodic sum capacity C_e behaves in terms of P_0^f and P_1^f for a given $K^f < \overline{K}^f$.

To this end, we refer to the above two equations and recall that $P_0^f = \alpha^{-1}\hat{P}_1^f$. *Then*, it can be achieved that for a given $\overline{K}^f$ FUEs and $K^f < \overline{K}^f$, P_0^f and P_1^f should satisfy

$$P_0^f \le \frac{\eta \mathrm{P}_r^m}{\overline{K}^f + \alpha}\left(\frac{r^{f_o^c}}{r^{f_o}}\right)^{L_2^f/10}$$

$$P_1^f \le \frac{\overline{K}^f \alpha^{-1} - K^f \alpha^{-1} + 1}{\overline{K}^f + \alpha}\eta \mathrm{P}_r^m \left(\frac{r^{f_o^c}}{r^{f_o}}\right)^{L_2^f/10}$$

so that $I_o^{fm} \le I_o$ and $E^f \le E_o$ are maintained simultaneously.

It is well known that the expression of the ergodic sum capacity of a femto cell can be expressed as a function of the SINR by the best femto UE. That is, $C_e = \log_2\left(1+\bar{\rho}x^*\right)$ where $x^* = E(\rho^{f_{i^*}})$. Using the above two power expressions as well as the asymptotic expression for the distribution of x^* [135], the asymptotic expression for the ergodic sum capacity can be obtained as a function only of K^f after mathematical operations as [136]

$$C_e = \log_2\left(1+\tilde{\rho}G^{K^f}\left(\mu(K^f,d)+\beta(K^f,d)\right)\right)$$

where $\tilde{\rho} = \bar{\rho}/P_1^f$ and we denote that

$$G^{K^f} = \frac{\overline{K}^f - K^f + \alpha}{\overline{K}^f + \alpha}\eta \mathrm{P}_r^m \left(\frac{r^{f_o^c}}{r^{f_o}}\right)^{L_2^f/10} \frac{\mu(K^f,d)+\beta(K^f,d)\varpi}{\mu(\overline{K}^f,d)+\beta(\overline{K}^f,d)\varpi}$$

is the resulting power gain as compared to the extreme case when $K^f = \overline{K}^f$.

6.1.4 Numerical Results

Consider a co–channel femtocells network, where each femto service coverage has a radius of 10 (meters). We illustrate in this section numerical results for the performance of a femtocell-or-interest that is deployed at the distance *do* ∈ {50; · · · ; 100} (meters) with respect to the MBS. Let the given interference threshold be η ∈{10−2; 10−3}, and the system parameters $\alpha = 4/3$, the number *d* of antenna at the FAP is d ∈ {1; 2; 4} and $\overline{K}^f \in \{4,\cdots,20\}$ are used.

In Figure 6-1, the normalized interference toward the macrocell by its receiving power from macrocell own users is depicted versus the relative distance (*do*) between the FAP and the MBS. As can be seen in this figure, as *do* gets shorter, the interference by the proposed scheme remains at the target level while the interference by the conventional cases increases as *do* decreases. Therefore, it can be observed from this figure that the use of properly adjusted P_0^f benefits in maintaining the interference under the target level at various distances *do*.

As compared to the non self-organized conventional case when using both a fixed $K^f = \overline{K}^f$ and a constant P_0^f, Figure 6-2 depicts the ergodic sum capacity versus the average SNR $\tilde{\rho}$ in the case when optimizing both P_0^f and K^f. As per this figure, the proposed admission control and resource allocation scheme is superior to the conventional case. In particular, when *do* = 100 (meters), it can be seen in this figure that at Ce = 3 bits/s/Hz/cell, the case when autonomously adjusting both P_0^f and the optimal value of K^f obtains about 16 dBm power gain against the conventional case. It is worth mentioning that such a gain is achieved with no extra sum energy usage.

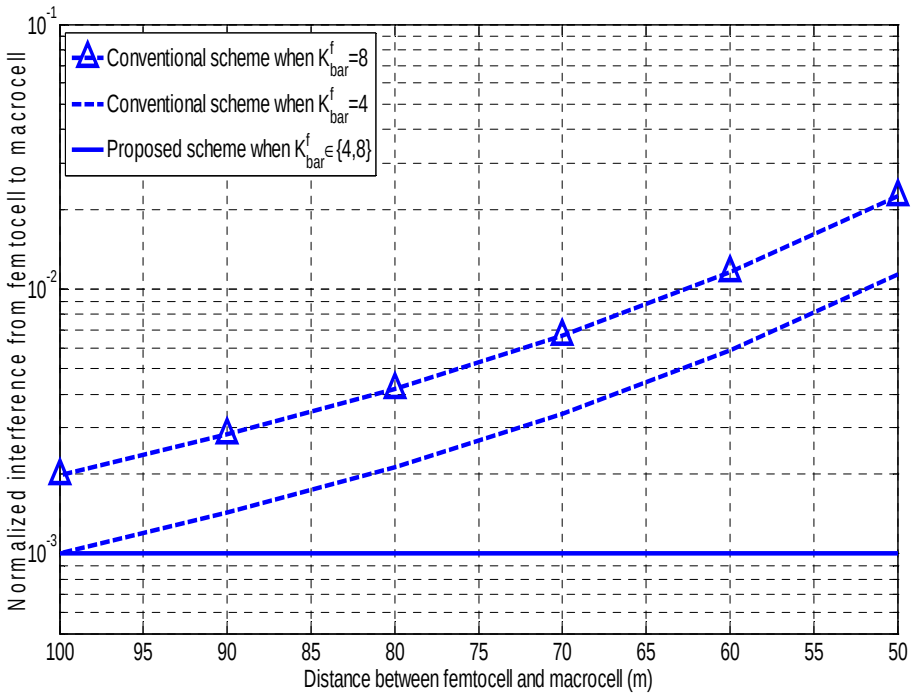

Figure 6-1: Comparison of the proposed scheme against the conventional one when using no adjustment on P_0^f and a fixed $K^f = \overline{K}^f$ has been illustrated in terms of the normalized interference from femtocell to macrocell versus d_o. For this comparison, $\overline{K}^f \in \{4,8\}, K^f = \overline{K}^f$, $d_o \in \{50,100\}$ m, $r^{f_o} = 10$ m, $\eta = 0.001$, $\alpha = 4/3$, and $d = 2$ are used.

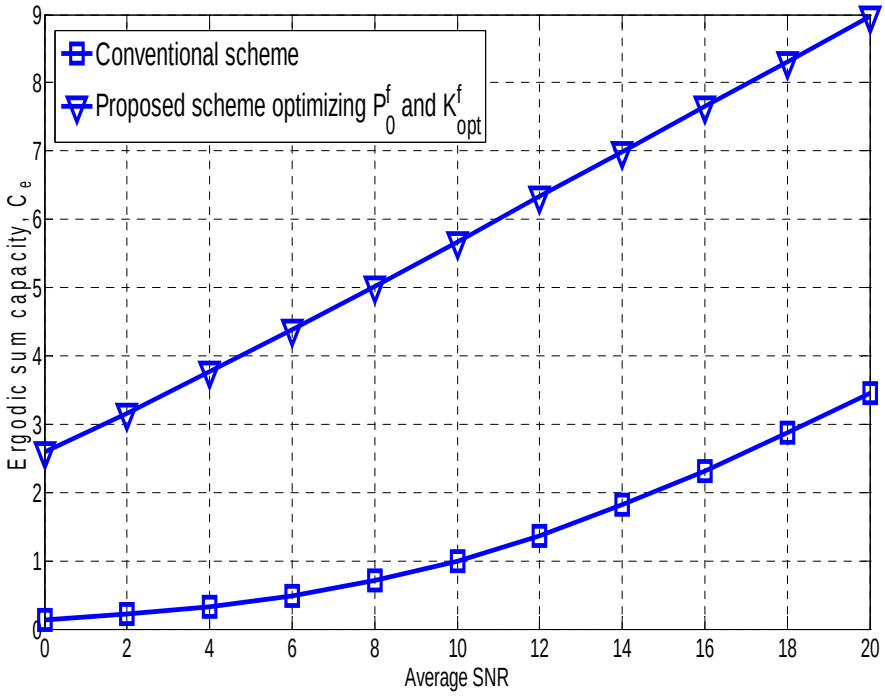

Figure 6-2: Comparison of the case when optimizing both P_0^f and the value of K^f to the conventional case has been depicted in terms of C_e versus the average SNR: $d = 4$, $\overline{K}^f = 8$, $K^f \in \{1,...,\overline{K}^f\}$, $d_o = 100$ m, $r^{f_o} = 10$ m, $\eta = 0.001$, and $\alpha = 4/3$ are used.

6.1.5 Conclusion

In this section, a two–tier co–channel femto cells network was considered. We proposed an admission control and resource allocation scheme in a distributed fashion, which aims at balancing the energy usage by femto cell users between the signalling and the data transmission. Developing the generic energy usage model by the femto cell users, it was proposed to autonomously select both the number of activated femto cell users and their power levels. In the worst case interference scenario towards the macrocell, the performance of the proposed system has been analyzed and the achievable gain was analyzed by presenting the asymptotic ergodic sum capacity expression in the closed–form under the realistic constraints on the interference– and the energy–requirements. Clearly, it is noted from the results in this work that when self-organizing the energy usage of a femto cell of interest, the proposed scheme benefits the enhanced cell capacity with no extra sum energy usage within the femto cell.

6.2 RF Front-End Functionalities for Self-Optimization

Fitting the downlink transmitted power in admissible levels and working with accurate transmitted power is the desirable working state for the transmitter. In 6.2.1 an implementation of power control for downlink that combines open-loop and closed-loop is described as solution to both, following changes of transmitted power desired in power control method in self-optimization, and accurate operation during periods with “temporal fitted power”. As “temporal fitted power” we refer to periods in which transmitted power suffer no change of level. Also the implementation of mechanisms that allows automated detection of potential user load in uplink is described in Section 6.2.2. This mechanism is useful to implement energy saving when there are periods of low user load or no user at all. In Section 6.2.3 an estimation of power consumption for the front-end is shown.

6.2.1 Implementation of Power Control in downlink

Closed-loop power control described in Section 2.2.2 refers to feedback power control implemented. It determines the error between the measured transmitted power and the desired transmited power. Based on this error, the system adjust the transmit power by adjusting the gain amplifier.

Open-loop refers to power control adjust the transmitted power in response to power control commands produced by operational parameters and/or environmental conditions. This open-loop does not include any means to verifying the accuracy of the transmit power. The combination of open-loop with closed-loop avoids [35] that the transmit power drift away from the desired transmit power. This change from desired working point can drive to violation of absolute power requirements. The block diagram is shown in Figure 6-3

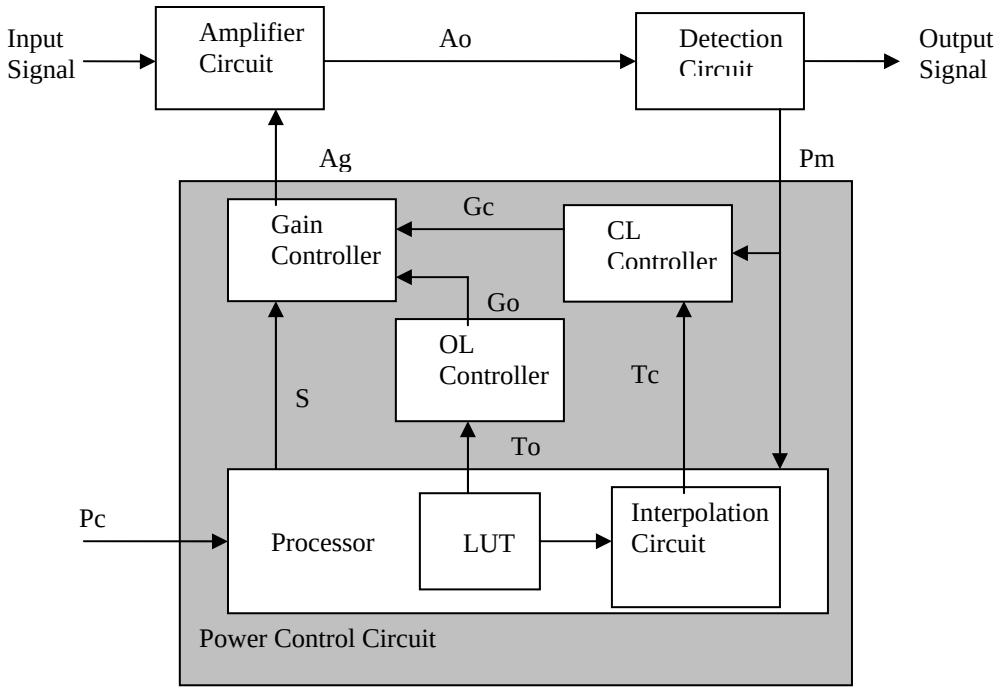

Figure 6-3: Closed-Open Loop Control Power Transmitter Block diagram

Detection Circuit extracts a small portion of the amplified signal Ao, measures the power, provides the measured power Pm to the Power Control Circuit and delivers the output signal to the radiating system.

The Amplifier Circuit has one variable gain amplifier (VGA) to amplify the input signal obtaining the output signal at a desired level. The VGA varies its response in accord to Ag provided from Power control circuit. Apart from the VGA, the Amplifier Circuit has a High Power Amplifier HPA that provides the desired level of the Output signal.

Power Control Circuit generates the gain control signal Ag responsive to power control commands Pc and/or the measured power Pm from the Detection Circuit during open and closed loop. It also adjusts Ag during transitions between both loops in a way that there are no power deviations.

The processor includes a look-up table and an interpolation circuit. In response to a power command, the processor executes the look-up table to obtain closed and open loop references, Tc and To. It also generates the selection signal S to the gain controller in response of a detected power Pm. When Pm meets or exceeds a predetermined threshold, processor generates S to instruct the gain controller to select closed-loop gain adjustment Gc. If it is less then a threshold processor generates S to instruct the gain controller to select the open-loop gain controller Go.

The Look-up table (LUT) stores a plurality of open-loop and closed loop references in an ordered list corresponding to the power control levels.

Interpolation Circuit modifies the closed-loop reference Tc to provide a finer resolution than available with look-up table alone. Modifying the closed-loop reference Tc when transitioning from open-loop to closed-loop control avoids the large steps that cause the undesirable discontinuities.

The closed-loop controller generates the closed loop gain adjustment based on the difference between the measured power Pm and the closed-loop reference Tc. It includes a combiner and VGA converter. The combiner determines the power difference between Pm and Tc during close-loop, where Tc digitized target power level selected from the look-up table based on a selected power command Pc. The converter maps this difference of power to a digitized VGA value to generate the closed-loop gain Gc.

VGAOpen-loop controller generates the open-loop gain Go based on the open-loop reference to and provides open gain Go to the gain controller.

The power control circuit adjusts the gain of the variable gain amplifier to meet the power requirements. To do this, the gain controller selects one of the closed-loop and open-loop gain adjustment values and adjusts a gain control signal Ag based on the selected gain adjustment. The gain controller comprises a switch and a register.

6.2.2 Aspects related to uplink RF Front-End

The listening capability of the femtocells may be enabled independently from other functions of the cell [139]. In that case, those cells may monitor, when requested, interference over thermal (IoT) ratio, which is obtained based on Received Interference Power and Thermal Noise Power (RIP) and (TNP) [41]. When a femtocell detects high load, it may request the other femtocells within its coverage to provide their IoT measurements, and then using its proprietary algorithm, in most cases the femtocell will be able to find out which hotspot cells are the most appropriate to serve higher load. Therefore, those femtocells could activate the appropriate cells for boosting capacity while keeping other femtocells in sleep mode. The femtocells can also use their own IoT (RIP and TNP) to compare with a threshold. If the signal is high enough the femtocell leaves its sleeping state/ Eco-mode and takes care of the potential traffic in the surrounding.

Letting this functionality working in automated mode the Eco-mode [140] can be activated when the load is under the threshold level. In Figure 6-4 a Front-End scheme with uplink level threshold comparator to activate the eco-mode is included with the functionalities described for downlink power control described in Section 6.2.1

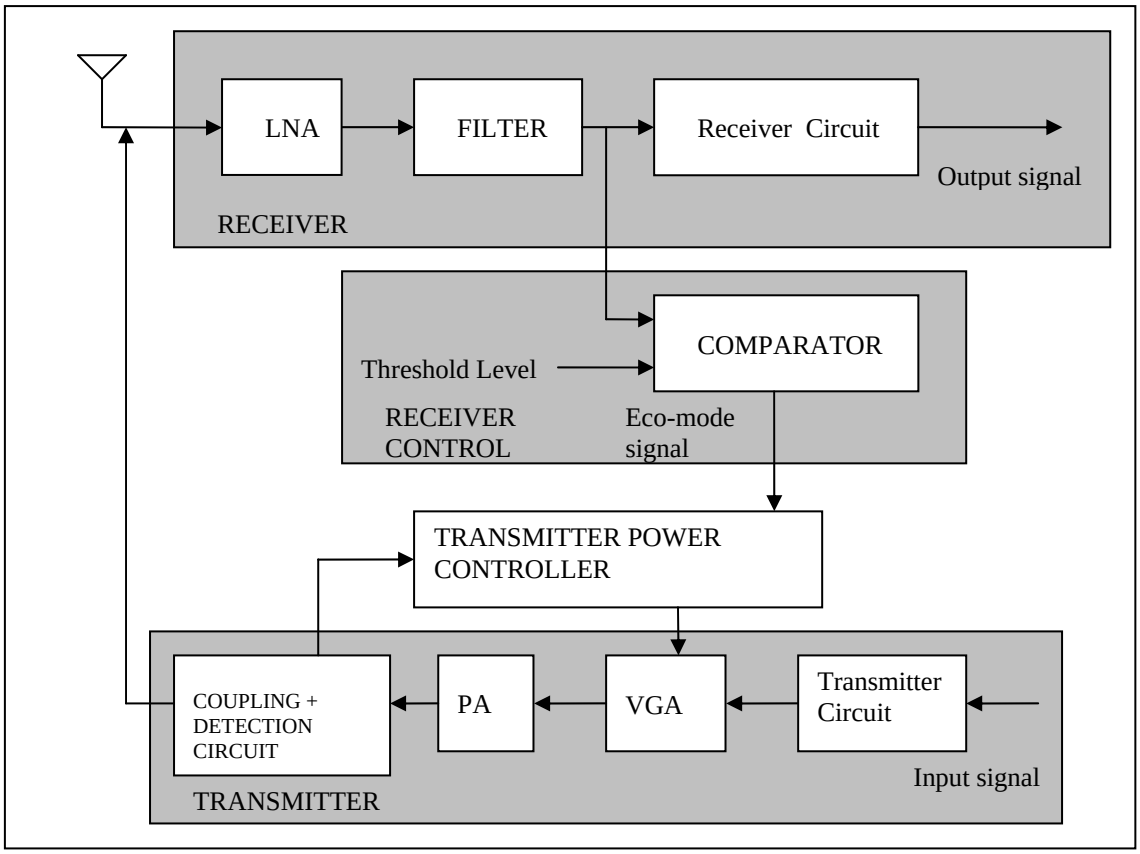

Figure 6-4: RF Front-End main modules.

6.2.3 Impact on energy saving

There are various factors impacting on the development of RF components and systems that are being researched and investigated. For general communications systems, for example, there is the continuous movement towards smaller, secure systems that have increased functionality and reduced power consumption.

The receiver or the transmitter has to switch to the standard or to the operator featuring the more efficient characteristics. There are also similar requirements concerning battery and performance management. In fact, relating to the electromagnetic environment, the performance of the receiver/transmitter can be more or less relaxed in order to save energy, which is a key issue in the case of portable communications. In this case the system has to be smart enough to choose the best configuration by trading off the electrical performance (that is, linearity and noise figure) and the power consumption [142].

The simplest way to describe a wireless communication module [141] could be defined as described in Figure 6-5.

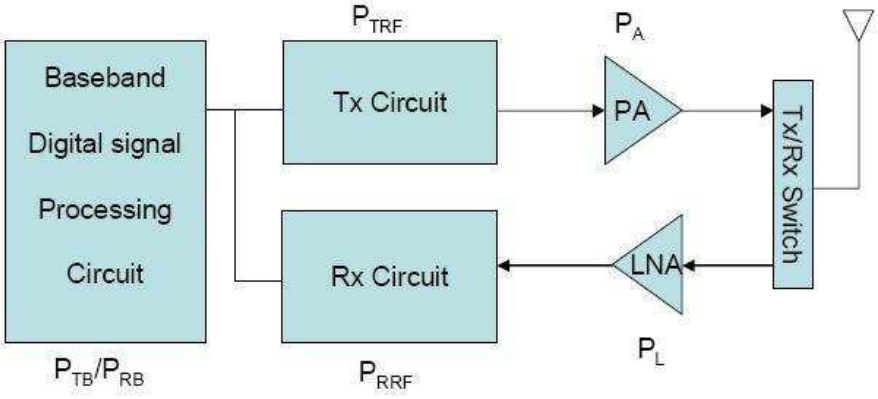

Figure 6-5: Communication Module Structure.

Based on the structure and power consumption of each component, the total power consumption for transmitting and for receiving, denoted by P_T and P_R, are specifically given by:

$$P_T(d) = P_{TB} + P_{TRF} + P_A(d) = P_{T0} + P_A(d) \quad (6.12)$$

$$P_R = P_{RB} + P_{RRF} + P_L = P_{R0} \quad (6.13)$$

where $P_A(d)$ is the power consumption of the power amplifier which is a function of the transmission range, d, that is the desired coverage and interference level. Since P_{TB} and P_{TRF} do not depend on the transmission range, the two components can be modelled as a constant, P_{T0}. Similarly, the power consumption of the receiving circuitry can be modelled as a constant, P_{RO}, since P_{RB} and P_{RRF} are clearly not dependent on transmission range, and P_L is also a constant while assuming that the LNA is properly designed and biased to provide the necessary sensitivity to reliably receive, demodulate and decode a minimum power signal, $P_{Rx\text{-}min}$.

While there are many types of RF power amplifiers, the total power consumption of a power amplifier, $P_A(d)$, will depend on many factors including the specific hardware implementation, DC bias condition, load characteristics, operating frequency and PA output power.

The power amplifier delivers RF output power, *PTx*, to the antenna. In general, the required RF output power, $P_{Tx}(d)$ for reliable transmission will depend on the transmission range, *d*, this is the desired coverage and interference to other cells and foreign users.

The total power consumption of the PA is given by P_{DC} and is the same as *PA* defined above. The ratio of RF output power to DC input power is called the drain efficiency (denoted as η) and is given by:

$$\eta = P_{Tx} / P_{DC} \quad (6.14)$$

By definition, the drain efficiency of a PA will be less than 100%. For example, simple class A power amplifiers have a maximum drain efficiency of 50% as equal amounts of power are dissipated in the bias circuitry and in the load. The drain efficiency will typically vary when the output power delivered to the load changes. In particular, for most types of power amplifiers, the drain efficiency increases while P_{Tx} is increasing and reaches its maximum value when P_{Tx} reaches the maximum output power, P_{max}.

By combining the concept of drain efficiency with the formula described in the previous part of this section, the power consumption of the communication module can be modelled as:

$$P_{T(d)} = P_{T0} + P_{Tx}(d)/\eta \quad (6.15)$$

$$P_R = P_{R0} \quad (6.16)$$

During dormant or Eco modes the total consumption is: $P_{total} = P_T(d) + P_R = P_{T0} + P_{R0}$ (6.17) if the PA is completely switched-off.

Some RF components that can be used to implement FAP transmitter and receiver have Enabling Entries that can be used to implement power saving periods when the FAP enters a no user load period. During these periods transmitter can be shunted down and only receiver operates in order to detect user load.
Base band dual amplifiers used in Tx circuit that appear in Figure 6-5, using current available devices to amplify signals I/Q to enter in modulator, consume 1W in normal operation mode and they reduce its consume to less than 10mW [137] using shunt-down option. I/Q modulators, also part of Tx circuit, with shunt down mode can pass from 250mW normal operation mode to less than 1mW in sleep mode [138]. Current power amplifiers used in LTE handsets even incorporate internal coupler to use in the power control loop. This type of devices also has saving operation modes that reduce consume.

7. Extensions to the Mobile and Relay Femto Scenarios

The following section investigates both fixed and mobile femtocell relays. First, leveraging on the TDD underlay at UL FDD proposal [175], [176], a full duplexing transmission scheme is presented in which a femtocell relay transmits and receives simultaneously. Second, preliminary results on the mobile femtocell relay are presented thereafter.

7.1 Full Duplex Based Transmission for Fixed Femtocell Relays

Cooperative communication is an alternative to achieve spatial diversity even with single antenna devices [148]. In a cooperative scheme a relay helps the source to communicate with the destination, and its behaviour is dictated by the cooperative protocols such as amplify-and-forward (AF) and the decode-and-forward (DF), or their variants selective and incremental [148-149]. In the Selective-DF (SDF) the relay station forwards the source message only if it is error free. Nevertheless, with half-duplex (HD) radios the cooperation suffers from a multiplexing loss, because the relay listen in a first time slot and then retransmits the message in a second slot. Several solutions have been proposed trying to overcome the problem of HD constraint as in [150-151] and references therein. On the other hand, incremental cooperative protocols, such as incremental-DF (IDF), can overcome the spectral inefficiency of HD cooperation through the exploitation of a return channel between nodes [148-149]. In the IDF protocol the relay only cooperates with the source if a retransmission is requested by the destination, so that it is not necessary to previously allocate a time slot for the relay operation.

Furthermore, cooperative FD relaying does not suffer from multiplexing loss and hence can achieve higher capacity than HD cooperative protocols [149]. Nonetheles, perfect isolation between transmitted and received signals is often not possible. In practice, isolating the transmitted and received signals is not straightforward, once the transmitted power is normally much larger than the received power [149]. Probably the most known FD schemes are multi-hop (FD-MH) and block Markov encoding (FD-BM).

Multi-hop is the simplest relaying technique while FD-BM is quite complex to implement, albeit being the best known performance achieving FD scheme [149,152]. In [152] the FD-BM technique is analysed and the authors derive the outage probability of an ideal cooperative FD-BM scheme. On the other hand, practical FD schemes have been proposed in which it is considered that there is a power leakage between transmitted and received signals, also known as loop interference or self-interference [153,154,155]. For instance, the authors in [153] show that practical FD-MH scheme is feasible even if the relay faces strong self-interference. Moreover, it is also shown that FD-MH relaying enhances capacity when compared to the HD scheme. In addition, similar conclusions were obtained in [154-156]. In our proposed solution, we consider a practical FD relay, with loop interference, which may operate under a multi-hop relaying scheme. We assume that the relay employs the DF protocol. Moreover, we assume that the relay receivers are able to apply successive interference cancelation (SIC) [**157**] on the received signals. Therefore, based on [**157-158**] we determine the rate regions and evaluate the individual outage probabilities. Due to the causality constraint the relay is not able to remove the self-interference through SIC, which reduces its performance when compared to the ideal FD relay (no loop interference). Nevertheless, we show that even in the presence of a strong interference link the FD-MH scheme is feasible.

7.1.1 System Model

Consider the uplink (UL) of a heterogeneous network composed of a femtocell and a macrocell. The latter is characterized by one macro user (MU) communicating with its serving macrocell base station (MBS), while the former is composed of a source (S), which can be a femto user, communicating with a destination (D), which can be seen as another femto user. The communication is established through the help of a full-duplex relay (R), which can be seen as either a femto base station or dedicated relay.

There are at least two possible scenarios regarding the position of the MU:

1. The MU is far from the femtocell, and therefore the femtocell can operate normally considering that the MU does not interfere with the femtocell.
2. The MU is close to the femtocell and therefore interferes with the femtocell communication.

Figure 7-1 illustrates the heterogeneous network, in which we emphasize the interference links. Notice that we assume a practical full-duplex relay which suffers self-interference (loop interference). As aforementioned the FD relay can be transmit and receive simultaneously. Nevertheless, perfect isolation between transmitted and received signals is often not possible, once isolating the transmitted and received signals is not straightforward given that transmitted power is normally much larger than the received power [148]. Therefore, we assume a self-interference signal which is the leakage of power from the transmitted to the received signal. We model the self-interference link as a Rayleigh fading channel, considering that the antenna isolation considerably reduces the LOS component and that the general behaviour of the channel is due to scattering [155].

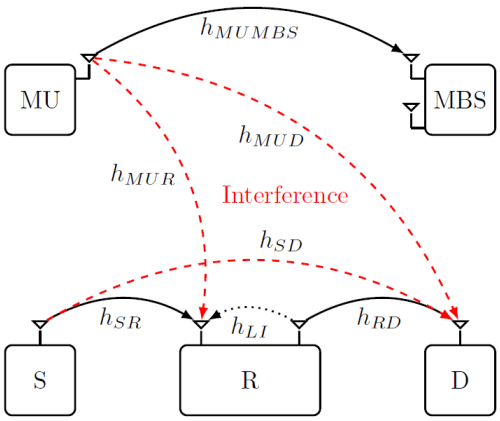

Figure 7-1: Heterogeneous network composed of a cellular macrocell and a femtocell. Note that the femtocell user uses a relay node to expand its coverage and improve throughput performance.

We assume that either R or D is able to employ successive interference cancellation (SIC) on the MU interference signal. Moreover, we assume that the SD link is seen as interference at D, and therefore can

also be removed through SIC. In this case, we can see the channel as a three-user multiple access channels, and the rate regions can be defined as in [157-158]. As shown in [159], SIC can be applied in cellular networks, while an example of application on a femtocell scenario can be found in [160-161], where half-duplex nodes are able to cancel the interference through SIC.

7.1.2 Numerical Results

We present the initial set of results based on the proposed scheme. We assume that the MU is far away from the femtocell. Therefore, the interference caused by the MU can be neglected. Figure 7-2 shows the overall outage probability considering that the MU is far from the femtocell. It can be seen that FD-MH (ideal case) considerably increases the performance, even in the presence of strong self-interference and strong interference at the destination. In this case, we conclude that the self-interference causes a lower reduction on performance when compared to the interference at D. On the other hand, Figure 7-3 illustrates the overall throughput as a function of the average SNR of the S-D link. From the figure we can see that the FD-MH considerably increases the performance achieving in the ideal case 10dB of gain in SNR when compared to the direct transmission. Notice that the throughput is limited by the S-D interference. Therefore, we aim in the next steps to define the outage probability and rate regions and apply SIC at the relay and at the destination. Through SIC, we aim to achieve a performance close to the ideal FD-MH which serves as a benchmark.

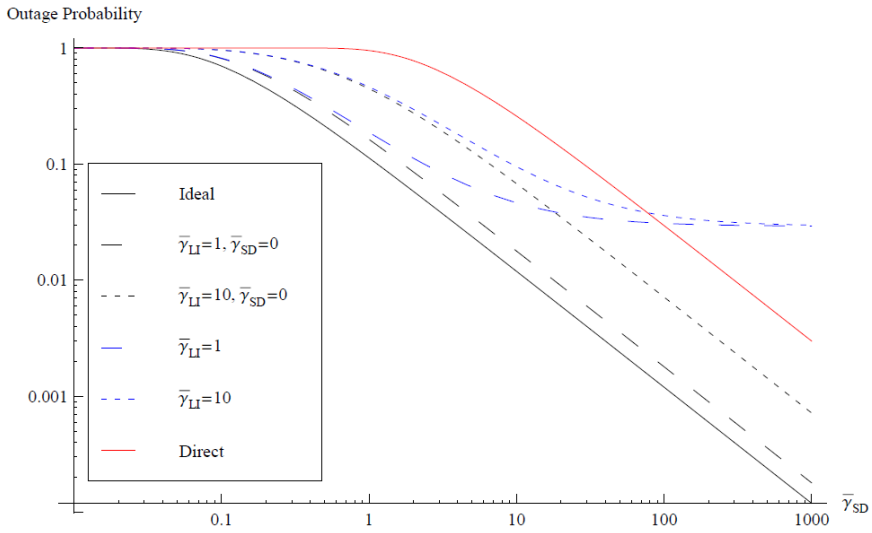

Figure 7-2: Overall outage probability. The proposed scheme considerably increases performance. However, the performance of the FD-MH is reduced by the interference at the relay (self-interference) or at the destination.

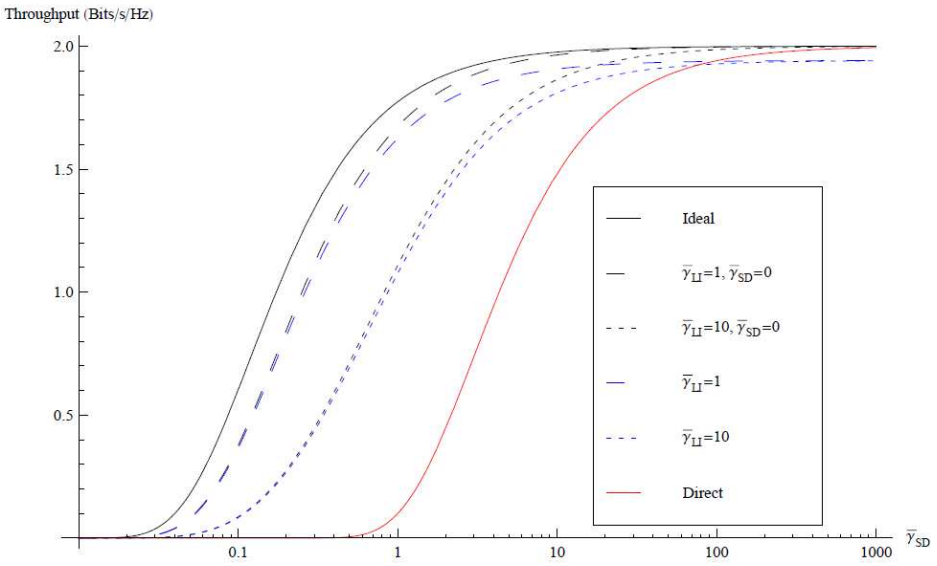

Figure 7-3: Overall Throughput. FD-MH considerably increases the throughput performance when compared to the direct transmission.

7.1.3 Conclusion and Next Steps

We have shown preliminary result about the usage of full duplex transmission for small cells, in which a femtocell base station serves a fixed relay. In the near future, we will define the rate regions and the outage probability of the proposed scheme considering that the MU is close to the femtocell. Moreover, we will analyse the throughput for the second case in which the MU is close to the femtocell. In addition, we plan to expand the proposed scenario considering that the femtocell can serve as a relay for the MU user exploiting different possibilities of backhauling, such as wired and wireless.

7.2 Moving Femtocell Relays

7.2.1 Problem Statement

Fixed relay nodes are one of the main enhancing technologies adopted in LTE-A (3GPP release-10), and provide enhanced cellular coverage by increasing the infrastructure density, at a lower cost and with shorter deployment time than traditional base stations. A coordinated and cooperative relay system (CCRS) consists of a closed group of moving relays (MR) mounted onto transportation vehicles, such as high speed trains, passenger ships, or buses. The CCRS provides innovative architecture enhancements for LTE-A systems, extending the concept of relaying from static areas, to densely populated, high speed transport systems, in order to provide efficient and reliable cellular coverage for passengers. The MRs and local macro cells thereof may operate in shared spectrum and network resources of the donor cellular system. The deployment of CCRS should be an integrated extension of the donor cellular network in terms of network protocols, capabilities, capacity, and MRs must appear to user terminals as traditional cells, in order to maintain compatibility with LTE user equipment (UE).

The 3GPP requirements for LTE-A state that network architectures should remain as unchanged as possible, while considering support of advanced features, such as carrier aggregation for flexible spectrum use (FSU), plug and play eNodeBs for self-organising and self-optimising networks (SON), and new relay architectures. Particularly backwards compatibility must be maintained with LTE (release 8) networks, when considering relay architectures, i.e. LTE user equipment (UE) must be able to access LTE-A systems, and vice versa.
The deployment scenario, characterized by a densely populated, closed coverage area, containing potentially hundreds, to thousands of potential mobile users poses many challenges:

- Resource allocation in order to provide sufficiently high data-rates for the base station to MR backhaul link(s), in order to support the potentially high number of users onboard, while maintaining fair sharing of resources with normal macro-cell users.

- As a MR cell may be travelling across cities, or even countries, for hours or even days, a robust cell configuration scheme against all possible changes of donor cellular systems along the route is desirable.
- Duplexing operation is essential, i.e. how to allocate and schedule resources for a RN to switch back and forth between communicating with donor eNodeB (DeNB) and communicating with UE efficiently, without impact on existing structures and operation of the air interface of the donor cellular systems.

7.2.2 CCRS System Model

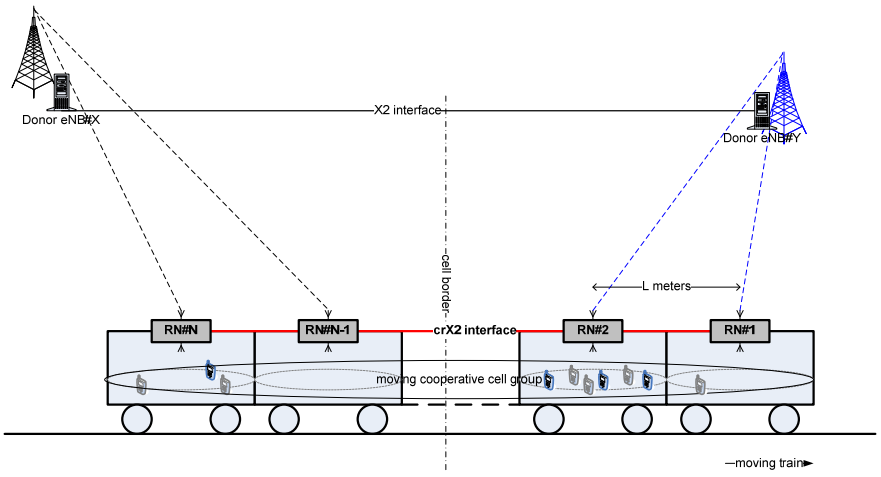

Figure 7-4: Considered network topology with two donor eNodeBs and a mobile femtocell train.

The CCRS is made up of a group of MRs, each of which is responsible for a local cell (within a carriage) and which may have a backhaul link established with a eNodeB. The CCRS may be connected to multiple eNodeBs at any given time, as well as multiple parallel backhaul links to the same eNodeB. The donor cellular system may control and coordinate these mobile backhaul links, together with smart cooperation between the MRs inside the CCRS. A new interface is defined (crX2) interconnecting the MRs, used for cooperation in duplexing operation, load-balancing and capacity sharing amongst the MRs and the local cells thereof, and connection and mobility management. The crX2 interface may be wired or wireless, and if wireless preferably out of band to avoid interference to cellular users.

7.2.3 Simulation Description

The primary assumption made for simulation of the CCRS is that the backhaul link (eNodeB to MR) is the capacity bottleneck of the whole system. It is therefore assumed that the MRs are able to share the backhaul capacity effectively amongst the served users through the access link (MR to UE) within the train. Therefore the access link is not modeled in the simulator, and the throughput of train users when served by a MR is calculated by simply dividing the backhaul throughput of the MR by the number of users of the MR. The duplexing operation of the MR is half duplex with a static 2:2 split for backhaul and access link communication. Simulations are carried out where all train users are connected to the network through a MR, or all train users are connected directly to a macro eNodeB.

7.2.4 Simulation Layout Generation

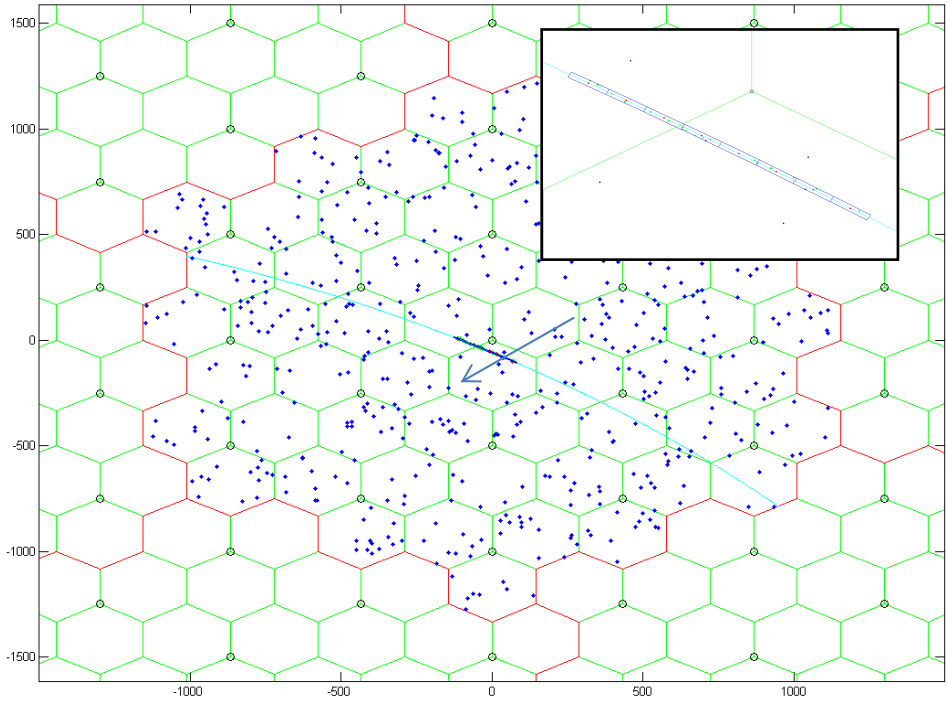

Figure 7-5: System layout generation highlighting the mobile femtocell's trajectory.

The simulator layout consists of 19 tri-sector eNodeBs, forming a 57 cell central layout. The 57 cells are then replicated around the edges of the central cell layout, to form the 399 cell wrap-around model shown in Figure 7-4. The wrap-around model is used so that there are equal levels of intra-cell interference at all cells in the central layout. Macro UEs are evenly distributed throughout the 57 central cells (blue points). A train consisting of 8 carriages is dropped randomly on a track (cyan) that runs through the cell layout with radius of 4Km (typical for high speed train lines), such that the whole of the train is always inside the central 57 cells. A second train may also be dropped traveling in the opposite direction, however for the following simulations only one train was dropped in the layout. Each carriage has a MR (red points) at the center, and train UEs (green points) are evenly distributed throughout and inside the carriages (dark blue border). The trains UEs are paired with the MR on the carriage in which they are located, if they are connected to the MR, otherwise they are paired with the closest 57 cells as are the normal macro users.

Moving Relay and train UE Channel Model

All links use the Urban Macro fast-fading model, and shadowing with distance dependent correlation. The path-loss model used for the normal macro users is also urban macro. The path-loss model used for the backhaul link from eNodeB to MR is "Macro-to-relay" in 36.814-v150 table A.2.1.1.2-2:

$$PL_{LOS}(R) = 100.7 + 23.5log_{10}(R)$$

$$PL_{NLOS}(R) = 125.2 + 36.3log_{10}(R)$$
$$PLOS(R) = \min\left(\frac{0.018}{R}, 1\right) * \left(1 - e^{\left(-\frac{R}{0.072}\right)}\right) + e^{\left(-\frac{R}{0.072}\right)}$$

In the case of the train users connected directly to the eNodeB, the same path-loss model is used for the eNodeB to train user link as the eNodeB to MR link, with a 5dB penetration loss added.

Scheduling and resource allocation

For the following simulations, round-robin scheduling is used. Each macro user is assigned one time slot. Train users connected directly to a macro eNodeB are scheduled in the same way as normal macro users. MRs are allocated as many timeslots as there are train users they are serving, so the total number of time slots allocated for all MR is equal to the total number of train users. When train users are served through a MR however effectively two time slots are allocated per user, as every time slot following a timeslot allocated to a MR is left blank. A simulation parameter 'MR Selection' allows for only the strongest MR in a given cell to be scheduled. In this case the time slots for users within carriages of the 'disabled' MR are allocated to the scheduled MR. It is assumed that the MR are able to cooperate amongst themselves to serve all users in all carriages fairly in this case. In the following simulations, the parameter was disabled however, and all MR serving train users are allocated resources.

Simulation Parameters

Table 7-1: Simulation assumptions

System Bandwidth	10Mhz (50 PRB)
Propagation environment	Urban Macro
Base station sites	19 (57cells)
Base-station Tx Antennas	1
User Rx Antennas (macro and train)	2
MRN Rx Antennas	4
MRN Rx Antenna height	5m
Train velocity	300Km/h
Train carriage length	30m
Train carriage penetration loss (eNodeB to train user)	5dB
Number of Macro users	570
Number of trains	1
Number of carriages per train (= Number of MRN)	8
Number of train users	20
MRN Duplex	Half Duplex, static 2:2 split
Scheduling (backhaul link)	Round Robin, 1 time slot per user
Number of drops	400
Channel samples per drop	300 (1ms between samples = TTI)
Traffic Model	Full-Buffer

Two simulation cases are considered. In the first case all train users are connected directly to the network through a macro eNB. In the second simulation case all train users are connected to the network through a MRN.

Simulation Results

Macro Users (bps/Hz)	Train Users (Direct Connection)	Train users (Connected through MR)	Cell (All Cells)	Cells Serving MR	Cells Serving Train Users (Directly)
1.7618	**1.3592**	**0.9477**	**1.7467**	**1.3636**	**1.6371**

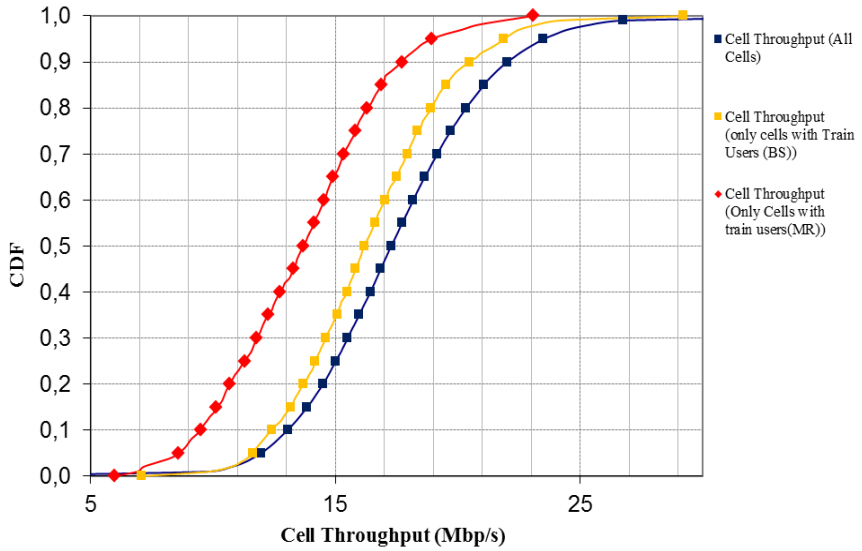

Figure 7-6: cumulative distribution function (CDF) of the cell throughput for users connected to the mobile relay and donor eNodeB, respectively

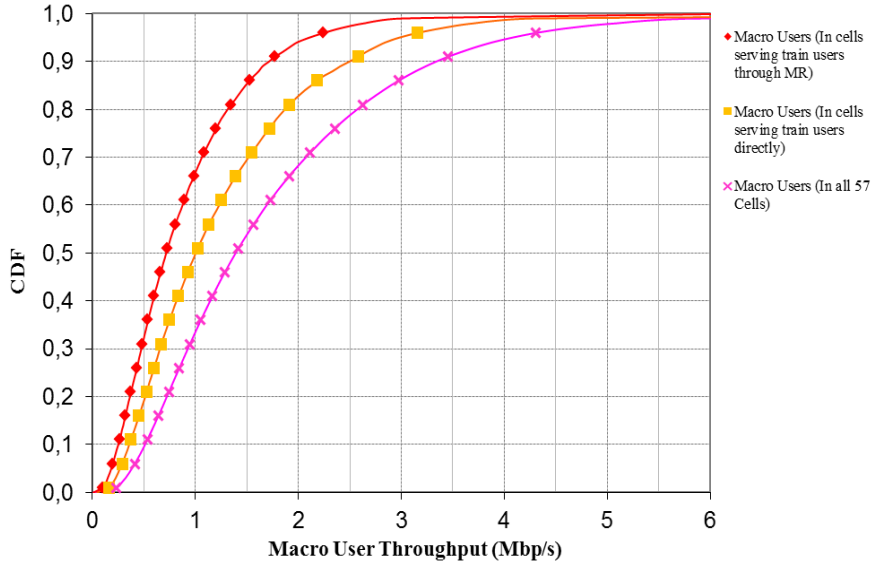

Figure 7-7: cumulative distribution function (CDF) of the macrocell user throughput for users connected to the mobile relay and donor eNodeB, respectively

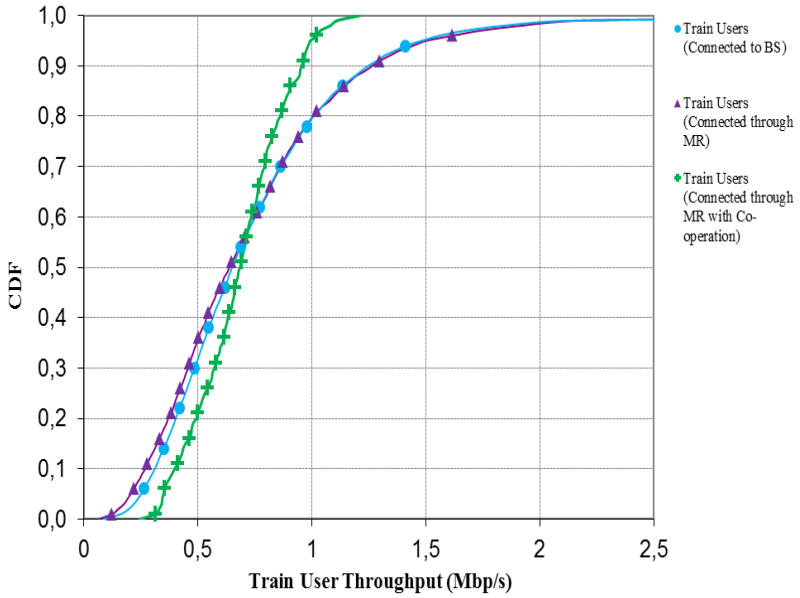

Figure 7-8: cumulative distribution function (CDF) of the train user throughputs.

Table 7-1 shows the average spectral efficiency of the macro users, train users connected through the MRs and connected directly to the base stations, as well as the average spectral efficiency of all cells, cells serving macro users and MR, as well as cells serving macro users and train users directly. The results show that there is a large loss in spectral efficiency when serving train users through an MR, due to the half-duplex operation of the MR. As a result the spectral efficiency of the cell sites serving the MR is also lower than the average for all cell sites, and the cell sites serving train users directly.
Figure 7-7 shows a CDF plot of user throughput for macro users throughout all cell sites, macro users in cell sites also serving train users directly, and macro users in cell sites also serving train users indirectly through MRs. There is a significant decrease in throughput of macro users that are located in cells serving train users, due to having to share resources. There is another significant drop in throughput for the macro users in these cells when the train users are served through MR compared to the case where the train users are connected directly to the base station. In this case, due to the half-duplex operation of the MR, train users when connected through the MR effectively take up two-time slots, thus further reducing the available resources for the normal macro users. The effect of half-duplex operation is again shown in Figure 7-6 which shows cell throughput for all cells, for cells serving train users through MRs, and cells serving train users directly. Cell throughput in cells serving train users is decreased compared to all cells in the layout, however it is reduced even more so in the case of serving users through MRs.

Figure 7-8 shows the throughput of train users when connected directly to the network through a base station, train users when connected to MRs, and train users when connected to MRs that are cooperating. The throughputs of train users are calculated by sharing the backhaul bandwidth of a MR by the number of train users that MR is serving, e.g. the number of users inside the carriage. For the cooperating case throughput is calculated as the sum of the throughputs of all the backhaul links to the train, shared equally by all the users inside the train. In the case of cooperating, the users are train users are sharing resources in a fairer manner, and hence there is less variance in throughput. The results are very similar for the case of the train users being connected directly to the network and being connected through a MR. However the half-duplex operation increased the amount of resources required in this case, since the scheduler does not schedule resources in the TTI following a transmission to a MR.

7.2.5 Conclusions and future work

The initial simulation results of the high speed train scenario show that in the case of the chosen simulation parameters, the CCRS does not improve the throughput of users aboard the train. However

with cooperation, the CCRS does improve resource sharing at lower capacity for the train users, at the cost of the throughput of normal macro users in the cells the train is located in. Further research is needed to evaluate the potential system performance improvement provided by MRN concept. Simulator development now focuses on optimization of the backhaul MIMO-OFDMA link capacity, through link adaptation and scheduling. Another future research topic is related to the full duplex operation with MRN. It would not be a fair assumption that the backhaul link is the capacity bottleneck if the MRN operation were full-duplex, as interference to train UE from macro eNBs would be significant. Simulator development underway includes modeling of the access link (MRN to train UE), which will allow for simulation of CCRS with full-duplex operation.

8. Concluding Remarks

This document has discussed the latest findings within WP4 tasks where the following research iterms were carried out. First, an overview of self-organization networking (SON) techniques was given with a taxonomy and state-of-the art literature on interference management in the context of SO, distributed machine learning and RF front-end functionalities thereby laying the foundation of the proposed SON-enabling techniques.

Next, the architectural requirements of SON 3GPP & BeFEMTO HeNB were discussed in addition to a look into recent Release 10 additions to SON functions and the extension to interference management case. With respect to SON for interference minimization, the impacts of dominant interference conditions in the downlink when macro UEs are in close proximity of femtocells were assessed. Markedly, the BeFEMTO milestone of 8 bps/Hz average femtocell spectral efficiency was achieved in a macro/femto network equipped with 4x4 antennas MIMO spatial multiplexing mode.

Furthermore, SON-enablers for interference minimization were examined as a means of minimizing the overall interference per resource block (RB) generated outside the femtocell coverage range while reducing the transmission power in each RB. Finally, spectral efficiency enhancement on the access link of outdoor fixed relay femtocells through SO of eNB antennas tilt was also investigated.

With respect to SON for radio resource management, a set of innovative SON-enablers for radio resource management were presented. First, the SON paradigm of docitive learning was presented where a femto BS learns the interference control policy acquired by an already active neighboring femtocell, leading to significant energy saving during the startup and learning process. Second, femtocell-aided macrocell transmission is presented as a means of improving the performance of cell-edge macrocell users with a reward mechanisms using spectrum leasing for cooperative femtocells.
Finally, interference coordination schemes in the spatial domain were analyzed and shown to improve the performance of UEs suffering from strong interference.
With respect to SON for energy efficiency, an admission control and resource allocation scheme was proposed, aiming at balancing the energy usage by femto cell users between the signalling and the data transmission. Additionally, RF front-end functionalities for SON weree presented including an implementation of power control for downlink combining both open-loop and closed-loop.

Last but not least, the BeFEMTO use of case of fixed and mobile femtocell relays within Task 4.4 was studied and preliminary results were provided for the case where the macrocell user is far away from the femtocell. First, full duplex transmission was studied in the context of full duplex femtocell relays in an indoor environment where the goal was to extend the coverage of indoor users.

Therein, femtocells were reusing the macrocell uplink FDD band whose concept was also studied in Work Package 3 Task 3.2. As far as mobile femtocell relays are concerned, a set of preliminary results were provided for indoor passengers with a main emphasis on the in-band backhaul from donor eNodeB-to moving relays.

The research activities performed in this deliverable report lay the foundation for further activities toward the main focus of WP4, that is, innovative developments of self-organizing femtocell radio access.
Finally, the following Table 8-1 summarizes the major innovations which are targeting the 8 bps/Hz.

Table 8-1 Average spectral efficiencies of main contributions

Innovations	Average femtocell spectral efficiency [bps/Hz]
SON MIMO based techniques for interference mitigation	8
Docitive networks	8
spectrum leasing as an incentive for macro-femtocell cooperation	~6
spatial and time domain based interference coordination in heteregenous networks	7
Energy aware self-organized networking enabled co-channel femtocell	8

9. References

[1] Z. Bharucha, H. Haas, G. Auer, and I. Cosovic, “Femto-cell resource partitioning,” in Proc. of IEEE Globecom Workshop, November 2009.

[2] S. M. Floriano De Rango, Fiore Veltri, “Interdisciplinary issues for the management of next generation autonomic wireless networks nature inspired techniques,” *Int. J. Mobile Network Design and Innoviation*, vol. 2, pp. 3–4, 2007.

[3] S. Haykin, “Cognitive dynamic systems,” *Proceedings of the IEEE*, vol. 94, no. 11, pp. 1910–1911, 2006.

[4] 3GPP TS 36.300 – E-UTRAN Overall description

[5] “Cognitive radio: brain-empowered wireless communications,” *IEEE Journal on Selected Areas in Communications*, vol. 23, no. 2, pp. 201–220, 2005.

[6] A. Spilling, A. Nix, M. Beach, and T. Harrold, “Self-organization in future mobile communications,” *Electronics Communication Engineering Journal*, vol. 12, no. 3, pp. 133 –147, jun 2000.

[7] E. Yanmaz, O. Tonguz, and S. Dixit, “Wlc09-3: Self-organization in cellular wireless networks via fixed relay nodes,” in Global Telecommunications Conference, 2006. GLOBECOM ’06. IEEE, nov. 2006, pp.1 –5.

[8] C. Prehofer and C. Bettstetter, “Self-organization in communication networks: principles and design paradigms,” IEEE Communications Magazine, vol. 43, no. 7, pp. 78–85, 2005.

[9] W. Elmenreich and H. de Meer, “Self-organizing networked systems for technical applications: A discussion on open issues,” *IWOS 2008*, vol. LNCS 5343, pp. 1–9, 2008.

[10] Carlos Gershenson and Francis Heylighen, When Can We Call a System Self-Organizing? Lecture Notes in Computer Science, 2003, Volume 2801/2003, 606-614, DOI: 10.1007/978-3-540-39432-7_65

[11] J. S. Harsini and F. Lahouti, “Adaptive transmission policy design for delay-sensitive and bursty packet traffic over wireless fading channels,” *IEEE Transactions on Wireless Communications*, vol. 8, no. 2, pp. 776–786, 2009.

[12] H. Zhu, T. Buot, R. Nagaike, and S. Harmen, “Load balancing in wcdma systems by adjusting pilot power,” in *Proc. 5th Int Wireless Personal Multimedia Communications Symp*, vol. 3, 2002, pp. 936–940.

[13] R. Giuliano, F. Mazzenga, and F. Vatalaro, “Adaptive cell sectorization for umts third generation cdma systems,” in *Proc. VTC 2001 Spring Vehicular Technology Conf. IEEE VTS 53rd*, vol. 1, 2001, pp. 219–223.

[14] A. Spilling, A.G.; Nix, A.R.; , "Aspects of self-organization in cellular networks," *Personal, Indoor and Mobile Radio Communications, 1998. The Ninth IEEE International Symposium on* , vol.2, no., pp.682-686 vol.2, 8-11 Sep 1998 doi: 10.1109/PIMRC.1998.734341

[15] “Aspects of self-organization in cellular networks,” in *PIMRC98*, vol. 2, 8-11 1998, pp. 682 –686 vol.2.

[16] L. Badia, M. Boaretto, and M. Zorzi, “Neural self-organization for the packet scheduling in wireless networks,” in *Wireless Communications and Networking Conference, 2004. WCNC. 2004 IEEE*, vol. 3, 21-25 2004, pp. 1927 – 1932 Vol.3.

[17] S. Dixit and E. Yanmaz, “Self-organization of relay-based next generation radio access networks (RANs),” in *Personal Wireless Communications, 2005. ICPWC 2005. 2005 IEEE International Conference on*, 23-25 2005, pp. 197 – 201.

[18] F. Pantisano, M. Bennis, W. Saad, and M. Debbah, "Spectrum Leasing as an Incentive towards Uplink Interference Mitigation in Two-tier Femtocell Networks," IEEE Journal on Selected Areas in Communications, special issue on Femtocells, 2011.

[19] A. Imran, M. A. Imran, and R. Tafazolli, "A novel self-organizing framework for adaptive frequency reuse and deployment in future cellular networks," in *Proc. IEEE 21st Int Personal Indoor and Mobile Radio Communications (PIMRC) Symp*, 2010, pp. 2354–2359.

[20] I. F. Akyildiz, W. Y. Lee, M. C. Vuran, and S. Mohanty, "NeXt generation dynamic spectrum access / cognitive radio wireless networks: A survey," *Computer Networks Journal (Elsevier)*, vol. 50, Issue 13, pp. 2127–2159, September 2006.

[21] A. De Domenico, E. Calvanese Strinati, and M. G. Di Benedetto, "A Survey on MAC strategies for Cognitive Radio Networks," *to be published in IEEE Communication Surveys and Tutorials*, 2012. Available at IEEExplore.

[22] K. Cho, W. Lee, D. Yoon, K. Hyun, and Y. S. Choi, "Resource allocation for orthogonal and co-channel femtocells in a hierarchical cell structure," in *IEEE International Symposium on Consumer Electronics*, May 2009, pp. 655–656.

[23] I. Guvenc, M. R. Jeong, F. Watanabe, and H. Inamura, "A hybrid frequency assignment for femtocells and coverage area analysis for cochannel operation," *IEEE Communications Letters*, vol. 12, no. 12, pp. 880–882, December 2008.

[24] Y. Bai, J. Zhou, and L. Chen, "Hybrid spectrum sharing for coexistence of macrocell and femtocell," in *IEEE International Conference on Communications Technology and Applications*, October 2009, pp. 162–166.

[25] H. Claussen, "Performance of Macro- and Co-Channel Femtocells in a Hierarchical Cell Structure," in *IEEE International Symposium on Personal, Indoor and Mobile Radio Communications*, September 2007, pp. 1 –5.

[26] Y. Y. Li, M. Macuha, E. S. Sousa, T. Sato, and M. Nanri, "Cognitive interference management in 3G femtocells," in *IEEE International Symposium on Personal, Indoor and Mobile Radio Communications*, September 2009, pp. 1118–1122.

[27] M. Andrews, V. Capdevielle, A. Feki, and P. Gupta, "Autonomous spectrum sharing for mixed LTE femto and macro cells deployments," in Proc. of IEEE INFOCOM, March 2010.

[28] A. Ruihong, Z. Xin, C. Gen, Z. Ruiming, and S. Lin, "Interference avoidance and adaptive fraction frequency reuse in a hierarchical cell structure," in Proc. of IEEE WCNC, April 2010.

[29] K. Sundaresan and S. Rangarajan, "Efficient resource management in OFDMA femtocells," in Proc. of ACM MobiHoc, May 2009.

[30] T.-H. Kim and T.-J. Lee, "Throughput enhancement of macro and femto networks by frequency reuse and pilot sensing," in Proc. of IEEE IPCCC, December 2008.

[31] X. Chu, Y. Wu, L. Benmesbah, and W.-K. Ling, "Resource allocation in hybrid macro/femto networks," in Proc. of IEEE WCNCW, April 2010.

[32] V. Chandrasekhar and J. Andrews, "Spectrum allocation in tiered cellular networks," *IEEE Transactions on Communications*, vol. 57, no. 10, pp. 3059–3068, October 2009.

[33] Q. Su, A. Huango, Z. Wu, G. Yu, Z. Zhang, K. Xu, and J. Yang, "A distributed dynamic spectrum access and power allocation algorithm for Femtocell networks," in *International Conference on Wireless Communications Signal Processing*, November 2009, pp. 1–5

[34] H. A. Mahmoud and I. Guvenc, "A comparative study of different deployment modes for femtocell networks," in Proc. of PIMRC, September 2009.

[35] Gustavson et al. , "Continuous alternating closed-open loop power control" , www.freepatentsonline.com/

[36] 3GPP TS 36.104 "Evolved Universal Terrestrial Radio Access (E-UTRA); Base station (BS) radio transmission and reception ", V10.0.0, Dec. 2010

[37] Steve Egolf, "Intelligent Power Management: A Method to Improve 2G/3G Handset Talk Time", Microwave Journal, vol.50 , no.7, July 2007

[38] Jackie Johnson, “How Mobile Devices Users are Impacting the Future of RF Front Ends”, Microwave Journal, vol. 53, no.11, Nov. 2010 supplement

[39] 3GPP TR 36.921, Home eNodeB (HeNB) Radio Frequency (RF) Requirements Analysis (FDD), 3rd Generation Partnership Project, March 2010.

[40] Patel et all, “Femtocell and Beacon Transmit Power Self-Calibration” www.qualcom.com

[41] 3GPP TS 36.214 “Evolved Universal Terrestrial Radio Access (E-UTRA); Physical layer; Measurements”, V10.0.0, Dec. 2010.

[42] R. Bellman, Dynamic Programming, Princeton Univ. Press, Princeton, NJ, 1957.

[43] G. Brown, Iterative solution of games by fictitious play, in: Activity Analysis of Production and Allocation, John Wiley and Sons, New York, 1951.

[44] R. Powers, Y. Shoham, New criteria and a new algorithm for learning in multiagent systems, in: Proc. of Advances in Neural Information Processing Systems (NISP2004), pp. 1089–1096.

[45] G. Tesauro, Extending Q-learning to general adaptive multi-agent systems, in: Proc. of Advances in Neural Information Processing Systems (NISP2003), pp. 1089–1096.

[46] J. Salo, G. Del Galdo, J. Salmi, P. Kysti, M. Milojevic, D. Laselva, and C. Schneider, “MATLAB implementation of the 3GPP Spatial Channel Model (3GPP TR 25.996).” On-line, Jan. 2005. http://www.tkk.fi/Units/Radio/scm/.

[47] M. Weinberg, J.S. Rosenschein, Best response multi-agent learning in non stationary environments, in: Proc. of 3rd International Joint Conference on Autonomous Agents and Multi agent systems (AAMAS 2004), pp. 506–513.

[48] J. Nie, , J. Nie, and S. Haykin, “A Q-learning-based dynamic channel assignment technique for mobile communication systems,” In IEEE Transactions on Vehicular Technology, vol. 48, no. 5, pp. 1676 –1687, Sept 1999.

[49] C. J. Watkins and P. Dayan, “Technical note: Q-learning,” Machine Learning, vol. 8, pp. 279–292, 1992.

[50] M.L. Littman, Markov games as a framework for multi-agent reinforcement learning, in: Proc. of the 11th International Conference on machine Learning, pp. 157–163.

[51] C. Claus, C. Boutilier, The dynamics of reinforcement learning in cooperative multi-agent systems, in: Proc. of the 15th national Conference on Artificial Intelligence, pp. 746–752.

[52] J. Hu, M. Wellman, Nash Q-learning for general-sum stochastic games, J. Mach. Learn. Res. 4 (2003) 1039–1069.

[53] L. Panait and S. Luke, “Cooperative multi-agent learning: The state of the art,” Autonomous Agents and Multi-Agent Systems, vol. 3, no. 11, pp. 383–434, Nov. 2005.

[54] G. Scutari, D. P. Palomar, and S. Barbarossa, “Asynchronous iterative waterfilling for gaussian frequency-selective interference channels,” IEEE Transanctions on Information Theory, vol. 54, no. 7, pp. 2868–2878, Jul 2008.

[55] G. Brown, Iterative solution of games by fictitious play, in: Activity Analysis of Production and Allocation, John Wiley and Sons, New York, 1951.

[56] R. Powers, Y. Shoham, New criteria and a new algorithm for learning in multiagent systems, in: Proc. of Advances in Neural Information Processing Systems (NISP2004), pp. 1089–1096.

[57] G. Tesauro, Extending Q-learning to general adaptive multi-agent systems, in: Proc. of Advances in Neural Information Processing Systems (NISP2003), pp. 1089–1096.

[58] M. Weinberg, J.S. Rosenschein, Best response multi-agent learning in non stationary environments, in: Proc. of 3rd International Joint Conference on Autonomous Agents and Multi agent systems (AAMAS 2004), pp. 506–513.

[59] M.L. Littman, Markov games as a framework for multi-agent reinforcement learning, in: Proc. of the 11th International Conference on machine Learning, pp. 157–163.

[60] C. Claus, C. Boutilier, The dynamics of reinforcement learning in cooperative multi-agent systems, in: Proc. of the 15th national Conference on Artificial Intelligence, pp. 746–752.

[61] M.L. Littman, Friend-or-foe Q-learning in general-sum games, in: Proc. of the 18th International Conference on machine Learning.

[62] J. Hu, M. Wellman, Nash Q-learning for general-sum stochastic games, J. Mach. Learn. Res. 4 (2003) 1039–1069.

[63] J. Nie, , J. Nie, and S. Haykin, "A Q-learning-based dynamic channel assignment technique for mobile communication systems," In IEEE Transactions on Vehicular Technology, vol. 48, no. 5, pp. 1676 –1687, Sept 1999.

[64] C. J. Watkins and P. Dayan, "Technical note: Q-learning," Machine Learning, vol. 8, pp. 279–292, 1992.

[65] A. Greenwald, K. Hall, Correlated Q-learning, in: Proc. of 20th International Conference on Machine Learning (ICML 2003), pp. 242–249.

[66] V. Kononen, Asymmetric multiagent reinforcement learning, in: Proc. of IEEE/ WIC International Conference on Intelligent Agent Technology (IAT 2003), pp. 336–342.

[67] A. Greenwald, A. Jafari, A class of no-regret algorithms and game-theoretic equilibria, in: Proc. of2003Computational Learning Theory Conference, pp.1–11.

[68] Y. Freund, R. Schapire, A decision-theoretic generalization of online learning and an application to boosting, in: Proc. of 2nd European Computational Learning Theory Conference, pp. 23–37.

[69] A. Greenwald, K. Hall, Correlated Q-learning, in: Proc. of 20th International Conference on Machine Learning (ICML 2003), pp. 242–249.

[70] V. Kononen, Asymmetric multiagent reinforcement learning, in: Proc. of IEEE/ WIC International Conference on Intelligent Agent Technology (IAT 2003), pp. 336–342.

[71] A. Greenwald, A. Jafari, A class of no-regret algorithms and game-theoretic equilibria, in: Proc. of2003Computational Learning Theory Conference, pp.1–11.

[72] Y. Freund, R. Schapire, A decision-theoretic generalization of online learning and an application to boosting, in: Proc. of 2nd European Computational Learning Theory Conference, pp. 23–37.

[73] M. Tan, Multi-Agent Reinforcement Learning: Independent vs. Cooperative Agents, in: M.N. Huhns, M.P. Singh (Eds.), Morgan Kaufmann, San Francisco, CA, USA, 1993, pp. 451–480.

[74] M.N. Ahmadabadi, M. Asadpour, Expertness based cooperative Q-learning, IEEE Transactions on Systems, Man, and Cybernetics, Part B 32 (2002) 66–76.

[75] Celtic gandalf project homepage: http://www.celtic-gandalf.org/.

[76] End to end efficiency project homepage: http://www.ict-e3.eu/.

[77] SOCRATES, "Deliverable d2.1: use cases for self-organizing networks, eu strep socrates (infso-ict-216284)," Tech. Rep., March 2008.

[78] NGMN, "Use cases related to self-organizing networks, overall description."

[79] 3GPP, "Self-organizing networks; concepts and requirements," 3GPP TS 32.500 .

[80] ——, "Telecommunication management; self-configuration of network elements; concepts and integration reference point (IRP) requirements,"3GPP TS 32.501.

[81] ——, "Telecommunication management; automatic neighbour relation (anr) management; concepts and requirements," 3GPP TS 32.511.

[82] ——, "Self-organizing networks (SON) policy network resource model (NRM) integration reference point (IRP)," 3GPP TS 32.521 v10.0.0.

[83] ——, "Telecommunications management; self-healing OAM; concepts and requirements," 3GPP TS 32.541.

[84] 3GPP TS 36.300 – E-UTRAN Overall description

[85] ——, “Information model for Type 1 interface HeNB to HeNB Management System (HeMS)”, 3GPP TS 32.592

[86] R3-101557, SON use cases analysis for scenarios with HeNB, Qualcomm Inc.

[87] BeFemto D7.1 documentation

[88] R3-103411, Mobility Robustness Optimization for HeNB, Qualcomm Inc.

[89] T.-H. Kim and T.-J. Lee, “Throughput enhancement of macro and femto networks by frequency reuse and pilot sensing,” in *Proc. of IEEE IPCCC*, December 2008.

[90] G. Boudreau, J. Panicker, N. Guo, R. Chang, N. Wang, and S. Vrzic, “Interference coordination and cancellation for 4g networks,” in IEEE Communications Magazine, April 2009.

[91] S. H. Ali and V. C. M. Leung, “Dynamic frequency allocation in fractional frequency reused ofdma networks,” in Trans. of IEEE on Wireless Communications, August 2009.

[92] A. Simonsson, “Frequency reuse and intercell interference co-ordination in E-UTRA,” in Proc. of IEEE VTC Spring, April 2007.

[93] B. Krasniqi, M. Wrulich, and C. F. Mecklenbrauker, “Network-load dependent partial frequency reuse for lte,” in Proc. of ISCIT, September 2009.

[94] M.-S. Kim, M. R. Jeong, F. Watanabe, and F. Tobagi, “Band-distributed channel-aware fractional frequency reuse in ofdma systems,” in Proc. of IEEE VTC Fall, September 2009.

[95] S.-E. Elayoubi and B. Fourestie, “On frequency allocation in 3G LTE systems,” in Proc. of PIMRC, September 2006.

[96] M. Rahman and H. Yanikomeroglu, “Enhancing cell-edge performance: A downlink dynamic interference avoidance scheme with inter-cell coordination,” in Trans. of IEEE on Wireless Communications, April 2010.

[97] Befemto D4.1 “Preliminary SON Enabling & Multi-Cell RRM Techniques for Networked Femtocells”, Dec. 2010

[98] B. Zubin, S. Andreas, A. Gunther, and H. Harald, “Dynamic Resource Partitioning for Downlink Femto-to-Macro-Cell Interference Avoidance,” EURASIP Journal on Wireless Communications and Networking, vol. 2010, 2010.

[99] 3GPP TSG-RAN1#62, “R1-105082, Way Forward on eICIC for non- CA based HetNets,” August 2010.

[100] E.C. Strinati, A. De Domenico, A. Duda, "Ghost femtocells: A novel radio resource management scheme for OFDMA based networks," Wireless Communications and Networking Conference (WCNC), 2011 IEEE , vol., no., pp.108-113, 28-31 March 2011

[101] S. Uygungelen, G. Auer, and Z. Bharucha, “Graph-Based Dynamic Frequency Reuse in Femtocell Networks,” in *Proc. of the 73rd IEEE Vehicular Technology Conference (VTC)*, Budapest, Hungary, May 15–18 2011.

[102] R. Chang, Z. Tao, J. Zhang, and C.-C. Kuo, “A Graph Approach to Dynamic Fractional Frequency Reuse (FFR) in Multi-Cell OFDMA Networks,” in *Proc. of the IEEE International Conference on Communications (ICC)*, Jun. 14–18 2009, pp. 1–6.

[103] M. C. Necker, “Integrated Scheduling and Interference Coordination in Cellular OFDMA Networks,” in *Proc. of the Fourth International Conference on Broadband Communications, Networks and Systems (BROADNETS)*, Sep. 10–14 2007, pp. 559–566.

[104] M. C. Necker, “A Graph-Based Scheme for Distributed Interference Coordination in Cellular OFDMA Networks,” in *Proc. of the IEEE Vehicular Technology Conference (VTC)*, May 11–14 2008, pp. 713–718.

[105] D. Brélaz, “New Methods to Color the Vertices of A Graph,” *Communications of the ACM*, vol. 22, no. 4, pp. 251–256, Apr. 1979.

[106] L. Kleinrock and F. Tobagi, “Packet Switching in Radio Channels: Part I–Carrier Sense Multiple-Access Modes and Their Throughput-Delay Characteristics,” *IEEE Transactions on Communications*, vol. 23, no. 12, pp. 1400–1416, Dec. 1975.

[107] 3GPP TS 36.213, Evolved Universal Terrestrial Radio Access (E-UTRA) Physical layer procedures (Release 9), 3rd Generation Partnership Project, December 2010.

[108] 3GPP TS 25.469, "UTRAN Iuh interface Home Nobe B (HNB) application part (HNBAP) signalling (release 9)," vol. 9.2.0. Jun.,

[109] 3GPP TS 36.211, "Evolved universal terrestrial radio access network (E-UTRAN); physical channels and modulation (release 9)," vol. 9.1.0., Mar. 2010.

[110] EU FP7-ICT BeFEMTO project, ``Preliminary SON enabling & multi-cell RRM techniques for networked femtocells'', D4.1, Dec. 2010

[111] BeFEMTO, Description of Work, 2009.

[112] Jackie Johnson, "How Mobile Devices Users are Impacting the Future of RF Front Ends", Microwave Journal, vo. 53, no.11, Nov. 2010 supplement

[113] 3GPP, "3GPP TSG RAN WG4 (Radio) Meeting 51: Simulation assumptions and parameters for FDD HeNB RF requirements," tech. rep., 4-8 May 2009.

[114] 3GPP TSG RAN, "3GPP TR.25.814, Physical Layer Aspects for Evolved UTRA (Release 7)," *v7.1.0*, September 2006.

[115] 3GPP TSG-RAN4#51, Alcatel-Lucent, picoChip Designs, and Vodafone, "R4-092042, Simulation assumptions and parameters for FDD HENB RF requirements," May 2009.

[116] L.H. Ozarow, S. Shamai, and A.D. Wyner, "Information theoretic considerations for cellular mobile radio," *Transactions on Vehicular Technology*, vol. 43, no. 2, pp. 359–378, may 1994.

[117] G. Ungerboeck, "Channel coding with multilevel/phase signals," *IEEE Transactions on Information Theory*,, vol. 28, no. 1, pp. 55–67, January 1982.

[118] D. Chase, "Code Combining–A Maximum-Likelihood Decoding Approach for Combining an Arbitrary Number of Noisy Packets," *IEEE Transactions on Communications*, vol. 33, no. 5, pp. 385–393, May 1985.

[119] W. Saad, Z. Han, M. Debbah, A. Hjørungnes, and T. Bas¸ar, "Coalition game theory for communication networks: A tutorial," *IEEE Signal Processing Mag., Special issue on Game Theory in Signal Processing and Communications*, vol. 26, no. 5, pp. 77–97, Sept. 2009.

[120] R. Menon, A. B. MacKenzie, J. E. Hicks, R. M. Buehrer, and J. H. Reed, "A game-theoretic framework for interference avoidance," *IEEE Transactions on Communications*, vol. 57, no. 4, pp. 1087–1098, Apr. 2009.

[121] E. Altman, T. Bas¸ar, and R. Srikant, "Nash equilibria for combined flow control and routing in networks: asymptotic behaviour for a large number of users," *IEEE Trans. Automatic Control*, vol. 47, pp. 917–930, Jun. 2002.

[122] V. Vukadinovic and G. Karlsson, "Video streaming in 3.5G: On throughput-delay performance of proportional fair scheduling," in *Proc. of IEEE Symp. on Modeling, Analysis and Simulation of Comp. and Telecom. Systems (MASCOTS) 2006*, Monterey, CA, USA, 11-14 Sept. 2006.

[123] L. K´oczy, "A recursive core for partition function form games," *Theory and Decision*, vol. 63, no. 1, pp. 41–51, August 2007. [Online]. Available: http://www.springerlink.com/content/5v61j22882l77j33/fulltext.pdf

[124] ——, "Stationary quasi-perfect equilibrium partitions constitute the recursive core," no. 028, 2008. [Online]. Available: http://edocs.ub.unimaas.nl/loader/file.asp?id=1329

[125] ——, "Stationary consistent equilibrium coalition structures constitute the recursive core," no. 0905, Aug. 2009. [Online]. Available: http://ideas.repec.org/p/pkk/wpaper/0905.html

[126] ——, "Sequential coalition formation and the core in the presence of externalities," *Games and Economic Behavior*, vol. 66, no. 1, pp. 559–565, May 2009. [Online]. Available: http://uni-obuda.hu/users/vecseya/RePEc/pkk/wpaper/0801.pdf

[127] S. Boyd and L. Vandenberghe, *Convex Optimization*. New York, USA: Cambridge University Press, Sept. 2004.

[128] 3GPP, “Physical layer aspects for evolved UTRA (Release 7),” *3GPP Technical report (TR 25.814) v7.1.0*, Oct. 2006.

[129] G. Chalkiadakis, E. Elkind, E. Markakis, M. Polukarov, and N. R. Jennings, “Cooperative games with overlapping coalitions,” *Journal of Artificial Intelligence Research*, vol. 39, pp. 179– 216, 2010.

[130] 3GPP TS 36.211, “Evolved universal terrestrial radio access network (E-UTRAN); physical channels and modulation (release 9),” vol. 9.1.0., Mar. 2010.

[131] EU FP7-ICT BeFEMTO project, ``Preliminary SON enabling & multi-cell RRM techniques for networked femtocells’’, D4.1, Dec. 2010

[132] BeFEMTO, Description of Work, 2009.

[133] J. Giese, M.A. Amin, S. Brueck, “Application of Coordinated Beam Selection in Heterogeneous LTE-Advanced Networks”, IEEE ISWCS, Aachen, Germany, November 2011

[134] S.Brueck, “Heterogeneous Networks in LTE-Advanced”, Invited Paper, IEEE ISWCS, Aachen, Germany, November 2011.

[135] E. Castillo, *Extreme Value Theory in Engineering*. San Diego: Academic Press, Inc, 1988.

[136] Y. Ko, A. U. Quddus, R. Tafazolli, “On distributed optimum energy usage in a two-tier co-channel femtocells network”, submitted to IEEE Trans. Wireless Commun., Aug. 2011

[137] http://www.analog.com/en/specialty-amplifiers/variable-gain-amplifiers/ad8372/products/product.html

[138] http://www.rfmd.com/CS/Documents/2483DS.pdf

[139] 3GPP TR 36.927 “Evolved Universal Terrestrial Radio Access (E-UTRA); Potential solutions for energy saving for E.UTRAN”, V1.0.0, Nov. 2010.

[140] Befemto D2.1 “Description of baseline reference systems, use cases, requirements, evaluation and impact on business model”, Dec. 2010

[141] Qin Wang, Mark Hempstead and Woodward Yang, “A Realistic Power Consumption Model for Wireless Sensor Networks Devices”, IEEE SECON 2006 proceedings, pp 286-295

[142] Robert Plana, “ What is hot in RF component and Systems”, Microwave Journal, vol. 49, no 2, Feb. 2006

[143] Viering, I.; Dottling, M.; Lobinger, A.; , "A Mathematical Perspective of Self-Optimizing Wireless Networks," *Communications, 2009. ICC '09. IEEE International Conference on* , vol., no., pp.1-6, 14-18 June 2009 doi: 10.1109/ICC.2009.5198628

[144] P.E.Gill, W. Murray and Wright,M. H. “Practical Optimization”, London, Academic Press 1981

[145] Powell, M. “A fast algorithm for nonlinearly constrained optimization calculations, Numerical Analysis”, Springer Berlin / Heidelberg, 1978

[146] P. B. S. Lissaman ;Carl A. Shollenberger, “Formation Flight of Birds” Science 22 May 1970: Vol. 168 no. 3934 pp. 1003-1005 ,DOI: 10.1126/science.168.3934.1003

[147] A. Ghosh, R. Ratasuk, B. Mondal, N. Mangalvedhe, and T. Thomas, “LTE-Advanced: Next-Generation Wireless Broadband Technology,” IEEE Transactions on Wireless Communications, June 2010.

[148] J. C. Ikuno, M. Wrulich, and M. Rupp, “System Level Simulation of LTE Networks,” in Proc. IEEE VTC Spring, May 2010.

[149] K. C. Beh, A. Doufexi, and S. Armour, “On the Performance of SU-MIMO and MU-MIMO in 3GPP LTE Downlink,” in Proc. of IEEE PIMRC, September 2009.

[150] Z. Bai, C. Spiegel, G. H. Bruck, P. Jung, M. Horvat, J. Berkmann, C. Drewes, and B. Gunzelmann, “On the Physical Layer Performance with Rank Indicator Selection in LTE/LTE-Advanced System,” in Proc. of IEEE PIMRC, September 2010.

[151] M. Simsek, T. Akbudak, B. Zhao, and A. Czylwik, “An LTE-Femtocell Dynamic System Level Simulator,” in Proc. of International ITG Workshop on Smart Antennas, February 2010.

[152] V. Chandrasekhar, M. Kountouris, and J. G. Andrews, “Coverage in Multi-Antenna Two-Tier Networks,” IEEE Transactions on Wireless Communications, October 2009.

[153] J. G. Andrews, W. Choi, and R. W. H. Jr., “Overcoming Interference in Spatial Multiplexing MIMO Cellular Networks,” IEEE Transactions On Wireless Communications, December 2007.

[154] P. Lee, T. Lee, J. Jeong, and J. Shin, “Interference Management in LTE Femtocell Systems Using Fractional Frequency Reuse,” in Proc. of ICACT, February 2010.

[155] V. Chandrasekhar, J. G. Andrews, T. Muharemovic, Z. Shen, and A. Gatherer, “Power Control in Two-tier Femtocell Networks,” IEEE Transactions on Wireless Communications, August 2009.

[156] A. Galindo-Serrano and L. Giupponi, “Distributed Q-Learning for Interference Control in OFDMA-Based Femtocell Networks,” in Proc. of VTC Spring, May 2010.

[157] D. S. Baum, J. Hansen, G. D. Galdo, M. Milojevic, J. Salo, and P. Kysti, “An Interim Channel Model for Beyond-3G Systems Extending the 3GPP Spatial Channel Model (SCM),” in Proc. of IEEE VTC Spring, May 2005.

[158] K. Ramadas and R. Jain, “WiMAX System Evaluation Methodology,” WiMAX Forum, Tech. Rep., January 2007.

[159] M. Maqbool, M. Lalam, and T. Lestable, “Comparison of Femto Cell Deployment Models for an Interference Avoidance Technique,” in Proc. of European Workshop on Broadband Femtocell Networks, June 2011.

[160] Femto Forum, “Interference Management in OFDMA Femtocells,” Tech. Rep., March 2008. [Online]. Available: www.femtoforum.org

[161] J. Laneman, D. Tse, G. Wornell, “Cooperative Diversity in Wireless Networks: Efficient Protocols and Outage Behavior,” IEEE Transactions on Information Theory, vol. 50 no.12, 2004.

[162] G. Kramer, M. Gastpar, P. Gupta, “Cooperative Strategies and Capacity Theorems for Relay Networks,” IEEE Transactions on Information Theory, vol. 51, no. 9, 2005.

[163] R. Tannious, A. Nosratinia, “Spectrally-efficient relay selection with limited feedback,” IEEE Journal on Selected Areas in Communications, vol. 26, no. 8, 2008.

[164] H. Alves, RD. Souza, ”Selective Decode-and-Forward Using Fixed Relays and Packet Accumulation,” IEEE Communications Letters, vol. 15, no. 7, 2011.

[165] Y. Zhu, Y. Xin, Kam PY, “Outage Probability of Rician Fading Relay Channels,” IEEE Transactions on Vehicular Technology, vol.57, no. 4 2008.

[166] T. Riihonen, S. Werner, R. Wichman, “On the feasibility of full-duplex relaying in the presence of loop interference,” In Signal Processing Advances in Wireless Communications. SPAWC '09 – Workshops, 2009.

[167] T. Riihonen, S. Werner, R. Wichman, “Optimized gain control for single-frequency relaying with loop interference,”. IEEE Transactions on Wireless Communications, vol. 8, no.6, 2009.

[168] T. Kwon, S. Lim, S. Choi, D. Hong, “Optimal Duplex Mode for DF Relay in Terms of the Outage Probability,” IEEE Transactions on Vehicular Technology 2010, 59(7):3628 {3634.

[169] T. Riihonen, S. Werner, R. Wichman, “Comparison of Full-Duplex and Half-Duplex Modes with a Fixed Amplify-and-Forward Relay,” In Wireless Communications and Networking Conference, 2009.

[170] TM. Cover, JM. Thomas, “Elements of Information Theory,” Hoboken, New Jersey: Wiley-Interscience, 2 ed., 2006.

[171] Narasimhan R: Individual Outage Rate Regions for Fading Multiple Access Channels. In 2007 IEEE International Symposium on Information Theory, 2007.

[172] J. Andrews, “Interference cancellation for cellular systems: a contemporary overview,” IEEE Wireless Communications, vol. 12, no.2, 2005.

[173] B. Kaufman, E, Erkip J. Lilleberg, and B. Aazhang, “Femtocells in Cellular Radio Networks with Successive Interference Cancellation,” In ICC'2011 Workshops 2011.

[174] A. Adhikary, V. Ntranos, G. Caire, “Cognitive femtocells: Breaking the spatial reuse barrier of cellular systems,” In IEEE Information Theory and Applications Workshop, 2011.

[175] F. Pantisano, K. Ghaboosi, M. Bennis, and R. Verdone,”A self-organizing solution for interferecne avoidance in TDD underlay femtocells,” IEEE ASILOMAR, Nov. 2010.

[176] C. Lima, M. Bennis, K. Ghaboosi, and M. Latva-aho, “Interference management for self-organized femtocell towards deployed green networks,” IEEE PIMRC (W-GREEN), 26-29 September 2010.

[177] 3GPP TR 36.814, “Further advancements for E-UTRA physical layer aspects”, V9.0.0, March. 2010

[178] Z. Altman, R. Skehill. R. Barco, L. Moltsen, R. Brennan, A. Samhat, R. Khanafer, H. Dubreil, M. Barry, B. Solana, “The Celtic Gandalf framework,” *Electrotechnical Conference, 2006. MELECON 2006. IEEE Mediterranean* , vol., no., pp.595-598, 16-19 May 2006 doi: 10.1109/MELCON.2006.1653171